THE DEVELOPMENT OF SHAFT FRICTION AND END BEARING FOR PILES IN HOMOGENEOUS AND LAYERED SOILS

by

S.N. WERSCHING BSc.

Thesis presented in fulfilment of the requirement for the Degree of Doctor of Philosophy, Council for National Academic Awards, London, 1987.

Sponsoring Establishment

Department of Civil Engineering and Building,

The Polytechnic of Wales, U.K.

Collaborating Establishment

Building Research Station, Watford, U.K.

March 1987

CERTIFICATION OF RESEARCH

This is to certify that, except when specific reference to other investigations is made, the work described in this Dissertation is the result of the investigation of the candidate.

S.N. Wersching

S.N. Wersching

(Candidate)

19/3/87

(Date)

G.O. Rowlands

G.O. Rowlands

(Director of Studies)

19/3/87

(Date)

R. Delpak

R. Delpak

(Supervisor)

19th March '87

(Date)

DECLARATION

This is to certify that neither this thesis, nor any part of it, has been presented, or is being currently submitted, in candidature for any degree at any other Academic Institution.

S. N. Waschka

(Candidate)

ACKNOWLEDGEMENTS

The author wishes to express his thanks to Mr. G. O. Rowlands, his Director of Studies, and Dr. R. Delpak, his Supervisor, at the Polytechnic of Wales for their assistance.

He wishes to extend his gratitude to Mr. R. W. Cooke of the Building Research Establishment for his advice and suggestions.

The author acknowledges the help and guidance offered by the technical staff of the Polytechnic of Wales, in the design and production of the testing apparatus. Particular thanks are extended to Mr. B. Lloyd and Mr. L. Whiteman for their assistance in the Geotechnics Laboratory.

Finally, he is indebted to Mrs. J. M. Werscheing for typing this thesis, and for the encouragement and understanding she has given throughout the duration of this study.

SUMMARY

THE DEVELOPMENT OF SHAFT FRICTION AND END BEARING FOR PILES IN HOMOGENEOUS AND LAYERED SOILS

by

S.N.WERSCHING

This thesis examines the behaviour of a 114.0 mm diameter segmental tubular steel pile jacked into loose sand, and loose sand overlying clay. The soil was placed under controlled conditions in a 3.0 m diameter by 3.0 m deep concrete tank.

The variation in local unit shaft friction and radial effective stress was monitored along the pile shaft, together with the distribution of axial load within the pile. Density changes within the sand were recorded at the end of pile installation. Vertical displacements and vertical effective stresses within the sand were recorded. In the case of the layered soil profile the shear and vertical effective stresses generated on the sand/clay interface were monitored.

Data from both the pile and soil instrumentation was recorded throughout pile installation and load testing, consisting of CRP, ML and CRU tests, by an Orion Data Logger which was interfaced with a Commodore PET micro computer. Each stage of the test was controlled by a 'Management' program, written by the author. This also recorded the incoming raw data on a floppy disc and reduced the raw data, outputting a hard copy as the test proceeded.

The results showed:

(i) The local unit shaft friction and radial effective stress is practically constant along a pile shaft in sand for a given pile embedment, and increases at a diminishing rate with pile embedment.

(ii) The average coefficient of earth pressure, K_s, at ultimate load in loose sand exceeds K_p for shallow pile embedments.

(iii) At full pile embedment and ultimate load the local coefficient of earth pressure, K_z, may greatly exceed K_p near the top of the pile and tend to a lower limiting value of 0.5 near the pile base.

(iv) Axial stresses within the sand around the pile shaft are reduced by the development of arching. Adjacent to the pile shaft the radial effective stress is the major axial stress.

(v) The development of shaft friction is directly related to displacements within the surrounding sand and on the sand/clay interface.

(vi) The presence of an underlying clay layer effects the development of shaft friction to a limited height above the sand/clay interface.

(vii) The drawdown of sand into the underlying clay had a direct effect the local unit shaft friction developed within the clay.

NOTATIONS

A_b = Pile base area

A_s = Pile shaft area

A_k, B_k = Bearing capacity factors (Berezantzev, 1961)

B = Foundation width or pile diameter

B_t = Diameter of testing tank

C = Empirical compaction factor

C_u = Undrained shear strength

D_b = Foundation depth

D_c = Critical depth

D_r = Relative density

E = Elastic modulus

E_u = Undrained elastic modulus

e = Voids ratio

f_a = Maximum allowable elastic stress in outer fibres of BOST web

f_s = Average unit shaft resistance

f_{sf} = Average unit shaft friction at failure

f_n = Average stress developed within the webs of the BOST due to an applied normal load

f_y = Yield stress

f_z = Local unit shaft friction

f_{zf} = Local unit shaft friction at failure

G = Shear modulus

G_s = Specific gravity

K_a = Active earth pressure coefficient

K_o = 'At rest' earth pressure coefficient

K_p = Passive earth pressure coeffient

K_s = Average lateral earth pressure coefficient acting on pile shaft at failure

K_z = Local lateral earth pressure coeffient acting on pile shaft at failure

l = Distance between web centres on one gauged face of the BOST

M_p = Fully plastic moment in the webs of the BOST at failure

N_γ, N_q, N_c = Bearing capacity factors

N_q^* = Base bearing capacity factor encorporating shape factor

P_s = Shear load applied to active face of the BOST

P_{sa} = Maximum allowable shear load on the BOST

P_{sf} = Applied shear load causing failure of the BOST

P_n = Normal load applied to active face of the BOST

Q_a = Applied load

Q_{af} = Applied load at failure

Q_{amax} = Maximum applied load

Q_{aw} = Applied working load

Q_b = Pile base resistance

Q_{bf} = Pile base resistance at failure

Q_s = Pile shaft resistance

Q_{sf} = Pile shaft resistance at failure

Q_t = Total pile resistance

Q_f = Bearing capacity at failure

q_{bf} = Unit base resistance at failure

q_{sf} = Average unit shaft resistance at failure

R = Radial displacement of the soil

R_{max} = Surface roughness coefficient

r = Radius from the pile axis

Sr = Degree of saturation

t = Web thickness of the BOST

V = Vertical displacement of the soil

W = Total width of a web on the BOST

Z = Depth

Z_e = Depth at which the ratio of effective overburden stress to effective radial stress is equal to K_s

Z'_e = Shaft bearing capacity factor

Z_i = Depth to sand/clay interface

α = Pile shaft adhesion factor

α_T = Surcharge reduction factor (Berezantzev, 1961)

γ = Unit weight of soil

γ_D = Unit weight of overburden (Berezantzev, 1961)

Δ = Lateral displacement of the active face of the BOST due to an applied shear load

Δ_* = Change in '$*$', where '$*$' is any of the notations included herein

δ' = Effective friction angle between pile shaft and soil at failure

ε_v = Volumetric strain

ε_z = Elastic vertical strain

ε_θ = Elastic circumferential strain

θ = Rotation at webs of the BOST for an applied shear load of P_{sf}

ν = Poisson's Ratio

ζ_γ, ζ_q = Shape factors

ρ_d = Dry density

σ_r = Radial stress

σ'_r = Radial effective stress

σ'_{ri} = Radial effective stress acting on the sand/clay interface

σ'_z = Vertical effective stress

σ'_{zf} = Vertical effective stress adjacent to pile shaft at failure

σ'_{zi} = Vertical effective stress acting on the sand/clay interface

σ'_{θ} = Circumferential effective stress

σ'_1 = Major principal effective stress

σ'_2 = Intermediate principal effective stress

σ'_3 = Minor principal effective stress

ϕ' = Angle of effective internal friction

τ_f = Shear strength of sand at failure

τ_i = Shear stress acting on the sand/clay interface

ω = Moisture content

ω_b = Pile base settlement

ω_s = Mean pile shaft settlement

ω_t = Pile butt settlement

CONTENTS

CHAPTER 3 SOIL PROPERTIES AND PRELIMINARY INVESTIGATIONS

CHAPTER 4 TESTING FACILITIES, CONTROL AND MONITORING SYSTEM

CHAPTER 5 PILE AND SOIL INSTRUMENTATION

LIST OF TABLES

LIST OF FIGURES

CHAPTER 3

CHAPTER 4

CHAPTER 5

CHAPTER 7

LIST OF PLATES

CHAPTER 5

CHAPTER 6

CHAPTER 1

INTRODUCTION AND OBJECTIVES

CHAPTER 1

INTRODUCTION AND OBJECTIVES

1.1 Introduction

This study forms part of an on-going investigation at the Polytechnic of Wales into the performance of piled foundations in layered soils. The programme was instigated by Perren (1978) who undertook a case study on the choice, construction and performance of piled foundations in glacial till, for a number of viaducts forming part of the M4 between Port Talbot and Bridgend in West Glamorgan. Among the types tested were bored piles which were placed with the aid of temporary casings. The tills in this region, in common with the rest of South Wales, are primarily granular in nature due to the fluvio-glacial conditions which prevailed in the valleys at the limits of the ice sheet during deposition (Weltman and Healy, 1978). The granular nature of the till allowed the inflow of ground water into the pile casing, which meant that the concrete had to be placed using a tremie. A number of the trial piles were founded in an underlying clay stratum. This effectively sealed the base of the temporary casing and allowed the piles to be formed in 'dry' conditions once the water within the casings had been bailed-out. It was later agreed with the Engineer that all bored piles should be formed under 'dry' conditions by increasing pile lengths as necessary.

Kay (1980) set out to model the behaviour of a pile in a layered soil profile within the confines of the laboratory, under semi-full scale

conditions. The test programme was conducted with a 114.0 mm diameter pre-placed, segmental pile suitably instrumented to measure the distribution of axial load along the pile shaft. Sand was employed to represent the granular till. The underlying clay stratum was modelled using a frictionless cylinder which eliminated end bearing. The primary objectives of his study were to measure the distribution of shaft friction along the pile shaft and to determine the interaction of the pile with the surrounding sand. This was achieved with some success within the limits of the somewhat crude and insensitive instrumentation used.

The current research programme aims to improve and advance on the previous work by jacking a pile into a soil profile consisting of sand overlying clay.

An intensive instrumentation development programme was undertaken by the author which resulted in the production of a simple orthogonal stress transducer. This was used extensively as a boundary element along the pile shaft.

The soil profile was comprehensively instrumented in order to monitor vertical displacements within the soil using electrolytic levels (Cooke and Price, 1973(a)). Changes in sand density due to pile installation were recorded using a method developed by the author (Wersching et al, 1983). Effective vertical and shear stresses developed on the sand/clay interface were monitored throughout the test programme using an array of diaphragm pressure transducers and shear stress transducers.

1.2 Objectives of the Investigation

At present, investigations into the behaviour of a pile within a layered soil profile, consisting of sand overlying clay are extremely limited. Principal contributors to this aspect of piling are Meyerhof and Tomlinson. The data reported in these papers was obtained with relatively limited instrumentation in both the pile and the soil.

The purpose of the author's investigation is to study the behaviour and interaction of a pile with one particular soil geometry of sand overlying clay. The sole variable throughout this study was to be the undrained shear strength (C_u) of the clay, since this influences the deformability of the clay. The programme was to be initiated with a test in a homogeneous sand profile in order to obtain a set of comparative data. However, due to circumstances beyond the author's control, the test programme had to be substantially curtailed and revised. Time allowed for only two tests in a homogeneous sand profile to check for repeatability, and a single test in a layered soil profile. A second test would have required an additional 2 months which, at the time, was unacceptable to all concerned.

CHAPTER 2

LITERATURE REVIEW

CHAPTER 2

LITERATURE REVIEW

2.1 Introduction

In recent years significant advances have been made in the analytical modelling and design of piles in cohesive soils. This work was primarily instigated by the needs of the offshore oil industry where both pile size and environmental conditions make load testing impractical. By comparison, our increase in the understanding of the behaviour of piles in non-cohesive soils is limited. Still less attention has been directed towards the behaviour of piles in a layered soil profile. This chapter aims to outline the current understanding of the performance of straight sided, large displacement piles in both non-cohesive and layered soils (sand overyling clay).

2.2 Non-cohesive Soils

The ultimate bearing capacity of a single pile is evaluated as the sum of two discrete components; namely, the base and shaft resistance.

Thus:

$$Q_f = q_{bf}A_b + f_{sf}A_s \qquad (2.1)$$

where:

Q_f = bearing capacity at failure,

q_{bf} = unit base resistance at failure,

f_{sf} = average unit shaft resistance at failure,

A_b = pile base area,

A_s = pile shaft area.

Equation 2.1 assumes the mass of the displaced soil to be equal to the mass of the embedded portion of the pile.

The geometric terms A_b and A_s may be quantified with a reasonable degree of confidence. However, the evaluation of q_{bf} and f_{sf} is somewhat subjective. The development of theoretical formula to evaluate q_{bf} and f_{sf} are necessarily based on a number of fundamental assumptions which, in general, simplify the true conditions encountered either in the laboratory or the field. It is the validity of the assumptions that determines the accuracy of any theory.

2.2.1 Unit Base Resistance at Failure

The assumptions common to many of the accepted theories used to evaluate the unit base resistance at failure of a pile are; that the pile is a rigid hard body and has a rough base, and that the soil is a homogeneous, rigid plastic medium which conforms with the Mohr-Coulomb strength criterion. A further requirement, which can vary from one theory to another, is that of a representative kinomatic failure mechanism with

defined boundaries and discontinuities. Of the many theories expounded, those which have received greatest acceptance amongst practicing engineers in the United kingdom are: Terzaghi (1943); Meyerhof (1951) and Berezantzev et al (1961). All of these theories are founded fundamentally on the above assumptions. However, there is some variation in the assumed kinomatic failure mechanism. Further, Berezantzev et al (1961) was the first to consider the geometry in terms of an axisymetric problem, the other theories being based on a biaxial solution.

Other theories have been developed where the problem has been considered in terms of an expanding cavity within an elastoplastic medium, the first of which was Bishop et al (1945).

Traditionally, the unit base resistance at failure, of a pile founded in a non-cohesive soil, is given by:

$$q_{bf} = \tfrac{1}{2}\gamma B N_\gamma \zeta_\gamma + \gamma D_b N_q \zeta_q \qquad (2.2)$$

where:

γ = unit weight of soil,

B = foundation width,

D_b = foundation depth,

N_γ, N_q = bearing capacity factors,

ζ_γ, ζ_q = shape factors.

N_γ and N_q are dimensionless functions of ϕ' and the assumed kinomatic failure mechanism (Coyle and Castello, 1981), and refer to the biaxial

problem of a continuous strip footing.

The shape factors are empirically/semi-empirically derived coefficients which relate the bearing capacity factors of a continuous strip footing to that of a circular or rectangular prismatic footing (Sherman et al, 1974).

At depth, the first term in Equation 2.2, which is a function of the foundation width (B), is small in comparison with the second term, which is a function of foundation depth (D_b), and may therefore be neglected (Coyle and Castello, 1981). Since most piles are prismatic and of either circular or square section, a single shape factor (ζ_q) may be used (Vesic, 1967). Thus allowing a new bearing capacity factor to be defined which includes the shape factor.

Equation 2.2, therefore, becomes:

$$q_{bf} = \gamma D_b N_q^* \qquad (2.3)$$

where:

$$N_q^* = N_q \zeta_q$$

The equation reported by Berezantzev et al (1961) for the unit base resistance at failure of a pile, is of a different form to that of Equation 2.2. That is:

$$q_{bf} = A_k \gamma B_k + B_k \alpha_T \gamma_D D_b \qquad (2.4)$$

where:

A_k, B_k = dimensionless bearing capacity factors dependant upon, ϕ',

γ = unit weight of soil at pile base level,

γ_D = unit weight of overburden,

α_T = overburden reduction factor dependent upon both D_b/B, and ϕ'.

Applying the same reasoning to Equation 2.4 as was applied to Equation 2.2:

$$q_{bf} = B_k \alpha_T \gamma_D D_b \qquad (2.5)$$

From which it may be surmised that:

$$N_q^* = B_k \alpha_T$$

Therefore, according to Berezantzev et al (1961), N_q^* is a function of both D_b/B and ϕ'.

Vesic (1963) presented, in graphical format, the variation in N_q^* with ϕ' for a number of published theories. This showed that for any given value of ϕ', N_q^* can vary by an order of magnitude, and illustrates that the true failure mechanism is not, generally, well understood (Coyle and Castello, 1981).

Equation 2.3, which is the generally accepted form, implies that q_{bf}

increases linearly with pile embedment (D_b). This has been known not to be the case for some time.

Kerisel (1961) conducted a series of large scale experiments with jacked piles of various diameter in a homogeneous sand mass. He concluded that N_q^* was not a unique function of ϕ' but was affected by B and D_b.

Vesic (1963) suggested that q_{bf} increased practically linearly (N_q^* being approximately constant) for shallow embedments of less than 4B for circular footings and 6B for rectangular footings. Further, for an embedment of about 15B, q_{bf} tended to a constant limiting value which was a function of sand density only.

The conclusions arrived at by Vesic (1963) were derived from a series of tests conducted with preplaced piles which were installed at discrete depths in increments of at least 4.5B. Thus, the statement that q_{bf} increased linearly at shallow depths cannot be regarded with confidence. Further, the unit base resistance at failure for the 52.0 mm diameter pile, upon which the above conclusions were primarily based, was evaluated by loading the pile base independently of the pile shaft. It was shown by Tejchman (1971) that q_{bf} can increase by about 10% due to the stresses developed in the soil by the action of friction along the pile shaft.

A series of large scale tests undertaken on jacked piles were reported by Kerisel (1964). From the results of these tests it was apparent that:

(i) Below a certain critical depth (D_c) q_{bf} attained a quasi-constant limiting value which appeared to be a function of sand density only.

(ii) The depth at which D_c was attained increased with B and sand density.

(iii) The variation in D_c with B was greater for higher sand densities.

It was evident from the results presented by Kerisel that q_{bf} did not increase linearly for shallow pile embedments, but increased at a progressively greater rate. With further pile embedment the rate of increase in q_{bf} gradually reduced and tended to a quasi-constant limiting value, which was a function of sand density. It appeared that the critical depth for a dense sand corresponded with a pile embedment of about 20B. In loose sand the critical depth was about 1.8 m, and was unaffected by pile diameter. Kerisel made the point that tests conducted with "pencil piles", which seldom exceed 1.0 m in depth, cannot have far reaching effects on our understanding of the behaviour of piles.

Vesic (1964) reported that D_c varied with sand density. For driven piles in loose sand D_c occurred at about 10B. In dense sand D_c increased to about 30B. For buried, preplaced piles in loose to medium dense sand D_c was the same as that for driven piles in loose sand. However, in dense sand D_c was attained at about 20B. Again, these observations were based upon tests in which both the pile base and the pile shaft were loaded independently.

More recent examples of critical depth behaviour have been reported by

Vesic (1970), Tavenas (1970) and Hanna and Tan (1973).

Vesic (1970) conducted tests on a 460.0 mm diameter by 15.7 m long, instrumented pile. The pile was driven into a deep deposit of medium dense to dense sand. Static load tests were conducted after each 3.0 m of penetration to full embedment. The results clearly showed the attainment of critical depth behaviour at about 20B.

Tavenas (1971) reported the development of critical depth behaviour in the field at 23B depth for a Herkules H800 pile, driven into a medium dense uniform medium sand.

Hanna and Tan (1973) undertook a series of laboratory scale experiments with long, slender, preplaced piles in a medium dense sand. Their results show the onset of critical depth behaviour at between 30 to 40B depth.

On the basis of the above studies it is evident that N_q^* is not solely a function of ϕ', but is also a function of D_b. The commonly expressed opinon is that the onset of limiting unit base resistance at the critical depth, is due to the stresses in the soil in the vicinity of the pile base attaining a quasi-constant limiting value. Thus, the soil stresses are no longer related to the initial effective overburden stress.

Vesic (1964) stated that at depth, generally in excess of 15B, the unit base resistance reached an asymptotic final value which was independent of the initial overburden stress, and appeared to be a function of the

relative density of the sand only. This was explained by the development of arching within the sand above the pile base. He further suggested, that a fundamental fallacy in the analysis of pile bearing capacity is the assumption that the stress condition at failure around the pile is the same as that prior to pile installation.

Vesic (1969(a)) stated that the initial state of stress in the vicinity of a pile may be very different from that prior to pile installation. Vertical stresses are generally increased below the pile base and decreased above the pile base.

Tavenas (1971) suggested that there are several weaknesses in the existing theories. These are:

(i) Unlikely kinomatic failure mechanisms for deep foundations.
(ii) Biaxial analysis of the problem.
(iii) Unverified stress distribution assumed around a pile.

Meyerhof (1976) suggested that the vertical effective stress near the pile base, at the onset of limiting unit base resistance, is practically independent of the effective overburden stress for a pile embedment of greater than the critical depth.

Hollaway et al (1978) stated that the overburden stress near the pile is affected by the load deformation conditions throughout pile installation and subsequent load testing.

2.2.2 Unit Shaft Resistance at Failure

By comparison with the number of theories dealing with the evaluation of the unit base resistance at failure, the procedure for evaluating the unit shaft resistance at failure remains relatively unchanged from the original concept proposed by Dörr (1922). This may be attributed, to some extent, to the practice of some engineers of neglecting the contribution of the pile shaft to the ultimate resistance of the pile in non-cohesive soils (Meyerhof, 1963; Robinsky and Morrison, 1964; Broms, 1966).

Norlund (1963) stated that unit shaft resistance of a pile is affected by the following:

(i) Effective friction angle of the soil.
(ii) Friction angle of the sliding surface.
(iii) Taper of pile.
(iv) Unit weight of soil.
(v) Length of pile.
(vi) Minimum perimeter encompassed by pile.
(vii) Volume of soil displaced by pile per unit length.

Other factors shown to affect the unit shaft resistance of a pile are:

(i) Applied load - tension, compression or torsion (Broms, 1964).
(ii) Method of installation - driven, jacked or bored (Vesic, 1964).

The generally accepted equation employed to evaluate the local unit shaft resistance at failure (f_{zf}) for a straight sided, cylindrical pile in non-cohesive soil is:

$$f_{zf} = K_z \sigma'_{zf} \text{Tan}\delta' \qquad (2.6)$$

where:

K_z = local lateral earth pressure coefficient,

σ'_{zf} = vertical effective stress adjacent to the pile shaft at failure,

δ' = effective friction angle between the pile shaft and the adjacent soil.

The problem facing the practicing engineer, however, is that of assigning representative values to each of the above terms, appropriate to the prevailing ground condition and pile type. It is generally assumed that K_z and $\text{Tan}\delta'$ are constant along the pile shaft and that σ'_{zf} is equal to the effective overburden stress at the depth in question prior to pile installation (Broms, 1966; Coyle and Castello, 1981).

On the basis of the above assumptions, f_{zf} increases linearly with depth along the pile shaft in a dry, homogeneous, non-cohesive soil. Thus, the shaft resistance at failure (Q_{sf}), as defined by Equation 2.7, increases with the square of pile embedment.

$$Q_{sf} = \tfrac{1}{2}\pi B D_b^2 K_s \text{Tan}\delta' \qquad (2.7)$$

where:

K_s = average lateral earth pressure coefficient.

However, the results from extensive field and laboratory tests have shown the above distribution and variation in shaft friction with depth and pile embedment to be incorrect.

Mohan et al (1963) recorded the axial load distribution in a cast in-situ pile (within which it may reasonably be assumed that the initial residual stresses are zero) in a medium dense sand. The distribution of local unit shaft friction along the pile, derived from the axial load distribution at ultimate load, increased at a decreasing rate with depth, attained a peak value, and reduced over the lower portion of the pile shaft.

Vesic (1964) conducted a series of tests with a 50.0 mm diameter, preplaced pile at discrete depths in homogeneous sand profiles. The total shaft load was recorded by loading the pile shaft independently of the pile base. Vesic reported that in dense sand f_{sf} increased linearly with pile embedment to a depth of 15B, beyond which f_{sf} was constant. In loose and medium dense sand he reported a linear increase in f_{sf} with pile embedment to 4B, beyond which f_{sf} was again constant. However, it should be noted that the shallowest pile embedment employed by Vesic in this series of tests was 5B. Vesic showed the constant limiting value of f_{sf} to be a function of the initial dry density of the sand.

Tavenas (1971) installed an instrumented Herkules pile H800 (nominally

305.0 mm in diameter) into a medium dense fine to medium sand in the field. It was found that f_{sf} tended to a constant limiting value for a pile embedment of about 7.0 m, corresponding to a critical depth of 23B.

Vesic (1970) reported the results of field tests on a 460.0 mm diameter by 15.7 m long steel pile, instrumented at six points along the shaft in order to monitor the distribution of axial load within the pile. The pile was installed in a dense to medium dense, medium sand. Static load tests were conducted at various pile embedments thoughout pile installation. From the recorded distribution of axial load at ultimate load, Vesic deduced the distribution of local unit shaft friction to be parabolic. For short piles f_{zf} was concentrated over the upper portion of the pile shaft, whilst in long piles the peak f_{zf} was concentrated over the lower portion of the shaft. Further, the average ultimate unit shaft resistance tended to a constant limiting value for a pile embedment of about 6.1 m, or 15B. It should be noted that although the pile was installed by driving, which results in the development of a system of residual stresses within the pile, the influence of the residual stresses do not appear to have been allowed for when calculating the distribution of f_{zf}. This observation is based on the reported distribution of axial load (associated with unloading the pile) for an applied load which was approximately equal to zero. This is further supported by the fact that Vesic reported that the total shaft load in both compression and tension was about the same, which is contrary to results reported elsewhere. Vesic also fails to report the distribution of axial load within the pile associated with tensile loading.

Gregersen et al (1973) installed a two sectioned, 16.0 m long, Brynildsen

pile of circular cross-section, 280.0 mm in diameter, into a uniform loose sand deposit, 30.0 m thick. The pile was instrumented to record the distribution of axial load. From the variation in axial load, which included the affects of residual stresses, Gregersen et al derived the distribution of f_{zf} along the pile shaft at ultimate load. Along the initial 8.0 m pile section they showed the distribution of f_{zf} to be approximately parabolic and concentrated over the upper portion of the pile shaft. However, for the 16.0 m pile f_{zf}, although generally parabolic, was concentrated over the lower portion of the pile shaft. It should be noted, however, that a number of data points relating to the axial load distribution within the pile were not reported. Further, despite the authors reference to the sand being uniform, a significant increase in dry density is evident below 10.0 m depth. This would be a contributing factor to the increase in f_{zf} over the lower portion of the 16.0 m pile.

Hanna and Tan (1973) reported the results of tests conducted with long, slender, preplaced piles in a medium dense sand in the laboratory. They reported that f_{sf} increased with pile embedment to about 40B depth, beyond which f_{sf} was almost constant. The pile was instrumented with sensitive axial load cells in order to record the distribution of axial load in the pile, and hence evaluate the distribution of f_{zf}. The distribution of f_{zf} was reported by Hanna and Tan at ultimate load for a pile embedment of 45B, and takes into account the effects of residual stress. It was observed that f_{zf} increased rapidly at shallow depths of about 3B or less. The precise variation of f_{zf} at shallow depths is somewhat speculative due to the limitations of the instrumentation. At greater depth, f_{zf} increased at a much reduced rate, and attained a peak

value at about 15B above the pile base before reducing with proximity to the pile base.

The method of assessing the distribution of f_{zf} in all the cases quoted above is based upon the measurement of the variation in axial load along the pile shaft. Although this procedure is theoretically correct, it is very sensitive to the accuracy of the load cells and the author's "interpretation" of the results. These two facts can lead to an erroneous assessment of both the magnitude and distribution of f_{zf}.

In view of the differences between the theoretical and observed distribution of f_{zf}, the general observation and recommendation reported in the literature, in relation to the terms in Equation 2.6, are reviewed below.

Coefficients of earth pressure, K_s, K_z:

Meyerhof (1951) reported that K_s varied between 0.5 for loose sand, and 1.0 for dense sand. These results are based upon pile tests conducted in the field, and cone penetration tests. Data from the cone penetrometer showed $K_s Tan\delta'$ to reduce with depth. If $Tan\delta'$ is assumed to be relatively constant with depth, then K_s must reduce with depth of embedment. The limits reported by Meyerhof may, therefore, only be applicable to relatively shallow piles.

Mohan et al (1963) evaluated the variation in K_z along the shaft of a 8.5 m long, bored pile, installed in a soil profile consisting of 2.4 m of silty sand and debris overlying 8.5 m of medium dense sand. They

assumed that σ'_{zf} was equal to the initial overburden stress and that δ' was equal to ϕ'. Near the surface, above the water table, they reported K_z being equal to 4.5, which is greater than K_p (3.25). At depth, K_z reduced at a diminishing rate to 1.6 in the vicinity of the pile base.

Norlund (1963) evaluated the theoretical magnitude of K_s in terms of ϕ' and pile taper angle. The solution implies the assumption of zero vertical displacement in the soil mass. For straight sided piles K_s is approximately equal to 0.5, regardless of ϕ'. This fact is in conflict with the findings of other investigators.

Vesic (1964) reported values of K_s evaluated for both driven and buried piles of 100.0 mm diameter, for tests conducted both in the laboratory and the field. The function $K_s \text{Tan}\,\delta'$ was evaluated from the initial linear portion of the f_s/D_b profile, and relates therefore to a pile shaft above D_c. $\text{Tan}\,\delta'$ was taken as being equal to $\text{Tan}\,\phi'_{min}$.

Sand Density	Relative Density	K_s Driven	K_s Buried
Loose	0.2-0.4	2.5	1.6
Medium Dense	0.5-0.7	3.0	2.2
Dense	0.7-0.9	4.5	3.3

The results show that K_s is greater for driven piles than buried piles, and increases with sand density.

On the basis of results reported in the literature, Broms (1966) recommended values of K_s to be considered for design purposes.

Pile Type	Relative Density	
	Low	High
Steel	0.5	1.0
Concrete	1.0	2.0
Wood	1.5	4.0

The results for steel piles are applicable to small displacement piles; that is, 'H'-piles. The effect of pile taper has been taken into account for wooden piles, together with the large displacement volume of soil.

Hanna and Tan (1973) evaluated the distribution of K_s along a thin slender pile in medium dense sand. They assumed σ'_{zf} to be equal to the initial effective overburden stress, and that $\tan\delta'$ was constant along the pile shaft. At ultimate load their results showed that K_s reduced markedly over the upper 400.0 mm of the pile shaft (25.4B) and was relatively constant below this depth. Hanna and Tan (1973) also showed that K_z was dependent upon the load applied to the pile.

Meyerhof (1976) suggested that K_z may approach K_p near the top of the pile shaft, and be less than K_o near the pile base. Further, he analysed the results of tests conducted on piles at depths less than D_c. The results show K_s to increase with ϕ', and that K_s is affected by the method of pile installation, with bored, jacked and driven piles resulting in progressively higher values of K_s for a given ϕ'.

Coyle and Castello (1981) analysed a number of well documented field tests. They showed K_s to increase with ϕ', and decrease logarithmically with relative pile embedment (D_b/B). For a shallow pile embedment K_s tended to K_p, whilst for deep piles K_s approached K_a.

Vertical effective stress adjacent to the pile shaft at failure, σ'_{zf} :

Broms and Silberman (1964) proposed that the shaft friction developed in compression, acted to increase the effective overburden stress adjacent to the pile shaft, whilst tensile loading of the pile acted to reduce the effective overburden stress adjacent to the pile shaft. This phenomenom was proposed to explain the difference in compressive and tensile capacity of the pile shaft. However, such an explanation, although apparently plausible, does not explain the very low torsional resistance reported by the authors.

Vesic (1964) argued that the vertical effective stress adjacent to a pile shaft increased linearly for shallow depths only. Below a certain depth σ'_{zf} may tend to a constant value, which may or may not be preceded by a peak value. He attributed such a distribution to the development of arching in the sand above the pile base. He further stated that the assumption that the stress adjacent to a pile shaft was the same as that in the soil prior to pile installation, was a fundamental fallacy and proposed that the limiting value of f_{sf} was independent of the effective overburden stress and was a function of relative density only.

Robinsky and Morrison (1964) analysed the density variation within a sand mass due to the installation of a model displacement pile. They concluded that driving the pile resulted in the formation of a dense cylinder of sand, previously compacted by the pile base which surrounded a sleeve of loose sand adjacent to the pile shaft. The effect of this was to promote lateral arching within the sand profile and, therefore, reduce the lateral stresses acting on the pile shaft.

Hanna and Tan (1973) stated that the installation of a pile in the ground resulted in a rotation of the principal stress planes. Further, through back analysis of their model tests they showed σ'_{zf} to be greater than the initial effective overburden stress over the upper 250.0 mm (10B) of the pile shaft, equal to the effective overburden stress between 250.0 to 800.0 mm depth (10 to 23B), and essentially constant below 800.0 mm depth. In evaluating σ'_{zf} they assummed $\delta' = 25^0$ and $K_s = 0.24$.

Meyerhof (1976) stated that K_s reduced to less than K_o for very long piles, which he considered to be impossible. However, if σ'_{zf} was less than the initial effective overburden stress, then such low values of K_s for long piles are plausible.

Holloway et al (1978) stated that the effective overburden stress adjacent to a pile shaft was affected by the load deformation conditions throughout pile installation and the load test sequence.

Effective friction angle between the pile shaft and the adjacent soil, δ':

Potyondy (1961) was the first to report in detail, on the friction angle developed between a variety of soils and common construction materials. Among the soils tested was dry and saturated dense sand with an angle of internal friction of 43^0 and 38^0 respectively. The friction angle developed between the sand and a smooth (polished with fine 'sand' paper) and a rough (rusted with the loose material removed) steel plate was recorded. The following results were obtained.

Sand (ϕ')		Steel (δ')	
		Smooth	Rough
Dry	43^0	24^0	34^0
Saturated	38^0	24^0	-

Broms and Silberman (1964) assumed $\delta' = \phi'$ for rough piles and $\delta' = 23^0$ for smooth piles, regardless of the relative density of the sand, for a series of model tests conducted with 19.0 and 38.0 mm diameter piles.

Vesic (1964) assumed δ' between the sand and the shaft of a 100.0 mm steel diameter pile, tested both in the laboratory and the field, to be equal to ϕ'_{min}. This assumption was based upon the results of friction tests undertaken earlier with steel plates.

Broms (1966) proposed the following values of δ' for common pile materials.

Pile Material	Friction Angle δ'
Steel	20^0
Concrete	3/4 ϕ'
Wood	2/3 ϕ'

These conclusions were based upon the work of both Potyondy (1961) and Broms and Silberman (1964). Broms stated that the above values may, however, be conservative.

Coyle and Silberman (1967) conducted a series of tests using a modified triaxial device. The modifications allowed a steel pile element, surrounded by sand within the pressure cell, to be loaded externally. It

was assumed by Coyle and Silberman that the total shaft friction developed along the pile element was equal to the applied external load and that the radial effective stress was equal to the applied cell pressure. It was, therefore, possible to evaluate δ'. Their results show $\text{Tan}\delta'$ to reduce with increased confining pressure, which they equated to increased depth in the field. A limiting value of $\text{Tan}\delta' = 0.4$ (22^0) was proposed by the authors.

The above work was criticised by Healy and Meitzler (1968). They stated that values of $\text{Tan}\delta'$ between 0.9 and 0.4 were at odds with previous findings. Further, the assumption made by Coyle and Silberman (1967) that the lateral effective stress acting on the pile element during shearing was equal to the applied cell pressure, was in error since:

(i) Radial arching will increase or decrease the stresses on the pile element depending upon whether the sand dilates or contracts during shearing.

(ii) Radial friction and normal stresses against the frame will increase the effective lateral stress during shearing.

Butterfield and Andrawes (1973) undertook a series of direct shear tests with various materials in contact with either a dense or loose sand. Amongst the materials tested were polished mild steel and a steel plate to which sand grains had been glued. Butterfield and Andrawes reported both the static (δ'_s) and kinematic (δ'_k) friction angles for these two interfaces. Their results are outlined below.

Steel	Sand			
	loose ($\phi' = 33^0$)		Dense ($\phi' = 46^0$)	
	δ'_s	δ'_k	δ'_s	δ'_k
Polished	11.3^0	9.8^0	18.0^0	15.6^0
Glued Sand Grains	-	31.6^0	-	40.0^0

They concluded that the static friction angle is always greater than the kinematic friction angle by about 2^0.

Holloway et al (1978) undertook direct shear tests on a sand/steel interface and reported that δ' ranged between 23^0 and 30^0 for ϕ' between 31^0 and 35^0. For the purposes of analysis they chose an average ϕ' of 32^0 and a high α' of 30^0 due to the probable densification of the sand adjacent to the pile shaft.

Yoshimi and Kishida (1981) undertook a comprehensive study of the shear behaviour of various sand/metal interfaces. The three types of sand employed had different grain shapes and surface texture. Yoshimi and Kishida proposed that the surface roughness of the interface was the governing factor with regard to the friction angle, and that the relative density of the sand was of minor importance. Further, they showed that for surfaces within the usual range of roughness encounted for construction materials, shear zones developed within the sand near the interface immediately after slip occurred along the interface.

Acar et al (1982) conducted a series of direct shear tests to establish the effective friction angle between sand and various construction

materials. They showed that for a given normal effective stress the friction angle diminished with reduced relative density of the sand. Further, for a given normal effective stress the ratio δ'/ϕ' was practically constant and reduced with increased normal effective stress.

In view of the variability of the above parameters it is clear, in relation to both base and shaft resistance, that we do not have as yet a clear understanding of the mechanics of the problem. Until such time as this knowledge is gained, full scale pile load tests and back analysis of these parameters for a given site and pile type will remain an important part of checking and/or finalising the design of piles for major projects.

2.3 Layered Soils

Our present understanding of the behaviour and interaction of vertical axially loaded cylindrical piles in layered soils, consisting of sand overlying clay, is limited to the publications of two author's; namely, Tomlinson and Meyerhof.

Tomlinson (1970) reported the findings of a series of tests conducted on 168.0 mm diameter steel piles (some of which were instrumented) in London Clay. As part of a series of supplementary tests three uninstrumented piles were driven through sand into the London Clay. This was achieved by enlarging the holes, left after the extraction of previously installed piles, by drilling to a diameter of 0.6 m (equivalent to 3.6B). The holes were then back filled with sand and lightly tamped. It should be

noted that the above configuration could result in the stiff clay surrounding the sand offering unrealistic boundary conditions, thereby increasing the confining effect of the sand and increasing lateral stress on the pile shaft, resulting in an increase in shaft resistance within the sand.

Excavation of the piles showed that the sand had been drawn down into the underlying clay around the pile shaft in the form of a thin adherent skin to a depth of 0.53 m (3.2B).

The three test results were analysed in terms of total stress. Tomlinson established that very high adhesion factors (α) were obtained for piles with limited penetration into the underlying clay. It should be noted, however, that since the piles used were not instrumented Tomlinson had no means of accurately assessing that proportion of load carried by the section of the pile shaft in contact with the stiff clay.

The above results were further discussed by Tomlinson (1971), together with supportive data reported in the literature.

Meyerhof and Sastry (1978(b)) identified the principal problem associated with piling in layered soils, consisting of sand overlying clay, as being one of punching of the pile through the sand layer into the clay as the pile tip approached the sand/clay interface. To this end they undertook a series of model tests employing a 76.0 mm diameter instrumented pile. They suggested that the depth to which a pile may be driven in a layered soil, without punching through to the underlying softer soil, depended upon the ratio of the limiting unit point resistance of the two soils in

question. From the results of experiments they reported typical values of 1.5B for $q_{lw}/q_{ls} = 0.67$ and 6.0B for $q_{lw}/q_{ls} = 0.02$. Meyerhof and Sastry analysed the problem of punching and derived the following relationships.

$$q_p = q_i + 4s_p K_{ps} p_o h' \tan\phi_s / B \leq q_{ls} \qquad (2.8)$$

in which:

$$q_i = C_u N_{co} + \gamma(D + h')N_{qo} \leq q_{lw} \qquad (2.9)$$

where:

q_p = maximum unit point resistance in strong layers,

q_i = unit point resistance at the (lower) strong-weak soil interface,

C_u = undrained shear strength,

K_{ps} = average punching coefficient for a strip footing,

h' = maximum punching height,

p_o = effective overburden pressure at centre of h',

ϕ'_s = angle of internal friction of strong soil,

B = pile diameter,

γ = unit weight of soil,

D_b = depth of pile point,

N_{co}, N_{qo} = surface bearing capacity factors for circular footing on weaker soil,

q_{lw}, q_{ls} = limiting unit point resistance in homogeneous weak and strong soils respectively.

On the bases of these equations, Meyerhof and Sastry derived a family of curves for K_{ps} in terms of ϕ' and the ratio of strong soil layer thickness (H) to pile diameter (B).

The above papers generally illustrate the limit of our understanding of the interaction of piles in layered soils, consisting of sand overyling clay.

CHAPTER 3

SOIL PROPERTIES AND PRELIMINARY INVESTIGATIONS

CHAPTER 3

SOIL PROPERTIES AND PRELIMINARY INVESTIGATIONS

3.1 Introduction

The soils used in this investigation were a uniformly graded quartzitic Leighton Buzzard sand and a red-brown silty clay of low plasticity from the Mercia Mudstone (formerly Keuper Marl) geological formation.

The red-brown clay from the Mercia Mudstone was primarily chosen because of local availability and the experience gained with this material at the Polytechnic. In total, 2.5 Tonnes dry weight of clay was obtained and oven dried before being crushed and pulverized. The clay was then remixed to a conditioning moisture content of 15.0% and stored in sealed bins for approximately 18 months until required.

Standard index and strength tests were undertaken to classify the physical and mechanical properties of both soils.

3.2 Leighton Buzzard Sand

3.2.1 Specific Gravity

The specific gravity was determined as 2.71. This was calculated from the average of four tests undertaken in accordance with BS1377 (1975),

Test 6(B) for fine grained soils, on samples taken from different locations within the sand mass.

3.2.2 Partical Size Distribution

The partical size distribution was determined in accordance with BS1377 (1975), Test 7(B) by dry sieving. The average grading curve from six tests on randomly selected samples is presented on Figure 3.1. The uniformity and curvature coefficients were determined as ($C_u = D_{60}/D_{10}$) 1.79 and ($C_z = D_{30}/D_{60}D_{10}$) 1.38 respectively.

3.2.3 Moisture Content

The moisture content of six samples taken at random from the sand mass was established to BS1377 (1975), Test No 1(A) by oven drying, as less than 0.1%.

3.2.4 Maximum and Minimum Densities

The maximum and minimum densities were determined in accordance with the California Bearing Ratio Mould (CBR) and 2000 ml cylinder methods described by Akroyed (1957). These were established as 1780.2 kg/m^3 and 1520.0 kg/m^3 respectively. However, the average 'as-placed' density measured within the sand tank was 1470.0 kg/m^3, with a minimum of 1439.1 kg/m^3, both of which were less than the minimum value determined using the 2000 ml cylinder method. Consequently the Funnel method, also

described by Akroyed (1957), was used to establish the minimum density. This gave a value which was slightly higher than the average placement density. The minimum density was, therefore, taken as 1439.1 kg/m^3, corresponding to the minimum placement density measured during the test programme.

3.2.5 Variation in Angle of Internal Shearing Resistance with Density

Drained triaxial tests were conducted at a single cell pressure on 102.0 mm diameter specimens of saturated sand for a range of initial densities, at a constant rate of strain (1.524 mm/min) as described by Bishop and Henkel (1961). This approach was justified since Lambe and Whitman (1979) stated that the stress-strain behaviour of saturated and dry granular soils was virtually identical provided the rate of strain was sufficiently slow to prevent the build up of excess pore water pressures.

The variation in ϕ' with ρ_d was established at a cell pressure of 110.0 kPa (derived in Appendix 3.1), and is shown on Figure 3.2.

3.3 Mercia Mudstone

3.3.1 Index Test Sample Preparation

A representative sample of the clay for index and shear strength tests was obtained by removing a small quantity of clay from each batch after remixing from a dry state to the conditioning moisture content. To

accelerate the conditioning of the index test sample the clay was throughly mixed at an elevated moisture content of 30.0% and allowed to dry naturally, remixing as required in order to prevent the formation of a 'dry crust', to the initial moisture content of 15.0%.

3.3.2 Specific Gravity

To determine the specific gravity, four samples were prepared and tested in accordance with BS1377 (1975), Test 6(B) for fine grained soils, from which an average value of 2.78 was established.

3.3.3 Liquid and Plastic Limits

The liquid and plastic limits were determined in accordance with BS1377 (1975), Tests 2(A) and 3, as 39.0% and 19.5% respectively. These values are consistent with a clay of low plasticity.

3.3.4 Determination of Optimum Placement Technique

In view of the quantity of clay to be placed, approximately 1.2 m^3, a more expedient method of compacting the clay using a Kango hammer was considered, as opposed to the hand-kneading or hand-ramming techniques more generally employed (Clark and Meyerhof, 1972; and Butterfield and Ghosh, 1977).

In developing a suitable procedure, sufficient clay to amply fill a

150.0 mm concrete cube mould, in which the compaction tests were undertaken, was mixed to a moisture content of 20.0%. Determination of the density of the clay proved to be a problem since it was impossible to satisfactorily compact the clay within the mould to a depth of greater than 100.0 mm due to extrusion of the clay around the platten of the Kango hammer during compaction. Thus, a procedure for density determination outlined in Appendix 3.2 was developed and proved by the author.

To investigate the effect of layer thickness on the degree and uniformity of compaction, the clay was placed in two, three and four layers (approximately 50.0, 33.0 and 25.0 mm thick) in consecutive tests. Each layer was compacted using the Kango hammer with a 100.0 x 125.0 mm platten in accordance with the following:

(i) 5 seconds compaction at each platten location. Further penetration of the platten into the clay was minimal after this time.

(ii) A 50.0% overlap of platten area at subsequent locations. This ensured a kneading action during compaction.

(iii) Three complete passes over a given area of clay. Arbitrarily considered as the maximum number economically possible with respect to time as well as the minimum necessary for satisfactory compaction.

(iv) The clay surface was 'roughened' before placing the next layer to ensure good inter-layer bonding.

To ascertain the uniformity of compaction with depth the extruded sample was cut in half along a vertical plane with a 'cheese-wire'. Using the

liquid limit cone penetrometer as a probe, one half of the clay sample was sited beneath the cone with the cut face upper most. The cone was then raised 40.0 mm above the clay surface and allowed to fall freely. The penetration of the cone into the clay was recorded at 12.5 mm intervals along the centre line of the sample, an operation which was repeated at comparable depths on the other half sample. Average penetration verses depth are presented on Figure 3.3, together with the average sample moisture content (ω) and degree of saturation (Sr).

The results suggested a maximum layer thickness of 33.0 mm. This was later reduced to 30.0 mm, being a convenient sub-layer thickness of the 150.0 mm thick primary layers employed in the secondary clay tank during placement of the clay (Section 6.4.1 Refer).

3.3.5 Variation in Undrained Shear Strength with Moisture Content

Samples of clay were prepared as described in Section 3.3.4 over a range of moisture contents. Prior to removing five 38.0 mm diameter cores from each sample, opportunity was taken to calibrate a 'Pocket Penetrometer'. Measurements were taken at nine locations on a grid pattern over the surface of the compacted clay sample. The possibility of the compaction technique forming a hardened crust at the clay surface was discounted by taking a number of random measurements within the body of the sample after extrusion. The penetrometer readings were then related to the undrained shear strength of the sample (Figure 3.4).

Three of the five cores were tested under immediate undrained conditions at different cell pressures up to 1033.5 kPa, in accordance with BS1377

(1975), Test 21. The remaining two specimens from each batch were tested in unconfined compression to BS1377 (1975), Test 20. One of these was first coated in wax and stored for 28 days before testing as a check for thixotropic hardening, of which none was observed (Figure 3.5).

Specimens cut from the clay after extrusion were tested in accordance with Appendix 3.2 to determine bulk and dry density, moisture content and degree of saturation (Figure 3.6).

3.3.6 Consolidation Properties

Four Oedometer tests (two pairs) were performed in accordance with BS1377 (1975), Test 17, on samples removed from the clay profile during placement within the secondary clay tank. Five increments of stress were applied to each specimen, corresponding approximately to one half and the full clay overburden (10.0 and 20.0 kPa), the full overburden of the sand/clay profile (40.0 kPa) and two and four times this value (80.0 and 160.0 kPa). Plots of 'e-log p' for each sample indicated a behaviour typical of an over consolidated clay with a pre-consolidation pressure of about 30.0 kPa (less than the full overburden pressure).

The results indicated a maximum consolidation settlement of 17.3 mm, with 50.0% occurring within 27 days. This was based on the assumption of single drainage since the base and sides of the clay block within the secondary clay tank were enclosed within a continuous impermeable polythene membrane. In reality the drainage path was further restricted by a vinyl membrane applied to the clay surface to limit moisture migration into the overlying dry sand (Section 3.4.1 Refer).

The maximum settlement recorded on the surface of the clay was 4.6 mm over a period of 8 days from instrumenting the sand/clay interface to the start of the test.

3.4 Moisture Retention Membrane

The use of a membrane at the sand/clay interface was considered in order to inhibit the migration of moisture from the clay into the overlying dry sand. A physical barrier was considered acceptable provided it did not affect the mechanical properties of the interface. Brown and Meyerhof (1969) employed a barrier of liquid latex rubber when faced with a similar problem at the interface of two clays of different moisture content.

3.4.1 Moisture Retention Properties of the Trial Membranes

The moisture retention properties of two membranes were investigated, primarily selected for their liquid state of application. These were:

(i) Concrete curing membrane (CM90 Cormix)

(ii) Clear Vinyl Aerosole Spray (Fisons Scientific Apparatus).

The tests were conducted using twelve 38.0 mm diameter triaxial size clay samples prepared to a moisture content of 19.3%. The twelve samples were divided into three groups of four. Two groups were coated with the selected membranes, whilst the third group was left uncoated as a control. Moisture losses at room temperature were recorded over a 17 day

period (Figure 3.7). The concrete curing membrane was rejected at the end of this test due to inferior performance and brittle nature when 'dry'.

3.4.2 The Effects of the Vinyl Membrane on the Shear Behaviour of the Sand/Clay Interface

The effect of the vinyl membrane on the shear behaviour of the sand/clay interface was investigated for the conditions outlined below under normal stresses equivalent to one, five, twenty and fifty times the full sand overburden (one overburden being approximately equal to 20.0 kPa) within the sand tank, using a 60.0 x 60.0 mm shear box.

(i) No vinyl membrane.

(ii) The vinyl membrane was applied to the clay surface in two coats. The first was allowed to partially dry before applying the second. The specimen was then cured for 24 hrs.

(iii) As (ii), but before the second coat of vinyl was dry sand was sprinkled over the surface and moderate pressure applied to partially embed the sand grains into the clay. Excess sand was removed and a third light coating of vinyl applied prior to curing the specimen for 24 hrs.

For this investigation a block of clay was prepared to a moisture content of 19.1% in the 150.0 mm concrete cube mould in accordance with Section 3.3.4, from which twelve specimens were prepared to suit the 60.0 mm square shear box.

Each specimen was subjected to the relevant normal stress for 1 hr in the shear box in an attempt to minimise consolidation settlement during the test. The shear box was then dismantled and the clay specimen cut leaving a surface flush with the top of the lower half of the shear box. The membrane was then applied (if required) and the specimen removed for curing. Once the membrane was cured the specimen was replaced in the assembled shear box. Sand was then poured over the clay, filling the shear box, and the composite specimen sheared at 1.22 mm/min under the appropriate normal stress.

The results of these tests are presented on Figure 3.8. The shear stress has been normalized with respect to the applied normal stress. The test results show that the vinyl membrane in either form has very little influence on the shear properties of the interface. In the light of these findings it was decided to use the membrane in the form described in (iii), since it was felt that this was a slightly better model of field conditions due to the embedded sand grains.

Appendix 3.1

Derivation of the Triaxial Cell Pressure used in Establishing the $\phi - \rho_d$ Relationship for Leighton Buzzard Sand

Assuming relevant soil parameters for loose sand:

ρ_d = 1500.0 kg/m^3 (From Pilot Investigation)

γ = 14.7 kN/m^3

D_r = 0.18

According to Meyerhof (1956):

$\phi' = (28 + 15D_r)$ Degrees

Therefore:

$\phi' = 30.7^0$

Quoting from his Doctoral Thesis, Meyerhof (1951) suggested that the average normal stress on the shear planes below a deep foundation was about 20.0% of the ultimate base resistance (q_{bf})

$$q_{bf} = N_q^* \gamma D_b$$

In the case of driven piles, according to Meyerhof (1963), $N_q^* = 60$ for $\phi' = 30.7^0$. D_b = 1.845 m.

Therefore:

$$q_{bf} = 1627.3 \text{ kPa.}$$

The average normal stress on a shear plane at failure is therefore:

$$\sigma_n = 326.5 \text{ kPa}$$

It can be shown, from Mohr failure criteria, that for $\phi' = 30.7^0$ a cell pressure (σ'_3) of 216.1 kPa is required in order to obtain a normal stress of 326.5 kPa on the failure planes within the triaxial sample.

Triaxial tests were, therefore, conducted at approximately half this cell pressure, which provided a compromise between the relatively high stress levels anticipated below the pile base and the comparatively low stress levels adjacent to the pile shaft.

Hence:

$$\sigma'_3 = 110.0 \text{ kPa (Approximately 16.0 psi)}$$

Appendix 3.2

A Method of Estimating the Density of a Small Sample of Clay by Water Immersion

This procedure is a variation on the Water Immersion Method specified in BS1377 (1975), Test 15(E), in which the volume of a wax coated specimen is determined by placing it on a wire cradle suspended from the pan of a weighing balance, and immersing the specimen in water. In the author's method a small uncoated clay specimen was impaled on a fine needle suspended by a thread from a vertically adjustable support. The specimen was lowered, until fully immersed, into a beaker of de-aired water placed on the pan of a weighing balance. The increase in weight was equated directly to the specimen volume. A period of immersion of less than 2 seconds was required to attain a steady reading on the balance, for this reason wax coating was considered unnecessary.

In order to justify the above method a comparative test was conducted on a block of clay of known 'bulk' density. Precise details and results are given below.

A Proctor Compaction mould full of clay was prepared and the bulk density of the clay established as 2193.0 kg/m^3 in accordance with BS1377 (1975), Test 12.

The clay cylinder was extruded and cut lengthways into quadrants designated in a clockwise direction as a, b, c and d. Specimens prepared from diametrically opposite segments, a and c, were tested by direct immersion, while those from b and d were tested with a wax coating.

In preparing the individual specimens, each quadrant was subdivided into three portions. The top and bottom portions were discarded since they could have contained compaction irregularities due to boundary effects. The middle third was then further divided into three equal portions. From each of these a 25.0 mm square prism of clay, approximately 12.5 mm thick, was cut such that one corner of the clay prism was formed by the apex of the quadrant.

Each sample was weighed in air and, if appropriate, coated in wax and re-weighed prior to immersion. The increase in weight recorded on the balance was equated to the volume of the sample with no adjustment for the water temperature in accordance with BS1377 (1975), Test 15(E). This would introduce an error in volume measurement of -0.17%, assuming a water temperature of 20.0^{0}C.

The wax coated specimens gave densities ranging between 2149.7 and 2171.9 kg/m^{3} with a mean 2159.4 kg/m^{3}, an error of -1.16% (G_s of wax = 0.915). The uncoated specimens recorded densitites ranging between 2195.9 and 2202.2 kg/m^{3} with a mean of 2199.1 kg/m^{3}, corresponding to a +0.28% error. The small error in determining the density of the uncoated specimens could be due, in part, to the under-estimation of volume, since water temperature was not taken into account, and the slightly greater compactive effort applied to the central portion of the clay sample remote from boundary effects. Errors in calculating the density of the wax coated specimens were probably due to the inclusion of small air voids traped under the wax coating.

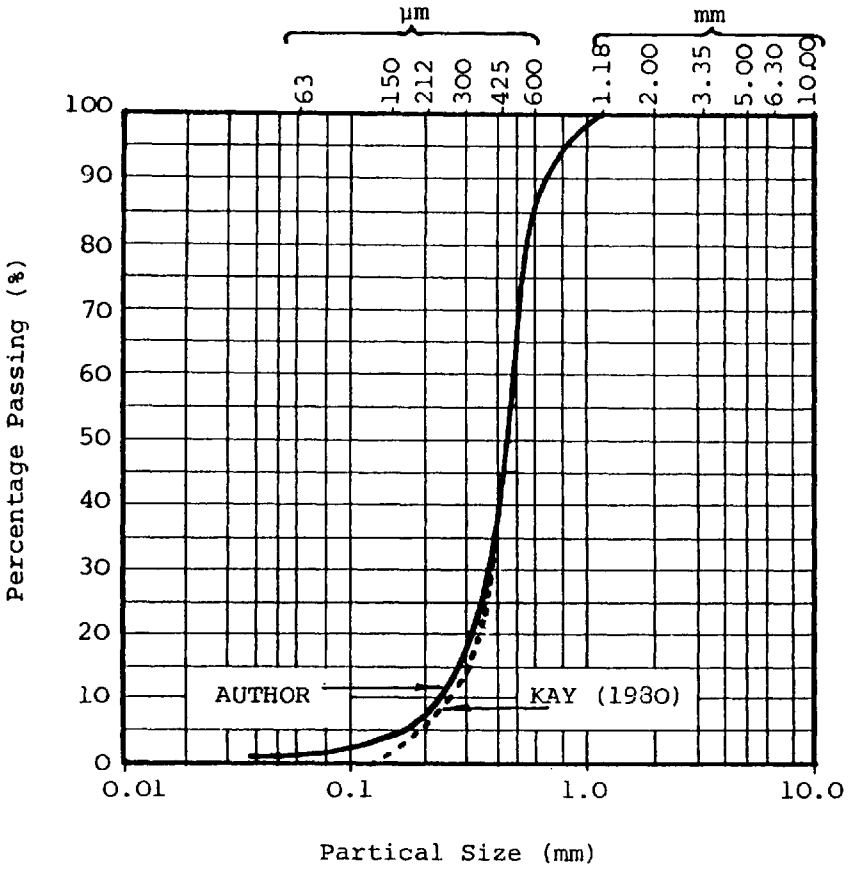

PARTICAL SIZE DISTRIBUTION FOR LEIGHTON BUZZARD SAND

FIGURE 3.1

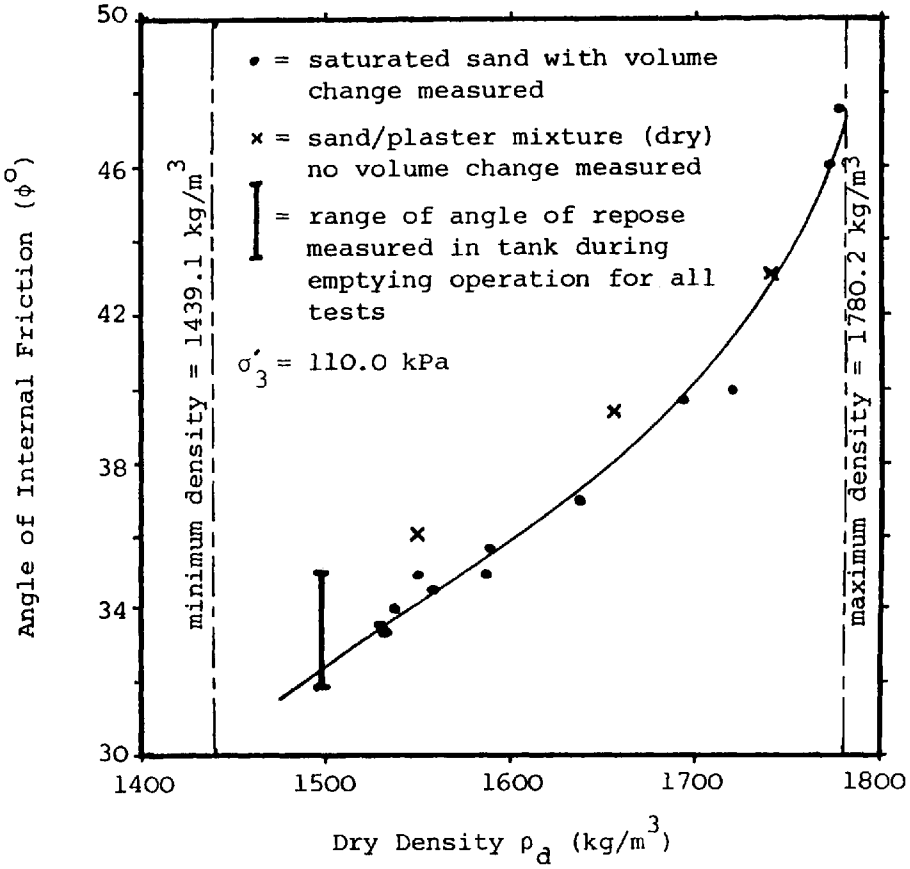

ANGLE OF INTERNAL FRICTION-DRY DENSITY RELATIONSHIP FOR LEIGHTON BUZZARD SAND FROM 102.0 MM DIAMETER DRAINED TRIAXIAL TESTS

FIGURE 3.2

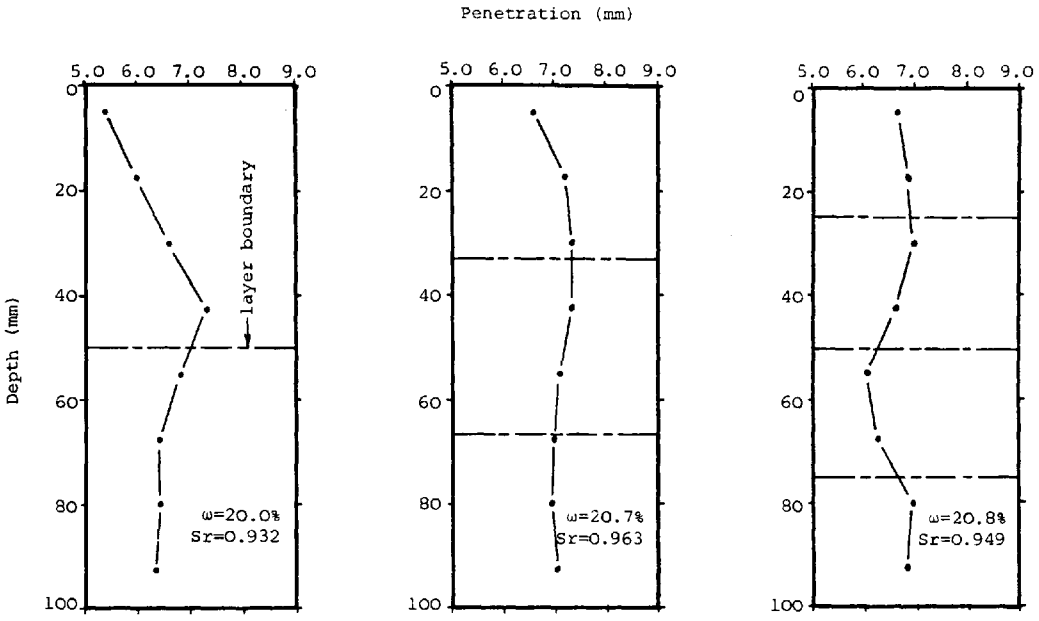

AVERAGE CONE PENETRATION INTO CLAY, COMPACTED WITH VARIOUS LAYER THICKNESS, VERSES DEPTH

FIGURE 3.3

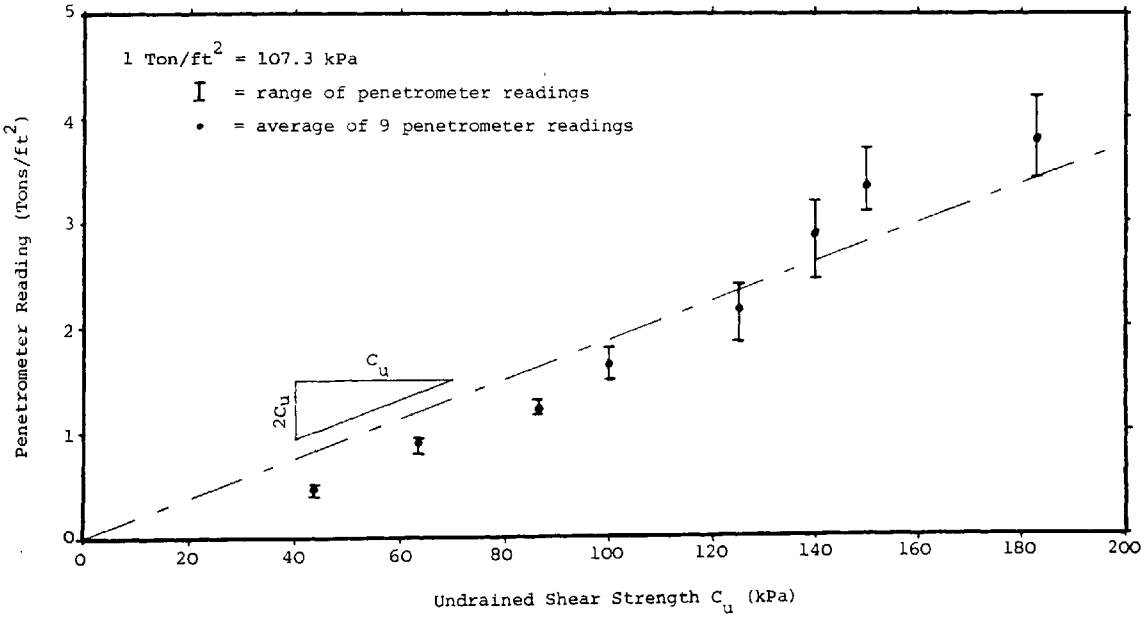

CORRELATION BETWEEN POCKET PENETROMETER READINGS AND UNDRAINED SHEAR STRENGTH OF CLAY

FIGURE 3.4

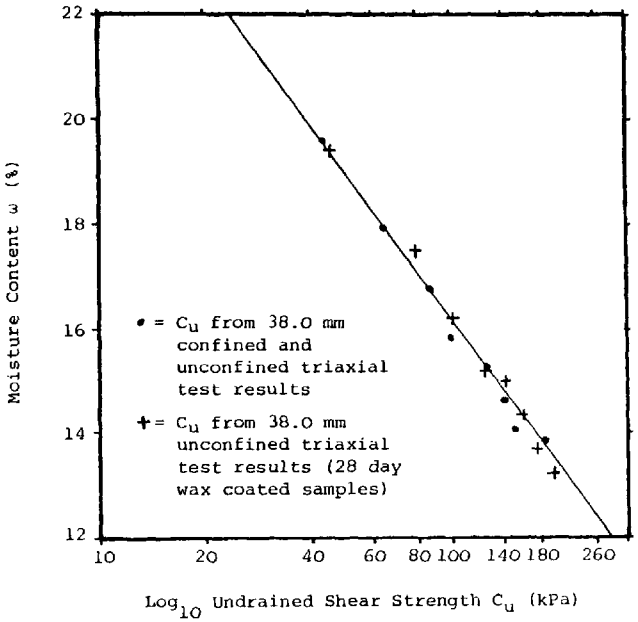

VARIATION IN UNDRAINED SHEAR STRENGTH OF CLAY WITH MOISTURE CONTENT

FIGURE 3.5

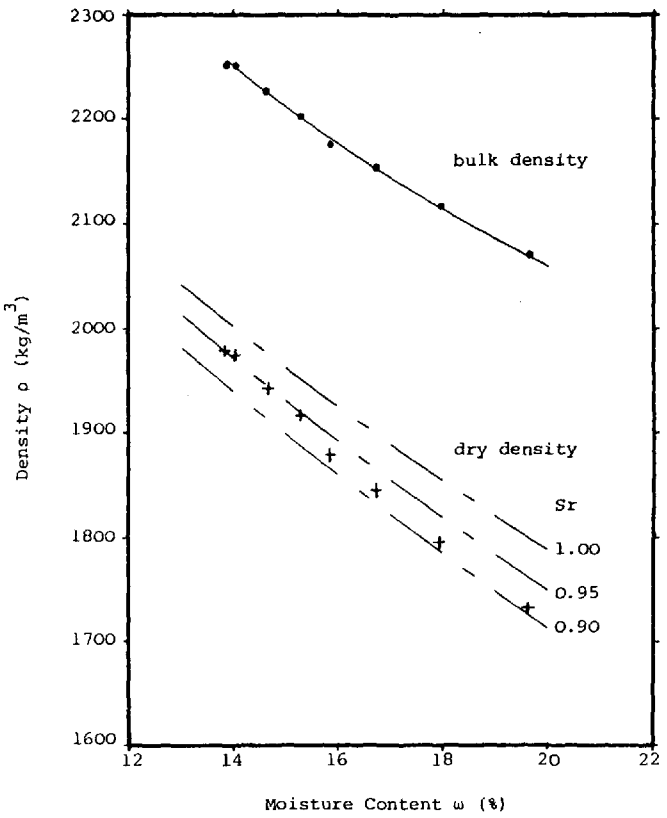

VARIATION IN BULK AND DRY DENSITY OF CLAY WITH MOISTURE CONTENT

FIGURE 3.6

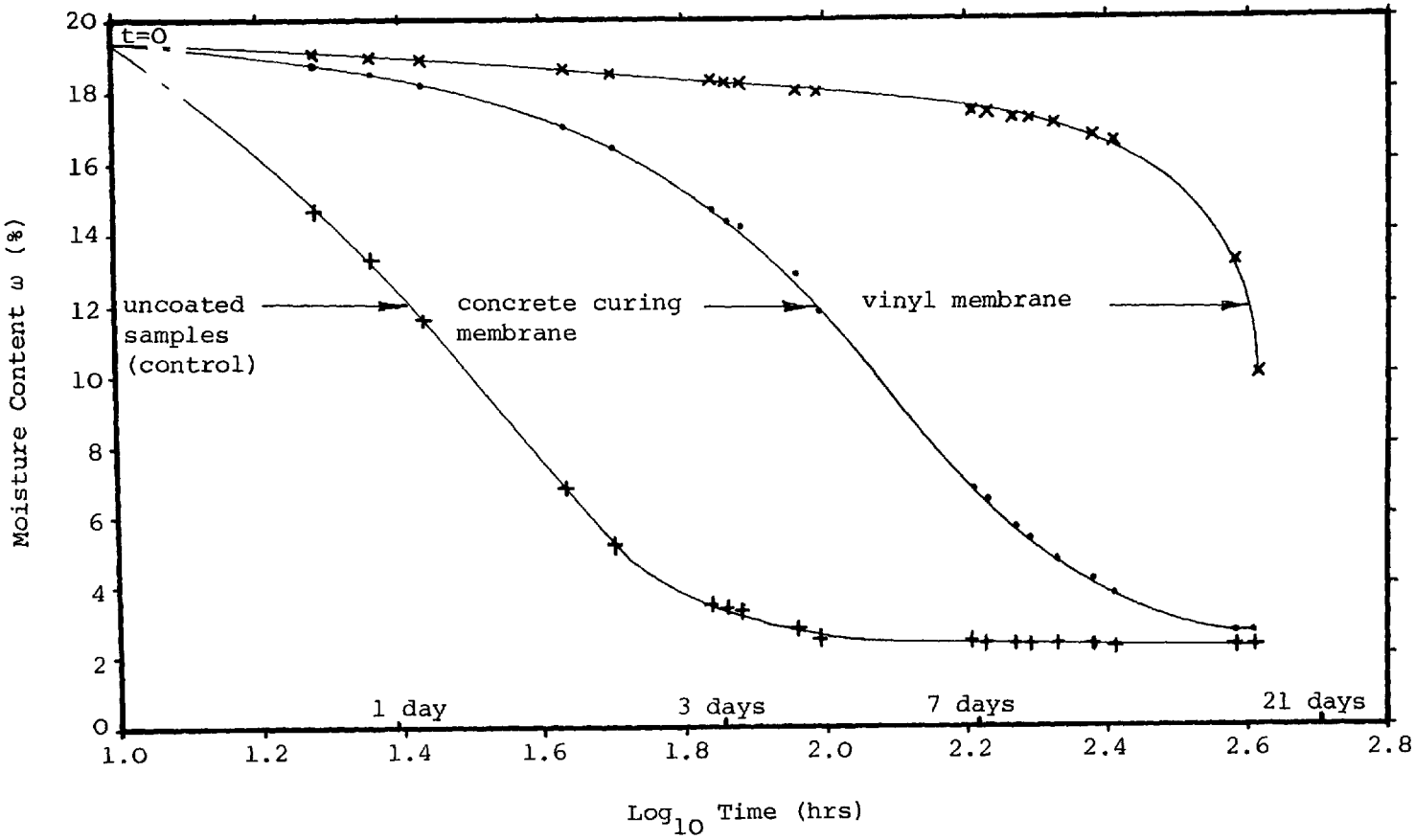

MOISTURE RETENTION PROPERTIES OF THE TRIAL MEMBRANES

FIGURE 3.7

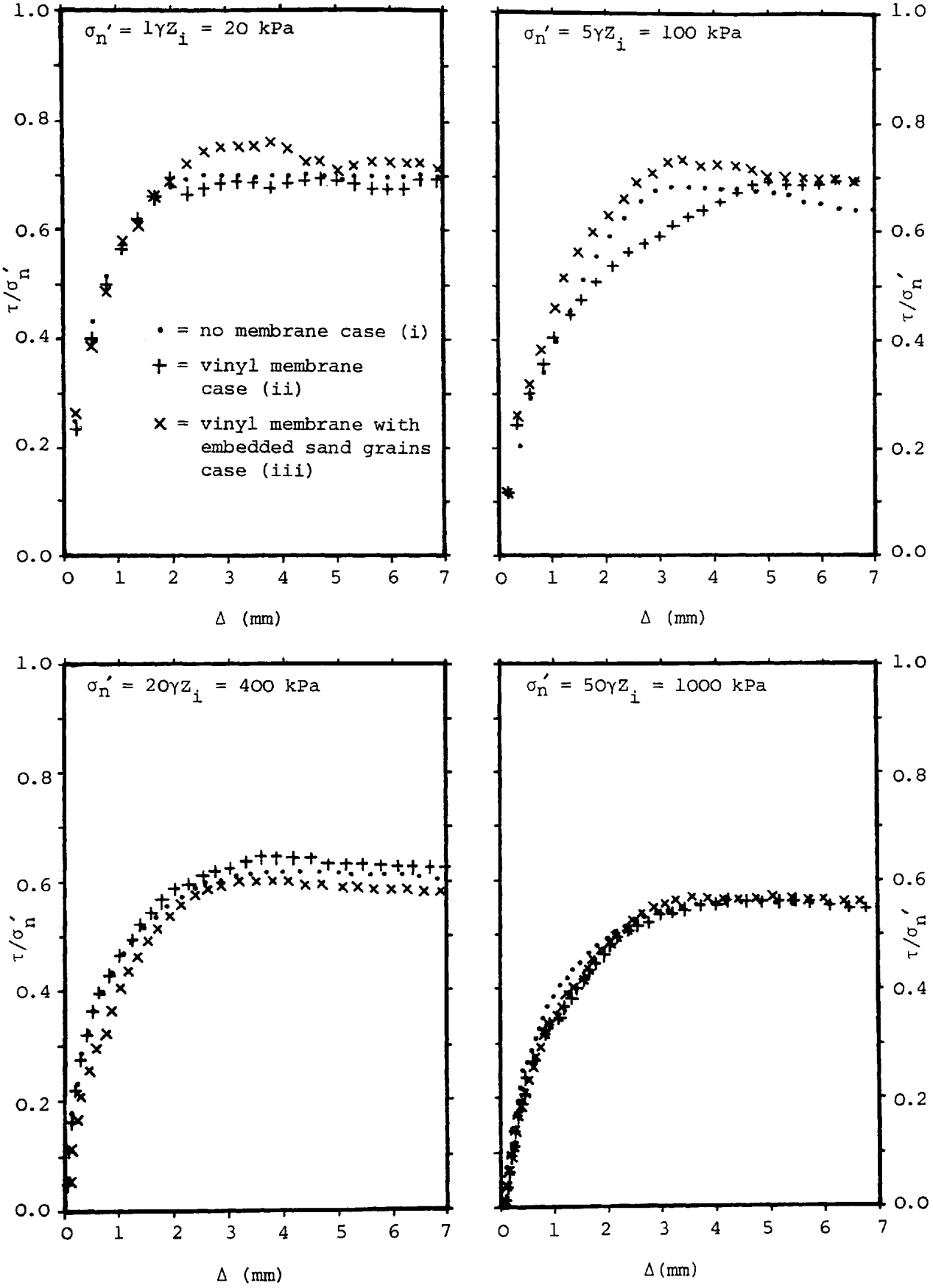

THE INFLUENCE OF THE VINYL MEMBRANE ON THE DEVELOPMENT OF SHEAR STRESS (τ) AT THE SAND/CLAY INTERFACE, NORMALISED WITH RESPECT TO THE APPLIED NORMAL STRESS (σ_n'), WITH RELATIVE DISPLACEMENT (Δ)

FIGURE 3.8

CHAPTER 4

TESTING FACILITIES, CONTROL AND MONITORING SYSTEM

CHAPTER 4

TESTING FACILITIES, CONTROL AND MONITORING SYSTEM

4.1 Introduction

The pile testing facilities available at the Polytechnic of Wales are described in detail by Kay (1980). It is, therefore, proposed to merely outline these in this chapter and to concentrate on the additions and modifications made to the system by the author.

4.2 Testing Facilities

4.2.1 Sand Tanks and Redler Conveyor System

A major feature in the Geotechnics Laboratory is the handed pair of bottom emptying sand tanks, 3.0 m in diameter by 3.0 m deep. These are separated by a Redler Conveyor which is used to transfer the sand between them (Figures 4.1 and 4.2). One tank is set-up for pile testing whilst the other serves as a sand reservoir. During the transfer operation, the Redler Conveyor lifts sand from the reservoir to a small enclosed hopper 2.5 m above laboratory floor level. From the hopper the sand flows under gravity via a segmental flexible hose, controlled by the operator, into the testing tank.

A problem encountered when conducting pile tests in a soil profile

enclosed by unrealistic boundary conditions, such as a rigid tank, is the influence of the tank on the test results. A review of the pile/tank geometries employed by other experimental investigators, and salient points from field and theoretical studies, was undertaken through a literature search. The author's study, conducted with a 114.0 mm diameter pile jacked to a depth of 1.845 m into a 2.500 m deep soil profile, has a tank/pile diameter ratio (B_t/B) of 26.0 with a pile base to tank base clearance of 5.7B. These clearances appeared to be adequate in view of the following observations.

Plantena and Nolet (1957) made soundings in the field around driven piles in sand using a Dutch Cone Penetrometer. From their results it was shown that a zone of disturbed sand extended to a distance of 4.5B below the pile base.

Meyerhof (1959) determined the theoretical limits of compaction in loose sand due to pile driving as 6.0B in overall width. This increased to between 7.0 and 8.0B a short distance below the base, and extending to about 5.0B below the pile base.

Kerisel (1964), working with loose sand, employed a minimum B_t/B of 40.0 with at least 10.0B between the pile base and tank base.

Robinsky and Morrison (1964), using radiographic techniques, observed a zone of 'visible' soil movement which extended to between 7.0 and 9.0B in overall width and to between 2.5 and 3.5B below the pile base. These limits increased to between 10.0 to 12.0B and 3.0 to 4.5B respectively for piles in medium dense sand.

Williams (1979), working with dense sand, found that as long as the final separation between the pile base and tank base exceeded 3.0B, then the jacking load applied to the pile was independent of the proximity of the tank base.

4.2.2 Secondary Clay Tank

The impracticality of placing 9.0 m^3 of clay to a depth of 1.250 m in the sand tank resulted in the author using a smaller, representatively sized clay sample accommodated in a secondary tank within the main sand tank.

The secondary tank was fabricated from Brathwaite panels. To further economise on the quantity of clay required the vertical corners of the tank were blocked off with wooden formers to produce a cylindrical clay sample 1.100 m in diameter by 1.130 m deep. In relation to the pile size the secondary clay tank provided a B_t/B of 9.6 and a pile base to tank base clearance of 5.0B, proportions which compared favourably with other case studies reported in literature. Even so, the influence of indeterminate boundary effects on the results should not be forgotten.

Clarke and Meyerhof (1972) drove a 76.0 mm diameter by 762.0 mm long pile, 508.0 mm into clay placed in a steel drum, 559.0 mm in diameter by 762.0 mm deep. Measurements were taken of soil stresses and displacements, as well as pore water pressures. This geometry gave a B_t/B of 7.3 and a base clearance of 3.3B.

Cooke and Price (1973(b)) jacked a 168.0 mm diameter instrumented pile into London Clay and monitored the variation in lateral displacement

within the soil with radius from the pile axis. They suggest that, from extrapolation of the results, some radial movement could be expected to a diameter of at least 9.0B in the soil above the pile base.

Holinquist and Matlock (1976) undertook a theoretical analysis of axially loaded piles in soft clay. They referred to the work of Seed and Reese (1955) in which it was found that excess pore water pressures due to pile driving extended to a diameter of about 11.0B. In view of this, Holinquist and Matlock assumed that shear strains caused by axial loading of the pile extended to the same distance, setting an outer limit for the vertical displacement of the soil.

Cooke et al (1979), working with a 168.0 mm diameter pile jacked into London Clay, monitored vertical displacements at depth to a diameter of 6.0 m (35.7B) during pile penetration and subsequent loading. Vertical displacement of the soil was observed to a diameter of 2.0 m (11.9B) at a depth of 0.5 m for a pile penetration of 1.0 m. This increased to greater than 3.0 m for penetrations in excess of 2.5 m, although displacements reduced rapidly with increased distance from the pile shaft.

Randolph et al (1979) investigated soil displacements around an 18.0 mm diameter pile pushed into clay using a diametrically sectioned model ($B_t/B = 15.6$). They found that radial soil displacements were minimal at depth beyond a zone 5.0B in diameter, and were smaller still within a region which extended to 6.0B below the clay surface. Further, from the displacement plots and displacement fields presented in their paper, it appeared that soil displacements beyond 3.0B below the pile base were minimal.

4.2.3 Hydraulic Jack and Reaction System

A 150.0 mm stroke, Dartec servo-hydraulic jack with integral 50.0 kN load cell was used to push the pile into the soil profile and conduct the load tests. The jack was mounted on a cross-head which could be raised and lowered over a 310.0 mm range on two threaded tie bars connected to the reaction frame. The reaction frame consisted of two RSJs fixed down to, and spanning, the sand tank on either side of the jack (Figure 4.2).

4.2.4 Pile Guide

As the pile was pushed into the soil profile from the surface, a means of 'frictionless' guidance was required to maintain the verticality of the pile throughout installation. In addition, a method of clamping the pile was required at the end of each jacking increment before any adjustments to the pile loading and displacement monitoring system were made and a new pile section added as necessary. The pile guide, designed by the author, provided restraint by a three-point contact around the pile circumference with 60.0 mm diameter roller bearings at two levels, 310.0 mm apart. A simple three-bolt arrangement incorporated in the pile guide served as an effective clamp.

The pile guide, attached to the underside of the reaction frame, was set-up to less than 1/500 of the vertical and in line with the jack axis using a 1.0 m section of 114.0 mm diameter pipe. To allow for any irregularities in the pile section a clearance of 0.38 mm (0.015") was provided by introducing sections of shim between the roller bearings and pipe section during alinement. A clearance of this magnitude allowed the

pile to deviate by an additional 1/270 from the vertical. The maximum possible non-verticality, assuming rigid conditions, was 1/175 which compared favourably with that permitted by CP2004 (1972) of 1/75.

4.2.5 Datum Frame

All soil and pile displacements were related to a 'rigid' datum frame. This was fixed below, and independent of, the reaction frame and consisted of a peripheral network of Dexion framing connected to two box sections which span the tank in line with the reaction frame RSJs.

4.3 Control and Monitoring System

The use of a micro computer interfaced with the jack control unit and data logger allowed the author to develop a comprehensive software package which 'managed' the entire test programme.

4.3.1 Orion 'A' Data Logger

An Orion 'A' data logger, controlled from a Commodore 4032 PET computer, monitored the 100 channels of instrumentation scanning them once per minute. All D.C. channels were scanned at a rate of 40 per second to an accuracy of 1.0 μV. This was the maximum rate at which 'background noise' due to an electrically aggressive environment could be filtered from the readings. The A.C. channels, connected to the electrolytic

levels, were scanned at a fixed rate of 5 per second to an accuracy of 1.0 μVrms.

4.3.2 Transducer Energization Power Supplies

It was not possible to use the internal 2.0 V D.C. supply of the data logger to energize the transducers as this would have restricted the number of monitoring channels. To maximise the performance of the various transducers, three different power supplies were required. Each supply was monitored for stability over a 10 day period, the results of which are presented on Table 4.1.

4.3.3 Jack Displacement Control Unit

The jack displacement control unit consisted of two items of equipment:

(i) A basic Dartec Jack Control Unit (JCU), which governed the jack displacement limits when functioning in displacement control mode, and the magnitude of any prescribed load when operating under load control.

(ii) A Wave-form Generator (WG), which supplied a ramp function of predetermined frequency to the JCU. The jack moved in phase with the ramp function when operating in displacement mode.

At this stage the author was faced with two independent and unsynchronised systems; the data acquisition and processing units (data logger and computer), and the pile loading system (JCU and WG). In an

effort to achieve a fully integrated system a successful attempt was made to interface the WG with the computer. This allowed the computer to have complete control over pile penetration, syncronising data acquisition with the start and finish of each penetration increment.

4.3.4 Commodore 4032 PET Computer and 'Management' Program

The full potential of the integrated system described above was only realised by the 'Management' program written by the author, for which a simplified flow chart is presented on Figures 4.3(a), (b) and (c). Included in the program were two small routines written in 'Basic' and 'Machine Code' by 'Solartron' (the data logger manufacturers). These allowed the transfer of data and instructions between the computer and data logger, since the two systems were not readily compatible.

Some of the main features of the 'Management' program are itemised below

(i) Interactive with the operator. Task selected from a prescribed menu.

(ii) Immediately before commencing a test sequence all data channels were scanned 10 times (once per minute). The results were averaged to give an initial 'zero' reading for each channel.

(iii) The length of each pile section was such that for each penetration increment of 100.0 mm, an adequate working clearance was always maintained between the pile butt/pile guide and the pile cap/jack load cell. It was, therefore, important to limit each penetration increment to

approximately 100.0 mm. This was achieved by monitoring the pile penetration with displacement transducers and automatically instructing the jack to 'reset' once a predetermined displacement limit was exceeded. As the instrumentation was scanned at minute intervals, the maximum by which any prescribed displacement limit could be exceeded was 10.0 mm (Section 6.5.1 Refer). An allowance was made for any excess embedment when calculating the next penetration increment.

(iv) Whilst the jack was operating in reset mode at the conclusion of each penetration increment, three further data scans were made of the instrumentation to monitor recovery in the pile/soil system.

(v) Allowance was made for the increase in pile self-weight as additional pile sections were added throughout pile installation.

(vi) Raw (unprocessed) data from every data scan was stored on a sequence of floppy disks.

(vii) All data, other than that from the electrolytic levels, was processed and a hard copy output between consecutive data scans. Soil displacements were calculated from the data disks at the conclusion of each test.

A modified version of the 'Management' program was produced to act as a back-up in the event of a systems failure. It differed only in that the initialization routine read the initial 'zero' values for each channel from a previous data disk of that test. The test could then be resumed once the fault had been rectified.

A schematic diagram of the layout of the data monitoring and load control system is shown on Figure 4.4.

TRANSDUCER	1.5 mm ORTHOGONAL STRESS TRANSDUCERS	ELECTROLYTIC LEVELS	ALL OTHER INSTRUMENTATION
SUPPLY	D.C.	A.C.	D.C.
NOMINAL VOLTAGE	11.000	5.000	3.000
MEAN VOLTAGE	11.014	4.957	2.999
STANDARD DEVIATION	0.013	0.037	0.006

STABILITY OF TRANSDUCER ENERGIZATION POWER SUPPLIES OVER A 10 DAY PERIOD

TABLE 4.1

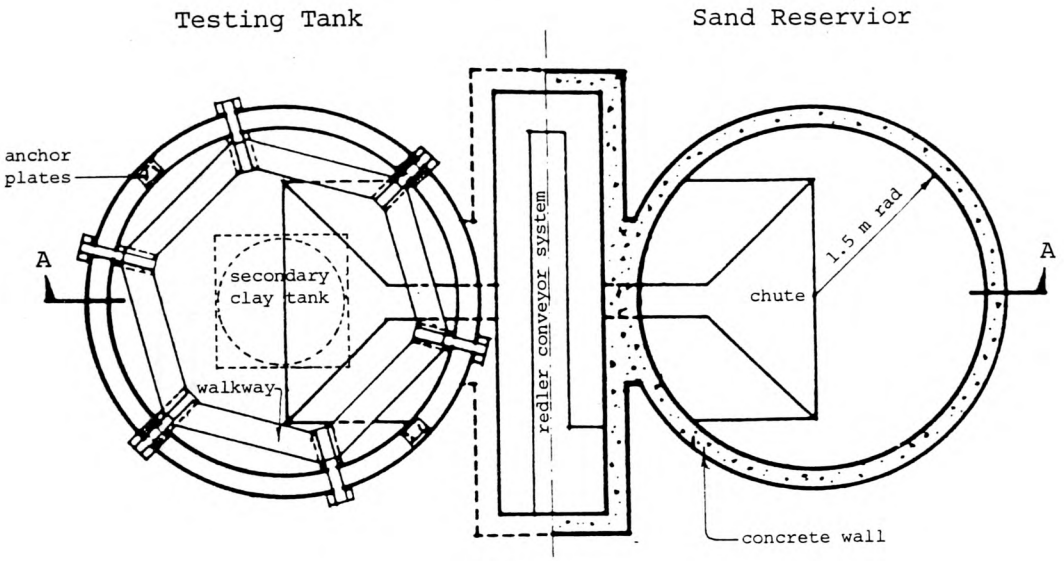

Half Plan

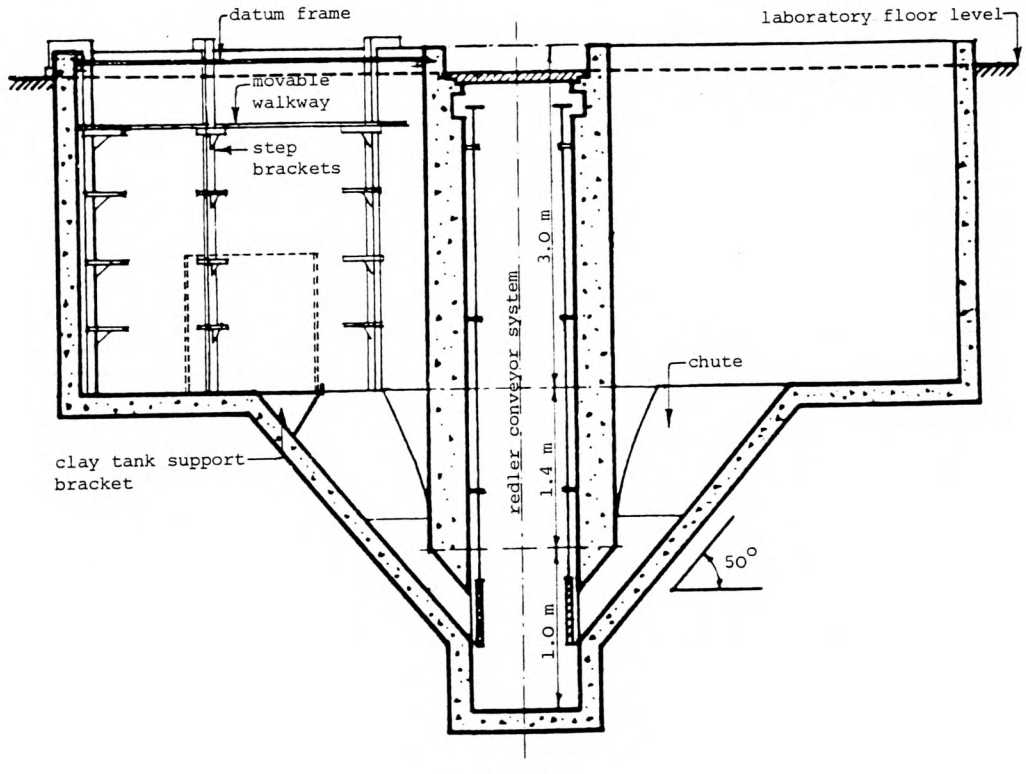

Section

SAND TANK AND REDLER CONVEYOR SYSTEM

FIGURE 4.1

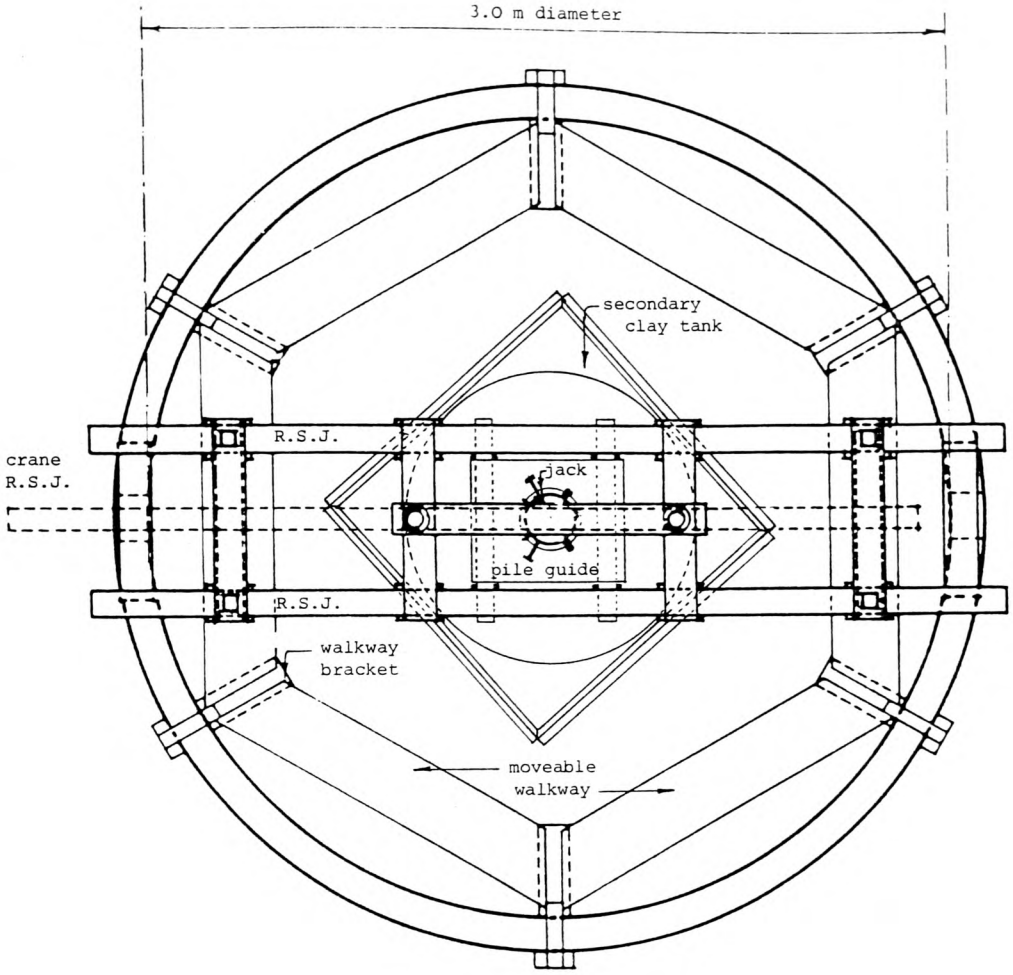

Plan

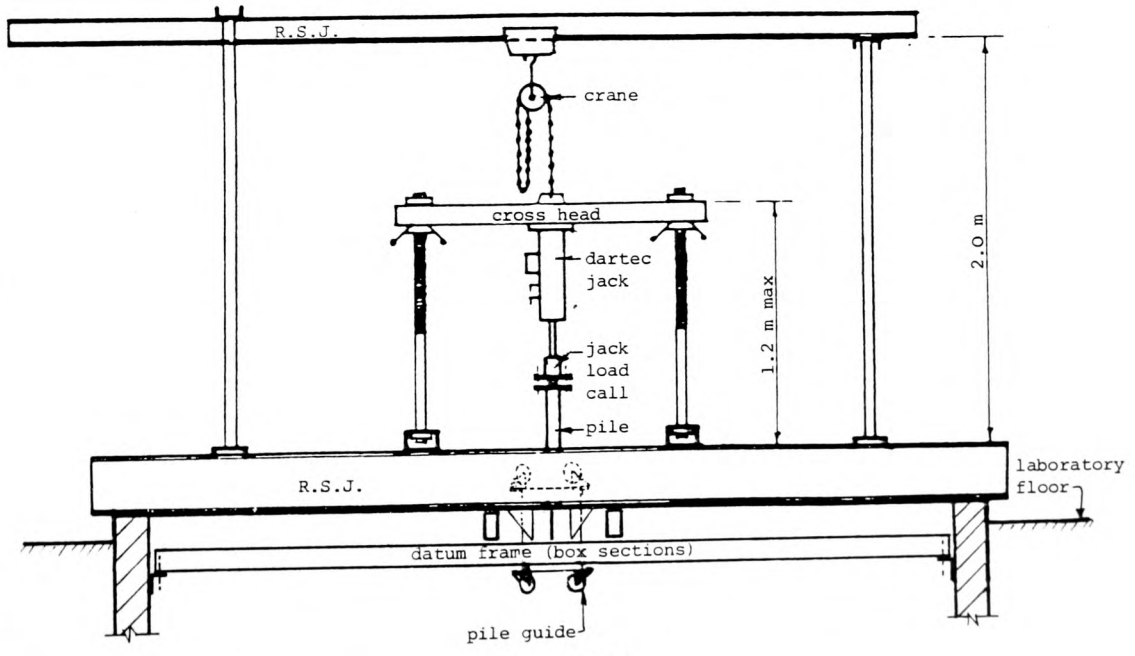

Elevation

LOADING FRAME, PILE GUIDE AND GANTRY CRANE

FIGURE 4.2

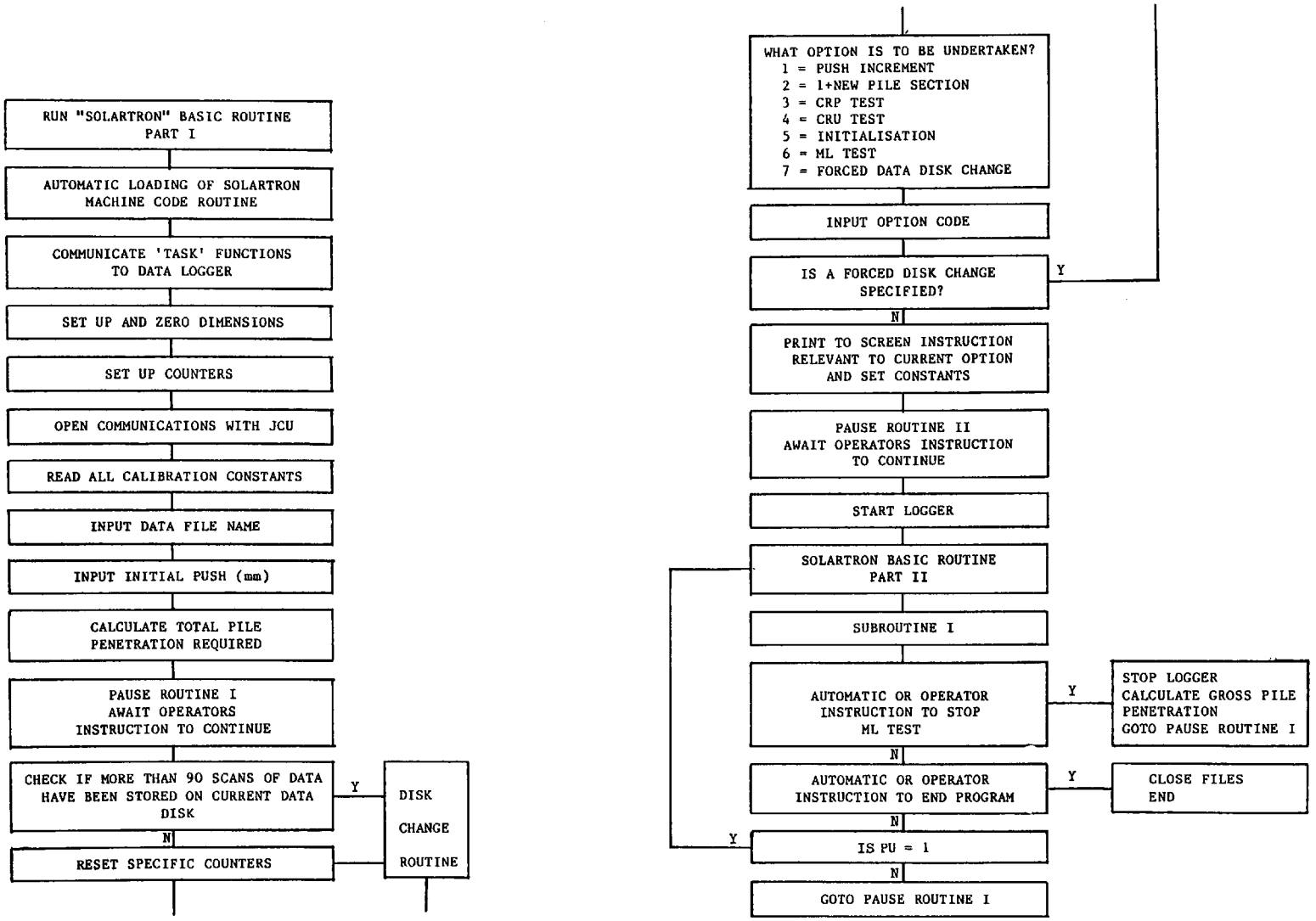

SIMPLIFIED FLOW CHART OF MANAGEMENT PROGRAM

FIGURE 4.3(a)

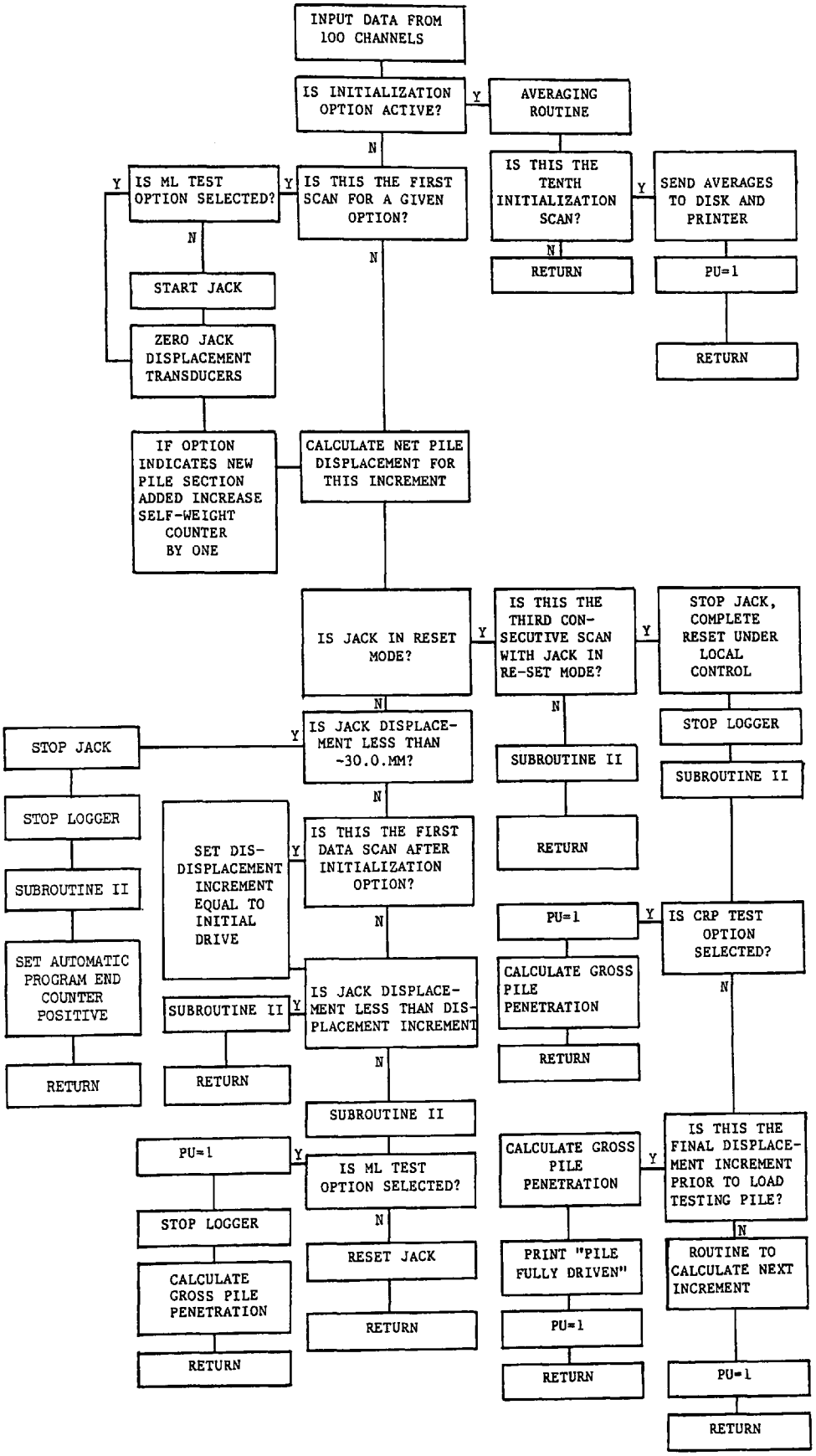

MANAGEMENT PROGRAM - SUBROUTINE I

FIGURE 4.3(b)

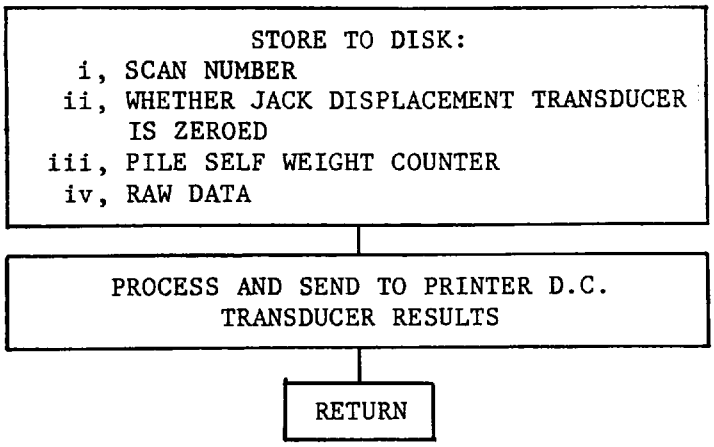

MANAGEMENT PROGRAM - SUBROUTINE II
FIGURE 4.3(c)

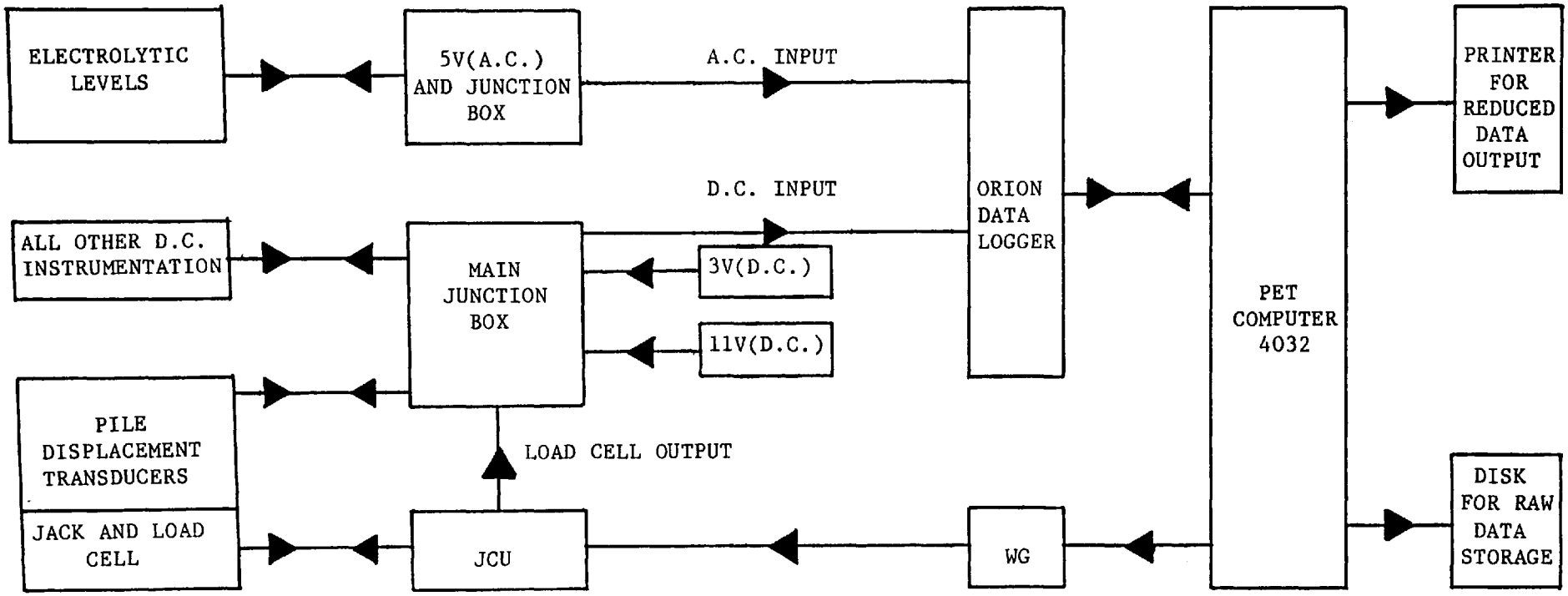

SCHEMATIC DIAGRAM SHOWING LAYOUT OF DATA RECORDING AND JACK CONTROL SYSTEM

FIGURE 4.4

CHAPTER 5

PILE AND SOIL INSTRUMENTATION

CHAPTER 5

PILE AND SOIL INSTRUMENTATION

5.1 Introduction

Instrumentation was installed in the pile and the soil in order to monitor their interaction.

The 114.0 mm diameter segmental tubular steel pile contained four 'core' type axial load cells (ALCs). The ALCs were complemented by nine pairs of boundary orthogonal stress transducers (BOSTs) which were installed in the pile wall, spaced more or less evenly along the embedded length of the pile shaft. The BOSTs in each pair were sited diametrically opposite each other.

Instrumentation installed within the sand and on the sand/clay interface monitored changes in sand density, vertical displacements and vertical effective stresses. Shear stresses were monitored on the sand/clay interface.

5.2 Pile Design and Instrumentation

A general arrangement of the pile developed by the author is presented on Figure 5.1(a). This shows the location of the pile instrumentation relative to the proposed layered soil profile.

The ALCs (Figure 5.2) were designed by and manufactured for Kay (1980). However, only one was strain gauged with a pair of quarter bridge circuits for use in his pile. It was, therefore, decided that the ALCs, modified to accommodate the BOSTs, were to form part of the instrumentation of the author's pile, thereby fixing the pile diameter. The most sensitive of the ALCs (ALC(a)) was used to monitor the load at the pile base by attaching a flat pile shoe to the bottom coupling. The surface of the underside of the shoe was considered to be rough due to the pattern of grooves left by the manufacturing process. This was justified since Meyerhof (1951) stated that in practice a base may always be considered rough for calculation purposes. The remaining ALCs were located such that when the pile was fully embedded within the layered soil profile they recorded the axial load in the pile at the level of the sand/clay interface (ALC(b)) and at middle third points within the overlying sand (ALC(c) and (d)). The incorporation of ALCs allowed a check to be made on the distribution and magnitude of shaft friction as suggested by Mansur and Kaufman (1956) and others.

Careful consideration was given to the number and distribution of BOSTs to be included in the pile in order to obtain, with a reasonable degree of accuracy, the profiles of radial stress (σ_r) and local unit shaft friction (f_z) acting on the pile shaft. This was, however, ultimately dictated by the number and length of the pipe segments which formed the pile.

The inclusion of independent boundary stress transducers presented a problem. The magnitude of the clearance between the active face of the transducer and the surrounding pile wall is critical in order to prevent the ingress and lodgement of sand particles which may affect performance.

There appeared to be two possible solutions to this problem:

(i) The clearance can be made small enough to prevent the entry of sand particles, and yet sufficiently large to allow the active face to displace under an applied shear stress. Such an approach was investigated by Arthur and Roscoe (1961). They showed that no 'wedging' or 'bridging' of sand grains occurred providing the clearance (c) was small in relation to the effective diameter (D_{10}) of the sand grains. In their investigation the ratio D_{10}/c was equal to 7.670, indicating a maximum allowable clearance of 0.030 mm for the Leighton Buzzard Sand used in this study. Such an approach also appears to have been employed by Butterfield and Johnston (1973) when investigating the stresses acting on a continuously penetrating pile in London Clay.

(ii) The clearance can be made larger and filled with a suitably flexible material. The influence of the filler on the transducers performance can then be taken into account during calibration. This technique was employed by Agarwal and Venkatesan (1965) and Williams (1979).

The author decided to use method (ii) since it offered other advantages. The most important of these being each panel, nominally 30.0 mm square, cut from the pile wall by a 'spark erosion' technique to form the transducer 'window', could be attached to the active element of the transducer resulting in an active face which maintained continuity of surface profile and texture along the pile shaft. Further, machining tolerances were increased which allowed faster production and assembly of the units.

A silicon rubber compound was considered as a suitable filler and was injected to a controlled depth (Section 5.4.5.1 Refer) into the 2.0 mm (nominal) clearance around the active face produced by the cutting electrode. An investigation had previously been undertaken to establish the load/deflection characteristics of the silicon rubber by attempting to simulate the behaviour of the transducer within the pile. The tests proved inconclusive since the equipment did not fully model the in-situ behaviour of the transducer. Despite this the data gathered was sufficiently encouraging to allow the pile construction programme to continue, leaving a final assessment of the influence of the silicon rubber to be established through in-situ calibration of the transducer (Section 5.4.5.3 Refer).

The method of connecting adjacent pile sections was dictated by the existing 'single' male couplings on the ALCs. Following Kay's (1980) example, the female half of the coupling was clamped to the male section by four 8.0 mm grub screws evenly spaced around the pile circumference. However, when tested to the maximum anticipated tensile load, this arrangement proved to be inadequate due to local yielding of the pile material around the grub screws. The number of screws used was, therefore, increased to eight. The results of a load test undertaken on a modified 'double' male coupling of the type used to connect the 'blank' pile sections employed above ground level, is presented on Figure 5.3. Displacements were recorded at three locations around the pile circumference, between two points 100.0 mm apart sited on opposite sides of the coupling. The theoretical elastic extension of a continuous 100.0 mm length of pile is also indicated together with the maximum tensile (negative) and compressive loads recorded during the course of the pile test programme. From this it can be seen that the coupling

design functioned reasonably satisfactory within the load range applied to the pile during the test programme.

In view of the segmental nature of the pile, which resulted in alternate male and female couplings being 'offered' to the jack as additional pile sections were attached to the pile during installation, two types of pile cap were required (Figure 5.1(b)). Both caps had similar features to allow free passage of the pile instrumentation wiring from the inside of the pile. This was achieved by means of a pair of diametrically opposite slots machined into the pile caps. A pair of diametrically opposite 'rigid' arms were attached to the top of each cap from which pile butt displacements were measured using two 125.0 mm linear variable displacement transducers (LVDTs).

5.3 'Core' Type Axial Load Cells

The ALCs consisted of a section of 114.0 mm diameter steel pipe (of the same specification as that from which the pile was fabricated) which surrounded a central hollow core, with a 'single' male coupling at either end. The bottom coupling and core were machined from a single billet of steel. The pipe section fitted over the core and rested on a rubber 'O'-ring on the bottom coupling. The top coupling was threaded on to the central core and was connected to the top of the sleeve. Since the outer sleeve was not fixed to the lower coupling, any load transmitted through the cell was carried via the central core. Different cell sensitivities were achieved by increasing the diameter of the central bore, thereby reducing the wall thickness of the core.

5.3.1 Instrumentation

All ALCs were instrumented with an eight gauge full-bridge circuit. The bridge circuits were applied to the cores in such a way as to eliminate the effects of bending due to non-axial loading and to take full advantage of the Poisson effect. Gauge bonding was undertaken by the author in accordance with Bulletin B-130-6 (Hot-Tack method) issued by Micro-Measurement, using a temperature cured adhesive (M-Bond 610).

5.3.2 Calibration Procedure

Initially an in-situ calibration procedure was considered whereby the pile, fully assembled within the empty sand tank, was to be loaded vertically against a rigid base using the Dartec jack, calibrating the ALCs against the integral load cell of the jack. This approach was subsequently abandoned due to technical and practical problems. The ALCs were, therefore, calibrated individually using a 200.0 kN capacity Instron Universal Materials Testing Machine. The Dartec jack load cell was calibrated against that of the Instron by a direct compression test. No significant discrepancy was observed between the loads recorded by the two load cells.

Arrangements were made for the calibration procedure to simulate, as near as possible, the loading conditions experienced by the ALCs when located within the pile. The Instron/ALC adaptors designed for this purpose were, however, unable to transmit both tensile and compressive loads. Calibration was, therefore undertaken in two parts. Sketches of the apparatus for the compressive and tensile calibration are shown on

Figures 5.4(a) and (b). In view of the greater sensitivity of ALC(a) (base load cell) calibration was undertaken within the limits ±35.0 kN, whilst the remainder were calibrated over the range +50.0.kN to -35.0 kN. During calibration the load was applied over four cycles in 5.0 kN increments to the maximum for the given range. After each loading cycle the ALC was given a quarter turn to minimise the effects of any non-axiality in the loading system. Prior to the initial calibration cycle, and after each quarter turn, the maximum calibration load was applied several times to the ALC; initally to strain cycle the strain gauges and core, and thereafter to 'bed in' the contact surfaces.

Calibration constants of 35.2 μV/kN/V (base load cell) and 19.2 μV/kN/V (average for the remaining three cells) were in good agreement with the theoretical values of 33.8 μV/kN/V and 19.4 μV/kN/V respectively.

A single ALC was calibrated both with and without the rubber 'O'-ring in place. It was established that approximately 0.18% of the applied axial load was transmitted via the sleeve and 'O'-ring, by-passing the core. A discrepancy of this magnitude was considered to be insignificant.

On completion of two tests, the trial investigation and the first test in homogeneous sand (S/S1), an on-site calibration was undertaken, as indicated on Figure 5.4(c), as the pile was extracted and dismantled after S/S1. The resulting calibration constants were in good agreement with those of the initial calibration.

5.3.3 Accuracy and Stability

According to the initial calibration data the ALCs were accurate, at the 95.0% confidence limit, to ±0.04 kN (toe load cell) and ±0.14 kN (average for the remaining three cells). On completion of the test programme the ALCs were recalibrated in compression only due to failure of the tensile Instron/ALC adaptors through repeated use. An average reduction in the calibration constants of 0.74% was observed between the initial calibration and the subsequent recalibration. This was within the limits of stability of the 3.0 V (nominal) energizing power supply.

For a 24 hr period, immediately prior to commencing each test, the stability of the ALCs was monitored under zero load. During this period the initial zero values were observed to fluctuate, on average, within the limits ±0.06 kN.

5.4 Boundary Orthogonal Stress Transducers

Numerous investigators have undertaken field and laboratory investigations to monitor and quantify the magnitude and distribution of shaft friction in various soil types under different loading conditions. However, few have attempted to record simultaneously the distribution of radial stress and local unit shaft friction (σ_r and f_z) acting on the pile shaft. Among those that have, with any degree of success for axially loaded piles are: in sand, Agarwal and Venkatesan (1965), Gregersen et al (1973), and Williams (1979); in clay, Seed and Reese (1955) in conjunction with Reese and Seed (1955), Butterfield and Johnston (1972), Clarke and Meyerhof (1972 and 1973) and Franceson

(1982). None of the above have considered the variation in σ_r with f_z.

In order to obtain information on the interdependence of the two boundary stresses, a means of monitoring these was required. The cost of 'off the shelf' Cambridge type contact stress transducers from Robinson Research was prohibitive in view of the number required to obtain worth-while data. It was therefore necessary for the author to develop a transducer for this purpose. The resulting design has a distinct advantage in terms of manufacture over other types of BOST employed in the field of geotechnics. The transducer requires only eight strain gauges which are located on the outer surfaces of the transducer body. Further, only elementary machining is required to produce the transducer body from a single billet of material.

Transducers of a similar cross-section to that of the author's have been employed in electronic weighing balances, the operational concept of such a transducer under an applied shear load is, therefore, not new. However, the adaption of this transducer section to monitor orthogonal stresses appears to be original.

5.4.1 Conceptual Mode of Operation

To understand the operational behaviour of the transducer consider the three loading conditions outlined below applied to the simplified transducer cross-sections presented on Figure 5.5. These show the resulting strains developed in the outer fibres of the vertical faces of the transducer section (referred to subsequently as 'Gauged Faces') for each loading condition.

(i) Normal Loading (P_n)

As a result of the reduction in section at points A, B, C and D (referred to from here on as 'Webs') the local strains at and around the webs will be higher than those at other points on the gauged faces. This is not strictly correct as will be shown later (Section 5.4.3 Refer), but serves to illustrate the point to be made.

(ii) Shear Loading (P_s)

Under the action of an applied shear load the active element of the transducer will be displaced laterally 'Δ', with the webs acting as elastic hinges. This will result in the section assuming the deformed profile shown in broken outline. Such a displacment mechanism produces diagonally opposite regions of intense compressive and tensile strain on the gauged faces at the webs.

(iii) Combined Normal and Shear Loading ($P_n + P_s$)

The third case is the algerbraic combination of the previous two cases.

If two independent half-bridge circuits are employed, with active gauges sited at A and D, and B and C respectively (Figure 5.6), any combination of orthogonal loads can be resolved.

That is:

$$Vc1 \propto (\varepsilon_n + \varepsilon_s)$$

or

$$Vc1 \propto (P_n + P_s)$$

and

$$Vc2 \propto (P_n - P_s)$$

Rearranging

$$P_s \propto (Vc1 - Vc2) \qquad (5.1)$$

and

$$P_n \propto (Vc1 + Vc2) \qquad (5.2)$$

The measurement of the eccentricity in an applied normal load, acting along the major axis of the transducer, was considered and disregarded since the variation in the intensity of the radial stress across the active face of the transducer in the field was deamed to be insignificant. Further, a small eccentricity developed by the radial stress during pile installation and testing should not affect the response of the transducer to any great extent, since the design is, at least in theory, self compensating for this.

5.4.2 Prototype Transducer

A prototype transducer was manufactured from a billet of 'readily available' aluminium alloy with a yield stress (f_y) of 270.0 N/mm^2 and elastic modulus (E) of 71.0 kN/mm^2.

A developed elevation of the prototype transducer is presented on Figure 5.7. This shows the location of the strain gauges, both active

and dummy (which were bonded in accordance with Bulletin B-127-5 issued by Micro-Measurement, with M-Bond 200, a Cyanoacrylate adhesive), and the interbridge wiring. The dummy gauges were located on the sides of the passive element, which may be considered relatively 'strain free', to minimise any adverse effects resulting from ambient temperature fluctuations local to the transducer. It was realised that the heat sink capacity of the webs and the passive element were different. Unfavourable effects, as a consequence of this, were minimised by allowing a 'warm up' period for the transducers to attain a stable operating temperature prior to calibration and testing. This procedure was adopted for all instrumentation described in this chapter.

5.4.2.1 Calibration Procedure

Prior to calibration, the transducer was subjected to a number of loading cycles within the proposed calibration limits (±1.5 kg in shear and 0.0 to 6.0 kg normally : 1.0 kg being equivalent to 13.0 kPa) to strain cycle the transducer body and the strain gauges. Calibration was undertaken by applying a series of 'dead' loads via a loading plate secured to the active element of the transducer. During calibration the transducer was subjected to three cycles of shear loading in 0.5 kg increments for each 1.0 kg increment of applied normal load. The resulting outputs were recorded on a Bruel and Kjaer Strain Indicator, Type 1526.

For each increment of normal load two first order polynomials were established, one for each bridge circuit, which defined the relationship between output and the applied shear load (Table 5.1). It was found that the intercept terms of the polynomials increased as a function of the

applied normal load, as defined by Equations 5.3 and 5.4.

$$C1i = 5.48P_n - 14.29 \qquad (5.3)$$

$$C2i = 9.44P_n + 13.02 \qquad (5.4)$$

The slope terms of the equations in Table 5.1 also increased marginally as a function of the applied normal load. However, using the average value had only a minimal effect on the accuracy of the measurement of an applied shear load, estimated as ±0.4%. By combining the average slope values with the appropriate C1i and C2i terms, two general equations (Equations 5.5 and 5.6) were formed which defined the response of each bridge circuit for any combination of loads within the calibration limits. These equations were transposed to solve directly for P_s and P_n in terms of Vc1 and Vc2.

$$Vc1 = 1024.78P_s + 5.48P_n - 14.92 \qquad (5.5)$$

$$Vc2 = -1047.10P_s + 9.44P_n + 13.20 \qquad (5.6)$$

In order to verify the above equations the transducer was subjected to a series of one hundred and thirty two different loading conditions, the results of which were analysed statistically. The average error in measuring an applied normal load was found to be -0.070 kg with a standard deviation of 0.110.kg, whilst in shear this reduced to 0.010 kg and 0.007 kg respectively.

5.4.2.2 Eccentric Normal Loads

Eccentricity in the normal load applied along the major axis of the active face of the transducer should not, from geometric considerations, significantly affect the response of the transducer. Any discrepancy between an applied eccentric normal load and that recorded, was probably due to a redistribution of stress between the upper and lower webs on the gauge faces. This would be compounded if all webs are not of the same thickness (t) and width (a or 2a), or if the strain gauges were misalined.

The effect of a normal load applied eccentrically along the minor axis of the active face was evaluated by considering the active element of the transducer as being 'stiff' with respect to the webs. This assumption permitted the behaviour of the gauge face to be analysed in terms of a 'rigid' beam analogy by considering the 'rigid' active element to be resting on three elastic supports (the webs), the central support being twice as stiff as the two outer supports. Such an approach showed that, irrespective of the degree of eccentricity, the load transmitted through the central web was always one half of the applied normal load. It is possible, however, for a degree of stress redistribution to occur between the upper and lower webs on the gauged face, in which case this relationship is not valid within the lower webs. However, such an approach serves as a useful first order approximation. As the neutral axis of the gauged face coincided with the centre line of the active strain gauges, bending effects about the minor axis were self compensating.

The results of eccentric normal load tests conducted along both axes of

the active face of the transducer are shown on Figure 5.8. The degree of eccentricity developed during the pile test programme will be small in comparison to those applied above. Thus, errors will be sufficiently small to be ignored.

5.4.3 Finite Element Model

Having established a viable transducer geometry, an indication of the effects of varying the web thicknesses 't' was required. This was achieved by modelling a simplified section, of unit thickness, in constant strain triangular finite elements. The web thicknesses chosen for this study were 0.5, 1.0 and 1.5 mm. Each section was subjected to two uniform loading conditions comparable with cases (i) and (ii) outlined in Section 5.4.1. The magnitude of the uniformally distributed load applied to the active face was 10.0 N. The resulting stress profiles generated in the outer fibres of one gauged face are shown on Figures 5.9(a) and (b) for the two loading conditions.

The stress profiles for an applied shear load were much as assumed in the initial concept. However, those as a consequence of an applied normal load differed significantly from the initial postulation. An investigation of nodal displacements along the gauged face showed that the crown of the webs moved outwards, sufficient in the extreme case to induce a tensile stress in the outer fibres of the webs.

An exponential relationship was found to exist between web thickness 't' and the lateral displacement 'Δ' of the active element for a given shear load. This was (with due allowance for the unit thickness of the finite

element model and the 10.0 N applied shear load):

$$\Delta = \frac{P_s \, t^{-2.116}}{1000} \qquad (5.7)$$

In which:

Δ = lateral displacement of active face (mm),

P_s = applied shear load (N),

t = web thickness (mm).

Equation 5.7 was applied to the prototype transducer (t = 0.917 mm) for the maximum applied shear load of 14.7 N (1.5 kg). This gave a theoretical displacement of 0.018 mm, which was 72.0% of the measured displacement (0.025 mm). Although agreement between the theoretical and measured displacement was not good, the equation may be used to estimate the approximate order of any displacement.

5.4.4 A Suggested Design Procedure

From consideration of the transducer geometry, the most likely mode of failure is that due to excessive lateral displacement of the active element under an applied shear load. Based on this assumption a design procedure involving plastic equilibrium was developed by the author.

Equating the internal and external work done at failure on the

transducer by an applied shear load, it may be shown that:

$$P_{sf}\theta l = 4M_p\theta \qquad (5.8)$$

where:

P_{sf} = applied shear load causing failure (N),

θ = rotation at webs (Radians),

l = distance between web centres on one gauged face (mm),

M_p = fully plastic moment in the webs at failure (N mm), given by:

$$M_p = \frac{f_y W t^2}{4} \qquad (5.9)$$

in which:

f_y = yield stress of transducer material (N/mm^2),

W = total width of a web (4a) (mm).

Combining equations (5.8) and (5.9)

$$t = kl^{\frac{1}{2}} \qquad (5.10)$$

where:

$$k = \frac{P_{sf}}{f_y W} \qquad (5.11)$$

If P_{sa} is substituted for P_{sf} and $\frac{2}{3}f_a$ is substituted for f_y in Equation 5.11, the variaton in 'l' with 't' is fixed and a suitable

transducer geometry can be established. The factor of $\frac{2}{3}$ is applied to f_a in order to convert the maximum allowable stress in the web from that associated with an elastic stress block to that corresponding with a notional plastic stress block.

An acceptable estimate of the average stress (f_n) developed in the webs due to an applied normal load (P_n) may be derived from simple theory, that is:

$$f_n = \frac{P_n}{2tW} \qquad (5.12)$$

The elastic stresses evaluated using the Plastic Design Method for a given shear load, and by simple theory for an applied normal load, are compared with those from the Finite Element Method study on Figures 5.9(a) and (b). The theoretical maximum stress in the webs, calculated using the Plastic Design Method for a 10.0 N shear load, are also compared with those derived from the Finite Element Method on Table 5.2. In addition the mean stress recorded in the webs of the prototype transducer for a 10.0 N shear load, as determined from the response of the strain gauges, is compared with that evaluated by the Plastic Design Method. The results show the Plastic Design Method to be reasonably accurate for web thicknesses of 1.0 mm or more. However, there was a gradual reduction in accuracy with decrease in web thickness (t). The divergence of the results may have been due in part to the acute internal angles of the finite elements at the webs, which can result in some loss of accuracy.

5.4.5 Production Transducers

The experience gained with the prototype BOST led to the introduction of a number of minor improvements in the design of the production BOST (Plate 5.1). The webs were effectively lengthened in an attempt to produce a more even 'flow' of stress along them. To improve the performance of the dummy gauges, the cross-sectional profile of the passive element was altered to increase the size of the 'unstressed' region. This allowed the overall height of the transducer to be reduced.

The production BOST bodies were manufactured from HE15W Aluminium Alloy, which is supplied in a naturally aged and solution treated condition. The properties of the alloy are: f_y = 390.0 N/mm^2 and E = 71.0 kN/mm^2. The maximum allowable working stress (f_a) was limited to $0.25f_y$ (about 90.0 N/mm^2) due to nonlinearity in the stress/strain profile at elevated stress levels. This was in line with the limits of f_a prescribed by Bransby (1973) for the same material; that is, 73.0 to 145.0 N/mm^2.

The Plastic Design Method showed that for optimum performance in the layered soil profile two specifications of BOST were required. These required web thicknesses of 0.6 and 1.5 mm in order to accommodate the anticipated maximum shear stresses developed on the pile shaft within sand and clay respectively.

Boundary elements should have a maximum tolerable stiffness. The corresponding theoretical stiffness of the BOSTs in shear was 0.340 kN/mm (t = 0.6 mm) and 2.357 kN/mm (t = 1.5 mm), which compared unfavourably with those measured of 0.219 kN/mm and 0.978 kN/mm respectively. The above stiffnesses were smaller than those of other transducers reported

in literature. That is, 13.0 kN/mm (Arthur and Roscoe, 1961); 2.5 kN/mm (calculated from transducer properties) Argarwal and Venkatesan, 1965; and 30.0 kN/mm (Butterfield and Johnston, 1973). A subsequent calculation based on the pile shaft load/settlement results, obtained during the ML tests, suggested that the initial stiffness of the soil adjacent to the pile was 5.0 N/mm and 26.0 N/mm per unit area equivalent to the size of the active face of the transducer (30.0 x 30.0 mm) in the sand and clay respectively. The transducers were, therefore, about 25 times stiffer than the adjacent soil. The maximum measured lateral displacement of the active face was 0.022 mm (t = 0.6 mm) and 0.044 mm (t = 1.5 mm) under the action of the maximum design shear load.

Trollope and Currie (1960), referring to diaphragm type pressure transducers, recommended that the central deflection of the diaphragm should be less than 1/2000 of the cell diameter in order to minimise arching effects over the cell. Calculations indicated that the active face of the BOSTs deflected substantially less than this due to an applied normal load, even when a least favourable simplified geometry was considered.

Bransby (1973) suggested that the minimum contact area between the active face of a boundary element and the soil was related to the grain size and uniformity of the soil. After reviewing the work of other investigators he proposed that a rectangular cell should have sides of length equivalent to at least fifty grain diameters. The grain size of Leighton Buzzard sand is typically 0.6 mm, requiring a contact area of 30.0 x 30.0 mm.

To further improve performance, the production BOSTs were instrumented

with 350.0Ω strain gauges. This allowed a relatively high energizing voltage to be used, resulting in a correspondingly greater output voltage per unit of applied load. The gauges were bonded with M-Bond 610 adhesive according to Bulletin B-130-6 ('Hot-Tack' Method) issued by Micro-Measurement.

5.4.5.1 Installation in Pile

A typical pair of BOSTs installed in a section of pile are shown on Plate 5.2. The fixing bracket has an open central section which allows the BOSTs to be located around the core of the axial load cells.

A wiring loom and a length of fifteen core cable was attached to each bracket prior to installation in a pile section. Once the bracket was in place the ends of the loom wire were passed out of the pile section through the adjacent window and connected to the BOST. The BOST was then inserted into the pile section through the window and attached to the bracket by two 2BA screws.

The 30.0 mm square active face panel, previously cut from the pile section to produce the window, was then attached to the active element of the BOST with three 6BA screws. At the same time any necessary adjustments were made to ensure that the active face panel was situated centrally and squarely within the window and was flush with the external profile of the pile. Each active face panel was located in the window from which it was originally cut.

The cut edges of the window and active face panel were thoroughly cleaned

and a strip of 3.0 mm outside diameter PVC pipe was inserted into the clearance to create a channel approximately 0.5 mm deep. The PVC pipe served as a backing former whilst the silicon rubber was injected into the channel, and was removed once the rubber had set after a period of about 24 hrs.

5.4.5.2 Calibration Procedure

An indication of the maximum probable shear and radial stresses to act on the BOSTs embedded in sand was estimated in accordance with the classical theory of shaft friction. Calibration ranges of ±27.5 kPa (±2.5 kg) in shear and +27.2 kPa (+2.5 kg) radially were considered appropriate, and included an allowance against overload.

For the BOSTs embedded in the clay with a notional undrained shear strength of 50.0 kPa, a total stress approach was considered in order to estimate the probable maximum shear stress developed on the BOSTs. Taking α = 1.25, after Tomlinson (1970), for sand overlying clay ($D_b < 10.0B$), the limits ±174.4 kPa (±16.0 kg) were deemed to be satisfactory in shear with due allowance against overload. In order to ascertain the probable maximum radial stress it was necessary to resort to the theories of 'cavity expansion' which require a knowledge of the ratio of undrained elastic modulus (E_u) to undrained shear strength (C_u) for the clay. Tests on 38.0 mm diameter triaxial samples of clay at a consistency corresponding to the notional C_u, indicated an E_u/C_u of about 40, evaluating E_u from the secant modulus at $\frac{1}{2}(\sigma_1 - \sigma_3)_f$. Thus, changes in total stress of $4.35C_u$ (Butterfield and Banerjee 1970), $3.59C_u$ (Kirby and Esrig, 1979(a)) and $5.50C_u$ (Randolph et al, 1979(a)) were predicted

adjacent to the pile shaft immediately after installation. It was considered probable that stresses of this magnitude would not develop due to the relatively shallow penetration of the pile into the clay, since the resulting displacement field within the clay would not conform with the general assumptions of the cavity expansion theory. In addition, the presence of a sand plug below the pile base throughout penetration of the clay, and the 'draw down' of sand grains around the pile shaft, would aid in the rapid dissipation of any excess pore water pressure which constitute a major portion of the total radial stress adjacent to the pile immediately after driving. Further, the degree of stress relief allowed by flexure of the secondary clay tank is an unknown factor. Consequently an upper limit of $5.0C_u$ was considered appropriate for calibration purposes. Calibration was undertaken to a maximum radial stress of 272.5 kPa, corresponding to an applied load of 25.0 kg.

Calibration was undertaken on individual pile sections supported horizontally in a loading frame (Plate 5.3). 'Dead' loads were applied to the active face of the BOST via a 6BA screw, the head of which had been modified to accommodate a harness and yolk through which the shear and radial stress components were applied. The modified screw replaced the central screw securing the 30.0 mm square active face panel to the active element of the BOST.

In order to reduce the calibration time a 'quick' method was developed in contrast to the 'rigorous' method outlined in Section 5.4.2.1. In the 'quick' method the calibration, factors relating to the shear stress component were determined by subjecting the transducer to three cycles of shear, whilst applying a constant radial stress equivalent to half the maximum radial calibration stress. Calibration factors defining the

radial stress component were determined by applying three cycles of radial stress in the absence of an applied shear stress.

A comparative study was undertaken between the 'rigorous' and 'quick' calibration methods using two BOSTs, one of each specification. The results showed a change in the calibration constants of 0.43% and 3.50% (t = 0.6 mm) and 0.07% and -1.40% (t = 1.5 mm) for the shear and radial stress calibration factors respectively. These were considered to be insignificant. The author was, therefore, justified in employing the 'quick' calibration method.

The calibration factors derived during the above investigation for the t = 1.5 mm BOSTs were of a low order. In an effort to increase the response of the t = 1.5 mm BOSTs the energizing voltage was raised from 3.0 to 11.0 V (nominal). This had the adverse effect, however, of increasing in direct proportion the hysteresis in the output of the bridge circuits.

Since the t = 1.5 mm BOSTs were to operate in both sand and clay they were initially calibrated within the calibration limits specified for the sand. A second calibration was then undertaken on the t = 1.5 mm BOSTs within the calibration limits prescribed for the clay. During the test in the layered soil profile a routine within the 'management' program calculated the position of the t = 1.5 mm BOSTs with respect to the sand/clay interface, and changed calibration factors accordingly once the BOSTs had penetrated below the sand/clay interface.

Prior to undertaking a full calibration of the transducers, a number of secondary investigations were conducted to ascertain the factors

influencing the in-situ performance of the BOSTs. These are outlined below.

5.4.5.3 Influence of Silicon Rubber Sealant

Four BOSTs, two of each specification, were calibrated in-situ both without and with the silicon rubber sealant in place. An increase in stiffness of the order of 13.4% (t = 0.6 mm) and 3.2% (t = 1.5 mm) was indicated under an applied shear stress by an equivalent reduction in the shear stress related calibration constants. A reduction in the radial stress calibration constants of typically 0.8% was recorded for all four transducers.

5.4.5.4 Influence of Screws Attaching the Active Face Panel to the Active Element

The influence of the three axially alined fixing screws, which attached the 30.0 mm square active face panel to the active element of the BOST, was established by calibrating four BOSTs, two of each specification, twice; alternatively with one of the outer-fixing screws removed. Changes in the shear and radial stress related calibration factors were typically within the limits of ±1.0% and ±5.0% (t = 0.6 mm) and ±0.5% and ±3.0% (t = 1.5 mm) respectively. Although these changes were not particularly significant they highlighted the importance of a procedure adopted earlier, in which the output of a given BOST was recorded under zero applied load prior to removing any of the active face panel fixing screws. This allowed the screw (or the calibration screw) to be replaced

with sufficient torque to restore the original output of the BOST under zero applied load.

5.4.5.5 Influence of Eccentric Radial Loads Along the Major Axis

A series of eccentric radial loads were applied along the major axis of four BOSTs, two of each specification, at two points equidistance either side of the minor axis. The eccentricity was sufficient to cause a 300.0% difference in the theoretical proportions of axial load transmitted through the gauge faces. A consistant error was observed between the measured and applied radial load of ±11.0%. This depended only upon which side of the minor axis the load was applied. Such an error may be considered insignificant for the reasons previously stated in Section 5.4.2.2.

5.4.5.6 Influence of Cross-Sensitivity

In order to verify the calibration factors and quantify any errors statistically, a logical sequence of combined stresses within the limit of the calibration range were applied to each BOST in turn. From the initial results it was apparent that the design suffered from a degree of cross-sensitivity with the applied shear stress influencing the resolved radial stress. No satisfactory explanation was established for this phenomenon. However, the increase in the shear stress dependent calibration factors with greater radial stress (Section 5.4.2.1 Refer) may have some bearing on this problem.

The magnitude of the discrepancy between the applied and resolved radial stress was found to be consistent and repeatable for an applied shear stress. It was therefore possible to derive, through a secondary calibration, a correction factor which related the error in the radial stress to the resolved shear stress. Two adjustment factors were derived for the t = 1.5 mm BOSTs which corresponded with the calibration limits for sand and clay respectively.

5.4.5.7 Creep Under Maximum Shear Stress

The response of both specification of BOST to a sustained shear stress was investigated. It was found that the resolved shear stress increased by 3.5% (t = 0.6 mm) and 0.5% (t = 1.5 mm) after 1.0 hour. The resolved radial stress drifted from an initial zero value by 0.9 kPa (t = 0.6 mm) and 4.9 kPa (t = 1.5 mm), amounts which were within of the limits of accuracy for the BOSTs.

5.4.5.8 Accuracy and Stability

All BOSTs were subjected to a logical sequence of combined stresses within the calibration limits for sand. The errors observed between the applied and resolved stresses were analysed statistically, from which it was estimated that the measured radial and shear stresses were accurate to ±1.33 kPa and ±0.56 kPa respectively within the 95.0% confidence limit. The six t = 1.5 mm BOST were subjected to a second series of combined stresses within the calibration limits for clay from which it was estimated that an accuracy of ±7.00 kPa and ±1.78 kPa was achieved

for the resolved radial and shear stress components respectively to the 95.0% confidence limit.

On conclusion of the test programme a semi-random sample of six BOSTs were retested in order to ascertain whether any variation in the calibration factors had developed. A semi-random sample was specified since it was to include at least two BOSTs of web thickness t = 1.5 mm and any others whose performance was considered to be in doubt. The results of this study are shown graphically on Figures 5.10(a) and (b), together with the respective 95.0% confidence limit for each calibration range. The results showed that, within the confines of the maximum working range, the accurracy of the BOSTs was comparable with that established during the initial calibration. Beyond the limits of the working range the t = 0.6 mm BOSTs tended to under-estimate both stress components, whilst the t = 1.5 mm BOSTs tended to under and over-estimate the radial and shear stress components respectively for both calibration ranges. The maximum working range shown on Figure 5.10(a) was exceeded by the pair of t = 0.6 mm BOSTs situated immediately above the sand/clay interface during the CRU test.

The under-registration of the t = 0.6 mm BOSTs was probably due to the 2.3% reduction in energizing voltage recorded during the test programme, and a degree of 'age-hardening' of the silicon rubber, thereby increasing the effective stiffness of the BOST with respect to an applied shear stress. Over-registration by the t = 1.5 mm BOSTs to an applied shear stress was probably due, at least in part, to the localized debonding of the silicon rubber around the 30.0 mm square active face panels, which was observed for some of the BOSTs, as a consequence of penetration into the clay.

A secondary check was undertaken on the performance of the transducers at the conclusion of each pile test. This was undertaken by calculating the shaft capacity at ultimate load during the maintained load and constant rate of uplift tests. The shaft capacity was first estimated using the results from the ALCs. This value was then compared with that derived by integrating the local shear stresses recorded by the BOSTs, over the embedded length of the pile shaft. Discrepancies between the two values, taking the ALC results as datum, were typically of the order 2.1% and -18.3% for compressive and tensile loading respectively. The relative magnitude of these errors gave support to the decision not to consider a proportion of the clearance around the 30.0 mm square active face panel as constituting part of the active face.

During the 24.0 hr monitoring period prior to commencing a test, the resolved radial and shear stress components were observed to drift from an initial zero value by, on average, ±1.0 kPa and ±0.1 kPa respectively.

5.5 Soil Instrumentation

The layout of the soil instrumentation was primarily designed to suit the layered soil profile, paying particular attention to monitoring the behaviour of the sand/clay interface. An attempt was made to monitor vertical displacements at various levels within the sand mass, as well as effective vertical stresses on the sand/clay interface. Local variations in sand density as a consequence of pile installation were also determined at the conclusion of the ML test, in accordance with a method developed by the author.

5.6 Vertical Displacements on the Surface of the Sand

Vertical displacements on the surface of the sand were measured using an array of 'weights' attached by a length of 0.35 mm diameter piano wire to Linear Variable Displacement Transducers (LVDTs).

A 'weight' was located on the surface of the sand directly below an LVDT, and was sufficiently heavy to overcome the force of the return spring within the LVDT. Rotation of the 'weight' in a vertical plane passing through the pile axis, as a result of the displaced surface profile, was accommodated by means of a pinned coupling which connected the 'weight' to the piano wire (Plate 5.4).

Kay (1980) showed that the use of piano wire, in conjunction with LVDTs, was a satisfactory arrangement for measuring soil displacements generated at depth around a preplaced pile. He also described in detail the procedure adopted by the author for calibrating the LVDTs. This employed a modified micrometer to impart a series of precise displacements to the transducer.

For horizontal surface displacements to significantly influence the measured vertical displacements, the magnitude of the horizontal displacement has to be relatively large in relation to the vertical displacement. As the diameter of the 'visible' displacement envelope reported by Robinsky and Morrison (1964) for loose sand was, at depth, only slightly greater than the minimum diameter of the surface instrumentation (5.5B), and reduced in diameter towards the surface, the influence of horizontal displacments can be ignored.

5.6.1 Accuracy and Stability

From the calibration data it was calculated that the LVDTs were accurate to ±0.010 mm and ±0.047 mm at the 95.0% confidence limit for the two types of LVDT employed. These had nominal maximum displacements of 11.0 mm and 25.0 mm respectively.

During the 24 hr monitoring period prior to undertaking a test the initial zero readings were observed to drift between the limits +0.025 mm and -0.050 mm. Such a variation was probably due to the consolidation settlement of the sand, power supply fluctuations and temperature effects.

5.7 Vertical Displacements Within the Body of the Soil

Vertical displacements within the sand and on, or at a depth corresponding to, the sand/clay interface were measured using Electrolytic Levels (ELs). These were constructed from Gravity Sensing Electrolytic Transducers supplied by IFO International. Transducers of a similar type were first reported as being used to monitor vertical displacements around piles by Cooke and Price (1973(a)).

Displacements were calculated by numerically integrating the rotations recorded by a 'train' of ELs at a given depth. The integration procedure introduced an unknown constant which was taken as being equal to the vertical displacement of the EL, in any train, furthest from the pile axis. This was measured by attaching the EL, via a length of piano wire, to an LVDT positioned above ground level. The author was justified in

employing this method since the closest approach of any such EL to the pile axis was 4.0B, which was at the limit of the zone of visible disturbance for loose sand (Robinsky and Morrison, 1964).

The specification of the ELs employed by the author was different from those detailed by Cooke and Price (1973(a)). It was therefore considered necessary to quantify the effects of temperature and axial misalinement on the performance of the ELs (Sections 5.7.4 and 5.7.5 Refer).

5.7.1 Specification and Design

Two types of gravity sensing transducer were employed to cover the range of rotational displacement anticipated within the soil profile. These were the 7650 and 7660 series Gravity Sensing Electrolytic Transducers with ranges of ±0.70 and ±0.21 radians respectively. Each transducer was 'wired up' and encapsulated in a length of perspex tubing for protection. In an attempt to reduce the aspect ratio and increase stability, small stabilizing 'wings' were attached to the protective casings (Plate 5.5).

All ELs were connected to a combined junction box/power supply which also contained a bank of fifty-six 1.0 kΩ resistors (two per EL) which formed the internal halves of the bridge circuits. The supply voltage, nominally 5.0 Vrms, was found to vary slightly as a function of the number of ELs connected. It was, therefore, essential to ensure that all ELs were connected to the power supply during calibration. A simplified circuit diagram for a single EL is shown on Figure 5.11.

5.7.2 Calibration Rig and Procedure

The calibration rig consisted of a 'rigid' beam, 120.0 mm long, which was pinned and free to rotate at one end. The other end rested on a pointed brass tip set on the end of a depth gauge probe, which was clamped into a slot in the base plate of the calibration rig. A machined channel and a short spigot, alined along the longitudinal axis of the calibration beam, provided positive seatings for the type 7660 and 7650 ELs respectively. The ELs were held securely in place throughout calibration by stout elastic bands (Plate 5.6).

Prior to calibration, the EL was first secured to the beam with the electrodes approximately vertical and in line with the beam axis. A travelling telescope, the cross-hairs of which had previously been set vertical and horizontal, was positioned square on to the end of the calibration beam and in line with the longitudinal axis of the EL. This was used to view the electrodes to ensure true axial alinement and verticality. The depth gauge was then adjusted, raising or lowering the beam as necessary, until the bridge response indicated a null voltage at which point the EL was considered to be horizontal (0.0 rad). From the horizontal position the beam was raised and lowered, using the depth gauge, between the limits ±60.0 mm (7650) and ±18.0 mm (7660) (corresponding to approximately ±0.61 rad and ±0.21 rad) in 5.0 mm and 2.0 mm increments respectively. Results derived with the beam elevated and depressed were considered, for simplicity, as two separate sets of data. The variation in bridge output (Vrms) with rotation (rad) was defined by a third order polynomial for each set of data.

5.7.3 Effects of Temperature

The effect of temperature on the response of the ELs was investigated for a range of rotations corresponding to nominal outputs of 0.10, 0.75 and 2.00 Vrms at temperatures of 14.0, 17.0 and 20.0^{0}C. Temperature control was achieved by immersing the ELs in a constant temperature water bath. Three of each type of EL were employed during the test. These were embedded in plasticine on a solid base within the water bath. Each group of ELs was arranged in a 'nose to tail' configuration forming an equilatrial triangle in plan, and inclined in the same direction relative to the local axis of each EL. The 'tail' end of an EL was that end through which the wiring passed. Such a configuration was adopted in an attempt to minimise errors resulting from physical disturbance during the test period, since a small global change in the orientation of the group would increase the output of some ELs and reduce that of others. Thus, the mean output of each group of ELs would remain approximately constant.

The results of the above investigation are shown on Figure 5.12. It was noted that although the rate of change in output with change in temperature increased with greater inclination, due to the non-linear nature of the transducers response, the apparent rotation per ^{0}C was relatively constant at about -200.0×10^{-6} rad/^{0}C (neglecting the 2.0 Vrms data, since the higher electrode in each EL was not adequately immersed in the electrolyte) and -1400.0×10^{-6} rad/^{0}C for the type 7660 and 7650 respectively.

5.7.4 Effects of Misalinement of the Longitudinal and Vertical Axes

The effect of longitudinal and vertical misalinement on the output of both types of EL was considered. Two angular scales were attached to two of the ELs, one of each type, alined with the vertical and longitudinal axes respectively. The angular scales allowed the ELs to be positioned on the calibration beam with the longitudinal and vertical axes, in turn, alined at 0.17 rad and 0.44 rad to the longitudinal and vertical axes of the calibration beam. This was achieved by viewing the scales through a travelling telescope. For each misalinement a full calibration was undertaken. From the results, of which only the 'elevated' portion of the calibration data is shown on Figures 5.13(a), (b) and 5.14(a), (b), it was apparent that both types of EL were reasonably tolerant to deviations of up to 0.17 rad on either axis. Within the normal operating range (elevated, with an output of typically 0.5 to 1.0 Vrms) for a deviation of 0.17 rad on either axes, the absolute errors were:

Transducer Series	Errors at 0.17 rad Deviation % (Radian x 10^{-6})	
	Axis Vertical	Axis Longitudinal
7650(±0.70 rad)	-0.005(97.0)	0.250(387.9)
7660(±0.21 rad)	-1.177(591.5)	1.965(979.3)

In reality errors are likely to be less than this since relative changes in rotation were used in the evaluation of vertical displacements.

In view of the adopted placement technique (Section 6.3 Refer) a generous

estimate of the maximum probable deviation in placing the ELs within a soil profile is ±0.050 rad. Placement errors of this magnitude will have an insignificant influence on the calculated displacements.

5.7.5 Accuracy and Stability

To the 95.0% confidence limit, accuracies of $\pm 969.6 \times 10^{-6}$ rad and $\pm 3199.7 \times 10^{-6}$ rad were predicted from the calibration data for the type 7660 amd 7650 transducers respectively. Ambient temperatures in the laboratory were found to vary between 18.0 and 21.0 ^{0}C during the period of calibration.

On completion of the test programme a random sample of six type 7660 and two type 7650 ELs were recalibrated in order to check for any change in the calibration factors. The results suggested that within the operating range a 3.0% reduction in output had developed. This could be explained by:

(i) A reduction in the energizing volatage of 1.8% over the duration of the test programme. This was within the limits of stability for the power supply.

(ii) The ambient temperature during recalibration was 21.0 to 22.0 ^{0}C, which was higher than that recorded during the initial calibration. An increase in temperature of 3.0^{0}C corresponds approximately to a 1.0% reduction in output.

The magnitude of any change in the performance of the ELs throughout the test programme was probably less than that stated above since the ambient

temperature of the sand was approximately 17.0 to 18.0^{0}C.

The average drift in the response of the ELs recorded during the 24 hr period prior to testing was small and within the limits of accuracy, and amounted to $\pm 190.0 \times 10^{-6}$ rad (7660) and $\pm 1000.0 \times 10^{-6}$ rad (7650).

An estimate was made of the probable error in calculating vertical displacments as a consequence of the development of horizontal displacements within the sand. This has the effect of reducing the spacing between successive ELs in any train. For the purpose of calculation a simplified horizontal soil displacement profile was considered, based on zero vertical and volumetric strain, and applied to a typical set of displacement data recorded at the end of pile installation. The analysis showed that vertical displacements would probably be under-estimated by typically 0.8%, which may be considered insignificant.

5.8 In-Situ Density Measurement of Dry Sand

A complete description of a method developed by the author for the in-situ density measurement of sand is given by Werscheing et al (1983), and which is reproduced in Appendix 5.1.

The method employs an unhydrated mixture of sand and plaster which is deposited in small quantities at strategic locations within the sand profile during construction. The plaster is hydrated, after the pile has been installed and tested, by the injection of a small amount of a water/detergent solution local to the sand/plaster mixture. Hydration of

the plaster has the effect of cementing together the sand grains in the sample and 'locking in' any volumetric strain. The samples are retrieved at the end of a test, and the dry density of each calculated. From the dry density of the sample it is possible to estimate the dry density of the uncemented sand, local to the sample, using a relationship previously derived through calibration.

During the course of the pile tests an inconsistancy in the $\phi'-\rho_d$ relationship, indicated on Figure 6 of Appendix 5.1 became evident. This figure should be disregarded and replaced by Figure 3.2.

5.8.1 Accuracy

Analysis of the calibration data suggested a relatively low level of accuracy of ± 31.8 kg/m^3 ($\pm 0.09\ D_r$) at the 95.0% confidence limit. The consistancy and limited scatter in the results derived during the test programme suggested that the method was more accurate than the above limits indicated. Densities calculated from density samples, sited remote from the pile, were in good agreement with those calculated for the contents of the two California Bearing Ratio (CBR) moulds which were retrieved from the sand profile after each test. Further, calculated and actual sand densities determined during the 'pilot' study also were in good agreement (Appendix 5.1, Table 3).

5.9 Diaphragm Pressure Transducers

The distribution of vertical effective stress at, or corresponding to

the level of the sand/clay interface was monitored using an array of three diametrically opposite pairs of Diaphragm Pressure Transducers (DPTs). The DPTs have a maximum capacity of 500.0 kPa and are instrumented with a full bridge circuit of four 350.0Ω strain gauges. Development and production of these transducers was undertaken at Nottingham University under the direction of Professor Brown.

Brown (1973) outlined the criteria for the design of DPTs and the factors which affect cell registration. These were:

(i) A low aspect ratio (A = Transducer Thickness/Transducer Diameter) for minimal stress redistribution across the diaphragm.

(ii) To achieve a uniform distribution of stress across the diaphragm the area of the diaphragm should not be greater than 45.0% of the total plan area of the transducer.

(iii) The diameter of the diaphragm should be greater than 50 times the mean partical size of the soil.

(iv) The diaphragm should be small enough to minimise the stress variation across it.

(v) A rigid annular ring should surround the diaphragm to reduce cross-sensitivity in a non-uniaxial stress field.

(vi) The diaphragm should be stiff in relation to the soil stiffness.

Brown (1973) omitted to set any limits for the deflection of the diaphragm under load. According to Trollope and Currie (1960) the maximum central deflection of the diaphragm should be less than 1/2000 of the transducer diameter in order to minimise arching effects. This

criterion was adequately satisfied by the transducer in question since the theoretical deflection, at maximum capacity, was five times less than the maximum allowable value.

The DPTs employed during the investigation were of the following specification:

Transducer Diameter = 62.5 mm

Transducer Thickness = 11.0 mm

Diaphragm Diameter = 37.5 mm

Diaphragm Thickness = 2.0 mm

E Transducer = 210.0 kN/mm^2

E Soil (Loose Sand)* = 30.2 N/mm^2

* From initial linear portion of the stress/strain profile derived from the 102.0.mm triaxial tests ($\phi' = 33.4^0$).

Brown (1973) defined the stiffness ratio in (vi) by a flexibility factor 'F', where:

$$F = \frac{\text{E Soil x Diaphragm diameter}}{\text{E Transducer x Diaphragm Thickness}}$$

which, together with the aspect ratio, is related to a cell registration factor 'C', where:

$$C = \frac{\text{Stress recorded by Transducer}}{\text{True or Field Stress}}$$

For a transducer of the above specification these factors are:

$A = 0.18 \qquad F = 0.947 \qquad C = 1.08$

As 'F' is less than 5, 'C' will be practically unaffected by moderate changes in soil modulus.

With regards to cross sensitivity resulting from a non-unaxial stress field, Brown (1973) concluded that although theoretically significant changes in 'C' were predicted, for practical purposes these were not great, being of the order of 6.0% maximum, and were swamped by what he called "practical factors" which resulted in a 10.0% discrepancy in test repeatability.

5.9.1 Calibration Procedure

Brown (1973) stated that the calibration procedure should reproduce the anticipated in-situ stress conditions. Plantema (1952) simulated the action of an indirect DPT set in the face of a concrete slab or wall, by recessing the DPT into a concrete slab in the base of the calibration chamber. At the time of calibration it was anticipated that a major portion of the test programme was to be undertaken with the DPT recessed in, and flush with, the surface of the clay at the sand/clay interface. In order to simulate this condition each DPT was set in a bed of plasticine on the base of the calibration chamber, a modified 150.0 mm 'Rowe' consolidation cell. Plasticine was used in preferance to clay in order to overcome the problems of consolidation and moisture migration that would otherwise have occurred during calibration. Subsequently an

annular wooden former was used to the same effect as the plasticine.

In order to determine a suitable calibration technique a single DPT was loaded over six cycles to 206.7 kPa (30.0 psi) in 34.5 kPa (5.0 psi) increments. This operation was undertaken five times with various thicknesses of sand (12.0, 25.0, 37.0 and 50.0 mm) between the DPT and the pressure diaphragm of the Rowe cell. At stresses greater than 140.0 kPa (20.0 psi) the results obtained with sand overlying the DPT showed a reduced response compared with that undertaken without the sand, Figure 7.15. This indicated the probable development of arching across the transducer diaphragm. The degree of arching did not appear to be a function of the depth of sand as might have been expected (Getzler et al 1968). However, for stresses within the anticipated working range (0.0 to 70.0 kPa) there was little variation in response of the DPT irrespective of the thickness of sand layer (Figure 7.16).

Getzler et al (1968) suggested that the factors which contribute to arching over buried structures were the magnitude of the applied stress and the sand rigidity. With regard to these points it was considered that only a limited degree of arching would develop across the DPTs due to the relatively low sand density and stress levels within the sand throughout pile installation and load testing. It was, therefore, decided to calibrate the transducers without sand in the calibration chamber.

Each transducer was calibrated over three loading cycles, applied in 34.5 kPa (5.0 psi) increments up to 206.7 kPa (30.0 psi). Prior to this and at the start of each load cycle, the system was pressurized to 206.7 kPa a number of times to ensure a good contact between adjacent

components within the calibration chamber.

5.9.2 Accuracy and Stability

The calibration factors obtained by the author compared favourably with those reported by the manufacturer. The calibration data indicated an average accuracy of ±2.8 kPa at the 95.0% confidence limit. In practice the performance of the DPTs was probably better than this, ignoring registration and other associated factors, since the calibration characteristics were slightly non-linear. This resulted in a standard deviation over the calibration range which was higher than might reasonably be expected over the smaller operating range.

Recalibration of the DPTs, on completion of the test programme, indicated a reduction in the overall accuracy of the transducers to ±3.8 kPa at the 95.0% confidence limit. However, the accuracy of the individual transducers established during the initial calibration was not consistent with that established on subsequent recalibration. This fact pointed to the influence of operator and practical factors. Further, the overall sensitivity of the DPTs reduced by 3.6%, 2.3% of which was directly accountable for by the reduction in energizing voltage.

During the 24 hr monitoring period prior to a test, the transducers drifted by typically ±0.78 kPa from the initial zero value.

5.10 Interface Shear Stress Transducers

The radial shear stress on the sand/clay interface was monitored by four pairs of Interface Shear Stress Transducers (ISSTs) developed by the author (Plate 5.7). Each consisted of a boxed (t = 1.5 mm) BOST body, instrumented with four 350.0Ω strain gauges applied in a full-bridge configuration. The gauges, bonded with M-Bond 610 adhesive in accordance with Bulletin B-130-6 ('Hot-Tack' method) issued by Micro-Measurement, were so arranged that diametrically opposite pairs in the bridge circuit were located on diagonally opposite webs on the transducer. Such an arrangement maximised the bridge circuit response to an applied shear stress and theoretically rendered it insensitive to an applied normal stress. Shear stresses developed on the sand/clay interface were transmitted to the transducer via a section of shear box ridge plate attached to the active element of the transducer. The clearance of 2.0 mm between the transducer body and the sides of the protective box was sealed with silicon rubber to a depth of 0.5 mm as described in Section 5.4.5.1.

5.10.1 Calibration Procedure

The calibration procedure was similar to that outlined in Section 5.4.5.2, with the exception that a normal stress was not applied to the transducer. The transducer was strain cycled prior to calibration, which was undertaken over three loading cycles in 39.2 kPa (3.0 kg) increments between the limits ±196.2 kPa (±15.0 kg).

5.10.2 Accuracy and Stablity

An assessment of cross-sensitivity was made by subjecting the transducer to a sequence of normal stresses, of the same magnitude as prescribed in Section 5.10.1, under zero applied shear stress. The response of the transducers to an applied normal stress was found to be, on average, 0.459 μV/kPa (6.0 μV/kg), which indicated that 1.25% of an applied normal stress was registered as an apparent shear stress. This level of cross-sensitivity was considered acceptable.

The accuracy of the transducers, neglecting cross-sensitivity effects, was on average ±1.69 kPa at the 95.0% confidence limit. Recalibration on completion of the test programme showed there to be little change in this value, although the average sensitivity of the ISSTs reduced by 4.17%. Again 2.3% of the reduction in sensitivity can be accounted for by a reduction in the energizing voltage. The progressive age hardening of the silicon rubber would further contribute to a reduction in sensitivity.

During the 24 hr monitoring period prior to each test the ISSTs were observed to drift by typically ±0.32 kPa from the initial zero value.

Appendix 5.1

Shaun N. Wersching,[1] *Ramiz Delpak*,[1] *and Gruff O. Rowlands*[1]

A Method of Estimating the In-Situ Density of Dry Uniformly Graded Sand Under Controlled Conditions of Placement

REFERENCE: Wersching, S. N., Delpak, R., and Rowlands, G. O., **"A Method of Estimating the In-Situ Density of Dry Uniformly Graded Sand Under Controlled Conditions of Placement,"** *Geotechnical Testing Journal*, GTJODJ, Vol. 6, No. 4, Dec. 1983, pp. 196-200.

ABSTRACT: One of the main problems faced by investigators working with dry sand is the inability to obtain undisturbed specimens from which fundamental soil parameters may be established. The two principal related variables in sand are density and the angle of internal shearing resistance. This paper describes a method of estimating the in-situ sand density from a small specimen of sand, the grains of which are cemented together using plaster. The method uses an unhydrated sand/plaster mixture that is deposited in pockets at strategic locations within the soil profile during its construction. The plaster is subsequently hydrated by the injection of a quantity of water through a small pipe venting at the location of the specimen. Such specimens are retrieved at the end of a test and their densities determined from which the density of the uncemented sand in the proximity of the specimen can be estimated using a relationship previously determined through calibration.

KEYWORDS: sands, density, shear strength, measurement, plaster, in situ

Nomenclature

e	Voids ratio
Gs	Specific gravity of sand
$Gs(sp)$	Specific gravity of sand/plaster mixture
Ms	Dry mass of uncemented sand within the mold
Msp	Dry mass of sand/plaster mixture
Mt	Dry mass of California Bearing Ratio (CBR) molds contents
Sr	Degree of saturation
Vs	Volume uncemented sand within the mold
Vsp	Volume of sand/plaster mixture within the mold
Vt	Volume of CBR mold
w	Moisture content
ρs	Dry density of uncemented sand
ρsp	Dry density of sand/plaster mixture
ρt	Mean dry density of mold contents
ρw	Density of water

Introduction

In connection with research work on semi-full scale piles in sand we have developed a practical method of estimating local densities within a larger mass of sand placed under controlled conditions.

[1]Research student and principal lecturers, respectively, Department of Civil Engineering and Building, The Polytechnic of Wales, Pontypridd, Wales, United Kingdom.

0149-6115/83/0012-0169$02.50

A variety of techniques have been used by various investigators to determine the in-situ mean and local density variations, resulting from model tests, in a laboratory prepared sand profile. A method employed by Jurny [1], which is similar in concept to that reported in this paper, was used to investigate the pore-size distribution in sand. The method required a trace amount of powdered thermally sensitive polymer to be mixed with the sand before placing. Then the entire specimen and container were heated to 170°C for 1 h to activate the polymer, binding the sand grains together. The latter operation of heating renders the technique impractical for all but small-scale model tests. Even so, any instrumentation must either be capable of withstanding the elevated temperatures or be removable without disturbance to the sand's structure. Further structural disturbance is likely to occur as a result of transporting the sand profile to the oven. Other methods require sophisticated equipment or operations or both, which disturb the sand's in-situ structure. These include nuclear density meter, spoon penetration test [2], thermal probe method [3], density tins [4], Danish Geotechnical Institute vacuum sampling apparatus [5], and plastic injection, wedge, tube, sand funnel, and rubber balloon-tube methods as discussed by Griffin [6].

This paper outlines a method of determining the local densities within a larger mass of sand by relating it to the density of a small specimen where grains are cemented together using Kaffir 'D' plaster, which permits retrieval of the specimen in an undisturbed state.

Material Properties

Sand

Air dry Leighton Buzzard sand, for which a typical grading curve is shown in Fig. 1, was used throughout the test program. The maximum and minimum densities [7] are 1780.2 kg/m^3 and 1520.0 kg/m^3, respectively; $Gs = 2.71$; the uniformity coefficient = 1.79; and the coefficient of curvature = 1.38.

Kaffir 'D' Plaster

Kaffir 'D' is a gypsum based plaster chosen for its fast setting time during which it expands minimally; a typical 100/30 (plaster/water) mixture expands 0.2 to 0.25%. Further, when heated to a temperature in the range of 105 to 110°C for 24 h the plaster releases most of the combined water of hydration reverting mainly to the initial semi-hydrate state [8].

FIG. 3—*CBR mold with sand/plaster mixture and injection pipe in position (paper former removed).*

sand and plaster. This was then immersed in a bath of water within a vacuum dessicator and the air evacuated. The pressure within the chamber was then gradually increased to atmospheric, saturating the specimen.

A fine wire harness was used to lift the specimen from the bath, and any surplus surface water was allowed to drain before suspending the specimen in a beaker of water placed upon a balance. The increase in weight was equated to the volume of the specimen. This was then used in the determination of the specimen's specific gravity (Table 1). That is

$Gs(sp)$ = mass of specimen dry/volume of specimen − volume of voids and combined water

TABLE 1—*Specific gravity of sand plaster mixtures.*

Test	Dry Mass of Specimens, g	Volume of Solids[a] Volume of Specimen − Volume of Moisture in Specimen, cL	Specific Gravity of Specimen
8	140.45	84.50 − 30.60 = 53.90	2.606
9	132.80	80.30 − 31.35 = 48.95	2.713
10	146.55	87.40 − 31.90 = 55.90	2.640
11	140.65	86.50 − 33.70 = 52.80	2.660
12	135.40	85.20 − 35.20 = 50.00	2.708
13	143.10	79.30 − 26.20 = 53.10	2.695
14	138.80	87.00 − 36.20 = 50.80	2.732

[a]Specimen volumes differ slightly to those presented in Table 2 where they have been calculated using the mean value of $Gs(sp)$.

$Gs(sp)$ = mass of specimen solids/volume of specimen solids

$$Gs(sp)\ \text{mean} = 2.680 \tag{1}$$

Results are shown in Table 1.

On removing a specimen from the vacuum dessictor (or beaker in tests 8 to 14) the excess surface water was again allowed to drain before weighing the saturated specimen in air and drying in an oven at 105°C for 24 h to determine the specimen moisture content.

Using the above information, that is, specific gravity of the hydrated sand/plaster mixture $Gs(sp)$ and its moisture content w, it is possible to determine the dry density of the sand/plaster specimen ρsp

$$\rho sp = \rho w \cdot Gs(sp) / (1 + e) \tag{2}$$

where

$$e = w \cdot Gs(sp) \tag{3}$$

since the degree of saturation Sr is unity.

Calculation of Uncemented Sand Density

It was observed that the calculated density of the sand/plaster mixture was, in all cases, greater than the mean density of the contents of the mold. Thus it was necessary to establish a relationship

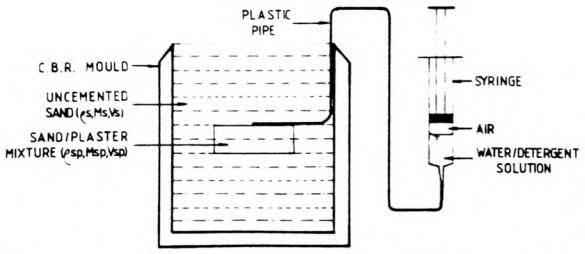

FIG. 4—*Sand profile within CBR mold and arrangement for injecting water/detergent solution.*

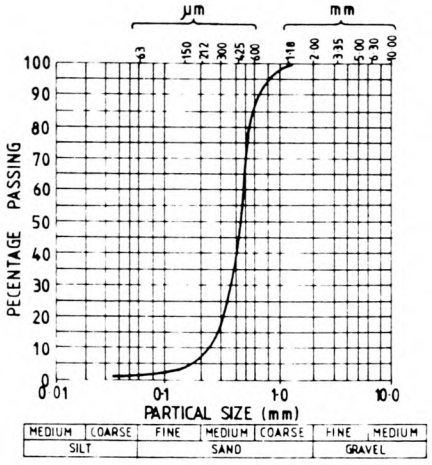

FIG. 1—*Typical grading curve of Leighton Buzzard sand.*

Optimum Plaster Content

The principal factor dictating the sand/plaster ratio was one of strength as the hydrated specimen must be capable of withstanding reasonable handling. This was investigated by preparing specimens containing 2, 4, 6, 8, and 10% plaster by mass. After hydration the specimens were examined and broken by hand to give an indication of strength. It was concluded from this that 7% plaster would be adequate.

Test Procedure

Specimen Compaction

The specimens were prepared in a standard California Bearing Ratio (CBR) mold. In order to obtain a range of sand densities various methods of placement were developed using sand without plaster. For the lowest densities (1504.9 to 1560.0 kg/m^3) the sand was placed by pouring freely from a pycnometer jar allowing a fall of up to 250 mm depending upon the degrees of compaction required. With the mid-range of densities (1560.0 to 1747.7 kg/m^3), the sand profile was built up in seven layers, each of which were initially placed in the loosest state using the pycnometer jar and subsequently tamped with a 150-mm-diameter platten. A small pneumatic vibrator was attached to the platten to achieve the highest density range (1747.7 to 1784.0 kg/m^3), and the number of layers increased to 14.

Specimens with Plaster

To evaluate the method, specimens of sand were prepared with a portion of the specimen consisting of the sand/plaster mixture. To do this, sand without plaster was first placed in a CBR mold to a depth of 75 mm by a method relevant to the density range under investigation. An annular paper former, 70 mm in diameter by 25 mm deep, was then positioned centrally on the sand surface (Fig. 2) and filled with the sand/plaster mixture by the same method adopted for placing the sand without plaster. However, before applying any necessary compaction to the sand/plaster specimen the level of the surrounding sand was made up to be equal to that of the mixture within the former. The former was then carefully lifted from the sand and physical compaction was applied if required. For the highest densities, where the sand was deposited in 14 layers, the operation of placing the sand/plaster mixture was performed in two 12.5-mm layers.

A length of plastic pipe, having an outside diameter of 3-mm and a 1-mm bore, was then inserted into the mold resting on the sand's surface to vent directly above the sand/plaster mixture (Fig. 3). The CBR mold was then filled with sand containing no plaster and compaction, as above, and the surface levelled before weighing (Fig. 4).

Twelve millilitres of a 0.2% detergent/water solution by volume together with 5 mL of air were drawn into a syringe and injected into the sand/plaster mixture via the plastic pipe.

The air serves two functions, acting as a buffer preventing any sudden high pressures resulting from erratic piston movement and freeing the pipe bore of liquid thus preventing back syphoning. A detergent was used in order to reduce any grain disturbance caused by surface tensile effects. The operation of injection was gradual and continuous taking about 30 s to complete thereby reducing the possibility of localized grain disturbance caused by high exit velocities from the pipe.

Sand/Plaster Density Measurement

At least 20 min was allowed after injection for hydration of the plaster before emptying the mold and retrieving the cemented specimen of

FIG. 2—*CBR mold containing sand and the paper former before placing the sand/plaster mixture.*

for the density of the uncemented sand in the mold, based upon the total dry mass Mt and total volume Vt of the CBR mold contents and the density of the sand/plaster mixture ρsp. With reference to Fig. 4

$$Mt = Ms + Msp \tag{4}$$

Putting Eq 4 in terms of density and volume

$$\rho t \cdot Vt = \rho s \cdot Vs + \rho sp \cdot Vsp \tag{5}$$

But

$$Vs = Vt - Vsp \tag{6}$$

From Eqs 5 and 6

$$\rho s = (\rho t \cdot Vt - \rho sp \cdot Vsp)/(Vt - Vsp) \tag{7}$$

Using Eq 2 in conjunction with

$$Vsp = \text{volume of sand/plaster solids} + \text{volume of voids} \tag{8}$$

Where it is assumed that the volume of voids is equal to the volume of water in the specimen. Therefore

$$Vsp = [Msp/Gs(sp) \cdot \rho w] + (Msp \cdot w/\rho w) \tag{9}$$

and

$$\rho t \cdot Vt = Mt \tag{10}$$

It can be shown that by substitution in to Eq 7

$$\rho s = \{Mt - [\rho w \cdot Gs(sp) \cdot (1 - e)] \cdot [Msp \cdot Gs(sp) \cdot \rho w + Msp \cdot w/\rho w]\} \{Vt - [Msp \cdot Gs(sp) \cdot \rho w + Msp \cdot w/\rho w]\} \tag{11}$$

The magnitude of this adjustment can be observed in Table 2. By plotting ρs against ρsp a relationship connecting these two parameters has been derived for which the equation

$$\rho s = 1.0485\, \rho sp - 134.4 \tag{12}$$

provides a good first order estimate (Fig. 5).

Discussion

We have successfully used this method of determining in-situ densities in pilot experiments on piles in sand. To illustrate the accuracy of the method, densities determined during the course of these tests are compared with the mean density as in each case the total

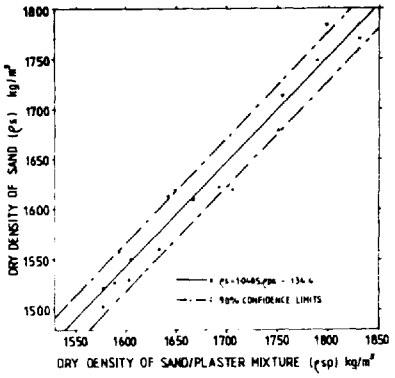

FIG. 5—*Variation of dry density of sand/plaster mixture ρsp with dry density of the surrounding uncemented sand ρs.*

TABLE 2—*Volume of CBR mold* Vt = 2.894 × 10^{-3} m^3.

	CBR Mold Contents		Cemented Sand/Plaster Specimen				Uncemented Sand
Test	Total Mass Mt, kg	Mean Density ρt, kg/m^3	Moisture Content w	Voids Ratio e	Calculated Volume Vsp, × 10^{-3} m^3	Density ρsp, kg/m^3	Density ρs, kg/m^3
1	4.362	1507.3	0.2609	0.6992	91.14	1577.2	1504.9
2	4.435	1532.5	0.2508	0.6721	85.95	1602.8	1530.3
3	4.668	1613.0	0.2269	0.6081	85.55	1666.6	1611.2
4	4.692	1621.3	0.2336	0.6260	88.55	1648.2	1620.4
5	4.698	1623.4	0.2133	0.5716	77.59	1705.3	1621.2
6	4.966	1716.0	0.1970	0.5280	82.90	1753.9	1715.0
7	4.866	1681.4	0.1985	0.5320	77.74	1749.3	1679.6
8	4.703	1625.1	0.2179	0.5840	83.01	1691.9	1623.3
9	4.677	1616.1	0.2360	0.6325	80.89	1641.7	1615.3
10	4.522	1562.5	0.2177	0.5834	86.59	1592.6	1558.4
11	4.523	1562.9	0.2396	0.6421	86.18	1632.1	1560.7
12	4.495	1553.2	0.2600	0.6700	84.37	1604.8	1551.8
13	5.164	1784.4	0.1831	0.4907	79.60	1797.8	1784.0
14	4.412	1524.5	0.2608	0.6989	87.99	1577.5	1522.8
15	5.063	1749.5	0.1856	0.4974	100.18	1789.8	1747.7
16	5.132	1773.3	0.1730	0.4636	97.92	1831.1	1771.4
17	4.426	1529.4	0.2567	0.6880	96.18	1587.7	1527.4

mass and volume of the sand profile was known (Table 3). However, at a later stage it is proposed to conduct a series of semi-full scale experiments using a fully instrumented 114.0-mm-diameter pile driven through a stratum of dry loose-sand deposited under controlled conditions in a 3.0-m-diameter tank. A number of sand/plaster specimens will be included at strategic locations within the sand profile during placement. Some of the specimens will be hydrated before driving the pile to monitor the initial as-placed density of the sand profile. The remainder being hydrated once the pile has been fully driven to record any density changes caused by driving.

The principal condition that must be fulfilled in order to permit the use of this method of density determination, when conduc model tests, is that the size of the sand/plaster specimen shoul small when considered in relation to the size of the model and the profile.

The influence of the dry plaster upon the shear strength of sand has been investigated at various densities. It can be seen I Fig. 6 that the angle of shearing resistance is increased by abou for a given density. Again providing the above condition is adh to, this effect can be ignored.

TABLE 3—*Comparison of mean density with that determined by the sand plaster method.*

Test	Average Density			Density According to Sand/Plaster Method	
	Mass, kg	Volume, m^3	Density, kg/m^3	Specimen 1, kg/m^3	Specimen 2, kg/m^3
1	141.516	0.092842	1524.3	1537.0	1526.6
2	66.830	0.044375	1506.0	1508.9	1508.1
3	65.830	0.043431	1511.5	1507.6	1494.1
4	64.750	0.042645	1518.3	1511.7	1518.6

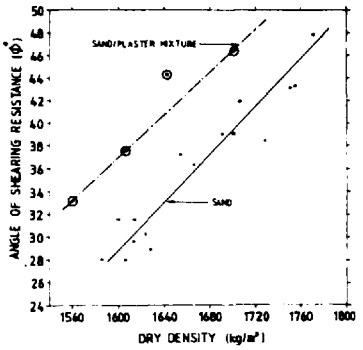

FIG. 6—*Variation in angle of internal shearing resistance with dry density for sand and the unhydrated sand/plaster mixture.*

Conclusion

The method outlined has been tried and has given satisfactor sults in a series of tests. But before applying the method, the influ of the sand/plaster mixture, in its hydrated or unhydrated stat the behavior of the sand mass in general, should be carefully sidered.

Acknowledgments

This paper is published by permission of Mr. R. D. McMu Head of Department of Civil Engineering and Building, The technic of Wales. The work described forms a part of the rese program on piles in granular soils carried out in the departr The student is supported by a Science and Engineering Res Council (SERC) studentship.

References

[1] Jurny, C. H., "Pore Size Distribution of Sandy Soils and the Pred of Permeability," Joint Highway Research Project, FHWA IN J 81 15, Purdue University, W. Lafayette, IN, Aug. 1981, 109 pp.

[2] Gibbs, H. J. and Holtz, W. G., "Research on Determining the D of Sand by Spoon Penetration Test," *4th International Conferer Soil Mechanical and Foundation Engineering*, Vol. 1, Butter Scientific Publications, London, 1957, pp. 35–39.

[3] Singh, G., Ergatoudis, J., and Siah, B. S., "A Laboratory Meth Measuring In-Situ Density Distributions in Dry Sand," *Geotec Testing Journal*, Vol. 2, No. 3, Sept. 1979, pp. 129–135.

[4] Kay, W. F., "The Development of Skin Friction in Semi-Full Scal Passing Through Granular Soils," Ph.D thesis, The Polytech Wales, Pontypridd, 1980.

[5] Mazurkiewicz, B. K., "Skin Friction on Model Piles in Sand, *Danish Geotechnical Institute, Bulletin, No. 25*, Copenhagen, pp. 13–48.

[6] Griffin, D. F., "Errors of In-Place Density Measurements in Coh less Soils," *Evaluation of Relative Density and Its Role in Geotec Projects Involving Cohesionless Soils, STP 523*, American Soci Testing and Materials, Philadelphia, 1973, pp. 195–206.

[7] Akroyd, T. N. W., *Laboratory Testing in Soil Engineering*, The M Press Ltd., London, 1957, pp. 41–42.

[8] Dinsdale, A., "The Effect of Heat on Plaster," *Transactions British Ceramic Society*, Vol. 52, 1953, pp. 614–631.

Normal load kg	Circuit	
	Vc1	Vc2
0.0	$1020.85P_s - 16.15$	$-1041.14P_s + 15.67$
1.0	$1024.47P_s - 4.20$	$-1044.85P_s + 18.38$
2.0	$1025.67P_s - 4.46$	$-1045.58P_s + 32.00$
3.0	$1026.70P_s - 0.43$	$-1046.83P_s + 42.75$
4.0	$1028.50P_s + 5.77$	$-1048.39P_s + 52.94$
5.0	$1029.87P_s + 17.01$	$-1050.22P_s + 55.99$
6.0	$1031.43P_s + 17.42$	$-1052.03P_s + 71.75$

EQUATIONS DEFINING THE VARIATION IN BRIDGE RESPONSE WITH APPLIED SHEAR LOAD UNDER SUCCESSIVE INCREMENTS OF NORMAL LOAD

TABLE 5.1

Method	Web Thickness 't'(mm)	Stress (N/mm^2)
	0.500	60.0
Plastic Design	1.000	15.0
	1.500	6.6
	0.500	45.0
Finite Elements	1.000	13.5
	1.500	6.2
Strain Gauges on Prototype Transducer	0.917	16.0
Plastic Design	0.917	17.8

MAXIMUM STRESS IN TRANSDUCER WEB DUE TO AN APPLIED SHEAR LOAD OF 10.0 NEWTONS

TABLE 5.2

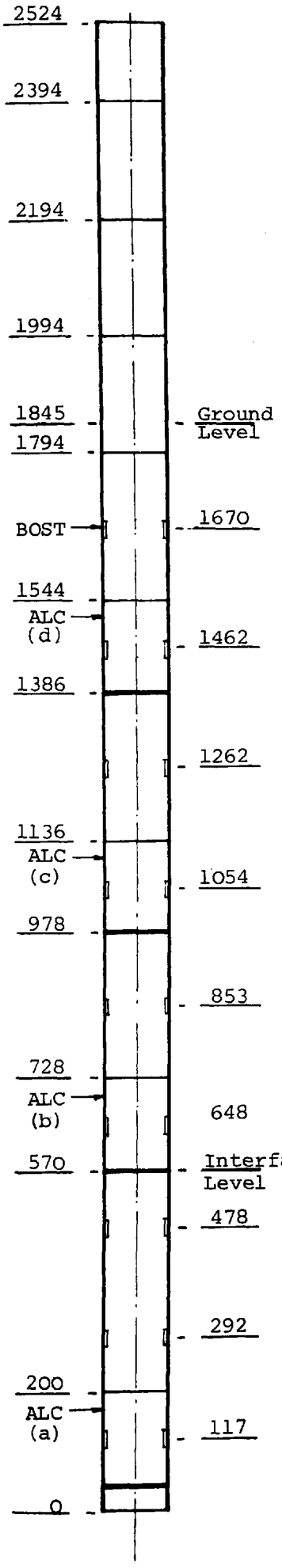

(a) General Arrangement of Composite Pile

1:100

(All Dimensions in mm)

BOST = boundary orthogonal stress transducer

ALC = axial load cell

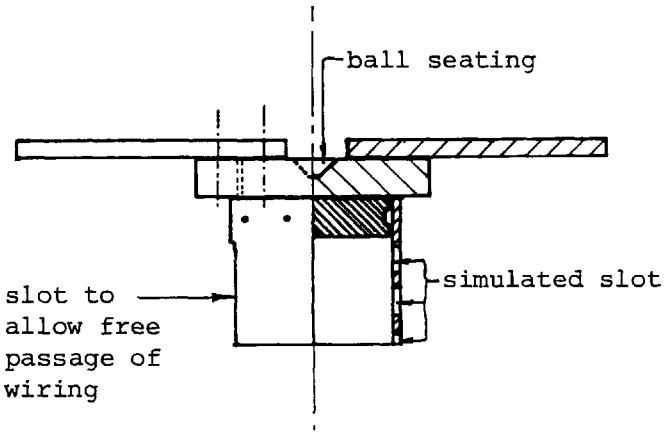

Female Pile Cap

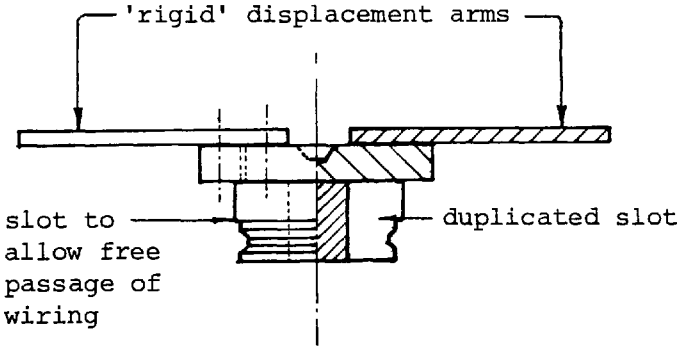

Male Pile Cap

(b) Half Section of Pile Caps

1:5

GENERAL DETAILS OF PILE AND PILE CAPS

FIGURE 5.1

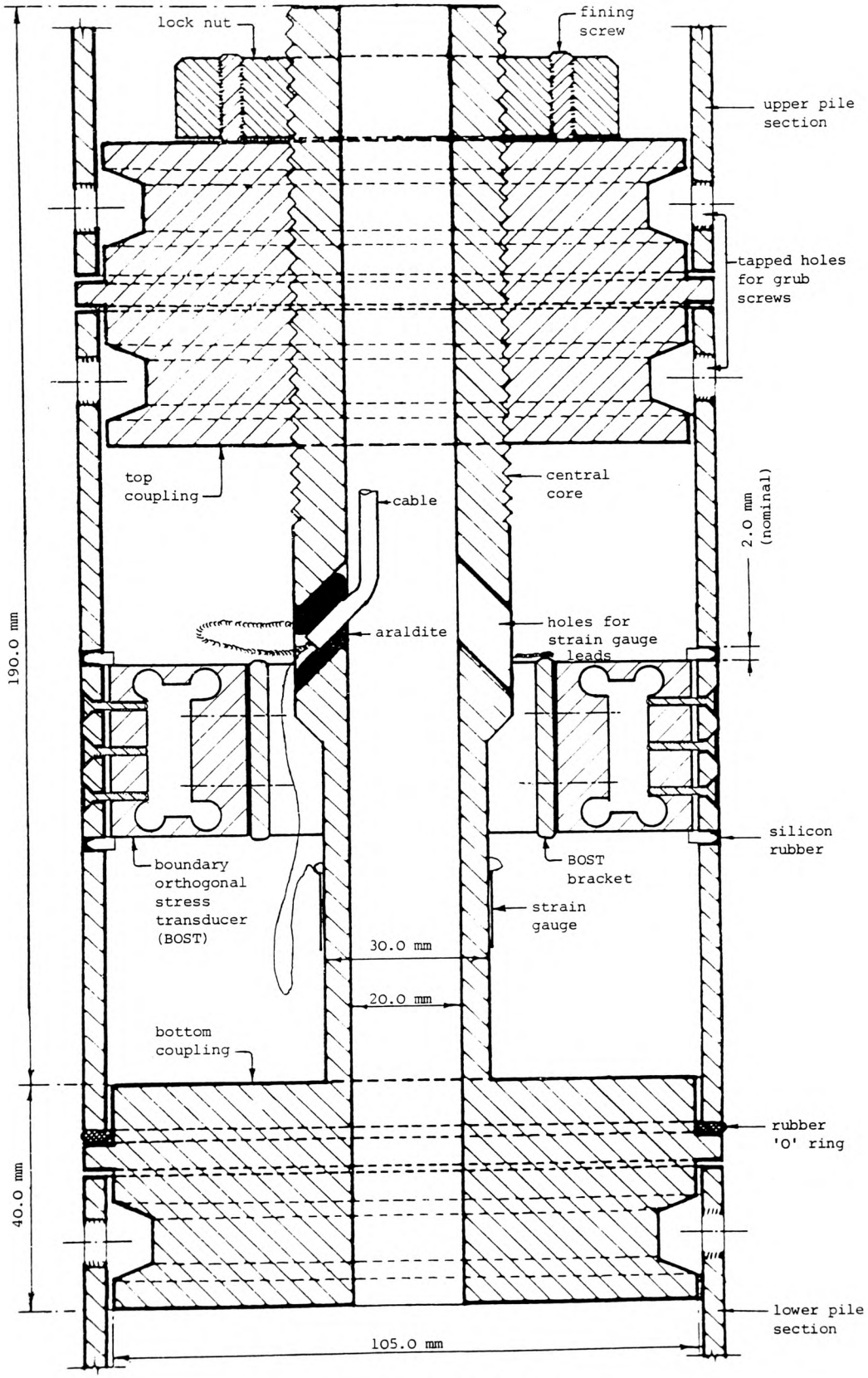

'CORE' TYPE AXIAL LOAD CELL

FIGURE 5.2

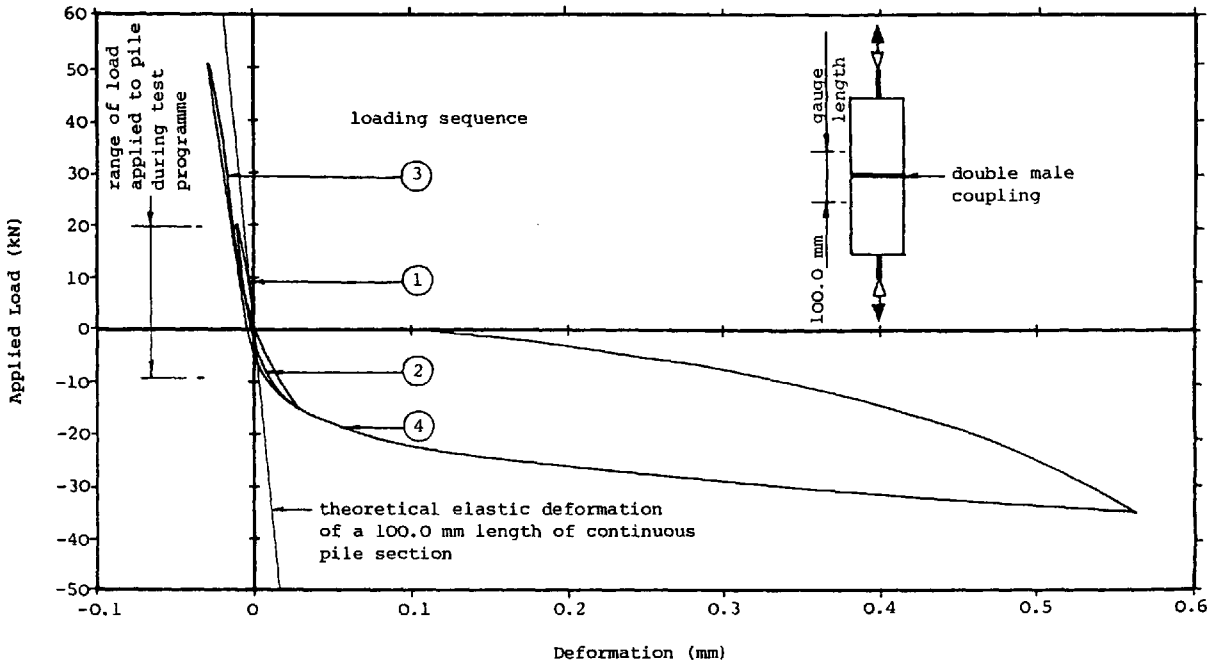

LOAD TEST RESULTS FOR A 100.0 mm LENGTH OF PILE INCORPORATING A MODIFIED DOUBLE MALE COUPLING

FIGURE 5.3

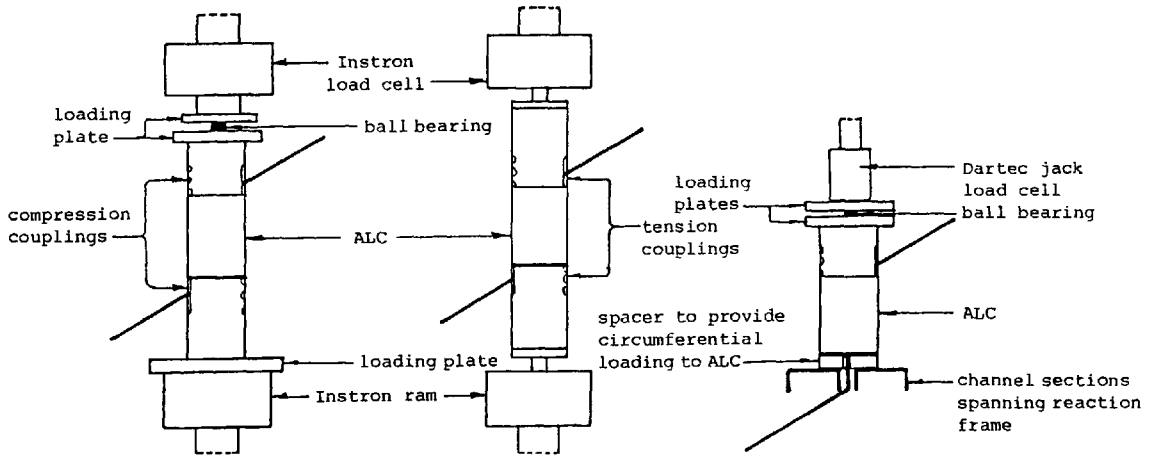

(a) Compressive (b) Tensile (c) On-Site

SKETCH OF CALIBRATION ARRANGEMENTS FOR AXIAL LOAD CELLS

FIGURE 5.4

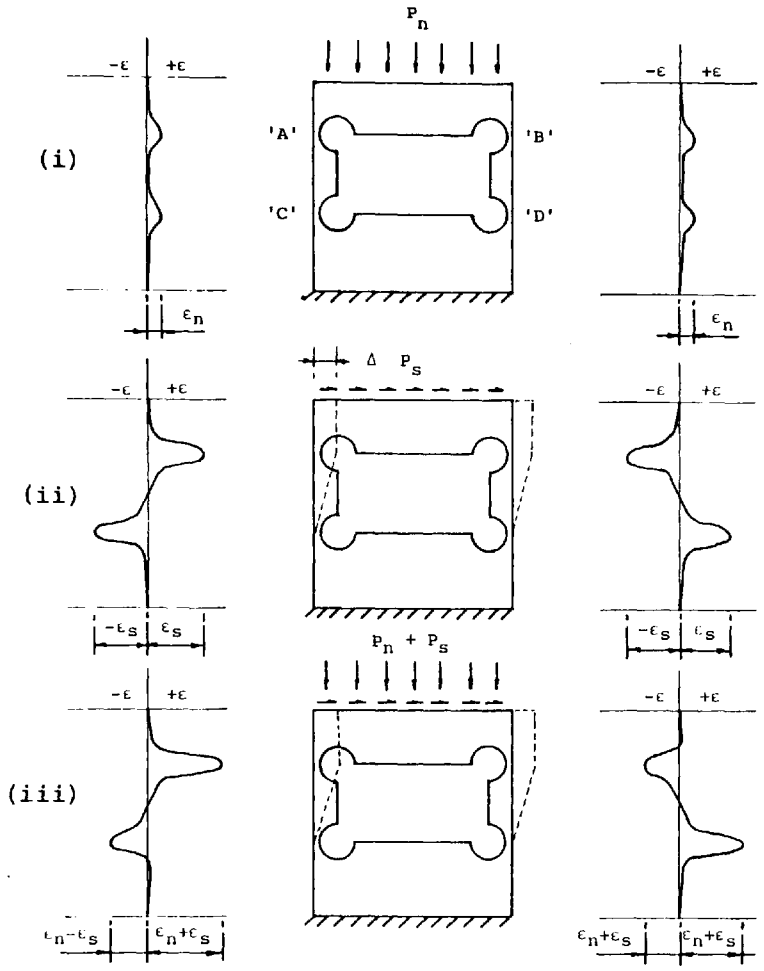

IDEALISED STRAIN (ε) PROFILES DEVELOPED ON THE 'GAUGED FACES' OF THE BOUNDARY ORTHOGONAL STRESS TRANSDUCER DUE TO THREE UNIFORM LOADING CONDITIONS

FIGURE 5.5

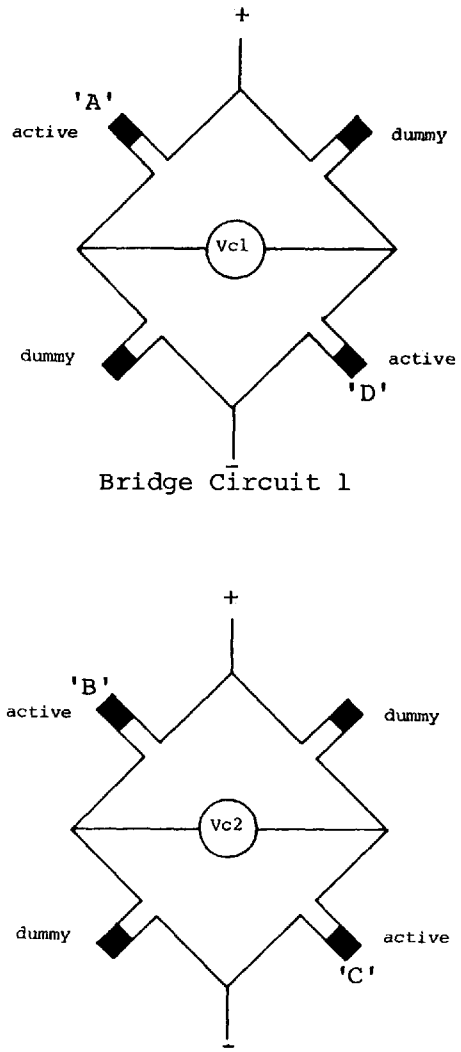

A DIAGRAMATIC REPRESENTATION OF THE TWO 'HALF'-BRIDGE CIRCUITS USED ON THE BOUNDARY ORTHOGONAL STRESS TRANSDUCERS

FIGURE 5.6

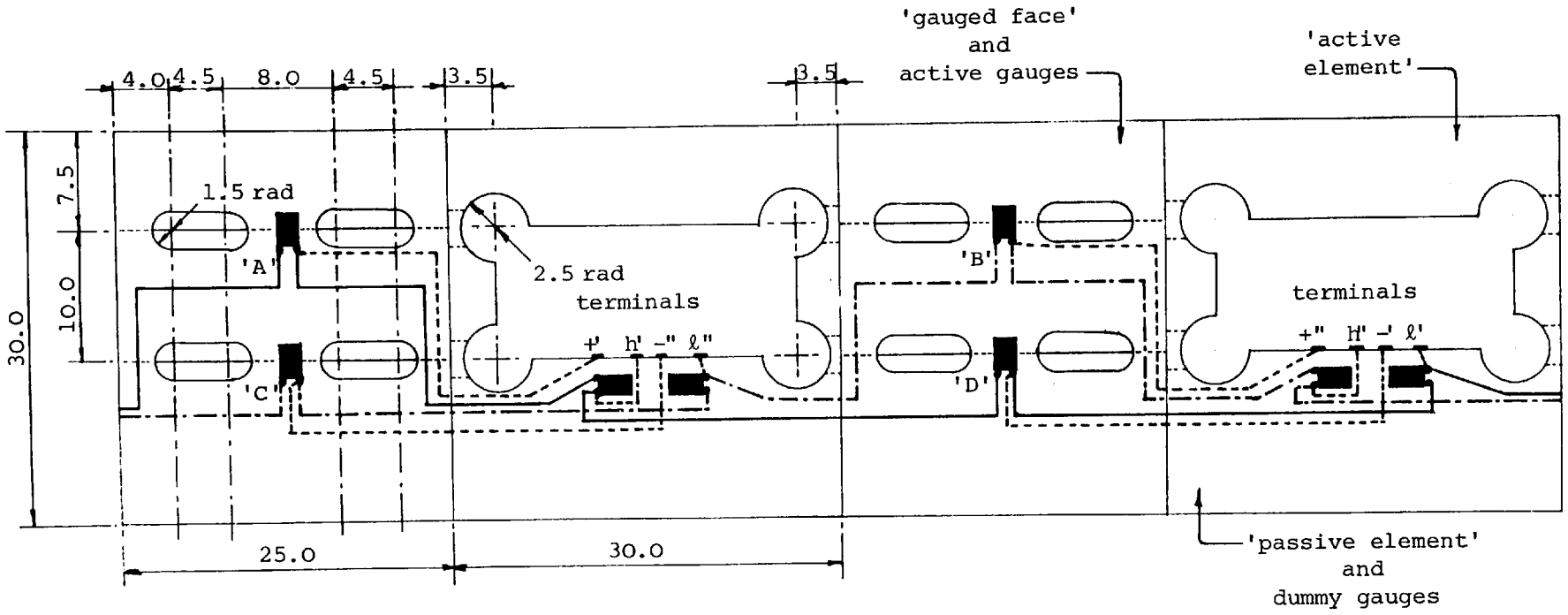

A DEVELOPED ELEVATION OF THE PROTOTYPE BOUNDARY ORTHOGONAL STRESS TRANSDUCER
SHOWING LOCATION OF STRAIN GAUGES AND INTERBRIDGE WIRING
(All Dimensions in mm)

FIGURE 5.7

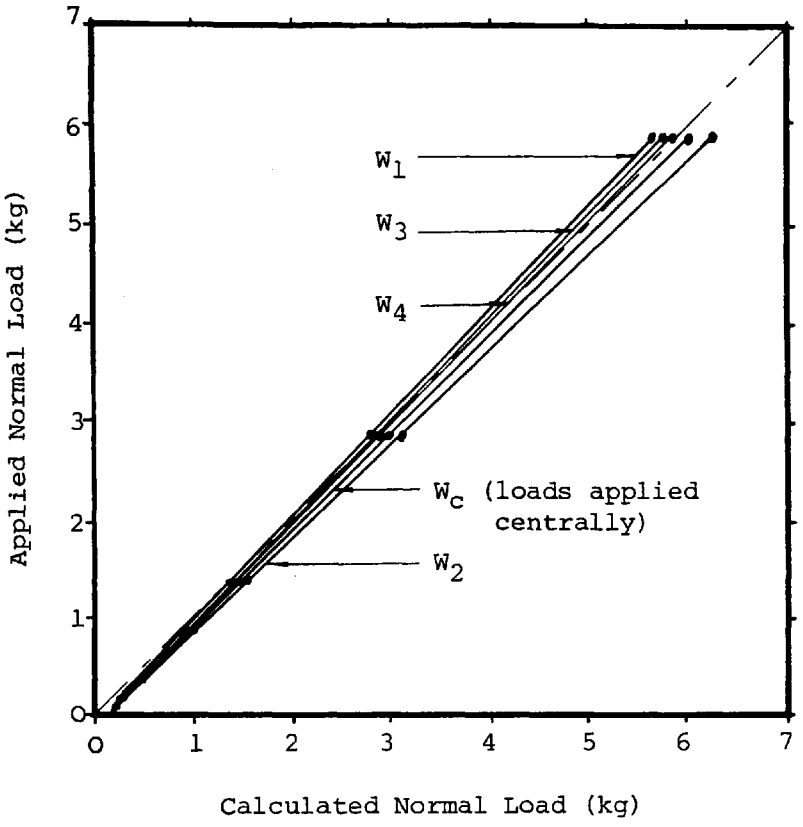

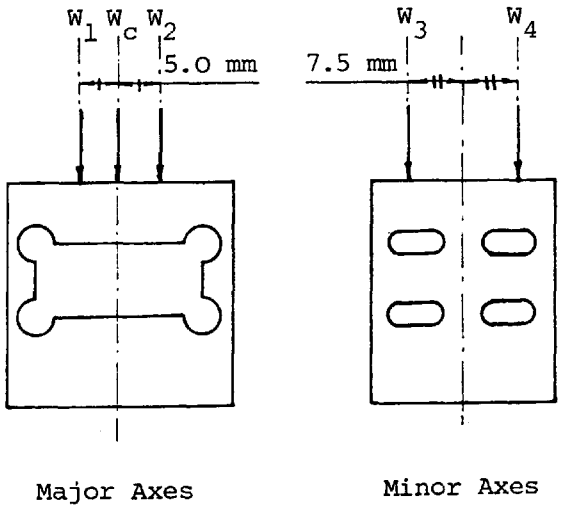

EFFECT OF ECCENTRIC NORMAL LOADING ALONG THE MAJOR AND MINOR AXES OF THE PROTOTYPE BOUNDARY ORTHOGONAL STRESS TRANSDUCER

FIGURE 5.8

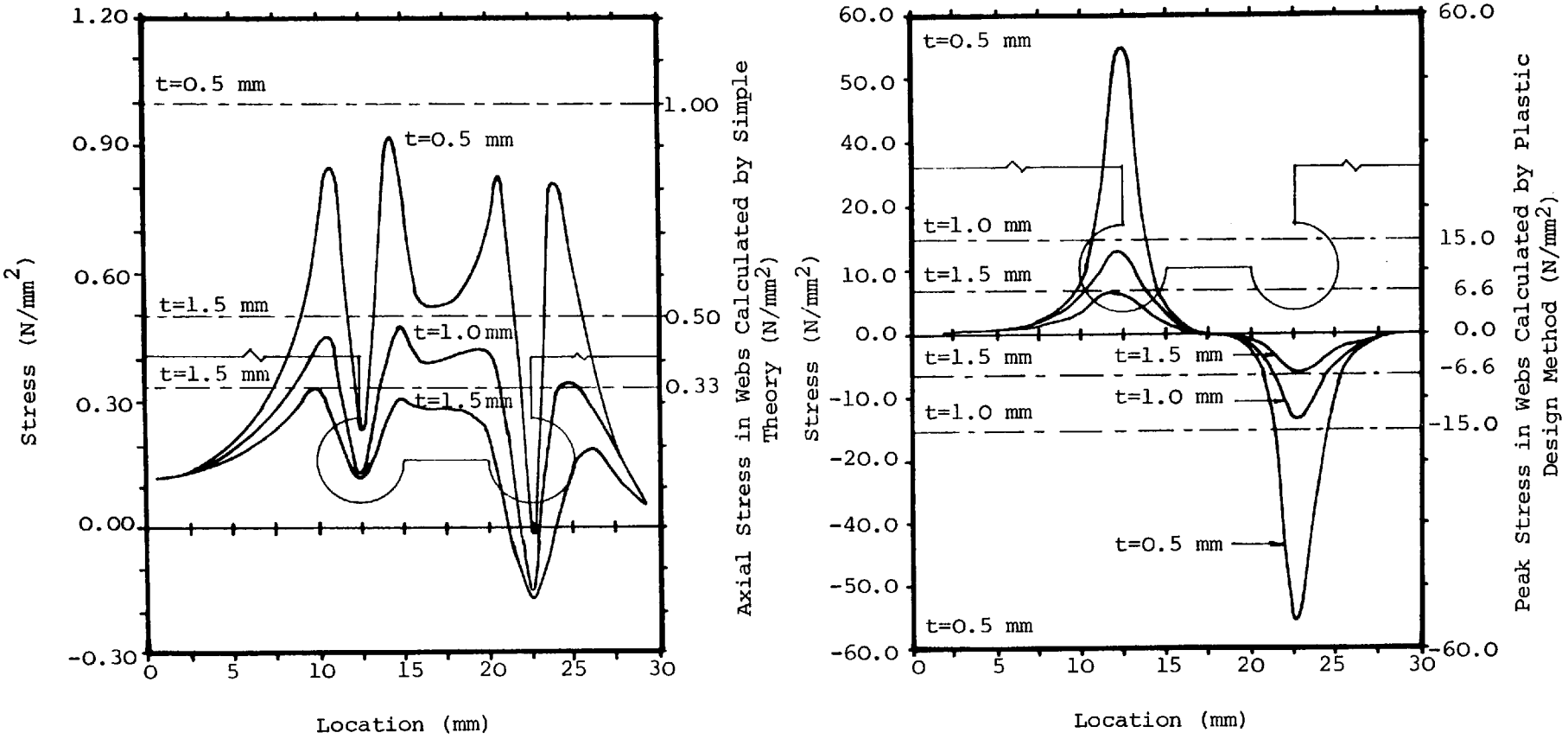

(a) Due to a Uniformally Distributed 10 N Normal Load Acting on the Active Face

(b) Due to a Uniformally Distributed 10 N Shear Load Acting on the Active Face

STRESS PROFILES PREDICTED BY THE FINITE ELEMENT METHOD ON THE GAUGED FACE OF A SIMPLIFIED ORTHOGONAL BOUNDARY STRESS TRANSDUCER SECTION FOR VARIOUS WEB THICKNESS (t)

FIGURE 5.9

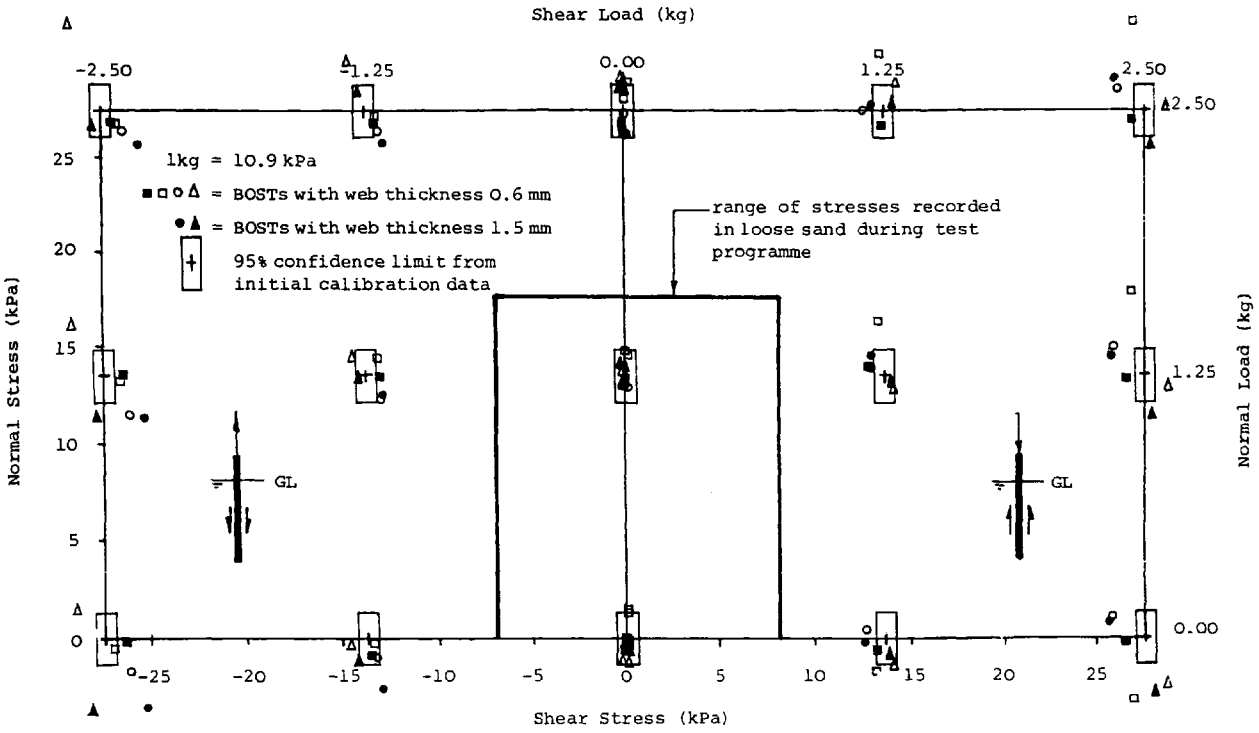

(a) Calibration Limits for Sand

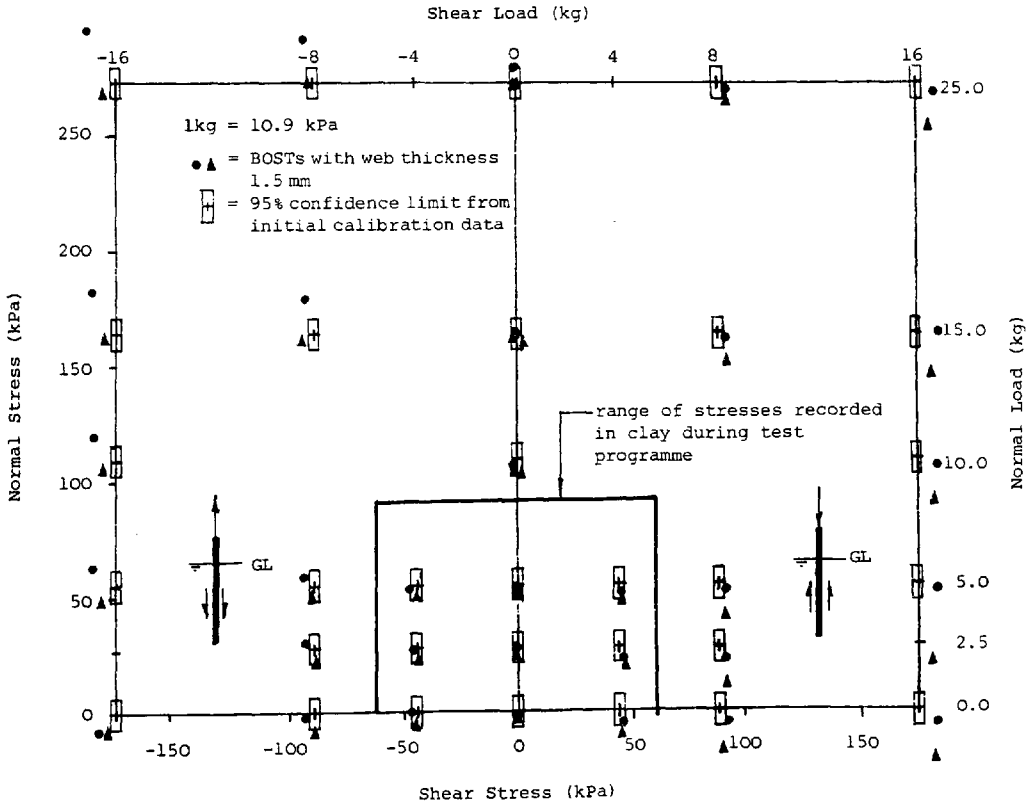

(b) Calibration Limits for Clay

ACCURACY OF A SEMI-RANDOM SAMPLE OF SIX BOUNDARY ORTHOGONAL STRESS TRANSDUCERS ON COMPLETION OF THE TEST PROGRAMME

FIGURE 5.10

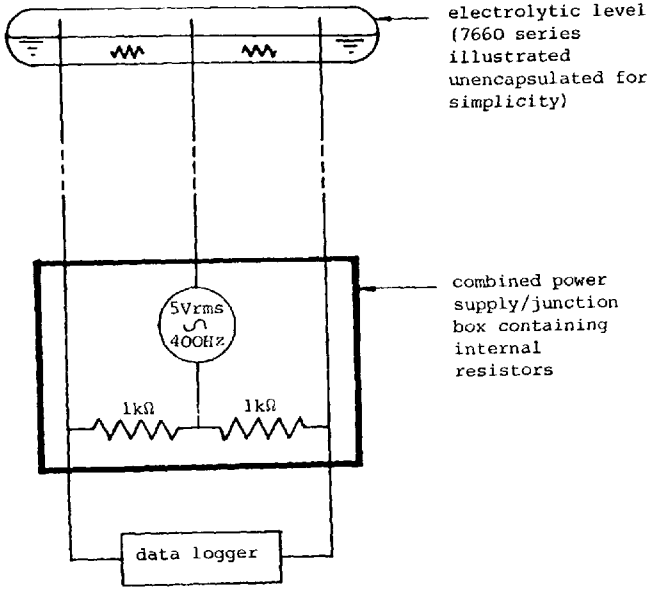

DIAGRAMATIC REPRESENTATION OF CIRCUITRY FOR THE ELECTROLYTIC LEVELS

FIGURE 5.11

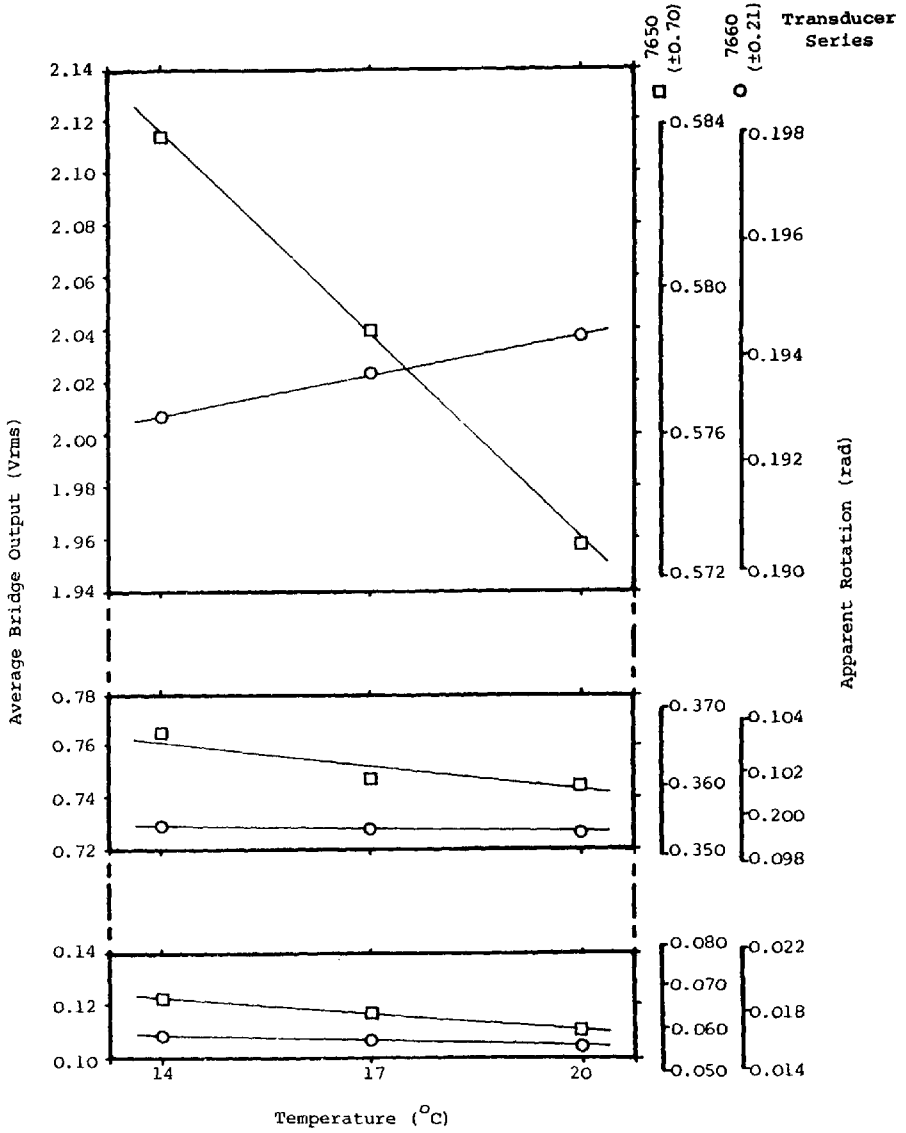

EFFECT OF TEMPERATURE ON THE AVERAGE BRIDGE OUTPUT FROM A GROUP OF THREE ELECTROLYTIC LEVELS OF EACH SERIES

FIGURE 5.12

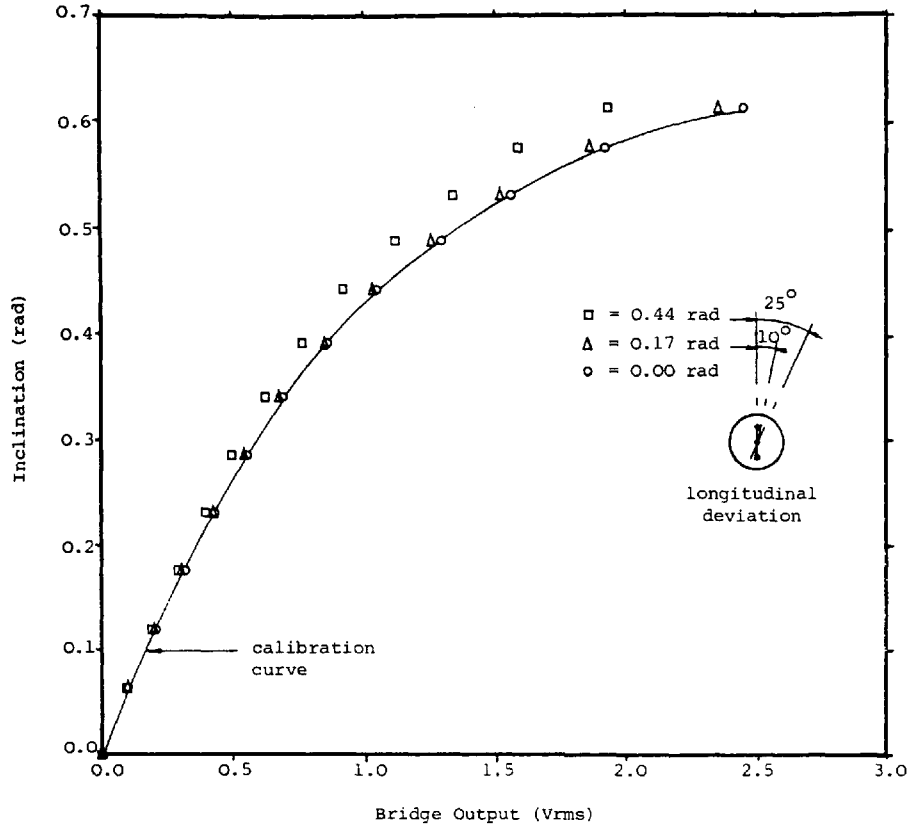

(a) 7650 Series

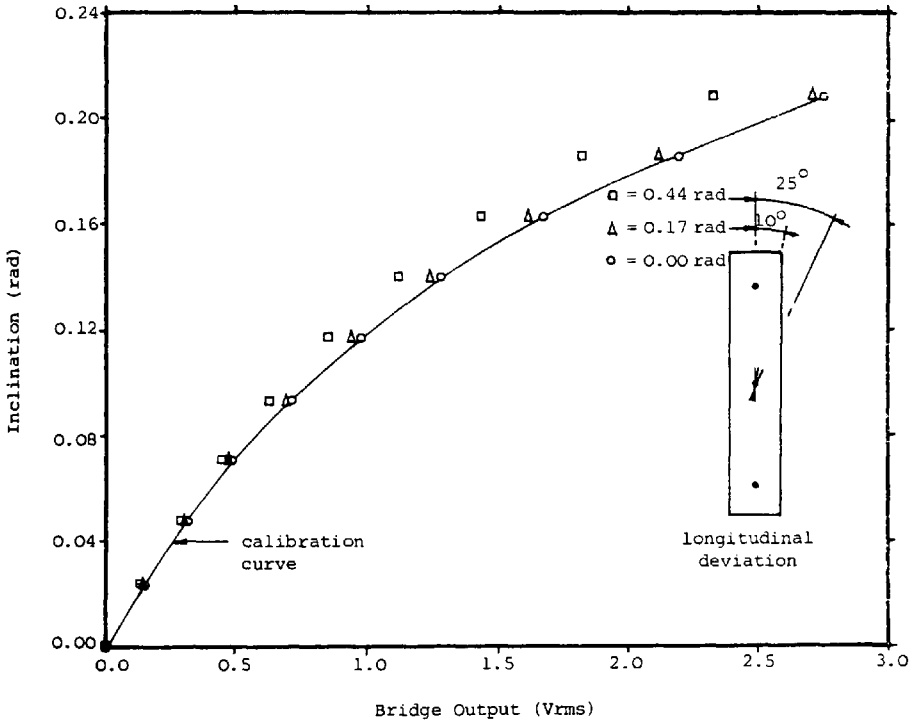

(b) 7660 Series

EFFECT OF MISALINEMENT OF THE LONGITUDINAL AXES OF THE CALIBRATION BEAM AND ELECTROLYTIC LEVEL ON BRIDGE OUTPUT

FIGURE 5.13

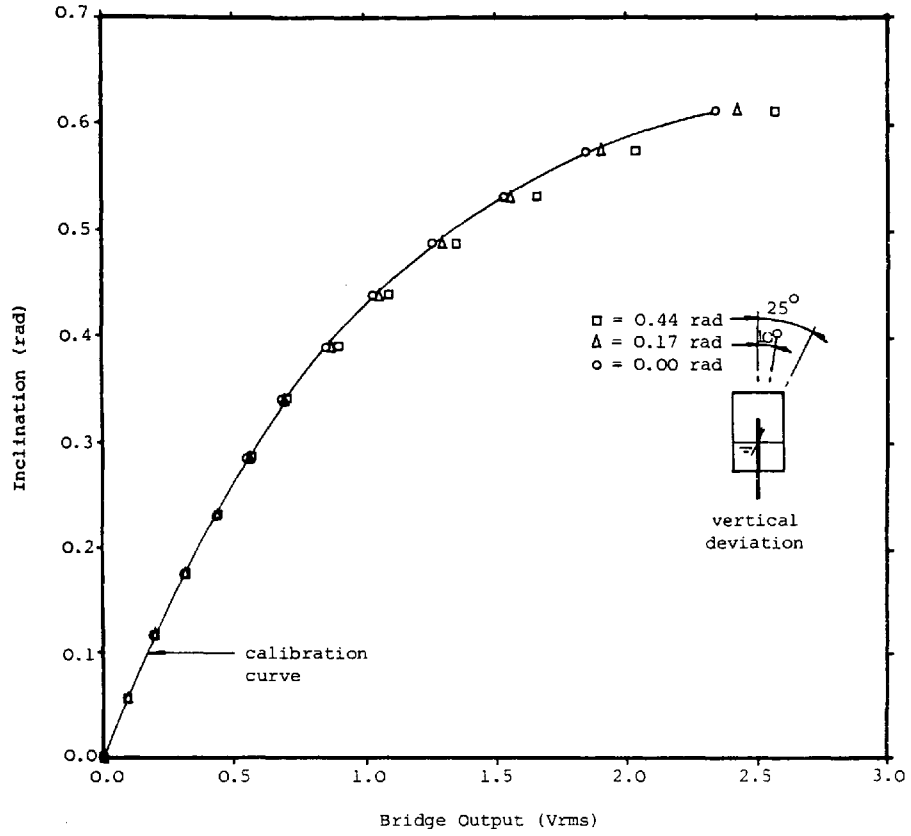

(a) 7650 Series

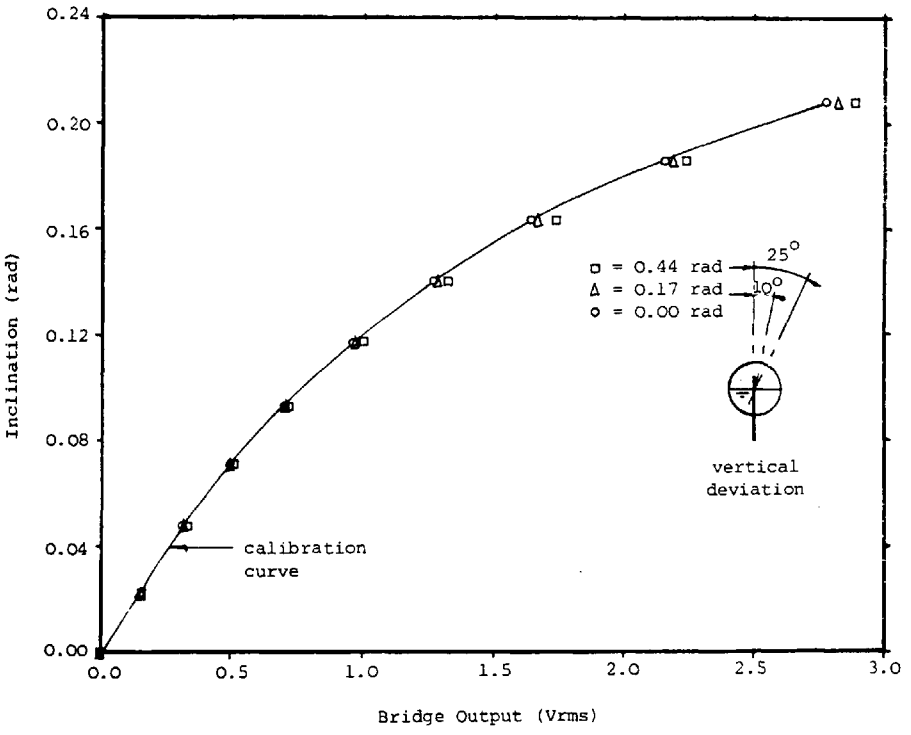

(b) 7660 Series

EFFECT OF MISALINEMENT OF THE VERTICAL AXES OF THE CALIBRATION BEAM AND ELECTROLYTIC LEVEL ON BRIDGE OUTPUT

FIGURE 5.14

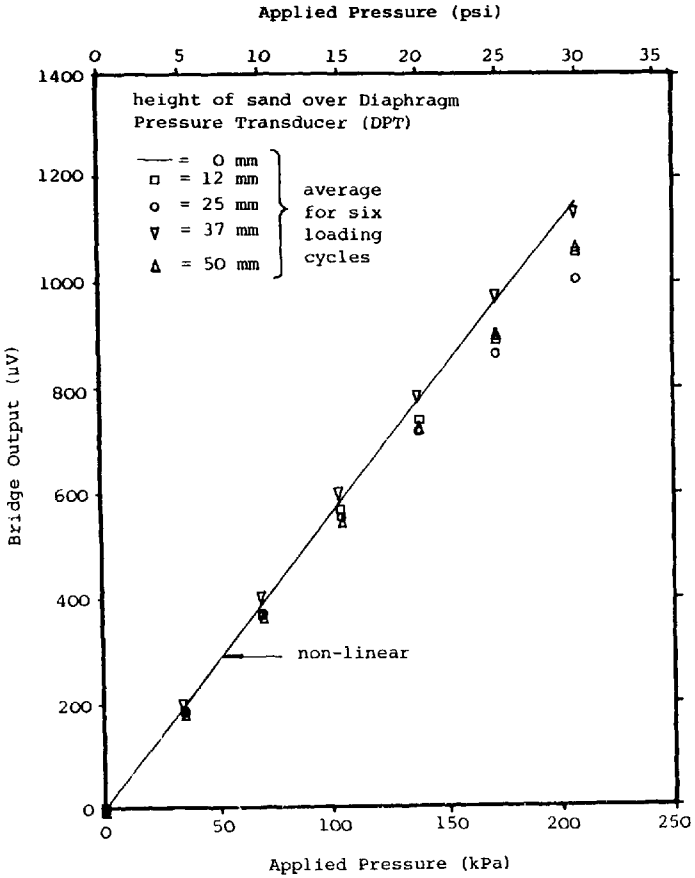

INFLUENCE OF DEPTH OF SAND COVER ON THE CALIBRATION CHARACTERISTICS OF A DIAPHRAGM PRESSURE TRANSDUCER

FIGURE 5.15

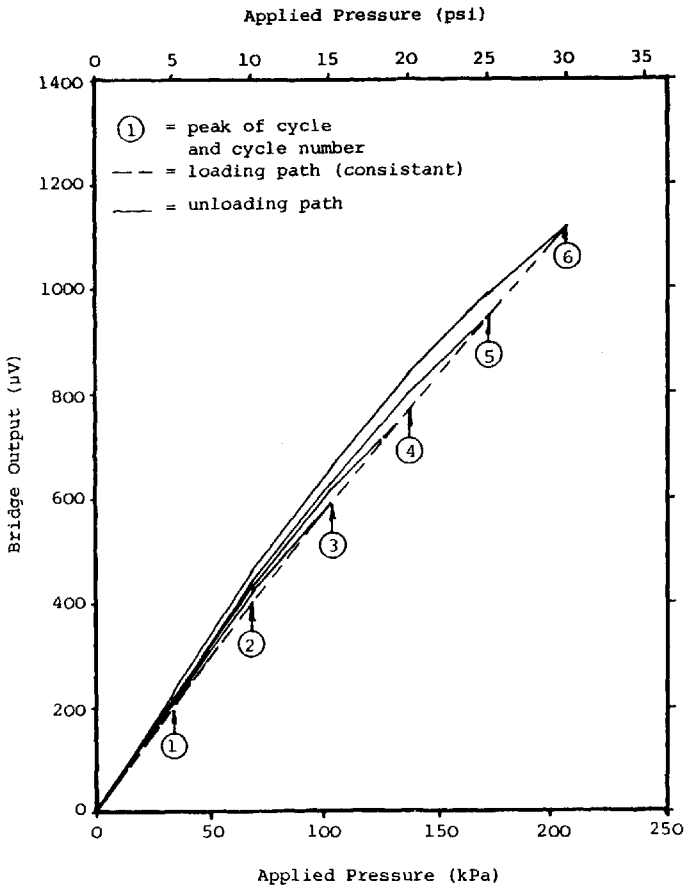

CALIBRATION CHARACTERISTICS OF A DIAPHRAGM PRESSURE TRANSDUCER WITH 50 mm OF SAND COVER UNDER AN INCREMENTED CYCLIC LOAD OF INCREASING MAGNITUDE

FIGURE 5.16

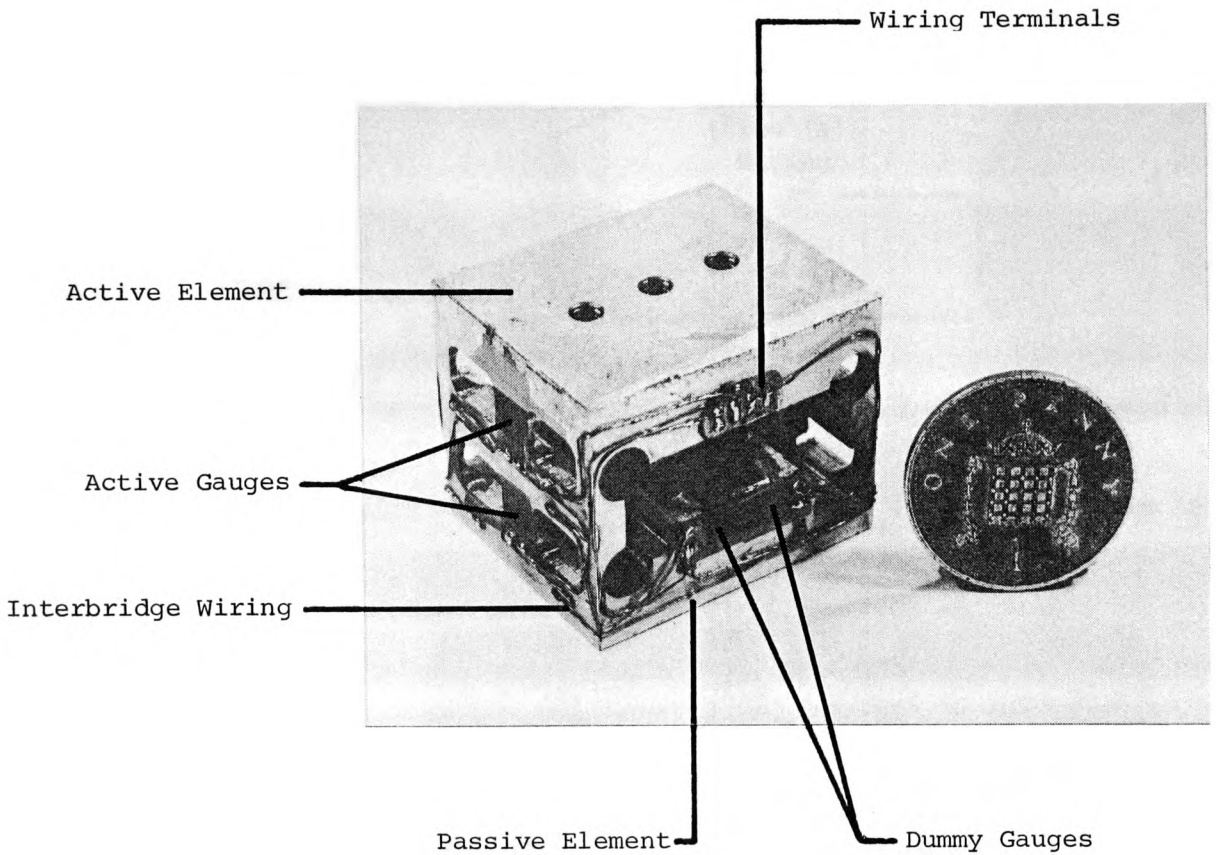

BOUNDARY ORTHOGONAL STRESS TRANSDUCER (t = 0.6 mm)

PLATE 5.1

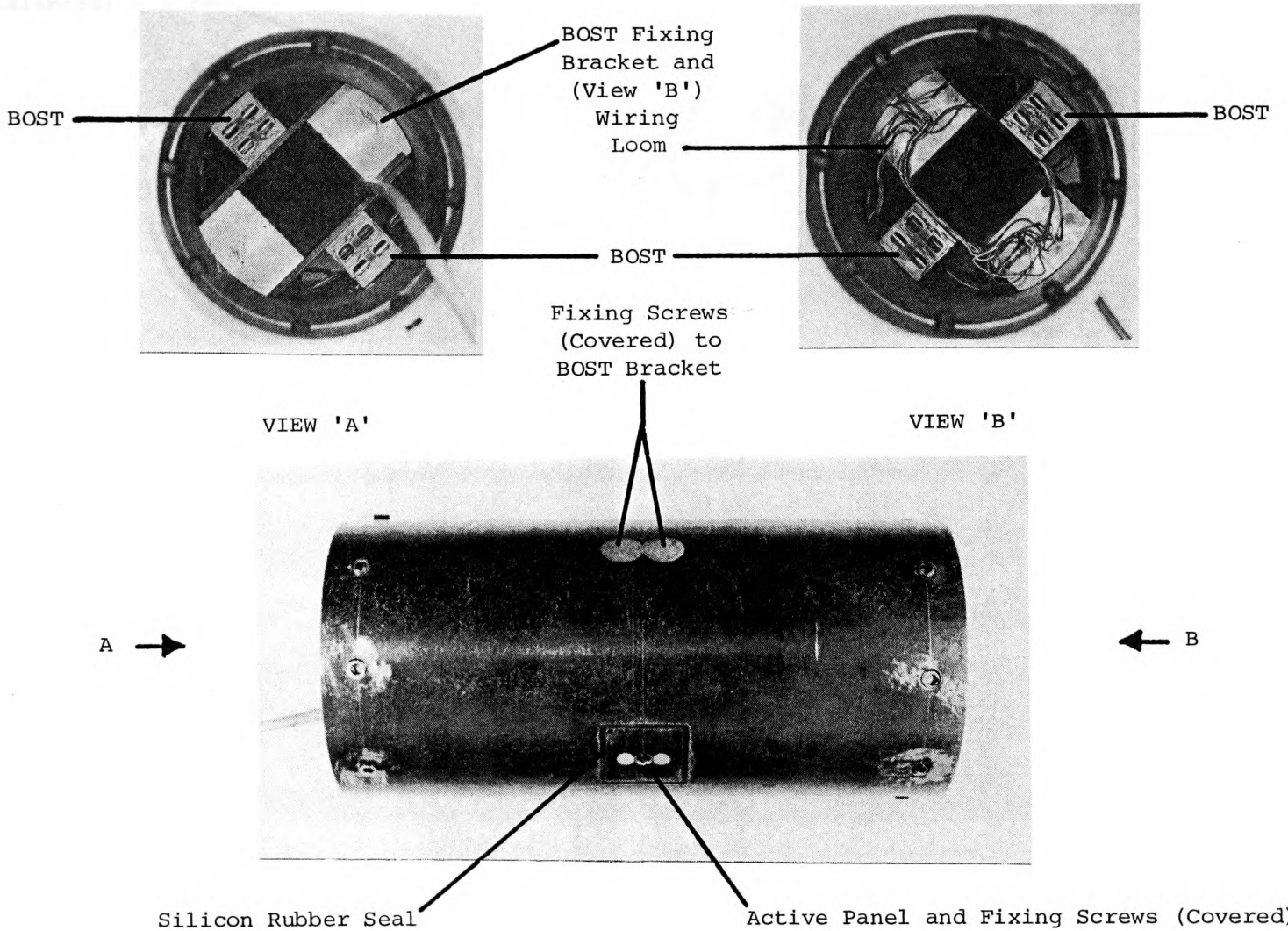

PILE SECTION WITH INSTALLED BOUNDARY ORTHOGONAL STRESS TRANSDUCERS

PLATE 5.2

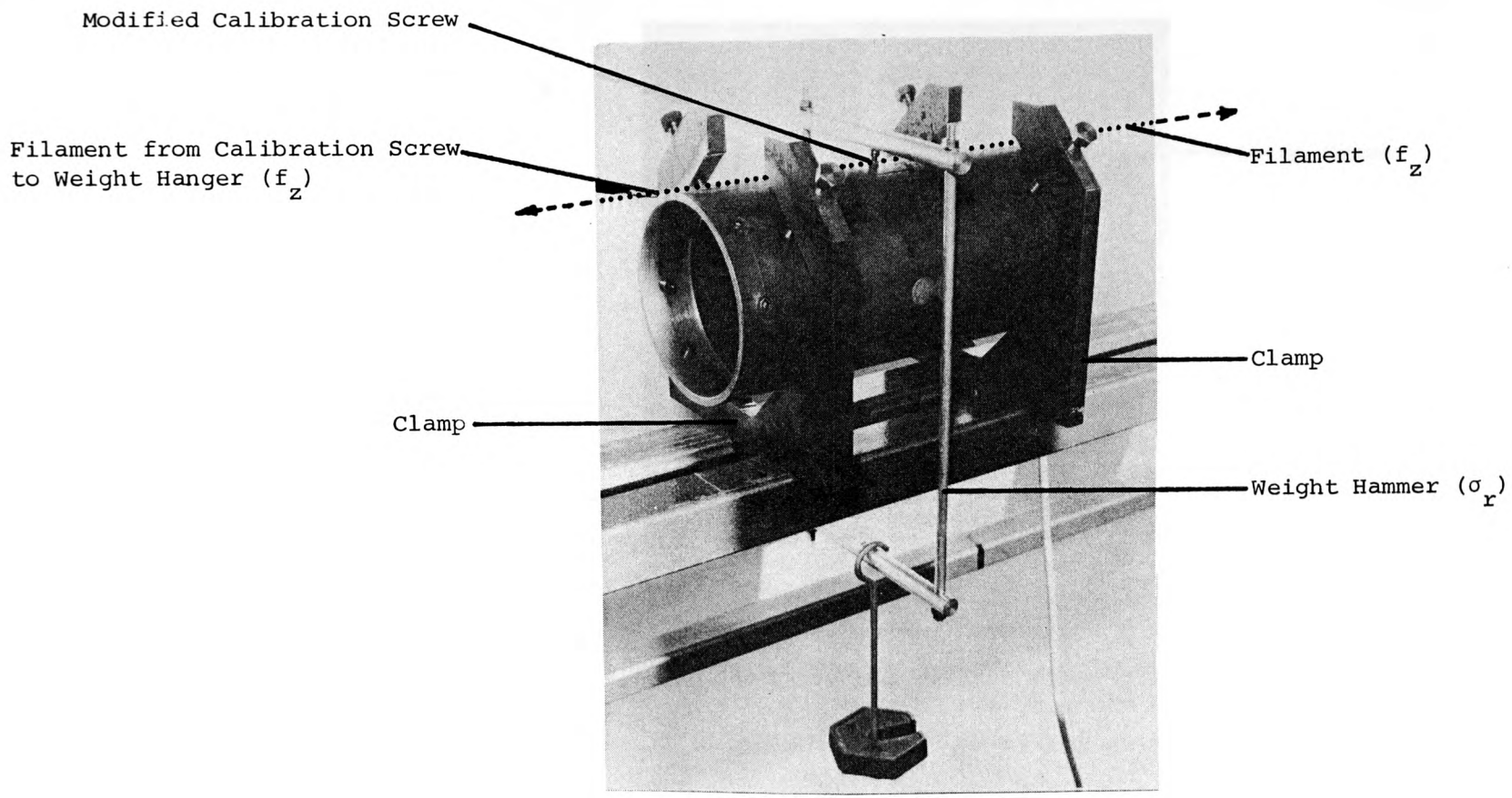

CALIBRATION RIG FOR BOUNDARY ORTHOGONAL STRESS TRANSDUCERS

PLATE 5.3

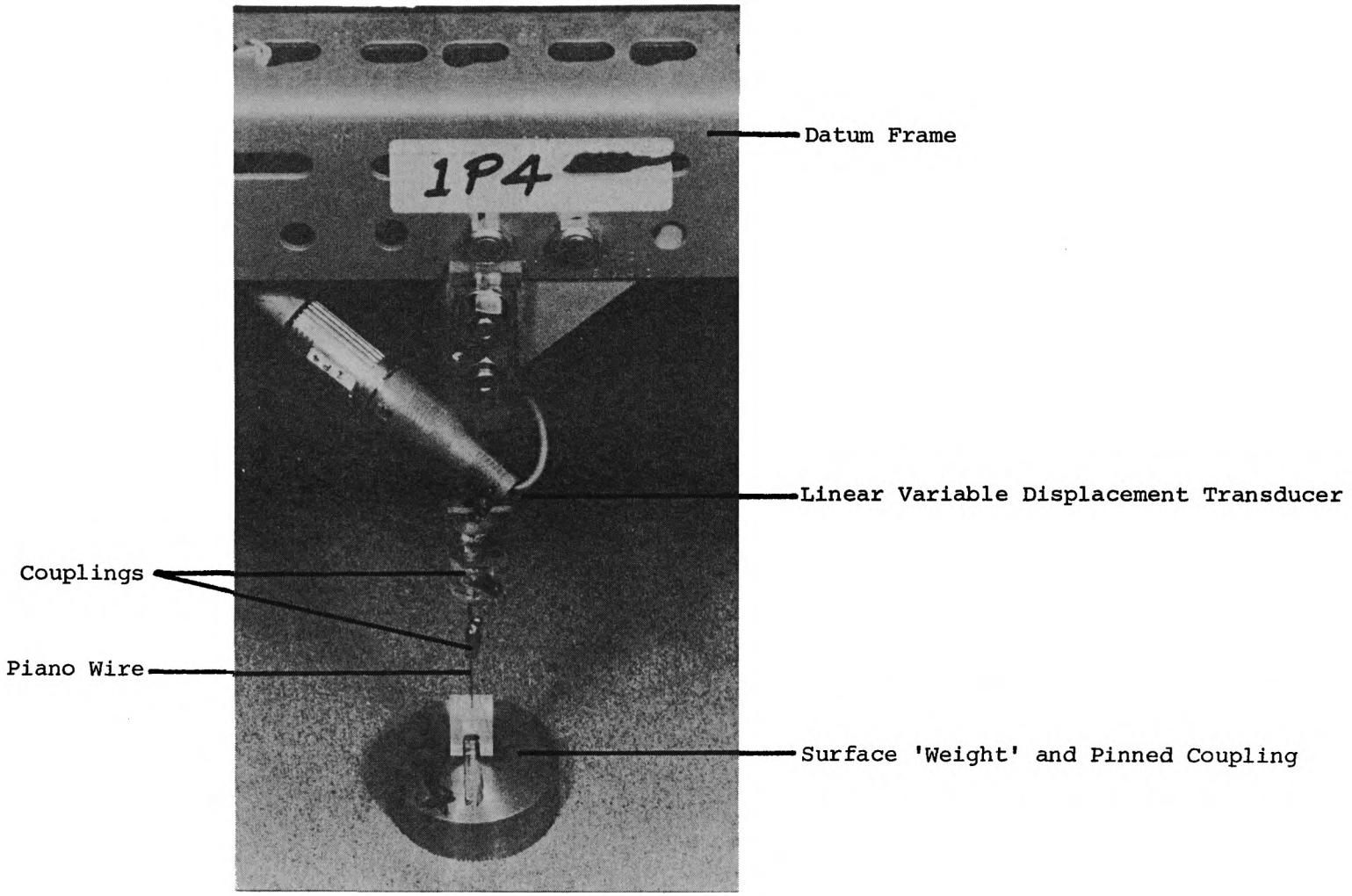

SURFACE DISPLACEMENT MONITORING SYSTEM

PLATE 5.4

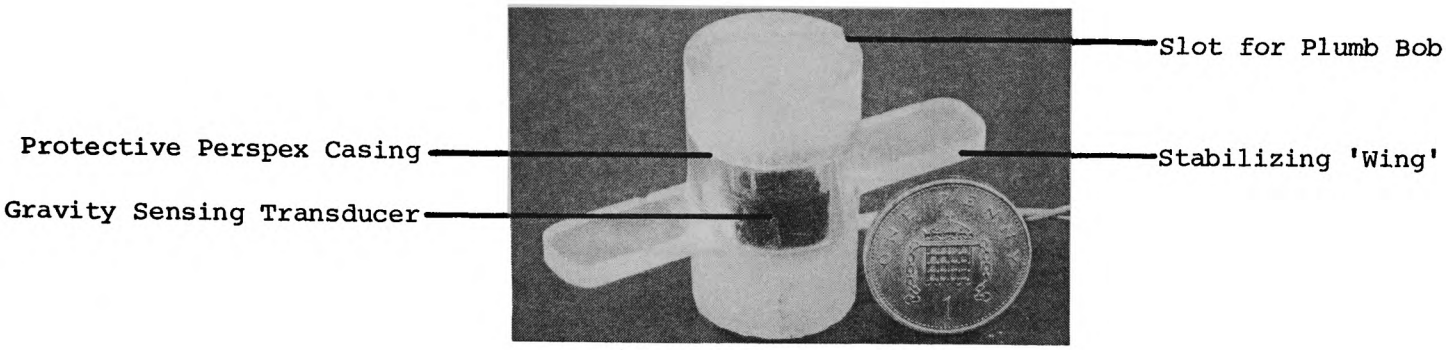

TYPE 7650

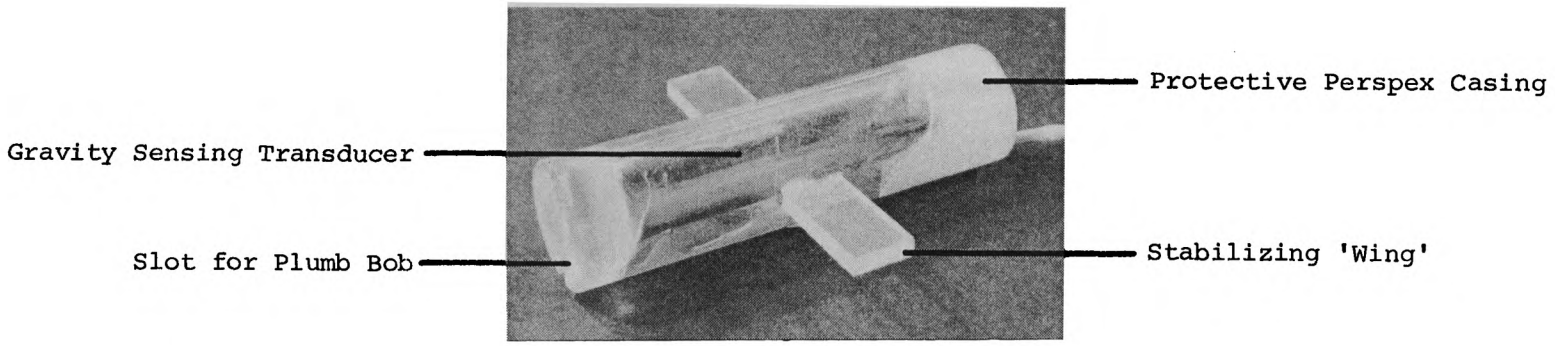

TYPE 7660

ELECTROLYTIC LEVELS

PLATE 5.5

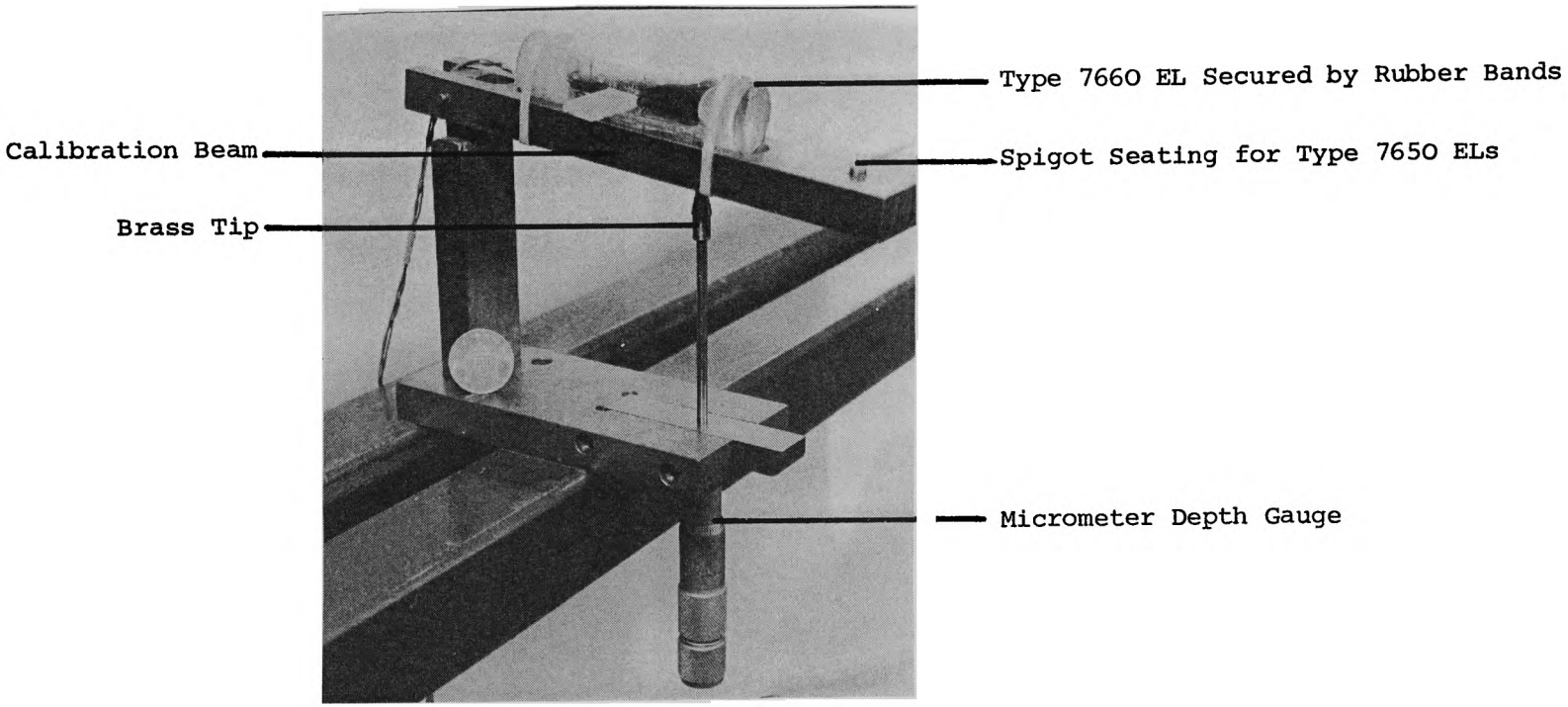

CALIBRATION RIG FOR ELECTROLYTIC LEVELS

PLATE 5.6

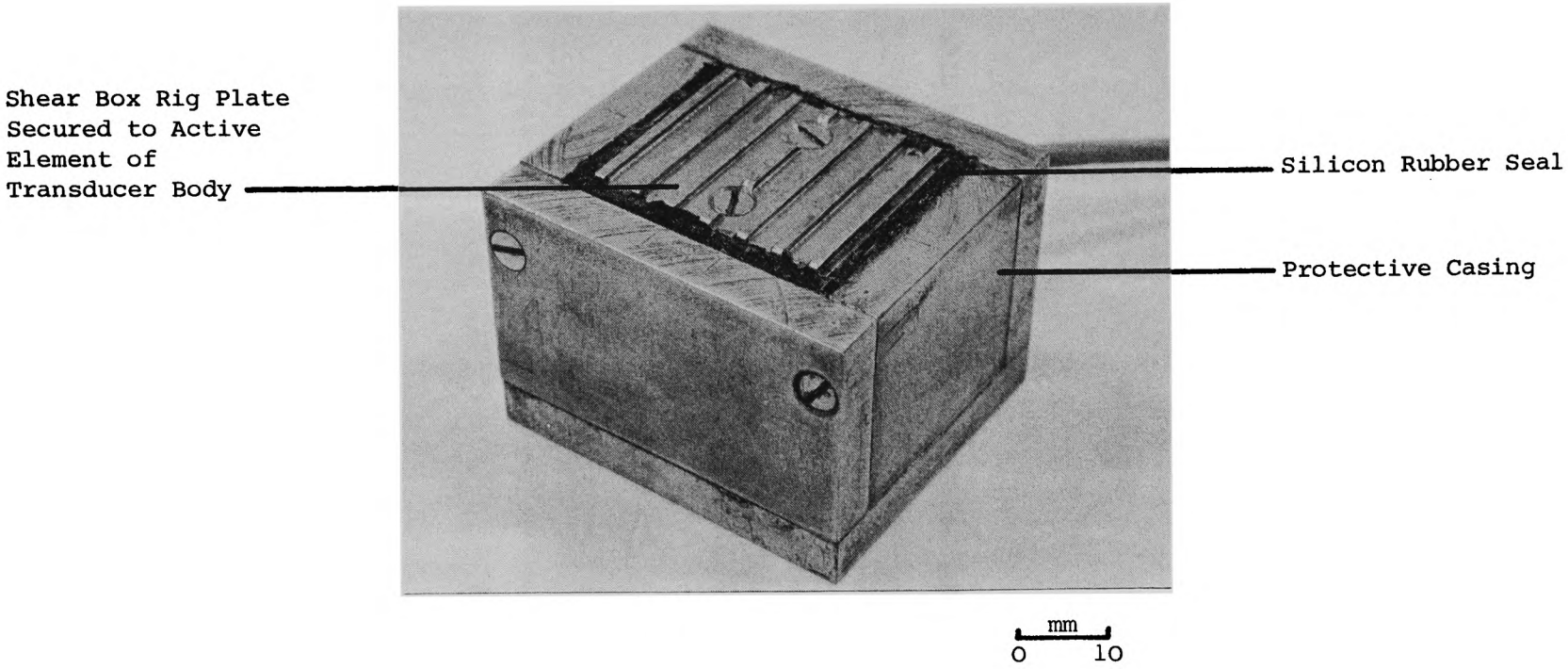

INTERFACE SHEAR STRESS TRANSDUCER

PLATE 5.7

CHAPTER 6

SOIL PLACEMENT AND INSTRUMENTATION, AND TEST PROCEDURES

CHAPTER 6

SOIL PLACEMENT AND INSTRUMENTATION, AND TEST PROCEDURES

6.1 Introduction

The techniques and procedures outlined in this chapter are those adopted as a consequence of a preliminary investigation, conducted with limited soil instrumentation in a homogeneous sand profile.

The sand was placed in ten 255.0 mm layers, which allowed the soil instrumentation to be located at various depths within the sand profile during construction. Each layer of soil instrumentation was placed in two 180^0 spirals. This arrangement permitted the duplication of instrumentation in diametrically opposite pairs and ensured that the resulting data was representative of the behaviour of the soil profile as a whole (Figures 6.1(a), (b) and 6.2). The minimum distance between any single item of instrumentation and the pile shaft was 103.0 mm, corresponding to a distance of 150.0 mm from the pile axis. This was arrived at after examination of the sand displacement profiles presented by Vesic (1963) and Robinsky and Morrison (1964). The latter reported that the most pronounced vertical displacements within the sand were generally within a distance of 0.25B from the pile shaft.

The possibility of the wiring/piping associated with the soil instrumentation acting as reinforcement within sand, was considered. To minimise any such effects the wiring/piping was radiated horizontally from the pile axis wherever possible, whilst that portion within the

immediate proximity of the pile, closer than 460.0 mm (4.0B), was concertinaed in order to accommodate the greater horizontal soil displacements anticipated within this region.

Initial concern over the possible damage to, or loss of, soil instrumentation during the tank emptying operation was proved to be unfounded during the preliminary investigation. However, the precaution was taken of relocating two electrolytic levels (ELs) and two density samples. These were A4I1 and A4I2, which were moved from stations 9 and 5 to 11 and 4 respectively. Density samples B5D5 and B1D3 were transferred from stations 8 and 9 to 10 and 11 respectively. Any remaining instrumentation within the 'critical sector', indicated on Figures 6.1(a) and (b), was readily recoverable by hand excavation.

6.2 Sand Placement Procedure

The sand placement apparatus employed by Kay (1980) consisted of a conic hood, housing a 2.36 mm mesh by 300.0 mm diameter sieve, attached to the end of a large flexible hose. The purpose of the sieve was to cause the sand to 'rain' into the tank during placement. This arrangement hindered placement since the equipment was heavy and difficult to manoeuvre; an undesirable feature in view of the quantity and sensitivity of the soil instrumentation. The conic hood was, therefore, dispensed with and the sand was allowed to fall freely from a height of approximately 100.0 mm from the open mouth of the hose. A bend was maintained in the lower portion of the hose in order to retard the sand flowing down the hose. It was realised that a technique of this nature could produce some stratification in the sand. The influence of this on the behaviour of

the pile was, however, considered to be mimimal in view of the relative size of the pile. During pile installation, however, the load/penetration profiles (Figures 7.1(a), (b) and (c)) indicated an increase in pile base resistance in the region of the third layer of density samples (D3s). This was almost certainly due to the higher placement density of sand layer 6 as a consequence of the additional 'work per unit volume' applied to the sand in placing and levelling the half layers above and below these density samples.

Checks were made on the density and uniformity of each sand layer during placement using a California Bearing Ratio (CBR) mould and a 12.7 mm diameter Dynamic Penetration Probe respectively. The CBR mould was placed on the surface of the previous sand layer, remote from any instrumentation. The sand was then placed, stopping only to excavate and retrieve the CBR mould once it had been completely covered by the sand. The density of the sand contained therein was then determined. This procedure was undertaken at two locations in each sand layer. On completion of each layer and prior to installing the instrumentation, a Dynamic Penetration Probe was driven through the upper two layers of sand and the number of blows per 50.0 mm penetration were recorded. This was undertaken at two diametrically opposite locations, alternating between points 'A' and 'B' (Figure 6.1(a)) with successive sand layers. The Dynamic Penetration Probe results and 'as placed' densities are presented on Figures 6.3 and 7.9(a), (b) and (c) respectively. It was concluded from these results that:

(i) Good repeatablity of sand density was achieved throughout the test programme.

(ii) The sand profile was relatively uniform with the exception of

layer 6, for which a higher driving resistance was clearly indicated by the Dynamic Penetration Probe results.

6.3 Procedure Adopted for Setting-Out Soil Instrumentation

The wall of the testing tank was marked-out to indicate the level of the various sand layers and the stations of all soil instrumentation.

The following procedure was employed to locate the instrumentation within the sand tank. A section of pipe, 114.0 mm in diameter by 380.0 mm long, with a pair of 'cross-wires' attached to one end which intersected on the longitudinal axis of the pipe, was clamped in the pile guide. A 'Plumb-Bob' was suspended from the intersection point of the cross-wires in order to project the pipe (pile) axis onto the surface of the sand layer in question, and the point marked. The end of a 1450.0 mm measuring rod (tank radius = 1500.0 mm), to which a small bubble level was secured in order to ensure that all distances measured were horizontal, was alined between the centre point and the appropriate station marker on the tank wall. The location of the instrument (radius from the pile axis) was then marked immediately adjacent to the edge of the measuring rod. It was estimated that instrumentation could be located to an accuracy of about ±5.0 mm by this method.

6.3.1 Sand/Plaster Density Samples

A paper former, as described in Appendix 5.1, was placed on the surface of the sand at the desired location. In order to identify the sample on

retrieval as the tank was emptied, a small paper label was placed on the sand within the former. The sand/plaster mixture was then poured from a 'Kilner' jar into the former, allowing a constant minimum fall and following a regular and even placement pattern. When full, sufficient sand to support the sand/plaster mixture was placed lightly around the former to the full height of the density sample, prior to carefully lifting the former free. This procedure was repeated for every density sample on a given layer before locating the water/detergent injection pipes. Each injection pipe was sited to vent centrally over a given density sample.

In addition to the array of samples used to monitor the change in sand density as a consequence of pile installation, two further density samples were included in each layer of density samples above 1275.0 mm (11.2B) depth at the outer limit of instrumentation. A further pair of density samples were sited midway between 1275.0 mm (11.2B) depth and the base of the sand tank. These samples were hydrated a day prior to testing in order to determine the initial density profile within the sand.

As a check on the performance of the density samples remote from the pile axis, two CBR moulds were placed diametrically opposite each other within sand layer 6, 300.0 mm in from the tank wall. These were left in place and retrieved on completion of the test, as the tank was emptied, in order to determine the density of the sand contained therein (Section 7.3.1 Refer).

6.3.2 Diaphragm Pressure Transducers

It was essential that the DPTs be placed horizontal. This was achieved with the aid of a small bubble level.

Once in place an initial zero reading was taken for each transducer. This allowed the increase in effective overburden stress to be monitored during sand placment. The increase in effective overburden stress recorded on completion of soil profiles S/S1 and S/M1 is given in Table 6.1 (values for S/S2 were not recorded). The magnitude of the measured and calculated effective overburden stresses for both profiles were in reasonable agreement.

6.3.3 Electrolytic Levels

The electrolytic levels (ELs) were energized with alternating current (A.C.) in order to prevent polarisation of the electrodes. A feature of A.C. is its nominal 'positive' polarity when measured in Vrms. This presented a minor difficulty with the operation of the ELs, since the output was always positive regardless of the inclination. In order to overcome this the ELs were initially installed inclined, dipping away from the pile axis. It was found that an inclination corresponding to an output of around 0.8 Vrms was sufficient to prevent the ELs rotating through and beyond the null point during pile installation. This obviated the need to change calibration constants during a test sequence. To ensure that the ELs were installed with the electrodes in a vertical plane, a miniature Plumb-Bob was suspended from a small 'gibbet' which located in a vertical slot on the end face of the protective casing of

the ELs. The slot in the protective casing was alined with the transducer electrodes. When the Plumb-Bob and the upright member of the 'gibbet' were in the same vertical plane along the longitudinal axis of the EL, the transducer electrodes were considered to be vertical (Plate 6.1). Radial alinement of the ELs was achieved by orientating the longitudinal axis of the EL with the edge of the measuring rod situated between the pile axis marker and the station marker on the wall of the sand tank.

6.3.4 Surface Displacement Transducers

The placement of the surface displacement transducers consisted of connecting the 'weights' (Section 5.6 Refer) to, and alining them vertically below, the array of LVDTs attached to the datum frame. It was important to ensure that the rotational axis of the 'weights' were tangential to the pile circumference. To permit both heave and settlement of the surface to be recorded, the LVDTs were adjusted to supply an initial output voltage equal to 33.0% of full scale deflection.

6.4 Preparation of the Secondary Clay Tank

Having previously assembled the secondary clay tank it was alined centrally below, and square to, the pile axis. The inside of the cylindrical wooden former was graduated into eight 150.0 mm layers, each of which was further divided into five 30.0 mm sub-layers. Each sub-layer represented the maximum thickness of a single layer of compacted clay (Section 3.3.4 Refer). The sides and base of the wooden

former were then lined with a continuous membrane of heavy duty polythene sheeting in order to limit moisture losses.

6.4.1 Remixing and Placement of the Clay

The clay had previously been mixed from a dry state to a conditioning moisture content of 15.0%, at which it was stored for approximately 18 months (Section 3.1 Refer). Samples of clay were removed from each conditioning bin in order to ascertain the initial moisture content of the clay prior to remixing to a target moisture content/shear strength of 19.0%/50.0 kPa. An indication of the shear strength of each batch at the end of remixing was obtained using a Pocket Penetrometer.

Sufficient clay was placed in the secondary clay tank to produce a layer 30.0 mm thick when compacted. Compaction was undertaken in accordance with Section 3.3.4. Each of the three passes over the clay surface were in a left to right direction, orientated at 120^0 to one another. During the compaction process the Kango hammer was inclined to ensure a better kneading action as the platten penetrated into the clay. After placing each 150.0 mm primary layer, four 38.0 mm diameter by 180.0 mm deep core samples were taken. Two of the samples were used to determine the unconfined compressive strength of the clay, the remainding two were used to monitor soil parameters such as moisture content, degree of saturation and bulk density (Figure 6.4). From layers 3 and 6, two 100.0 mm diameter by 150.0 mm deep clay cores were removed. From each of these a sample was prepared to suit the one dimensional consolidation apparatus. These were tested to determine the magnitude and duration of any consolidation settlement due to the self-weight of the clay and the sand

overburden (Section 3.3.6 Refer).

6.4.2 Application of Vinyl Membrane

The clay was placed to the full depth of the secondary tank and the surface trimmed and smoothed prior to applying the vinyl membrane in accordance with case (iii), outlined in Section 3.4.2.

6.4.3 Sand/Clay Interface Instrumentation

The procedure adopted for locating the instrumentation on the sand/clay interface was the same as that employed within the sand (Section 6.3 Refer). With one exception, namely that of the ISSTs, the type of instrumentation deployed on the sand/clay interface was the same as that at a comparable depth in S/S1 and S/S2. All instrumentation located on the sand/clay interface was recessed flush with the surface of the clay.

6.4.4 Sand Placement Around the Secondary Clay Tank

The procedure adopted for placing sand around the secondary clay tank was the same as that outlined in Section 6.2.

6.5 Pile Installation and Test Procedure

The pile was installed by jacking in increments of about 100.0 mm, at a

constant rate of displacement to a predetermined depth. Thereafter it was load tested in accordance with the following:

(i) Constant Rate of Penetration (CRP).

(ii) Maintained Load (ML).

(iii) Constant Rate of Uplift (CRU).

6.5.1 Pile Installation

The pile was jacked into the soil profile at a constant rate of 10.0 mm/min, in approximately 100.0 mm increments, to the target depth of 1845.0 mm (16.1B). This rate of installation was chosen since it was sufficiently fast to allow a complete test sequence to be undertaken in one working day, and yet slow enough to permit detailed monitoring of the installation history. It was estimated that the pile penetrated an additional 1.25 mm (1.1%B) during the time taken by the data logger to scan the 100 channels of instrumentation. This was considered to have an insignificant effect on the results.

The above rate of pile installation was of a similar order to those employed by other investigators working with piles of a comparable diameter.

Rate mm/min	Pile(B) mm	Soil medium	Reference
0.50 to 10.00*	200.0	sand	Koizumi (1971)
21.00	100.0	clay	Butterfield and Johnston (1973)
6.35	76.2	sand/clay	Meyerhof and Valsangkar (1977)
12.70	76.0	clay/loose and dense sand	Meyerhof and Sastry (1978(a))
3.75 to 15.00	168.0	clay	Cooke et al (1979)

* Rates reported refer to CRP test. Installation rates were not reported, however, the maximum possible jacking rate was 12.0 mm/min.

According to Cooke et al (1979) installing piles by jacking has several distinct advantages:

(i) The piles possess some of the characteristics of driven piles.

(ii) A complete load/penetration profile is obtained.

(iii) Short term load tests can be conveniently undertaken at a range of penetrations.

Pile verticality at the end of installation was calculated as 1/81 and 1/169 for S/S2 and S/M1 respectively (S/S1 was not recorded). These were within the limits set by CP2004 (1972) of 1/75 for vertical piles.

6.5.2 Constant Rate of Penetration Test

The capacity of the fully driven pile at 'failure' was determined by undertaking a CRP test. The resistance of a pile as determined by this method, assuming homogeneous soil conditions, can vary since the shear strength of the soil is affected by the rate of strain/penetration. According to Lambe and Whitman (1979) strain rates do not significantly influence the shear strength of dry sand, causing at most a 10.0% increase in Tanϕ'. A more realistic estimate of the increase in Tanϕ' is 1.0 to 2.0% for an increase in time to failure of 5.0 min to 5.0 millisec. However, the shear strength of a saturated soil under undrained conditions, such as that of the clay, may be increased by a factor of two with a reduction in time to failure of 1.0 hr to 5.0 millisec. This increase is due to the development of smaller excess pore water pressures with higher strain rates. In order to render the CRP test results comparable with the triaxial tests conducted on the soil, both were undertaken at the same rate (1.524 mm/min). The CRP test was terminated once the additional pile penetration had exceeded 30.0 mm (0.26B).

The influence of penetration rates on pile capacity are illustrated on Figure 6.5. Results from S/S2 conform with the idea of a higher soil shear strength with an increased rate of penetration. However, this effect was small and the ultimate pile capacity, as established from the installation data (10.0 mm/min) and the ML test, differ by ±3.0% respectively from that established from the CRP test. Similar observations were made in dense sand by Kerisel (1961) using a 45.0 mm diameter cone penetrometer, and Koizumi (1971) using a 200.0 mm pile. Comparable data from S/M1, where a majority of the pile capacity was

developed within the clay, indicated an increase in resistance with a reduced penetration rate. This was probably due to the clay not shearing under undrained conditions.

A suitable penetration rate for the CRP test of 0.813 mm/min (0.032 in/min) was recommended by Whitaker and Cooke (1961) for all soil types. However, they found that a rate of penetration one half to four times this value (0.407 to 3.252 mm/min) caused the load/penetration envelopes to diverge from the initial 0.813 mm/min envelope by not more than ±4.0% for a minimum penetration of 0.2B. Subsequently, Whitaker (1963) refined these limits to 0.762 mm/min (0.030 in/mm) for friction piles with an associated minimum penetration of 10.0% of the pile shaft diameter, and 1.524 mm/min (0.060 in/min) for end bearing piles with a minimum penetration of 25.0% of the pile base diameter, due to the greater displacement required to 'fail' a pile in non-cohesive soils. He further stated that providing the rate of penetration was steady, one half to twice the above rates were acceptable. The penetration rate employed by the author of 1.524 mm/min and minimum penetration of 0.26B complied with the above criteria.

In reality the CRP test was not conducted at a constant rate during the early stages of the test. This was due to the initial rapid build-up in pile resistance for a relatively small pile penetration. Thus, an element of the jack displacement was initially taken up in deflecting the reaction frame. Thereafter, the penetration rate was more or less constant. The maximum recorded initial deflection of the reaction frame was 2.3 mm. This was comparable with the maximum permitted movement of a pile displacement reference beam of 2.5 mm (Whitaker, 1963).

6.5.3 Maintained Load Test

The capacity of the pile at 'failure' was taken, for the purpose of calculating suitable loading increments during the ML test, as the maximum load applied to the pile during the CRP test prior to the jack being reset. The working load was taken as 40.0% of the 'failure' load, thereby assuming a factor of safety of 2.5. The pile was loaded in increments of 33.3% of the working load, since this supplied sufficient data points to define the load/settlement characteristics of the pile, as well as allowing the raw data from the ML test to be stored on a single floppy disk.

During the ML test the pile was loaded incrementally up to the working load and then unloaded in one step. The working load was then reapplied and incremental loading resumed until 'failure' was achieved. The pile was unloaded in two equal increments of load.

Cessation of movement was deemed to have occurred under each loading increment when the rate of penetration was less than 0.3 mm/hr. This was considered to have been achieved when the pile displacement, recorded in millimetres, was the same to two decimal places for three consecutive data scans. The minimum duration of any one loading increment was 10 mins. These criteria were in line with those proposed by Weltman (1980). The minimum rate of penetration was in reasonable agreement with that quoted by Poulos and Davis (1980) of 0.305 mm/hr, set by the ASTM, whilst CP2004 (1972) prescribes a minimum rate of 0.25 mm/hr.

At maximum load it was not always possible to fulfil the settlement rate criteria stated above, due to the extended period required to attain

equilibrium of the soil/pile system and the limited disk space available for storage of the raw data.

On completion of the ML test the sand/plaster density samples were hydrated, and a period of 20 mins allowed prior to undertaking the Constant Rate of Uplift (CRU) test.

6.5.4 Constant Rate of Uplift Test

The procedures adopted for this test, including the rate of displacement and displacement limit, were essentially the same as those of the CRP test. The test differed only in that the pile cap was securely clamped to the jack loading plate, attached to the integral load cell, which allowed tensile loads to be applied to the pile.

A strain controlled test, in preference to a stress controlled test, was undertaken in order to prevent the rapid withdrawal of the pile, which would otherwise have occurred once the ultimate uplift capacity of the pile was attained.

TEST NO	MEASURED							CALCULATED	PERCENTAGE DIFFERENCE
	1D3	1D2	1D1	2D1	2D2	2D3	Average	γZ_i	
S/S1	+16.71	+18.02	+18.31	+20.32	+17.76	+15.73	+17.81	+18.98	-6.2
S/M1	+21.44	+20.64	+21.59	+21.67	+18.95	+20.09	+20.73	+18.62	+11.2

COMPARISON OF THE SAND OVERBURDEN STRESS (kPa) RECORDED BY THE DIAPHRAGM PRESSURE TRANSDUCER WITH THAT CALCULATED FROM THE AVAILABLE SAND DENSITY DATA

TABLE 6.1

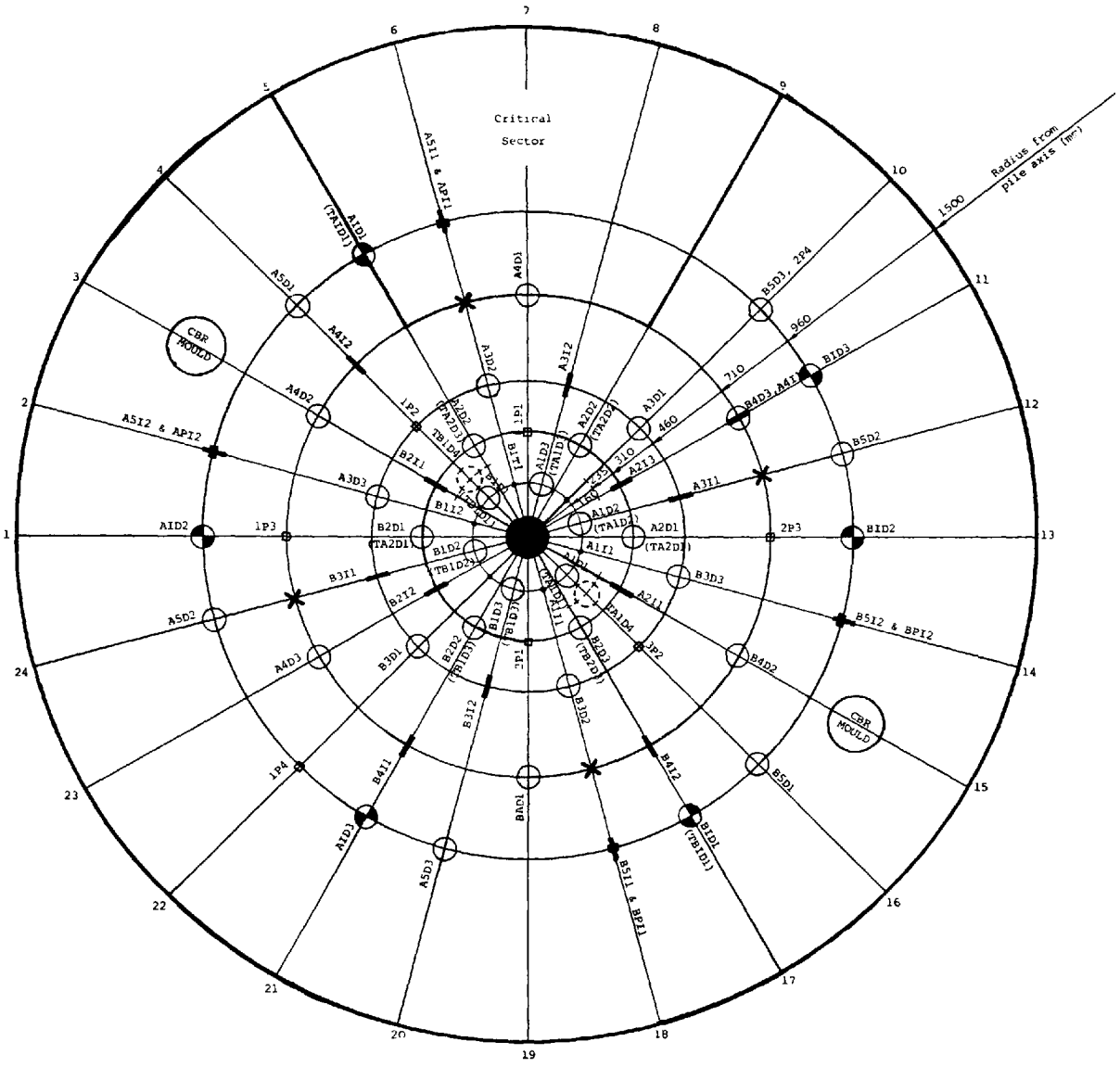

- series 7650 electrolytic levels
- series 7660 electrolytic levels
- series 7660 electrolytic levels connected to a LVDT
- surface displacement transducers
- sand/plaster density samples (those employed below Z=1275 mm in S/S1 and S/S2 are indicated in perenthesis)
- initial density sand/plaster density samples
- dynamic penetration probe locations

PLAN OF SOIL INSTRUMENTATION DEPLOYED IN SAND ABOVE INTERFACE LEVEL (Z_i = 1275.0 mm) IN ALL TESTS

FIGURE 6.1(a)

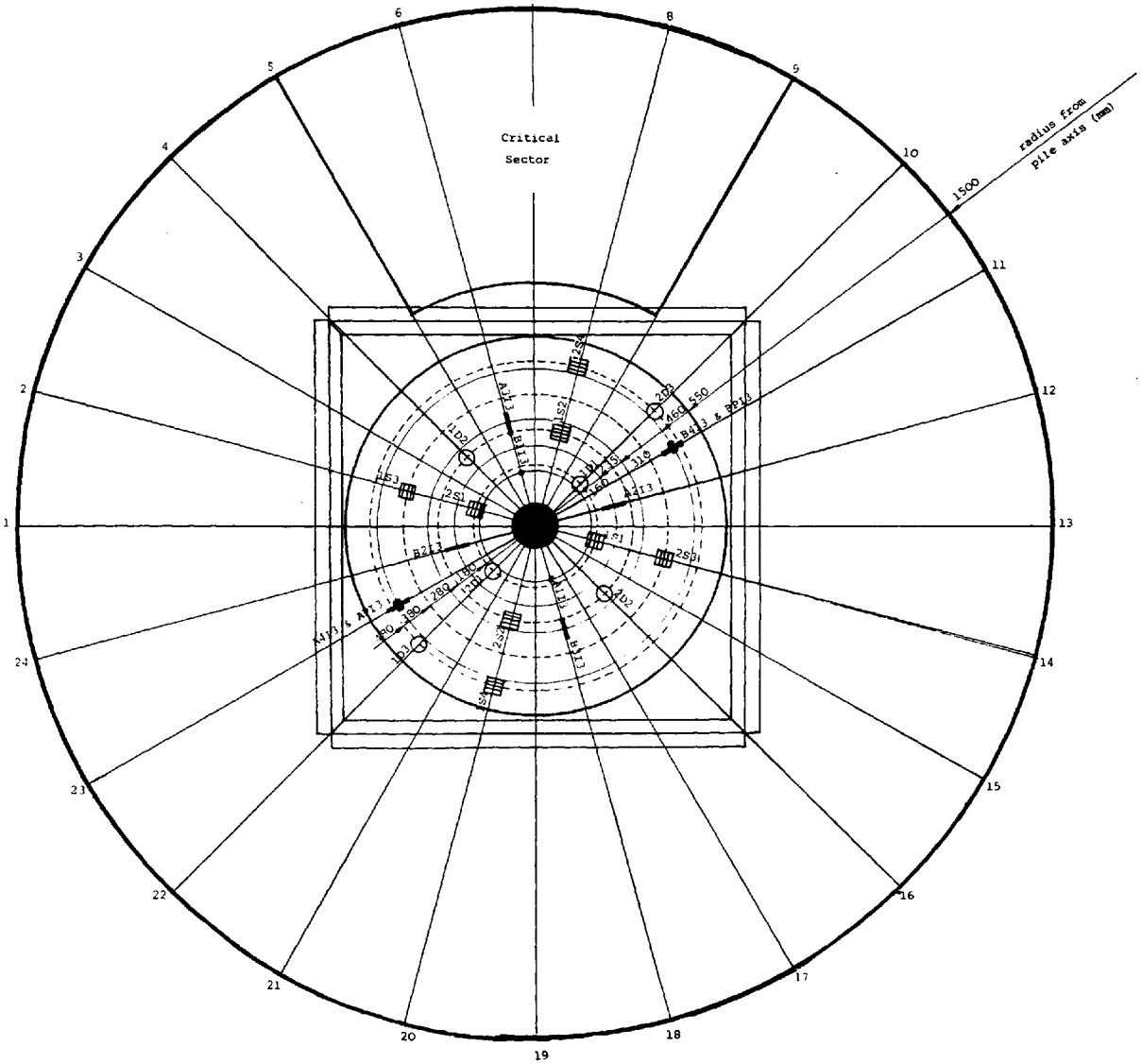

- series 7650 electrolytic levels
- series 7660 electrolytic levels
- series 7660 electrolytic levels connected to a LVDT
- diaphragm pressure transducers
- interface shear stress transducers

PLAN OF SOIL INSTRUMENTATION DEPLOYED ON THE SAND/CLAY INTERFACE (Z_i = 1275.0 mm) IN S/M1

FIGURE 6.1(b)

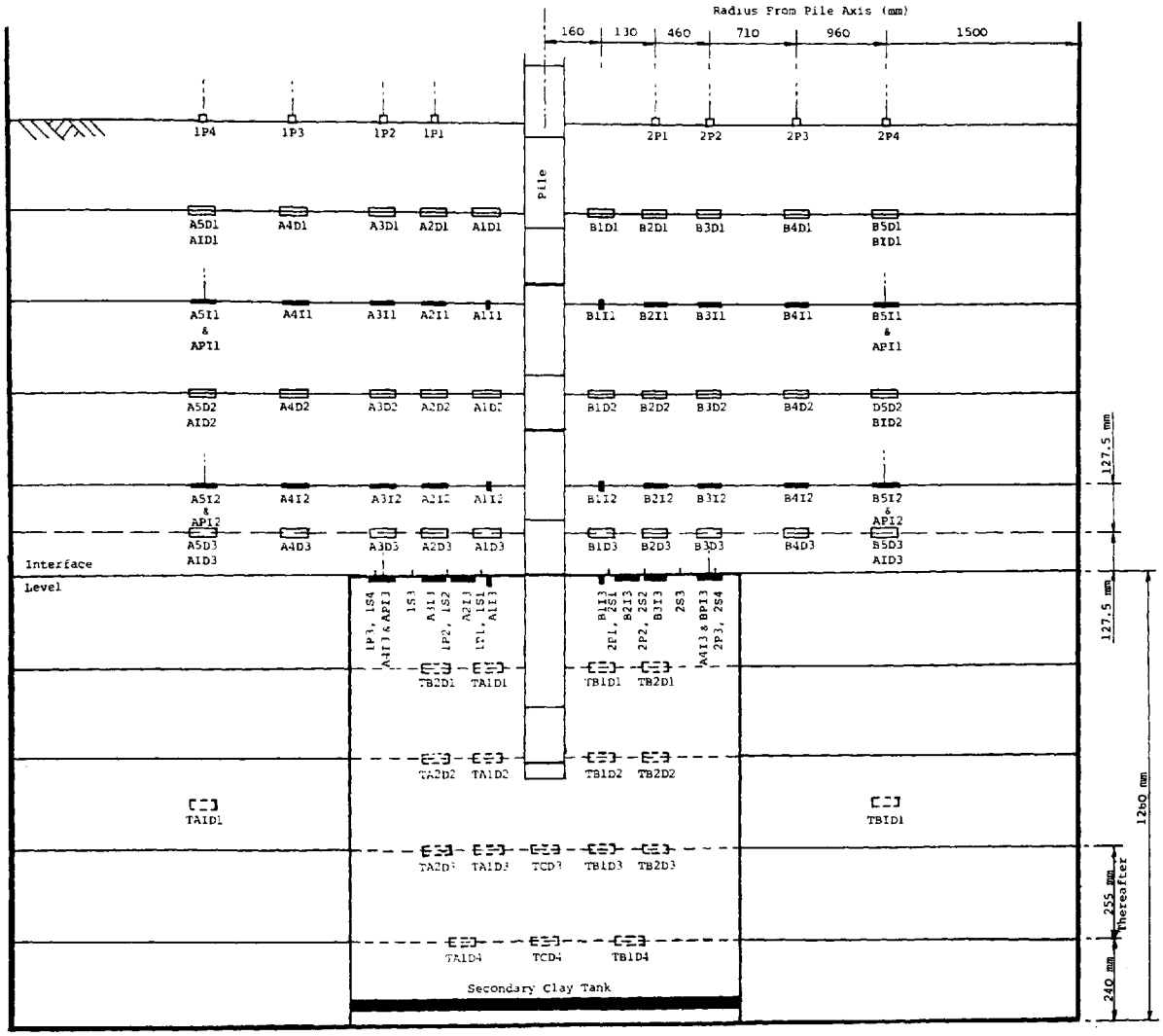

series 7650 electrolytic levels

series 7660 electrolytic levels

series 7660 electrolytic levels connected to a LVDT

surface displacement transducers

sand/plaster density samples

sand/plaster density samples employed below Z = 1275 mm in S/S1 and S/S2

(Interface shear transducers omitted in S/S1 and S/S2)
(Density samples below interface level omitted in S/M1)

A DIAMETRIC SECTION THROUGH S/M1 SHOWING THE ELEVATION AND RADIAL LOCATION OF THE SOIL INSTRUMENTATION TRANSPOSED ON TO A VERTICAL PLANE

FIGURE 6.2

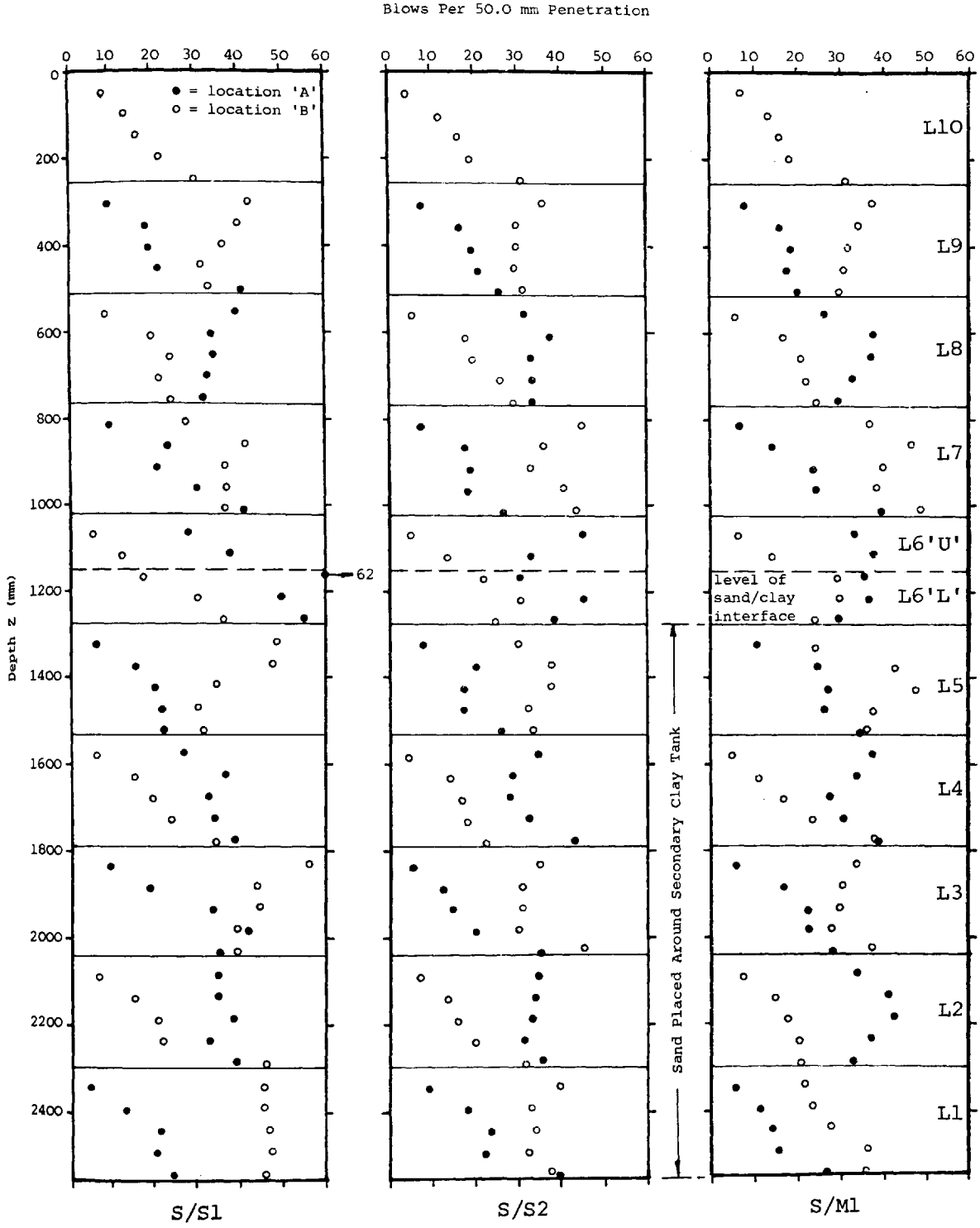

DYNAMIC PENETRATION PROBE RESULTS

FIGURE 6.3

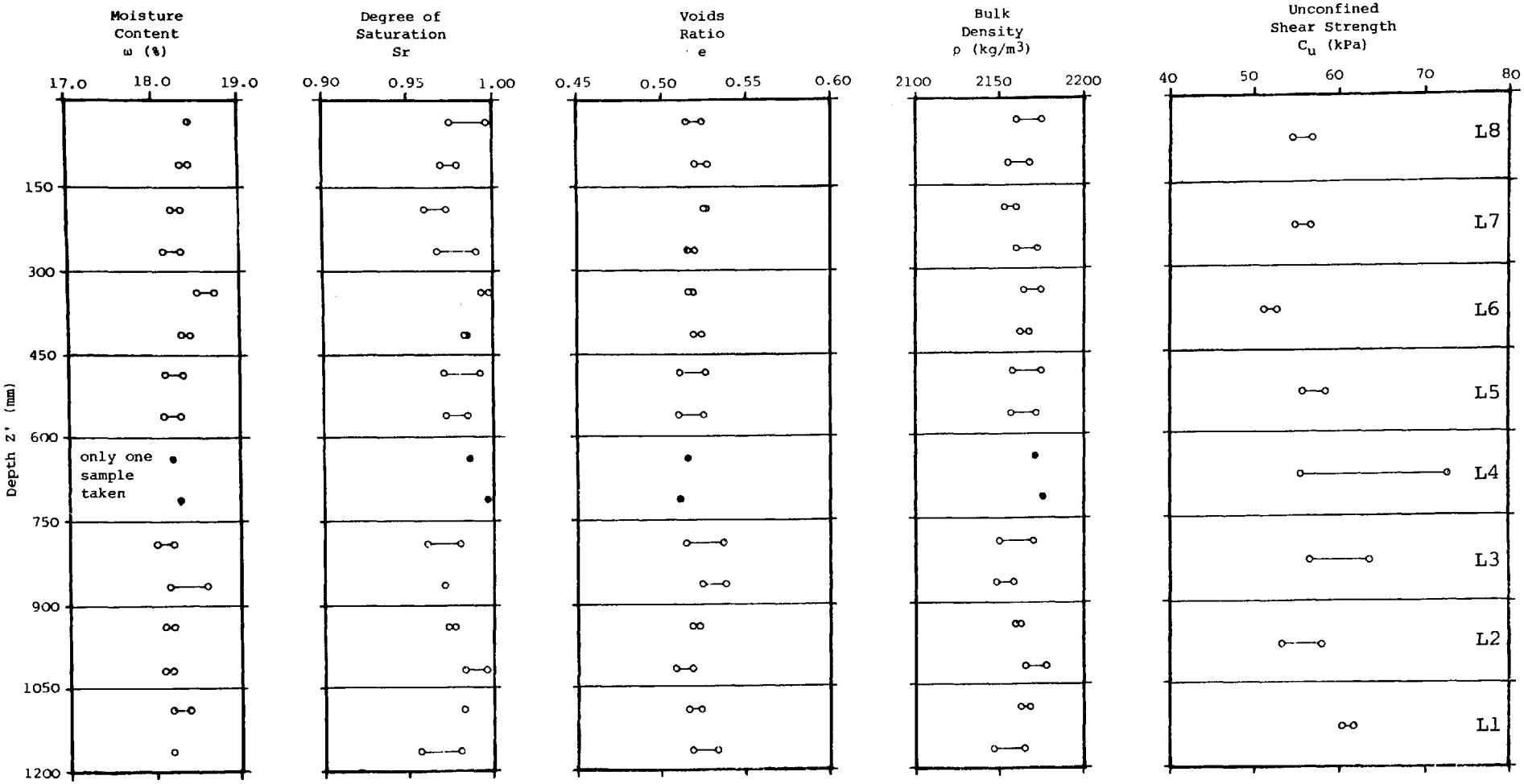

AS-PLACED PROPERTIES OR CLAY WITHIN SECONDARY CLAY TANK

FIGURE 6.4

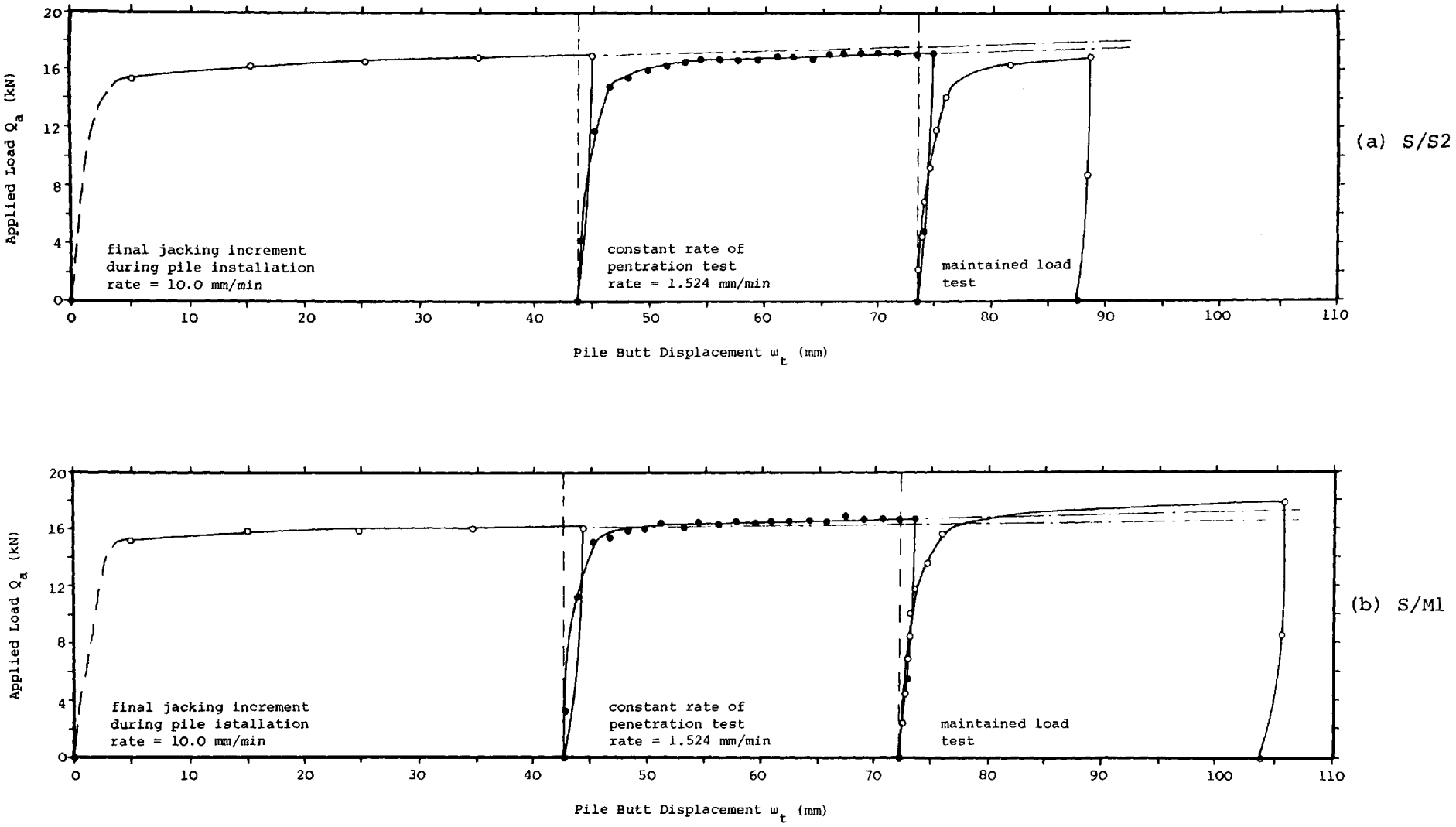

INFLUENCE OF PENETRATION RATE OF PILE CAPACITY

FIGURE 6.5

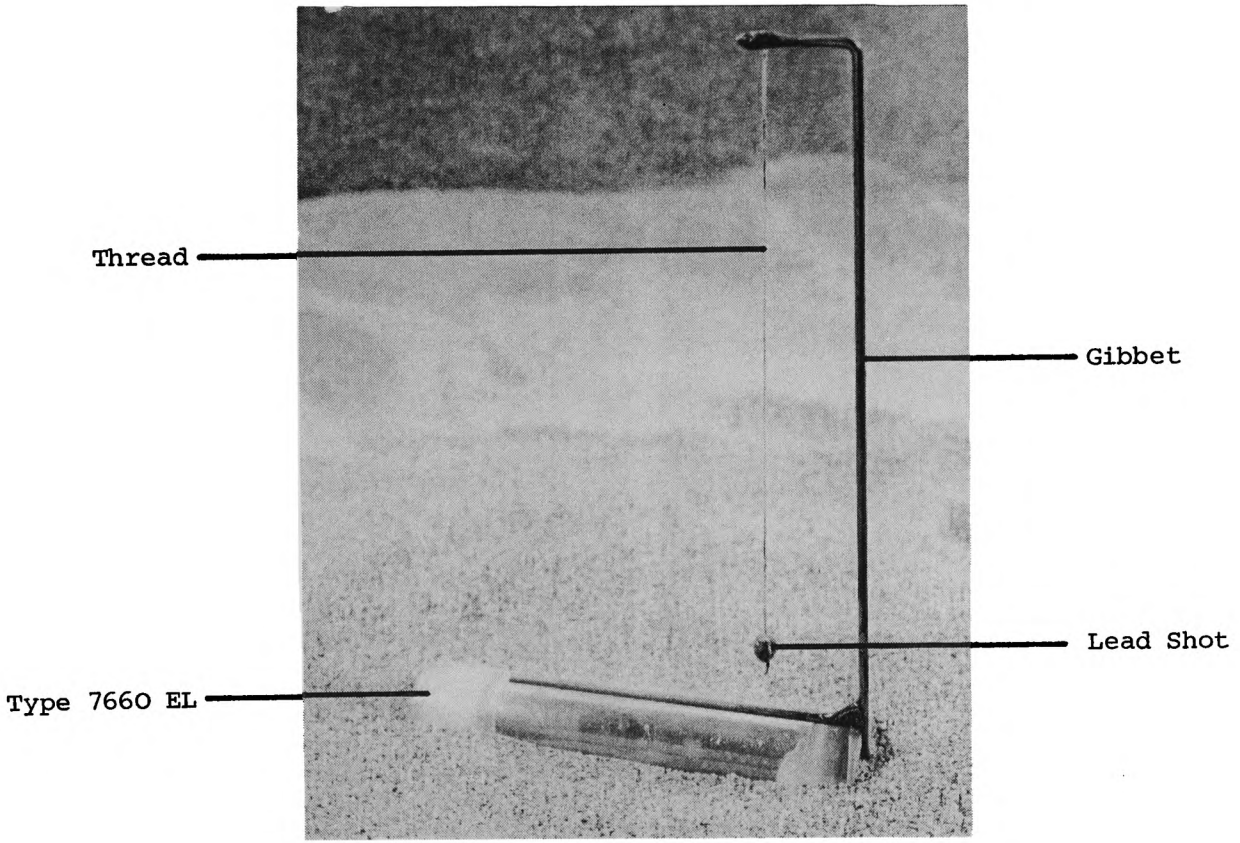

PLUMB BOB USED WHEN PLACING ELECTROLYTIC LEVELS

PLATE 6.1

CHAPTER 7

RESULTS, ANALYSIS AND DISCUSSION

CHAPTER 7

RESULTS, ANALYSIS AND DISCUSSION

7.1 Introduction

In view of the quantity of data generated during this study, the results from each set of instrumentation are considered separately in terms of their response during pile installation and subsequent load testing. Where appropriate, the results are discussed in relation to those from other instrumentation employed in this study and comparable data reported in literature.

For ease of reference the two tests conducted in the homogeneous sand profiles are referred to as S/S1 and S/S2, whilst that undertaken within the layered soil profile is referred to as S/M1.

7.2 Total, Base and Shaft Resistance

7.2.1 Pile Installation

7.2.1.1 Homogeneous Sand Profiles

The development of total pile resistance (Q_t) (the summation of pile self-weight and applied load (Q_a)) and base resistance (Q_b) with pile

embedment (D_b) is shown on Figures 7.1(a) and (b) for S/S1 and S/S2 respectively. The results relate to the last set of data recorded for each penetration increment throughout pile installation. The pile shaft resistance (Q_s) was taken as the difference between Q_t and Q_b.

To allow the results to be compared directly with those reported in literature, the development of Q_b is also reported in terms of unit base resistance (q_b). An anomaly in the rate of development of q_b with D_b was evident for a D_b of approximately 1140.0 mm (10.0B). During S/S1, q_b was thought to be exhibiting the on-set of 'text-book' critical depth (D_c) behaviour, ultimately attaining this at a D_b of 1345.0 mm (11.8B). This was subsequently viewed with some scepticism by the author, since Kerisel (1964) showed that an abrupt deviation in the $q_b - D_b$ profile at the onset of D_c was indicative of a dense sand and not a loose sand, where a gradual reduction in the rate of development of q_b with D_b was shown to occur. A systems failure during pile installation in S/S1 resulted in a delay of 2.3 hrs before the test was resumed. The delay was initially thought to be the cause of the further increase in q_b as recorded on resumption of the test. However, a subsequent closer inspection of the results showed that q_b had already started to increase prior to the systems failure. Superposition of the sand layer boundaries onto the $q_b - D_b$ profile revealed the probable cause of the 'irregularity', since it occurred approximately within the limits of sand layer 6. The higher placement density of this layer was clearly evident from the dynamic penetrometer results (Figure 6.3) and was attributed to the placement of this layer in half layers, L6'U' and L6'L', in order to install the D3 density samples.

For tests S/S1 and S/S2, the adverse influence of sand layer 6 on the

$q_b - D_b$ profile was effectively overcome by the construction of a smooth curve tangential to the $q_b - D_b$ profile immediately above and below sand layer 6.

The resulting modified profiles indicated that the rate of increase in q_b with D_b was initially non-linear and tending to increase with D_b, reaching a maximum rate for a D_b of 540.0 mm (4.6B). Thereafter, the rate of increase in q_b with D_b reduced with further pile penetration. A constant rate of increase in q_b was attained for D_b in excess of 1200.0 mm (10.5B), corresponding to D_c, at which q_b was typically 1060.0 kPa.

In general, good agreement was found to exist between the value of D_c recorded by the author and those reported in literature for loose sand. Vesic (1963) reported that the rate of increase in q_b with D_b was linear to a D_b of 4.0B for circular pre-placed piles. Thereafter, q_b gradually reduced to a constant value for a D_b of approximately 10.0B for both pre-placed and driven piles. Kerisel (1964) showed that for jacked piles of various diameter (B) in loose sand, D_c was a unique function unrelated to B. From the results presented by Kerisel (1964) it was estimated that D_c was attained at a depth of approximately 1800.0 mm (15.8B). Meyerhof (1976) presented the variation in D_c/B with ϕ' (after De Beer, 1971). This showed that for a sand of ϕ' equal to 32^0, D_c was equal to 8.5B.

The development of shaft resistance (Q_s) and the average unit shaft friction (f_s) is showed on Figures 7.2(a) and (b). A non-linear increase in Q_s with D_b, as implied by equation 7.1 for the ultimate pile shaft resistance (Q_{sf}), was observed to a D_b of 1000.0 mm (8.8B).

$$Q_{sf} \approx \tfrac{1}{2}\pi B D_b^2 \gamma K_s \tan\delta' \qquad (7.1)$$

where:

Q_{sf} = pile shaft resistance at failure,

B = pile shaft diameter,

D_b = foundation depth,

γ = unit weight of soil,

K_s = average lateral earth pressure coefficient acting on pile shaft at failure,

δ' = effective friction between pile shaft and soil at failure.

With further pile penetration, Q_b increased linearly with D_b. A similar observation was reported by Robinsky et al (1964). They reported that Q_s increased linearly with D_b, for D_b greater than 4.0B in tests conducted with straight sided model piles in loose sand.

The development of f_s with D_b was evaluated and, with due allowance for the scatter in the data, was observed to increase linearly to a D_b of approximately 1000.0 mm (8.8B). At greater D_b, a marked reduction in the rate of development of f_s was observed, which tended to a quasi-constant value of between 5.0 and 6.0 kPa for a D_b of 1200.0 mm (10.5B), the D_c for shaft resistance. The limiting value of f_s recorded by the author is in agreement with that reported by Vesic (1967) and Kerisel (1964) of 7.5 kPa (1.1 psi) and 5.9 kPa (0.60 T/m^2) respectively, for driven and jacked piles in loose sand.

The ratio of D_c(shaft) to D_c(base) in loose sand was calculated from the

data presented by Vesic (1967) as 0.5 and 1.0 for pre-placed and driven piles respectively. Meyerhof (1976) and Tavenas (1971) proposed a value of approximate unity from field tests on driven piles in sand. The value of unity as deduced from the author's results, is in agreement with those quoted above for driven piles.

7.2.1.2 Layered Soil Profile

The development of Q_b and Q_t during S/M1 is presented on Figure 7.1(c). The load-penetration profiles were modified in order to allow for the increased Q_b developed within sand layer 6. This was undertaken by calculating the difference in resistance between the actual and constructed portions of the profiles for Q_b and Q_t in S/S1 and S/S2 at a given D_b. The average difference for the two tests was then subtracted from the appropriate values recorded in S/M1 at the same D_b.

A comparison of the modified load-penetration profiles from all three tests (S/S1, S/S2 and S/M1), showed that the underlying clay did not influence the development of Q_b until the pile base was within 250.0 mm (2.2B) of the sand/clay interface. Further pile penetration resulted in a reduction in the rate of increase in Q_b. The maximum value of Q_b recorded in the overlying sand was 8.8 kN at 170.0 mm (1.5B) above the sand/clay interface. A minimum value of Q_b (7.4 kN) was attained at 170.0 mm (1.5B) below the sand/clay interface. With further pile penetration Q_b increased at a relatively constant rate. This was probably due to the increase in C_u with depth within the clay, established on completion of the test.

An appreciable increase in Q_t was recorded as the pile penetrated into the underlying clay, this was due of the greater Q_s developed within the clay.

The failure mechanism developed within the sand as the pile base approached the level of the sand/clay interface was described by Meyerhof and Sastry (1978(b)) as one of punching, in which a cylindrical mass of the stronger soil (sand) below the pile base was punched into the underlying weaker soil (clay). They established that the maximum height above the sand/clay interface (h') for punching failure to occur was related to the ratio of the limiting unit base resistance in a homogeneous profile of the weaker soil (q_{lw}) and the stronger soil (q_{ls}). In support of this they reported values of h' equal to 1.5B and 6.0B, which were associated with a q_{lw}/q_{ls} of 0.67 and 0.02 respectively. The author's test results indicated a h' of 175.0 mm (1.6B) for a q_{lw}/q_{ls} of 0.47.

The development of Q_s with D_b within in the overlying sand appeared to attain a linear rate of increase for a shallower D_b, approximately 700.0 mm (6.1B), than that observed for S/S1 and S/S2. This was also reflected in f_s which showed a reduced D_c of 700.0 mm (6.1B). The magnitude of f_s at D_c was approximately 1.5 kPa less than that reported for S/S1 and S/S2. The above was probably due to a reduced sand placement density, since a significant reduction in the local unit shaft friction (f_z), of the order of 0.5 to 1.0 kPa, was recorded by the BOSTs below a depth of 500.0 mm (4.3B) which coincided with the boundary between sand layers 8 and 9. Further, upon closer inspection of the $Q_b - D_b$ profile for S/M1, a slight reduction in the rate of increase of Q_b with D_b was observed below this depth, which was highlighted in the

variation in the back figured bearing capacity factor, N_q^* with depth (Figure 7.3). No obvious reduction in sand density was, however, evident at this depth from the dynamic penetration probe test results (Figure 6.3).

The magnitude of f_s at D_b equal to 1275.0 mm (11.2B), the depth to the sand/clay interface, was markedly higher than the preceding values by approximately 0.5 kPa. The results from the BOSTs indicated an approximate two fold increase in f_z and the radial effective stress (σ_r') acting on the pile shaft within the sand immediately above the sand/clay interface. An explanation for this is offered in Section 7.4.1.2.

As the pile penetrated below the sand/clay interface there was a rapid increase in Q_s, which continued at a diminishing rate for a pile embedment of greater than 330.0 mm (2.8B) below the sand/clay interface.

In calculating the magnitude of f_s within the underlying clay, it was assumed that Q_s within the overlying sand remained constant and was equal to the value recorded at D_b equal to the depth to the sand/clay interface. This approach was adopted by Meyerhof and Sastry (1978(a)) and Mansur and Kaufman (1956). The above assumption is not strictly correct, as is evident from the results of the BOSTs (Section 7.4.1.1 Refer). However, on the basis of this assumption the magnitude of f_s developed within the clay was found to increase with D_b, and attained a maximum rate of increase at a D_b of 200.0 mm (1.8B) below the sand/clay interface. This was found, on disection of the clay after the test, to approximately coincide with the depth to which sand was drawn down around the pile shaft into the clay; that is, 230.0 mm (2.0B). The maximum

value of f_s within the clay, 36.0 kPa, corresponded to a pile embedment of 430.0 mm (3.8B) below the sand/clay interface. Thereafter, f_s gradually reduced to 33.9 kPa at full pile embedment, 570.0 mm (5.0B) below the sand/clay interface.

7.2.1.3 Base Bearing Capacity Factors

The variation in the base bearing capacity factor, N_q^*, with D_b for S/S1 and S/S2 was evaluated by back analysis and is presented on Figure 7.3. This showed N_q^* to increase with D_b for shallow pile embedments, to a maximum value for a D_b of 540.0 mm (4.6B), or $0.45D_c$. Thereafter, N_q^* decreased at a diminishing rate with further pile embedment and tended to a limiting value of about 50 at full pile embedment, 1845.0 mm (16.1B). These finding were in agreement with those of Kerisel (1961), who showed that N_q^* was not a unique function of ϕ', but was influenced by D_b/B and B. Additional data presented by Kerisel (1964) indicated that the maximum value of N_q^* occurred at $0.45D_c$.

Berezantzev et al (1961) derived an expression (Equation 7.2) for q_{bf} in terms of the bearing capacity factors A_k and B_k, both of which are functions of ϕ'. The term B_k is also affected by a modification factor, α_T, which takes into account the reduction in surcharge pressure acting on a horizontal plane at the level of the pile base. The factor α_T is also a function of both D_b/B and ϕ'.

$$q_{bf} = A_k \gamma B + B_k \alpha_T \gamma_D D_b \qquad (7.2)$$

where:

q_{bf} = unit base resistance at failure,

A_k and B_k = bearing capacity factors,

γ and γ_D = unit weight of soil at base level and that forming the surcharge respectively,

B = pile diameter,

α_T = surcharge reduction factor, and

D_b = foundation depth.

The bearing capacity factors of Equation 7.2 were evaluated at various pile embedments for ϕ' equal to 32^0 and were equated to N_q^*. The results are presented on Figure 7.3. The magnitude of N_q^* at any depth was approximately one half of that established through back analysis. Meyerhof (1959) stated that the bearing capacity of piles driven in loose sand may be doubled due to compaction of the sand below the pile base, resulting in an increase in ϕ' of typically 4 to 6^0. To account for such an increase a modified ϕ' (Equation 7.3) was used as proposed by Kishida (1967).

$$\phi'_m = \tfrac{1}{2}(\phi' + 40) \qquad (7.3)$$

where:

ϕ'_m = angle of effective internal friction below pile base after installation,

ϕ' = angle of effective internal friction prior to pile installation.

The use of Equation 7.3, in conjunction with the bearing capacity factors derived by Berezantzev et al (1961), was advocated by Poulos and Davis (1981). The resulting modified values of N_q^* are in close agreement with the author's experimental values.

The variation in N_q^* with D_b, derived through back analysis of the results from S/M1, was in general agreement with that observed for S/S1 and S/S2 to a D_b of 1025.0 mm (9.0B), 250.0 mm (2.2B) above the sand/clay interface. The magnitude of N_q^* was, however, less than that derived in S/S1 and S/S2 by approximately 10.0% for D_b greater than 500.0 mm (4.4B). This gave further support to the existence of a lower sand density below this depth (Section 7.2.1.2 Refer). Further pile penetration resulted in a reduction in N_q^* as the pile base punched into the underlying clay.

The variation in N_c with D_b, derived through back analysis, gave no indication of the pile base behaving as a circular surface footing (that is, N_c equal to 6.2, Skempton (1951)) for D_b equal to the depth to the sand/clay interface, where N_c was equal to 12.5. For a pile embedment of 350.0 mm (3.0B) below the sand/clay interface, a minimum value of 10.0 was evaluated for N_c. With further penetration this increased to 10.5 at full pile embedment, 570.0 mm (5.0B) below the sand/clay interface.

Values of N_c greater than 9.0 are not uncommon. According to Vesic (1967), high values of N_c may be attributed to the soil deviating from a purely frictionless behaviour. Esrig and Kirby (1979(b)) stated that N_c was dependent upon a number of factors:

(i) The stress-strain behaviour of the clay; higher N_c with greater G/C_u.

(ii) For a given soil, N_c in over-consolidated clay may be expected to be less than N_c for a normally consolidated clay.

(iii) For a given over-consolidation ratio, N_c for a clay of low plasticity may be greater than N_c for a clay of a higher plasticity.

The probable reasons for the higher N_c values deduced by the author were:

For D_b equal to Z_i:

(i) The presence of an 'active' sand cone formed below the pile base. From the author's pilot study it was observed that for D_b equal to the depth to the sand/clay interface (Z_i), the clay surface below the pile base was depressed by the sand cone without being ruptured. The maximum depth of the depression was approximately 0.5B, and extended to a radius of approximately 1.0B from the pile axis. Sand trapped within this region would tend to distribute the base load over a greater surface area of clay than would be the case for a true surface footing, resulting in lower contact stresses on the surface of the clay.

(ii) A limited amount of moisture migration occurred into the overlying dry sand, resulting in some desiccation of the clay surface, thereby locally increasing C_u.

For D_b greater than Z_i:

(i) The sand cone formed beneath the pile base would tend to accelerate drainage and consolidation of the clay in the

proximity of the base, resulting in some increase in C_u.

(ii) The sand surcharge may aid in the development of a deep footing failure mechanism within the clay at relatively shallow depths.

(iii) The back figured values of N_c were calculated using the value of C_u at pile base level; the variation in C_u with depth was measured on completion of S/M1. However, the presence of the sand cone effectively lengthened the pile. The author may, therefore, have been justified in using C_u at a depth of approximately 55.0 mm (0.5B) below pile base level. This would reduce the derived values of N_c by approximately 0.5.

(iv) A small amount of shaft friction was developed on the sides of the pile shoe, estimated at typically 0.3 kN. This would result in a further limited reduction in N_c of typically 0.5.

7.2.1.4 Shaft Bearing Capacity Factors

Equation 7.1 assumes that the radial effective stress (σ'_r) increases linearly with depth and is directly related to the initial vertical effective stress (σ'_z) at that depth prior to pile installation by K_s, which is considered to be constant along the pile shaft. The variation in $K_s Tan\delta'$ with D_b was therefore evaluated by back analysis (Figure 7.4) Since $Tan\delta'$ was practically constant throughout pile installation, as will be shown subsequently (Section 7.4.1.3 Refer), K_s was quantifiable. The results showed that K_s was greater than the coefficient of passive earth pressure (K_p = 3.25) for a D_b less than 230.0 mm (2.0B). However, for small values of D_b, K_s was extremely sensitive to small fluctuations in Q_s. With further pile embedment K_s diminished at a reducing rate to a

value of approximately unity at full pile embedment, 1845.0 mm (16.1B).

Vesic (1977) established that for driven, high displacement piles, K_s could be as great as K_p for small pile embedments and reduced with increased pile embedment. He suggested that this reduction reflected the fact that the effective stresses in the region of the pile base were considerably less than the initial ground stresses.

Coyle and Castello (1979) analysed data from a number of pile tests in sand, from which they indicated that $\log K_s$ varied linearly with D_b/B for a given ϕ'. From their results it was apparent that a value of K_s equal to unity was reasonable for D_b equal to 16.1B and ϕ' equal to 32^0.

Within the overlying sand of S/M1 the variation in K_s was in agreement with that deduced for S/S1 and S/S2.

Within the underlying clay of S/M1 the back figured shaft adhesion factor (α) was deduced using the average value of C_u adjacent to the pile shaft. This approach gave an average value of typically 0.45, with a maximum of 0.54. The derived values of α were substantially less than those reported by Tomlinson (1970 and 1971) of 1.21, 0.74 and 1.60, corresponding to embedments of 18.0B, 18.0B and 9.0B respectively into the underlying clay for steel-tube piles driven through sands and gravels, and tested at 28 days. Tomlinson (1970) suggested that the high adhesion factors were due to the drawdown of the granular material into the clay, resulting in the development of greater skin friction over the upper portion of the pile shaft within the clay. This effect would, therefore, be most evident where the pile penetration of the clay was limited. Subsequent excavation of these piles revealed that sand was

drawn down into the underlying clay around the pile shaft forming a thin adhering skin to a depth of 530.0.mm (3.1B, B = 168.0 mm). This compared with the drawdown of sand observed by the author of 230.0mm (2.0B), with an absolute limit of 285.0 mm (2.5B) for S/M1.

7.2.1.5 Pile Butt and Soil Displacement Recovery

The pile butt recovery recorded at the conclusion of each jacking increment throughout pile installation is presented on Figure 7.5(a) for all tests.

The magnitude of the pile butt recovery recorded during S/S1 and S/S2 increased at a reducing rate with D_b, and attained a relatively constant value of approximately 1.0 mm (0.9%B) for a D_b of 1000.0 mm (8.8B). On resumption of pile installation during S/S1, after a delay of 2.3 hrs due to a systems failure, smaller pile butt recoveries were recorded at the conclusion of the two subsequent pile penetration increments. In total, an additional pile embedment of 250.0 mm (2.2B) was required before the pile butt recovery was again equal to the limiting value reported above. This was thought to be indicative of the relaxation of prestress within the soil below the pile base (Meyerhof, 1959), as a consequence of creep effects (Vesic, 1969(a)). However, no change in the intensity of the soil stresses was recorded by the stress transducers (BOSTs or DPTs).

The pile butt recovery profile for S/M1 approximated to those of S/S1 and S/S2 to a D_b of 800.0 mm (7.0B), 475.0 mm (4.2B) above the sand/clay interface. At greater depth the pile butt recovery increased rapidly to a maximum value of 2.7 mm (2.4%B) for a D_b of 1225.0 mm (10.7B), 50.0 mm

(0.4B) above the sand/clay interface. This diminished equally rapidly with further pile penetration, and attained a relatively stable value of 1.6 mm (1.4%B) for a D_b of greater than 1500.0 mm (10.4B), 225.0 mm (2.0B) below the sand/clay interface.

The soil displacement recovery recorded at a radius of 160.0 mm (1.4B) from the pile axis on the sand/clay interface, together with that recorded at an equivalent location within S/S1 and S/S2 throughout pile installation, is presented on Figure 7.5(b). In all tests, displacement recovery of the soil was not evident until the pile had attained a D_b of 600.0 mm (5.3B), 675.0 mm (5.9B) above the plane of instrumentation under consideration. For greater D_b the displacement recovery of the soil was observed to develop sinusoidally to a maximum value of typically 0.15 mm (0.12%B) for S/S1 and S/S2, and 0.8 mm (0.7%B) for S/M1 at a D_b of 1225.0 mm (10.7B). This was equal to the D_b at which maximum pile butt recovery was recorded in S/M1. With further pile embedment the amount of soil recovery reduced to a relatively constant value of typically 0.05.mm (0.05%B) for S/S1 and S/S2, and 0.3 mm (0.3%B) for S/M1 for D_b greater than 1500.0.mm (13.2B). This was equal to the D_b at which a constant limiting pile butt recovery was recorded during S/M1.

The probable radial distribution of soil recovery at a depth of 1275.0 mm was deduced for each test at the conclusion of the penetration increment corresponding to a D_b of 1225.0 mm (11.2B), and is presented on Figure 7.5(c). This indicated that:

(i) At any radius the displacement recovery of the sand/clay interface was greater than that of the sand alone.

(ii) Displacement recovery was greatest below the pile base and

diminished rapidly with distance from the pile axis.

(iii) The sand/clay interface displacement recovery profile tended to zero at a radius which was less than that of the secondary clay tank. This may, however, reflect the lack of sensitivity of the LVDTs, which recorded the vertical displacement of the outer EL, to small displacement reversals.

7.2.2 Constant Rate of Penetration Test

The amount of 'useful' data provided by the CRP test, Figures 7.6(a), (b) and (c), in comparison with that provided by the rest of the test programme, was limited. Therefore, only the results relating to the development of Q_t, Q_a, Q_b and Q_s (together with selected data from other items of instrumentation) are reported in this thesis.

The criterion employed to define pile failure throughout this study was that reported by Vesic (1963). Vesic (1963) established that for a loaded circular base at any depth in relatively loose sand (D_r less than 0.35) the failure mechanism was one of punching shear failure. This mode of failure is associated with a steady increase in base resistance with settlement. The maximum rate of settlement under these conditions may be expected at a settlement of about 15.0 to 20.0%B. Further, no surface heave occurs since the failure planes, which are vertical or slightly inclined, never reach the surface. Under these circumstances Vesic (1963) suggested that failure may be defined as the point at which the maximum rate of settlement is first observed.

Nine other failure criteria were reported by Vesic (1977) for piled foundations. He concluded that provided B was less than 300.0 mm, then they all resulted in the same Q_{af} to within ±10.0%. However, substantial discrepancies could result if the pile under test was very long or of a large diameter.

7.2.2.1 Homogeneous Sand Profiles

The results from S/S1 should be disregarded since the pile cap and loading plate, attached to the jack load cell, were clamped together prematurely in readiness for the CRU test. This resulted in a limited extraction of the pile as the jack 're-set' routine operated at the conclusion of the final penetration increment during pile installation. The pile was withdrawn approximately 9.0 mm (7.9%B) before the 're-set' instruction was cancelled. The results from S/S1, however, illustrate a number of interesting points.

(i) Extraction of the pile formed a void in the sand below the pile base, or at least produced a region of very loose sand. The initial rate of increase in Q_b, with pile butt displacement (ω_t), from the residual value of 0.1 kN was, therefore, small. The maximum rate of increase in Q_b with ω_t was recorded for a D_b equivalent to that which existed immediately prior to the extraction of the pile. At the conclusion of the CRP test, Q_b was equal to 14.3 kN, comparable with that recorded at the conclusion of the CRP test in S/S2 of 14.0 kN.

(ii) The residual Q_s was +0.8.kN. The distribution of residual

f_z, as recorded by the BOSTs, was considered equivalent to the residual shaft friction at the end of a CRU test; data not recorded. The initial rate of increase in Q_s with ω_t was less rapid than that observed in S/S2. Further, the ω_t required to achieve shaft failure (Q_{sf}) was approximately twice that recorded in S/S2, 6.5 mm (5.7%B) as opposed to 3.5 mm (3.1%B). For ω_t greater than that necessary to achieve shaft failure, Q_s remained relatively constant at 3.9 kN, and was comparable with that recorded in S/S2 of 4.5 kN.

In S/S2, Q_b increased rapidly from a residual value of 1.8 kN to 12.0 kN (90.0%Q_{bf}) for a ω_t of 3.5.mm (3.1%B), equal to that at which Q_{sf} was attained. With further ω_t the rate of increase in Q_b was greatly reduced and a ω_t of 12.0 mm (10.5%B) was required in order to achieve Q_{bf} (13.4 kN), beyond which only a small linear increase in Q_b was recorded with greater ω_t.

The residual Q_s of -0.9 kN increased rapidly to Q_{sf} (4.5 kN) for a ω_t of 3.5 mm (3.1%B), at which Q_s remained relatively constant with further ω_t.

Whilst the jack was re-setting at a rate of 1.524 mm/min at the conclusion of the CRP test in S/S2, the pile was subjected to a reduced Q_a of 5.0 kN (29.4%Q_{af}) as the first of the three data scans associated with the re-set mode was made. This corresponded with a pile butt recovery of -0.5 mm (0.4%B). The associated values of Q_b and Q_s were 6.5 kN and -0.6 kN (85.0% of the maximum residual capacity) respectively. A total pile butt displacement recovery of -1.2 mm (1.1%B) was recorded

at the conclusion of the test. Comparable values were also recorded in S/S1.

7.2.2.2 Layered Soil Profile

As the pile was loaded, Q_b increased from a residual value of 2.3 kN to Q_{bf} (8.1 kN) at a reduced rate per unit pile penetration than was observed in S/S2. However, a smaller ω_t was required in order to develop Q_{bf}; that is, 5.6 mm (4.9%B). For ω_t greater than that associated with Q_{bf}, Q_b continued to increase linearly, possibly as a consequence of the increase in undrained shear strength of the clay with depth.

From a residual value of -1.3 kN, Q_s increased to Q_{sf} (8.8.kN) for a ω_t of 5.6 mm (4.9%B), the same as that recorded at Q_{bf}. The distribution of Q_{sf} between the sand and clay was in the proportions 21.6% (1.9 kN) and 78.4% (6.9 kN) respectively. For ω_t greater than that associated with Q_{sf}, Q_s increased linearly with ω_t.

Upon unloading, as with S/S2, the pile shaft initially experienced the greatest reduction in load. For a Q_a of 5.6 kN (35.0%Q_{af}), in association with a pile butt recovery of -0.5 mm (0.4%B), Q_s and Q_b reduced to 5.6 kN and 5.4 kN (60.0% and 33.0% of their respective failure loads). A total pile butt displacement recovery of -1.6 mm (1.4%B) was recorded at the conclusion of the test.

7.2.3 Maintained Load Test

The ML test results are presented on Figures 7.7(a), (b) and (c). Base and mean shaft settlements (ω_b and ω_s) were calculated from the measured pile butt settlement (ω_t), with due allowance for the elastic behaviour of the pile.

7.2.3.1 Homogeneous Sand Profiles

The load-settlement profiles obtained from S/S1 for Q_t, Q_a and Q_b did not, on subsequent analysis, fulfil the failure criterion previously defined in Section 7.2.2. This was a consequence of plotting the data as the test progressed at too large a scale with respect to the settlement axis, which resulted in a premature assumption of pile failure. The effect of reducing the scale of the settlement axis is indicated on the plot of $Q_a - \omega_t$, together with tangents indicating the rate of increase in Q_a per unit pile penetration as recorded during the CRP tests for loads in excess of Q_{af}.

During the initial stage of the ML test significant base and shaft settlements were not deduced until Q_a was sufficient to overcome the residual Q_s. This was achieved with the first increment of Q_a, 33.3% of the applied working load (Q_{aw}), typically 2.2 kN, which was distributed equally between Q_s and Q_b, and resulted in a ω_s and ω_b of typically 0.07 mm (0.06%B) and 0.03 mm (0.03%B) respectively. With the application of further increments of Q_a, an abrupt increase in both ω_s and ω_b per unit of applied load was observed. ω_s continued to increase at greater rate per unit Q_b, whilst the rate of ω_s per unit Q_s remained relatively

constant at 0.31 mm/kN to a ω_s of 0.53 mm (0.47%B).

At Q_{aw}, (7.2 kN) ω_t, ω_b and ω_s were on average 0.61 mm (0.54%B), 0.44 mm (0.39%B) and 0.53 mm (0.47%B) respectively. Typically, 61.1% Q_{aw} (4.4 kN) was transmitted directly to the pile base.

Pile loading in S/S2 may have been terminated at, or very near the actual failure load for the pile. Thus, Q_{af} was equal to 17.2 kN and was associated with a ω_t of 15.0 mm (13.2%B). The associated Q_{bf} was 13.6.kN, for a ω_b of 14.6 mm (12.8%B). These values are greater than those reported by Vesic (1967). From the results of a rapid ML test conducted on a 101.6 mm diameter driven pile in loose sand, Vesic reported a base settlement of 6.0%B at failure.

In both S/S1 and S/S2, Q_{sf} was typically 4.4 kN and corresponded with a ω_s of approximately 2.9 mm (2.5%B), beyond which Q_s was constant with further ω_s. The magnitude of ω_s at Q_{sf} was smaller than that reported by Vesic (1967) of 8.4 mm for driven piles in a homogeneous dry, loose sand. Further, from a series of tests conducted in sand over a range of initial densities, with preplaced and driven piles of various diameter and embedded length, Vesic concluded that the relative displacement of the pile shaft necessary to attain Q_{sf} was independent of the above variables and depended only upon the absolute pile shaft displacement, for which an average value of 8.9 mm was reported.

The minimum rate of settlement attained under the final increment of Q_a in S/S1, did not fulfil the criterion of 0.3 mm/hr for the reasons previously outlined in Section 6.5.3. It is estimated that had the settlement criterion been achieved, ω_t would have been at most 1.0 mm

greater than that recorded at the conclusion of the test. Such an increase in settlement would not radically affect the shape of the load-settlement profiles, or the estimated failure loads.

Unloading the pile to $\frac{1}{2}Q_{amax}$, typically 8.5 kN, reduced Q_s and Q_b by almost an equal amount to 0.3 kN and 9.0 kN respectively. This represented a reduction in percentage terms of 94.0% and 36.0% respectively. The associated recovery in ω_t was on average -0.17 mm (0.15%B), with calculated recoveries in ω_s and ω_b of -0.09 mm (0.08%B) and -0.02 mm (0.02%B) respectively. This suggested that 88.2% of the recovery in ω_t was due to the elastic recovery of the pile. The removal of Q_a restored the pile to a state of residual load, in which Q_s and Q_b were equal to -1.0 kN and 1.8 kN, associated with a total recovery in ω_t, ω_s and ω_b of typically 1.24 mm (1.09%B), 0.96 mm (0.84%B) and 0.86 mm (0.75%B) respectively.

7.2.3.2 Layered Soil Profile

As in the cases of S/S1 and S/S2, both ω_b and ω_s were minimal until such time as Q_a was sufficient to overcome the residual Q_s. This again was achieved by the application of the first increment of Q_a (2.4 kN), $33.3\%Q_{aw}$, which was distributed between Q_s and Q_b in the proportions of 79.2% (1.9 kN) and 21.8% (0.5 kN) respectively, and was associated with a ω_t of 0.07 mm (0.06%B). The corresponding calculated values of ω_s and ω_b were approximately 0.04 mm (0.04%B) and zero respectively.

For Q_a in excess of $33.3\%Q_{aw}$, settlement rates increased abruptly. The rate of increase in Q_s per unit ω_s was 8.0 kN/mm which was sustained to a

ω_s of 0.39 mm (0.34%), corresponding with Q_{aw} (6.8 kN). The settlement rate of the pile base continued to increase per unit Q_b. The applied load of Q_{aw} was distributed between Q_s and Q_b in the proportions 72.1% (4.9 kN) and 27.9% (1.9 kN) respectively. Further, Q_s was distributed between the sand and clay in the proportions of 8.1% (0.3 kN) and 91.9% (3.4 kN) respectively.

It was difficult to establish the pile settlement at failure with certainty due to the sudden plunging failure of the pile which occurred during application of the final increment of Q_a. Therefore, the value stated below should only be considered as approximate. It was estimated from the variation in Q_a with ω_t, plotted to a reduced scale, that Q_{af} was 18.5 kN, corresponding to a ω_t of typically 10.0 mm (8.8%B). At this point the rate of increase in Q_a per unit ω_t was in reasonable agreement with that recorded during the latter stages of the CRP test.

It appeared that Q_{sf} and Q_{bf} were attained simultaneously, as in the CRP test, and were equal to 9.6 kN and 8.0 kN respectively. The distribution of Q_{sf} between the sand and clay was in the proportions of 24.0% (2.3 kN) and 76.0% (7.3 kN) respectively.

As 89.0% of Q_{amax} was transmitted to the underlying clay, the performance of the pile may reasonably be expected to compare with that of a pile embedded entirely in clay. However, the magnitude of the displacements required to achieve base and shaft failure were in excess of those reported in literature.

Clark and Meyerhof (1972) showed that the rate of mobilization of Q_s in clay, for small settlements, was greater than that for Q_b. They reported

that for a settlement of 1.0%B, Q_s and Q_b were 92.0% and 50.0% of the values recorded at failure.

Cooke and Whitaker (1961), experimenting with model piles in soft clay, established that settlements of 0.5%B and 10.0 to 15.0%B were required to mobilise Q_{sf} and Q_{bf} respectively.

As the pile was unloaded to $\frac{1}{2}Q_{amax}$ (8.8 kN) similar behavioural characteristics were observed to those reported for S/S1 and S/S2. However, a greater reduction in Q_s was recorded which was probably due to the greater displacement recovery in ω_t of -0.21 mm (0.18%B), typically 24.5% in excess of that reported for S/S1 and S/S2. The corresponding displacement recoveries in ω_s and ω_b were calculated to be -0.13 mm (0.11%B) and -0.06 mm (0.05%B), and were associated with a Q_s and Q_b of 3.3 kN and 6.4 kN respectively. Of Q_s, -0.4 kN and 3.7 kN were developed within the sand and clay respectively.

Upon complete removal of Q_a a total recovery in ω_t of -1.51 mm (1.32%B) was recorded, which was typically 21.8% greater than was reported for S/S1 and S/S2. The corresponding recoveries in ω_s and ω_b were -1.34 mm (1.18%B) and -1.17 mm (1.03%B) respectively. A residual Q_s of -1.6 kN was distributed equally between the sand and clay, and acted in conjunction with a residual base load of 2.5 kN.

7.2.4 Constant Rate of Uplift Test

The results from the CRU tests are presented on Figures 7.8(a), (b) and (c).

7.2.4.1 Homogeneous Sand Profiles

A pile butt uplift of typically -2.5 mm (2.2%B) was required in order to eliminate the residual Q_b. With further uplift the base load cell continued to record a small compressive load of between 0.10 and 0.15 kN. This suggested that the initial zero value of the base ALC had drifted slightly by an amount in excess of the average accuracy reported in Section 5.3.3 of ±0.062 kN.

On average, the post compressive residual Q_s accounted for 45.0% of the uplift Q_{sf}. Initially the rate of increase with Q_s was rapid for the first 1.0 mm (0.9%B) of ω_t. Thereafter the rate of increase reduced, reaching zero at Q_{sf}.

The magnitude of ω_t associated with Q_{sf} was typically twice that observed in the CRP test for Q_{sf}, that is -7.0.mm (6.1%B) as compared with 3.5 mm (3.1%B). Conversely, Q_{sf} was 44.4% of that recorded in the CRP test, 2.0 kN as compared with 4.5 kN. Thus, the magnitude of the tensile K_s is 44.4% of that in compression, assuming all other terms in Equation 7.1 to be constant for the given set of conditions. Similar observations were reported by Bergdahl and Wennerstrand (1976), Gregersen et al (1973), Tejchman (1971), Mazurkiewiz (1968), Vesic (1967), Broms and Silberman (1964) and Mansur and Kaufman (1956).

For ω_t in excess of that associated with Q_{sf}, a gradual reduction in Q_s was recorded, which was disproportionate to the amount of pile uplift. This may be compared with the CRP test in which a constant Q_s was recorded for ω_t in excess of that associated with Q_{sf}. The mechanics responsible for this behaviour are discussed in Section 7.4.3.1.

7.2.4.2 Layered Soil Profile

The residual Q_s accounted for 20.0% of that mobilised at Q_{sf}. The rate of development of Q_s with ω_t was rapid at first, but gradually decreased at an increasing rate to zero at Q_{sf}.

The ω_t required to achieve Q_{sf} (-7.4 kN) was -11.2 mm (9.8%B), approximately twice that required to attain Q_{sf} during the CRP test. The proportions of Q_{sf} developed within the sand and clay were 17.6% (-1.3 kN) and 82.4% (-6.1 kN) respectively. These values were 68.4% and 91.0% of the failure loads recorded during the CRP test.

Pile failure, defined relative to Q_a, corresponded to a load of -9.4 kN and was associated with a ω_t of -13.0 mm (11.4%B). Approximately -0.7kN of which was attributed to a suction force developed below the pile base.

For ω_t greater than that associated with Q_{sf}, a linear reduction in Q_a was recorded which occurred at a rate of 21.0 kN/m of pile uplift. This compared favourably with the rate of increase in Q_s recorded during the CRP test of 19.0 kN/m of pile penetration. Both of the above may primarily be attributed to the change in pile embedment within the clay.

7.3 Sand Density

Variations in the sand density due to pile installation were recorded using the method outlined in Appendix 5.1. The sand/plaster density samples were hydrated on completion of the ML tests. The results thus obtained were considered to be representative of the density variation

resulting from pile installation. These are presented on Figures 7.9(a), (b) and (c). All three sets of data were compatible above a depth of 1275.0 mm (11.2B), regardless of soil conditions below this level. They are, therefore, considered collectively in the subsequent discussion.

7.3.1 Uniformity of the Sand Profile Prior to Pile Installation

The average 'as-placed' density of each sand layer was estimated with the aid of a CBR mould. The results showed the 'as-placed' density of the sand to be typically 20.0 kg/m^3 ($0.06D_r$) less than the average density determined from the sand/plaster density samples hydrated 24 hrs prior to the start of each test. Such an increase was reasonable, since loose sand may consolidate and densify with time and increased overburden stress. The average sand density calculated within the two CBR moulds retrieved from the testing tank during the emptying operation, was within typically ±5.0 kg/m^3 ($\pm 0.015D_r$) of that evaluated from the initial density samples (DI3s) located at the same depth within the sand profile. In all tests the sand density evaluated from those density samples remote from the zone of densification, was in good agreement with that obtained from the initial density samples hydrated 24 hrs prior to the start of each test.

The variation in initial sand density with depth, as deduced from the initial density samples, was insignificant. Therefore, for the purposes of analysis, the average density appropriate to each test was used.

7.3.2 Volumetric Strains within the Sand Mass due to Pile Installation

The effect of pile installation on sand density was considered in terms of volumetric strain (ε_v). The variation in ε_v within the sand profiles is presented on Figure 7.10(a) for all tests. From these results it was concluded that the zone of densification around the pile shaft in loose sand, extended to a diameter of 1500.0 mm (13.2B). This was greater than the limit generally reported in literature for loose sand; that is, Kishida (1967), 7B; Broms (1966), 7 to 12B; Broms and Silberman (1964), 4 to 6B; Robinsky and Morrison (1964), 6 to 8B and Meyerhof (1959), 6B.

Adjacent to the upper portion of the pile shaft, ε_v was typically 3.0% at the closest point of measurement to the pile axis, 160.0 mm (1.4B). This was comparable with 4.0 to 8.0%ε_v recorded by Davidson et al (1981) at the same relative radius around a diametrically sectioned cone penetrometer pushed into loose sand (Figure 7.10(b)). Robinsky and Morrison (1964) presented the variation in D_r within a loose sand due to the installation of a model pile with a straight, rough shaft. Their results have been converted directly to ε_v by the author and are presented on Figure 7.10(c). The magnitude of ε_v was typically 3.0 to 5.0% at a radius of 1.4B from the pile axis. Both of the above results compare favourably with that reported by the author.

The results derived from the density samples sited at a depth of 1785.0 mm (15.7B), showed the existance of a zone within which ε_v was less near the pile shaft than at a radius of 310.0 mm (2.7B) from the pile axis. This trend appeared to be continued below pile base level where the 'on-axis' samples recorded a negative ε_v (dilatancy). The density samples removed from directly below the pile base were noticeably

thinner and of a greater diameter than the other density samples removed from the sand profile. This resulted in the samples possessing an increased surface area to volume ratio. Experience showed that density samples with a higher ratio of surface area to volume, tended to record a lower density. This was probably due to the greater portion of excess surface water to void water that such samples possessed, which effectively increased the calculated voids ratio of the sample.

With the exception of the results from the density samples sited directly below the pile base, the density variation within the sand around the pile base was in general agreement with that reported in literature.

Kerisel (1964) reported the volume changes within a loose sand profile at various depths, as recorded by an array of 'off-axis' cells developed for this purpose, due to the installation of a 216.0 mm diameter pile. Some doubt as to the validity of the results in absolute terms, is expressed by the author. However, two general observations may be made:

(i) A maximum ε_v was recorded when the pile base was immediately above the plane of instrumentation.

(ii) Above pile base level some relief of the maximum ε_v was observed. This was greatest for the cells near to the pile shaft.

The volumetric strain contours reported by Davison et al (1981) (Figure 7.10(b)) for loose sand, show that dilatancy can occur within the sand adjacent to a pile base. However, below the penetrometer base, which was of conic section, the ε_v contours were bulbous in shape and indicated a gradual increase in ε_v with proximity to the penetrometer base.

The contours of ε_v around a model pile in loose sand, as evaluated from the work of Robinsky and Morrison (1964) (Figure 7.10(c)), showed a general increase in density with proximity to the pile shaft. This was interspersed with localized regions of high and low density. At base level a region of low density was observed to one side of the pile. A density profile of this type would result in a radial distribution of ε_v similar to that recorded by the author. Directly below the pile base the ε_v contours turned inwards and upwards towards the pile base. This indicated that within a region between 1.0 and 2.0B below pile base level, the maximum ε_v on a given horizontal plane occurred at a radius of between 1.0 and 1.5B from the pile axis. This is in general agreement with the author's findings. Evidence of dilatancy was not observed below the pile base, which reinforces the author's doubts as to the validity of the result from the density samples sited immediately below the pile base.

As a first order approximation, it was calculated that the total reduction in void content of the sand due to pile installation in S/S1 and S/S2 was equal to 190.0% of the embedded volume of the pile. This compared with 170.0% as calculated from the average surface displacement profile at the end of the ML test.

7.3.3 Angle of Internal Shearing Resistance of the Sand Adjacent to the Pile Shaft

As the inner radial limit of density samples did not approach within 0.4B of the pile shaft, the sand density, and hence the angle of internal shearing resistance of the sand adjacent to the pile shaft, was

indeterminate. However, a survey of literature revealed the following:

Robinsky and Morrison (1964) stated that as the pile penetrated through the region of dense sand generated below the pile base, a thin sleeve of loose sand was created around the shaft. This was surrounded by a cylinder of denser sand, originally compacted by the pile base. The existance of a loose sleeve of sand was not evident from the author's results. However, a loose sleeve of sand adjacent to the pile shaft may be observed on Figure 7.10(b) extending to a radius of 1.3B. This showed that the closest approach of the author's density samples was approximately at the outer limit of the above zone. Adjacent to the penetrometer shaft ε_v was between the limits ±6.0%, which suggested that for a loose sand ϕ' adjacent to the pile shaft was, on average, the same as that prior to pile installation.

Poulos and Davis (1980) recommend a value for ϕ' adjacent to the pile shaft which was equal to the mean value below the pile base, before and after pile installation (Equation 7.4).

$$\phi'_s = \tfrac{3}{4}\phi' + 10 \qquad (7.4)$$

where:

ϕ'_s = angle of effective internal friction adjacent to pile shaft,

ϕ' = angle of effective internal friction prior to pile installation.

In view of the uncertainty regarding the value of ϕ' adjacent to the pile

shaft, for calculation purposes it was considered as being the same as that estimated for the sand prior to pile installation; that is, 32^0.

7.4 Boundary Orthogonal Stress Transducers

7.4.1 Pile Installation

The data presented in this section relates to a state of quasi-static equilibrium developed between the pile shaft and the soil during pile installation.

7.4.1.1 Homogeneous Sand Profiles

The average local unit shaft friction (f_z) recorded by each pair of BOSTs throughout pile installation, is present on Figures 7.11(a) and (b) as a function of pile embedment (D_b). It was observed that all BOSTs, regardless of their individual embedment, recorded a value of f_z which was a unique function of D_b. The results suggest that for a given D_b, f_z was constant along the pile shaft and increased in magnitude at a decreasing rate with greater D_b.

Feda (1963, 1976) suggested that f_z could be constant with depth along a pile shaft due to the effects of soil dilatancy on the pile shaft contact stresses. He concluded that the depth below which f_z first became constant was related to the amount of dilatancy the soil could undergo. For a highly dilatant soil a depth of typically 2.3 to 3.4 m was

required. Whereas for a soil of low dilatancy, f_z could be constant from ground level down.

Tentative extrapolation of the variation in f_z with D_b indicated a probable maximum value for f_z of 7.9 kPa at a D_b of 2850.0 mm (25.0B). The recorded maximum value of f_z (6.4 kPa) was in general agreement with the limiting value of f_s reported in Section 7.2.1.1, of 5.0 to 6.0 kPa.

The magnitude of f_z varied during pile installation, generally attaining a peak value at the start of each jacking increment. A further limited increase in f_z was observed towards the end of each jacking increment, although this was relatively small in comparison with the initial peak value. This behaviour was originally thought to be related to the relatively low stiffness of the BOSTs. However, comparable variations were observed in the development of Q_s.

During the initial stages of embedment of each pair of BOSTs, f_z developed relatively linearly at approximately 100.0 kPa/m of pile embedment, to the limiting value associated with the prevailing D_b.

The variation in σ'_r with D_b is not reported, since it was directly related to f_z by $1/\text{Tan}\delta'$, which was practically constant throughout pile installation (Section 7.4.1.3 Refer).

The residual values of f_z, developed at the conclusion of each jacking increment, followed the general trends reported for f_z throughout pile installation. The magnitude of the residual f_z was, however, typically one quarter of that recorded during pile installation.

7.4.1.2 Layered Soil Profile

The development of f_z within the overlying sand was comparable with that observed in S/S1 and S/S2, since it conformed with the unique function for the variation in f_z with D_b (Figure 7.11(c)). There were, however, two zones within the overlying sand where the development of f_z deviated from the idealized behaviour.

(i) Within a zone extending to 170.0.mm (1.5B) above the sand/clay interface, a significant increase in the rate of developement of f_z with D_b was recorded, which peaked at a value of typically 10.5 kPa immediately above the sand/clay interface. f_z remained relatively constant at this value irrespective of D_b. This was almost twice that recorded at the same depth in S/S1 and S/S2. A localised increase in f_z of this amount would account for the 0.5 kPa increase in f_z as indicated on Figure 7.2(c), for D_b equal to the depth to the sand/clay interface. Similar observations were reported by Meyerhof and Sastry (1978(a) and (b)). They suggested that this was due to the wedging action of the soil trapped between the rigid pile shaft and the deformable soil interface. Clemence and Brumund (1975) observed a sharp increase in f_z over the lower portion of a model pier in loose sand (the end of which passed through a rigid horizontal annular plate) to a height of 1.0B above pile base level. They considered that this was caused by the confining effect of the plate on the sand mass, which increased radial stresses on the pier resulting in a greater f_z.

(ii) Immediately above the zone outlined in (i) above, was a

region within which f_z was typically 0.5 to 1.0 kPa less than that recorded in S/S1 and S/S2. The start of this zone was evident at a depth of 500.0 mm (6.5B), and coincided with the boundary between sand layers 8 and 9. This gave further support to the existance of a lower sand density below sand layer 9 (Section 7.2.1.2 Refer).

The variation in residual f_z recorded in the sand to a depth of approximately 700.0 mm (6.1B), 575.0 mm (5.0B) above the sand/clay interface, conformed with that previously observed in relation to S/S1 and S/S2. However, as the BOSTs approached the sand/clay interface a significant increase in the residual f_z was recorded. A maximum value of typically -4.0 kPa was recorded within the sand immediately above the sand/clay interface. This was approximately twice the magnitude of residual f_z recorded at a comparable depth in S/S1 and S/S2. Such behaviour may be explained by the greater pile butt displacement recovery, as recorded at the conclusion of each penetration increment (Section 7.2.1.5 Refer). This effect was further enhanced by the increased in vertical effective stress generated within the sand to a limited height above the sand/clay interface, as a consequence of the greater displacement recovery of the clay surface (Section 7.2.1.5 Refer). This is discussed subsequently in Section 7.6.1.2.

The three pairs of BOSTs which penetrated into the clay, recorded practically identical variations in f_z with depth below the sand/clay interface. Typically, f_z increased linearly from 10.5 kPa, immediately below the sand/clay interface, to a maximum of 60.0 kPa at 230.0 mm (1.9B) below the sand/clay interface. The peak f_z coincided approximately with the maximum depth to which sand was drawn down around

the pile shaft into the underlying clay in a continuous layer. At greater depth a reduction in f_z was recorded, this was gradual at first but became progressively greater with depth. The maximum rate of reduction in f_z occurred at a depth of 320.0 mm (2.8B) below the sand/clay interface. This was comparable with the absolute limit to which sand was drawn down around the pile shaft into the underlying clay of 280.0 mm (2.5B). With further pile penetration, f_z tended towards a relatively constant value of typically 16.0 kPa. The observed distribution of f_z with depth below the sand/clay interface would account for the variation in Q_s, f_s and α, as shown on Figures 7.2 and 7.4.

Some doubt is expressed (Section 7.4.2.2 Refer) as to the validity of the residual f_z profile recorded within the clay, since this may reflect the lack of stiffness of the BOSTs relative to that of the clay.

7.4.1.3 Friction Angle Between the Pile Shaft and the Soil

The use of BOSTs obviated the need to undertake direct shear tests in order to determine the pile/soil friction angle (δ'). Figure 7.12 shows the variation in δ' ($Tan^{-1}(f_z/\sigma'_r)$) within the sand, throughout pile installation. The reported values relate to the last data scan at the end of each jacking increment. The results derived from the t = 1.5 mm BOSTs in S/S2 and S/M1 are excluded from these results. This was due, in the case of S/S2, to a poor connection with their power supply unit which resulted in periodic fluctuations in output. However, useful data was salvaged by undertaking a minor adjustment on these results. This required a knowledge of both δ', taken as the average value established from Figure 7.12 for S/S1 and S/S2, and the variation in f_z with D_b. The

results from the t = 1.5 mm BOSTs are also omitted in the case of S/M1, since it proved impossible to evaluate the amount of zero drift that occurred relative to σ'_r within the overlying sand during pile installation.

From Figure 7.12 it appeared that there was a slight reduction in δ' with depth, amounting to approximately 2^0. This occurred primarily within the upper 400.0 mm (3.5B) of the sand profit. However, for calculation purposes δ' was considered as being constant with depth and equal to the average value of 23.2^0. The results from S/M1 were omitted when calculating the average δ' in view of the adverse influence of the reduced sand density below 500.0 mm (4.4B) depth.

Coyle and Sulaiman (1967) suggested that δ' should reduce with depth in the field, on the basis of laboratory tests conducted on a pile element surrounded by sand within a modified triaxial cell. However, their procedure was criticised by Healy and Meitzler (1968) (Section 2.2.2 Refer).

A comparison of the average δ' reported by the author with those reported in literature for steel piles in sand proved favourable.

Reference	ϕ'	δ'
Coyle & Sulaiman (1967)	$(28\text{-}36)32^{0}$[a]	25^{0}
Hunter & Davisson (1969)	$(31\text{-}35)32^{0}$[a]	25^{0}
Holloway et al (1978)	$(31\text{-}35)32^{0}$[a]	$23\text{-}30^{0}$[b]
Author (1987)	32^{0}[a]	$23.2^{0}(24.3^{0})$[c]

a - Average value for range

b - Higher values relate to a higher ϕ'

c - Average value from ML test (static equilibrium)

Within the clay δ was directly affected by the prevailing pile/soil boundary conditions. To illustrate this the distribution of f_z developed within the clay during pile installation is reproduced on Figure 7.12, together with σ_r and δ.

The stresses acting on the pile shaft to a depth of 230.0 mm below the sand/clay interface were effective, due to the continuous layer of sand trapped between the pile shaft and the surrounding clay. Within this region the BOSTs recorded a linear increase in σ_r with depth from typically 20.0 kPa ($0.4C_u$) at the sand/clay interface to a maximum of 120.0 kPa ($1.8C_u$). This was associated with a proportionate increase in f_z as indicated by a relatively constant δ of typically 26 to 27^{0}, 3 to 4^{0} greater than that recorded within the overlying sand. The higher values of δ may be a consequence of the greater density of the sand trapped between the pile shaft and the clay. Results from the BOSTs located at 252.0 mm and 478.0 mm above pile base level, tended to show an increase in δ with depth below the sand/clay interface.

Between 230.0 and 290.0 mm (2.0 to 2.5B) below the sand/clay interface the soil in contact with the pile shaft consisted primarily of clay, interspersed with isolated sand grains. The contact stresses within this region may still have been effective since δ was essentially the same as that recorded above a depth of 230.0 mm (2.0B) below the sand/clay interface. However, within this region there was a general reduction in both f_z and σ_r.

At depths greater than 290.0 mm (2.5B) below the sand/clay interface the soil in contact with the pile shaft was clay, for which contact stresses of typically 16.0 kPa ($0.2C_u$) and 60.0 kPa ($0.8C_u$) were recorded for f_z and σ_r respectively, together with a δ of typically 15.0^0. A considerable variation in δ was observed, which ranged between 7 and 21^0. The state of stress at the pile/soil contact may be considered to be predominantly effective in view of the relatively short drainage paths as a result of the sand plug formed below the pile base and the drawn down of sand around the shaft.

From the results of both field and laboratory experiments, Clark and Meyerhof (1972) reported that a typical value for σ'_r acting on the pile shaft in clay was 1.6 C_u. This was greater than that reported by the author and may reflect the limited embedment of the pile into the clay and the 'flexibility' of the secondary clay tank.

The assumption of near effective stress conditions at the pile/clay interface is supported by Butterfield and Johnston (1973). They jacked a 100.0 mm diameter pile, instrumented with a type of BOST, 3.3 m into a stratified soil profile consisting of stiff, brown silty clay (2.5 m thick) overlying a stiff, dark grey silty clay of low sensitivity, which

contained small fissures at shallow depths. The rate of installation was 21.0 mm/min, more than twice that employed by the author. During intallation, followed by immediate extraction, a δ of $10^0 \pm 3^0$ was recorded in 72.0% of their results, with extremes of 4^0 and 20^0. They concluded that an appreciable and essentially constant proportion of σ_r was effective across the pile/clay interface.

7.4.1.4 Variation in the Local Coefficient of Earth Pressure with Depth and Pile Embedment

From the unique function for the variation in f_z with D_b, it was possible to calculate the magnitude of σ'_r acting on the pile shaft at any level within the sand for a given D_b, and hence evaluate the local earth pressure coefficient (K_z). It was assumed that the vertical effective stress (σ'_z) adjacent to the pile shaft at a given depth was equal to the effective overburden stress at that depth prior to pile installation, and that $\text{Tan}\delta'$ was constant at 0.429 (23.2^0) (Section 7.4.1.3 Refer) along the pile shaft. A linear relationship was found to exist between the variation in K_z with depth for a given D_b/B when both were plotted on logorithmic axes. This relationship is defined by Equation 7.5 within the limits of the test programme.

$$K_z = \left(\frac{B}{Z}\right)\left(\frac{D_b}{B}\right)^{0.791} \qquad (7.5)$$

Recorded values of σ'_r were used to evaluated K_z directly for a range of pile embedment and are presented on Figure 7.14 in conjunction with the variation in K_z as defined by Equation 7.5.

Equation 7.5 shows that K_z increases at a diminishing rate for a given B/Z with greater D_b/B. Further, the magnitude of K_z at any two points along the pile shaft (for a particular value of D_b/B) reduces inversely with the ratio of the depths. That is:

$$\frac{K_{z_1}}{K_{z_2}} = \frac{\frac{Z}{B}_2}{\frac{Z}{B}_1} \qquad (7.6)$$

Coyle and Sulaiman (1967) presented data relating to the development of f_z with shaft displacement at various depths along the shaft of a steel pile in sand. These were normalised with respect to the ultimate shear strength of the sand at that depth (τ_f). The ratio f_z/τ_f, equivalent to K_z, was evaluated for a displacement of 7.4 mm, sufficient to satisfy the criterion for pile shaft failure. The inverse relationship of Equation 7.6 was then applied to the data taking f_z/τ_f at a depth of 5.0 ft as datum. Reasonable agreement was established between the actual and derived distribution in view of the potential variability of field data.

Depth Z(ft)	K_z Actual f_z/τ_f	K_z According to Eq 7.6
5	7.00	7.00
15	2.21	2.33
25	1.22	1.40
35	0.81	1.00
45	0.52	0.78

Coyle and Sulaiman (1967) suggested that the very high values of K_z deduced at shallow depths, were due to the densification of the sand near

the top of the pile as a result of driving; thus, increasing τ_f. Therefore, if the actual value of τ_f adjacent to the upper portion of the pile shaft was known, the calculated magnitude of K_z would be less. Sand densities recorded near the surface by the author showed no indication of being greater than those recorded at depth. The probable cause of the higher values of K_z values near the surface was the erroneous assumption that σ_z' adjacent to pile shaft was equal to the effective overburden stress (γZ) prior to pile installation (Section 7.4.4.3 Refer).

K_s was determined by integrating Equation 7.5 between the limits of 1 to D_b/B (Equation 7.7). The variation in K_s, together with that of K_z, with D_b/B, is shown on Figure 7.15, from which it was observed that K_s tended to 1.7 for D_b/B greater than 10.

$$K_s = \frac{\left(\frac{D_b}{B}\right)^{0.791} \log_e\left(\frac{D_b}{B}\right)}{\frac{D_b}{B} - 1} \qquad (7.7)$$

The depth (Z_e) at which the ratio of effective overburden stress to σ_r' was equal to K_s is given by Equation 7.8. This equation was evaluated and is shown on Figures 7.14 and 7.15.

$$\frac{Z_e}{B} = \frac{\frac{D_b}{B} - 1}{\log_e\left(\frac{D_b}{B}\right)} \qquad (7.8)$$

It is apparent from Figure 7.15 that for D_b/B greater than 10,

Equation 7.8 can be approximated to:

$$\frac{Z_e}{B} = \frac{1}{4}\left(6 + \frac{D_b}{B}\right) \qquad (7.9)$$

Thus, Q_{sf} can be calculated from Equation 7.10:

$$Q_{sf} = \pi B D_b \gamma Z_e K_s \tan\delta' \qquad (7.10)$$

However, for $D_b/B > 10$, K_s tended to 1.7

Therefore,

$$Q_{sf} = \pi B D_b \gamma K'_e \tan\delta'$$

where:

$$K'_e = 0.425(6 + D_b/B)$$

The variation of K'_e with D_b/B is presented on Figure 7.15, together with values of K'_e deduced from experimental data presented in literature for piles tested in loose sand.

7.4.2 Maintained Load Test

7.4.2.1 Homogeneous Sand Profiles

The post-compressive residual f_z (Figures 7.16(a) and (b)) was negative and increased in intensity with depth from approximately -1.0 kPa near the surface to -1.7 kPa in the vicinity of the pile base. The first increment of Q_a, 2.3 kN ($33.3\%Q_{aw}$), was sufficient to reduce this to approximately zero at all points along the pile shaft.

At Q_{aw}, f_z tended to increase to a depth of approximately 1000.0 mm (8.8B). At greater depth f_z was relatively constant at 3.5 kPa. Unloading the pile and reapplying Q_{aw} had the effect of increasing f_z by typically 8.3%. This was also reflected in Q_s which was increased by 10.5%, and was associated with a 2.8% reduction in Q_b of about 0.17 kN.

For applied loads of greater than $133\%Q_{aw}$, the variation in f_z with Z was 'Dee' shaped, as described by Vesic (1970). This was due to a reduction in the rate of increase in f_z at the upper and lower limits of the pile shaft, and was first observed for Q_a in excess of 200.0% and $133.3\%Q_{aw}$ (9.3 and 13.9 kN) respectively, the latter being associated with a state of incipient shaft failure (Figures 7.7(a) and (b)). The above loads were associated with pile base and butt settlements of typically 2.16 mm (1.89%B) and 1.91 mm (1.67%B), and 0.97 mm (0.85%B) and 0.76 mm (0.66%B) respectively. The further development of f_z over the lower portion of the pile shaft was limited below 650.0 mm (5.7B) above pile base level.

Touma and Reese (1974) described a mechanism, in relation to bored piles

in sand, which accounted for the reduction in f_z above pile base level. They considered that the soil below the pile base was compressed due to the action of high stresses, which were sufficient to cause arching around the pile base. Two distinct zones were considered to develop around and above the pile base due to a displacement incompatibility between the sand above and below pile base level; namely, 'flow' and 'arching' zones. A reduction in stress levels adjacent to the pile shaft occurred within the flow zone, whilst increased stress levels were produced within the arching zone which surrounded the flow zone. The size of the zones was influenced by the sand density and the amount of base settlement, with dense sand generating the worst condition.

The irregular distribution of f_z along the pile shaft at Q_{amax} (17.4 kN) may be attributed to the state of quasi-static equilibrium developed between the pile and soil, since the minimum rate of settlement of 0.3 mm/hr was not attained.

Unloading the pile to $\frac{1}{2}Q_{amax}$ (8.5 kN) resulted in typically an 80.0% reduction in f_z to between 0.0 and 2.0 kPa, with the higher values occurring at depth. The distribution of f_z at $\frac{1}{2}Q_{amax}$ was different from that recorded during loading for a comparable Q_a of $133.3\%Q_{aw}$ (9.4 kN), being on average 3.0 kPa less at any depth. The greater reduction in f_z over the upper portion of the pile shaft may be considered indicative of the development of shaft friction as proposed by Hanna (1969) and expanded upon by Hanna and Tan (1971).

Upon removal of Q_a, f_z was again restored to the post-compressive residual distribution, and was comparable with that recorded at the start of the test.

The distribution of σ'_r along the pile shaft (Figures 7.17(a) and (b)) remained relatively unchanged from the post-compressive residual distribution until such time as Q_a approximately equal to $66.7\%Q_{aw}$ (4.6 kN). Thereafter, σ'_r increased progressively until such time as Q_a was equal to $133.3\%Q_{aw}$ (9.3 kN), beyond which the development of σ'_r was proportional to f_z, since f_z/σ'_r was equal to $\text{Tan}\delta'$. The reduction in σ'_r above pile base level for elevated values of Q_a, was in accord with the formation of a flow zone within the sand as described by Touma and Reese (1974). There was, however, no clear evidence of any significant increase in σ'_r associated with the formation of a zone of arching. Koizumi (1971) also reported a reduction in σ'_r over the lower portion of a pile shaft in sand. The stress changes in this case were recorded directly using earth pressure cells set into the pile wall.

The function $f_z/\sigma'_r = \text{Tan}\delta'$ was no longer valid as the pile was unloaded to $\frac{1}{2}Q_{amax}$ (8.5 kN). The distribution of σ'_r along the pile shaft at $\frac{1}{2}Q_{amax}$ was generally comparable with that recorded at a similar Q_a during loading; namely, $133.3\%Q_{aw}$ (9.3 kN). The magnitude of σ'_r at the upper and lower limits of the pile shaft, however, tended towards that recorded at Q_{aw} (7.2 kN). The reduced value of σ'_r immediately above pile base level suggested that the flow and arching zones within the sand remained partially mobilized.

The distribution σ'_r recorded upon removal of Q_a, was comparable with that recorded at the start of the test.

An indication of the distribution of K_z mobilized throughout pile loading may be obtained from Figures 7.17(a) and (b). For Q_a of less than, or equal to, $66.7\%Q_{aw}$ (4.6 kN), K_z tended to K_o over a significant portion

of the lower section of the pile shaft. However, at Q_{amax}, K_z varied from around 5.0 near the surface, greater than K_p, to approximately 0.6 near the base of the pile shaft.

7.4.2.2 Layered Soil Profile

The magnitude of the post-compressive residual f_z (Figure 7.18) within the overlying sand, was greater at any depth than that recorded in S/S1 and S/S2. This was due to the greater pile displacement recovery and increased stress levels generated in the sand directly above the sand/clay interface, as a result of the greater displacement recovery of the sand/clay interface (Sections 7.2.1.5 and 7.6.1.2).

As the pile was loaded, the rate of mobilization of f_z within the sand per unit Q_a was less than that observed in S/S1 and S/S2. This was due to the smaller relative displacment developed between the pile shaft and the adjacent sand per unit Q_a, as a consequence of a greater proportion of Q_a being resisted by the underlying clay, within which the shaft resistance was initially mobilized more rapidly for a given ω_s.

The reapplication of Q_{aw} increased f_z within the sand and clay by typically 10.6% and 0.8% respectively. This was associated with a total increase in Q_s of 3.7%, and a 2.6% reduction in Q_b of 0.14 kN. The average increase in f_z within the sand was 0.3 kPa, which was comparable with that observed in S/S1 and S/S2.

At Q_{amax}, the magnitude of f_z within the overlying sand appeared to be similar to that reported for S/S1 and S/S2. During pile installation a

significant increase in f_z was recorded to a height of 170.0 mm (1.5B) above the sand/clay interface (Section 7.4.1.2 Refer). This increase did not appear to be apparent during the ML test. From the f_z/D_b profiles presented on Figure 7.11(c) it was estimated that a maximum f_z of typically 10.5 kPa could be developed within the sand at, and immediately above, the sand/clay interface. Whilst that portion of the pile shaft immediately above the zone of influence of the clay may be subjected to a relatively uniform f_z of 6.6 kPa. Closer inspection of the results showed that both of these conditions were fulfilled, although they were obscured to some extent by scatter in the data.

Unloading the pile to $\frac{1}{2}Q_{amax}$ resulted in a reduction in f_z above a depth of 1000.0 mm (8.8B), which was greater by between 0.5 and 1.0 kPa than that recorded during S/S1 and S/S2. This was a consequence of the greater pile butt displacement recovery, which resulted in an increased relative displacement between the pile shaft and the adjacent sand. At depths greater than 1000.0 mm (8.8B) the reduction in f_z was less pronounced, whilst immediately above the sand/clay interface f_z was approximately 3.0 kPa, typically twice that recorded at a comparable depth in S/S1 and S/S2. This behaviour was a result of the increased stress levels and lower relative displacement developed between the pile shaft and the adjacent sand, as a consequence of the greater displacement recovery of the clay surface on unloading.

Upon removal of Q_a, the post-compressive residual distribution of f_z was again restored.

The residual distribution of f_z recorded within the underlying clay, may be erroneous since no satisfactory explanation can be offered for the

recorded distribution in terms of pile shaft/clay interaction.

At Q_{aw} (6.9 kN), ω_s was equal to 0.39 mm (0.34%B). f_z recorded at and beyond Q_{aw} was, therefore, considered to be representative of the actual state of stress acting on the pile shaft within the clay.

The magnitude of f_z developed within the clay for an applied load of 233.3%Q_{aw} (16.1 kN) conformed with the profile of maximum f_z recorded during pile installation. The reduction in f_z recorded by the lower two pairs of BOSTs at Q_{amax} (18.1 kN) was not, therefore, solely attributable to a reduction in stress levels adjacent to the shaft above pile base level (Touma and Reese, 1974), but reflected the prevailing pile shaft/clay boundary conditions.

Upon reducing the applied load to $\frac{1}{2}Q_{amax}$, (8.81 kN) the distribution of f_z within the clay was similar to that recorded for a Q_a of 133.3%Q_{aw} (9.6 kN) during loading.

On complete removal of Q_a the 'pseudo' post-compressive distribution of residual f_z was again recorded.

The development of σ_r' along the pile shaft within the overlying sand (Figure 7.19), remote from the influence of the underlying clay, was comparable with that reported for S/S1 and S/S2, with due allowance for the reduced settlement per unit Q_a The maximum σ_r' recorded immediately above the sand/clay interface was greater than that observed in S/S1 and S/S2 for the reasons previously outlined above.

The post-compressive residual σ_r developed within the clay lay typically

between the limits 0.75 to 1.05 C_u. A small increase in σ_r was recorded during loading which amounted to about 0.24 C_u (16.4 kPa) at Q_{amax} (18.1 kPa). The ratio $\Delta\sigma_r/\Delta f_z$ was typically 35.6%, compared with 120.0 to 130.0% recorded within the sand at the same depth in S/S1 and S/S2.

The limited increase in σ_r recorded during loading was in agreement with observations reported in literature.

Reese and Seed (1955) tested a 152.4 mm diameter instrumented pile in a 4.5 m stratum of soft, saturated clay and reported that loading caused little, if any, permanent effect on σ_r.

Esrig and Kirby (1979(a)), on the basis of a finite element study, suggested that the mean increase in the total normal stress acting on a pile shaft during loading was generally less than 0.1 f_z.

7.4.2.3 The Mobilization of Local Unit Shaft Friction, Radial Stress and Friction Angle with Mean Shaft Displacement

The mobilization of f_z, σ_r' and δ' with ω_s for S/S1 and S/S2 is presented on Figures 7.20(a) and (b). For clarity, only data from every second pair of BOSTs along the pile shaft is reported.

A ω_s of typically 0.06 mm (0.05%B), corresponding to an applied load of 2.5 kN (33.3%Q_{aw}), was required in order to nulify the post-compressive residual f_z. This agreed with the observations reported in relation to the development of Q_s (Section 7.2.3.1 Refer). For ω_s between the limits 0.06 and 0.87 mm (0.05 and 0.73%B), corresponding with applied loads of

2.5 to 9.6 kN (33.3 and 133.3%Q_{aw}), and with due allowance for the step in the f_z/ω_s profile as a consequence of the reapplication of Q_{aw}, the rate of development of f_z with ω_s was relatively linear. This agreed with the observed behaviour reported for Q_s in Section 7.2.3.1. The greatest rate of increase in f_z with ω_s was associated with the deeper BOSTs.

For ω_s in excess of 0.87 mm (0.73%B), corresponding with an applied load of 9.6 kN (133.3%Q_{aw}), f_z increased at a diminishing rate. This effect was most noticeable over the lower portion of the pile shaft and indicated that a base displacement slightly in excess of 0.71 mm (0.62%B) was required in order to mobilize the flow and arching zones (described by Touma and Reese (1974)) within the sand around the pile shaft to a height of 117.0 mm (1.0B) above pile base level. With further ω_s this effect was observed to propogate along the pile shaft, confirming the prognosis of Touma and Reese (1974) that the extent of the arching and flow zones was influenced by the amount of pile base settlement.

The rate of increase in f_z tended to zero at all points along the pile shaft for ω_s in excess of typically 2.2 mm (1.9%B), at which f_z was between 6.0 and 8.0 kPa. This was slightly less than the ω_s required to mobilize Q_{sf} (Section 7.2.3.1), and may be attributed to interpretation of the two sets of independent data.

For Q_a less than, or equal to, 4.7 kN (66.7%Q_{aw}), associated with a maximum ω_s of typically 0.29 mm (0.25%B), σ'_r was essentially constant at any given depth and tended to increase with depth. Thereafter, σ'_r increased at a progressively greater rate, attaining a maximum rate of increase for a ω_s of typically 0.87 mm (0.76%B), corresponding to an

applied load of approximately 9.6 kN (133.3%Q_{aw}). At greater ω_s the rate of increase in σ_r' with ω_s diminished and the magnitude of σ_r' varied in proportion with f_z, since the condition $f_z/\sigma_r' = \text{Tan}\,\delta'$ was attained.

The ratio of f_z to σ_r' is a measure of the degree of mobilization of δ'. This was initially 'negative' due to the negative post-compressive residual f_z. Application of the first loading increment reduced δ' to approximately zero along the entire length of the pile shaft. Thereafter, δ' increased at a diminishing rate to an average maximum value of Tan^{-1} 0.452 ($24.3^{\emptyset}$). This was attained at a ω_s of 1.20 mm (1.1%B), approximately one half of that required to mobilize the maximum f_z. At Q_{aw}, typically 6.9 kN, 80.0% of the maximum δ' was mobilized. At the point of mobilization of the maximum value of δ', f_z and Q_s were approximately 80.0% of their respective ultimate values. Further, f_z was marginally in excess of the limit of acceptable linear behaviour with respect to ω_s. The further increase in f_z may be attributed to the increase in σ_z' induced within the sand adjacent to the pile shaft at a given depth by the accumulative effect of f_z above the depth in question. This effect was taken into account theoretically by Birch-Hansen (1968) in calculating the ultimate resistance of a pile shaft in a granular medium.

the rate of mobilization of δ' with ω_s may reasonably be compared to the rate of increase in potential difference across a charging capacitor. Thus, if the ω_s required to reduce the residual friction angle to zero is ω_{sr}, then δ' for any ω_s in excess of ω_{sr} (ω_s') can be evaluated from Equation 7.10.

$$\text{Tan}\delta'_{\omega'_s} = (1 - e^{\alpha})\,\text{Tan}\delta' \qquad (7.10)$$

where:

$$\alpha = \frac{\omega_s - \omega_{sr}}{0.35} = \frac{\omega'_s}{0.35}$$

δ' = effective friction angle between the pile shaft and soil at failure (24.3^0)

ω'_s = displacement in excess of that required to eliminate the negative residual shaft friction.

Figures 7.20(c) and (d) show the development of f_z, σ_r and δ with ω_s for S/M1. The results from those BOSTs initially located at a depth of 414.0 mm and 823.0 mm within the sand were omitted for clarity.

The lower relative pile shaft/sand displacement per unit Q_a, and the higher post-compressive residual f_z, required a Q_a of slightly less than 4.7 kN ($66.6\%Q_{aw}$) in order to eliminate the post-compressive residual f_z developed within the overlying sand. The rate of development of f_z with ω_s was marginally less than that observed in S/S1 and S/S2, and the extent of acceptable linear behaviour tended to increase with depth from approximately 0.67 mm (0.59%B) at 207.0 mm (1.8B), 1068.0 mm (9.4B) above the sand/clay interface, to 1.66 mm (1.46%B) at 1024.0 mm (9.0B), 251.0 mm (2.2B) above the sand/clay interface. At a depth of 1229.0 mm (10.8B), 46.0 mm (0.4B) above the sand/clay interface, f_z tended to increase at a progressively greater rate for shaft displacements in excess of 1.01 mm (0.89%B). This was probably a consequence of the onset

of the wedging mechanism, as discussed in Section 7.4.1.2. The ω_s associated with f_{zf} could not be established with any certainty due to the limited amount of data. However, an upper limit of 3.6 mm (3.2%B) may be appropriate.

The change in σ_r' with ω_s underwent a pronounced reduction for ω_s less than 0.39 mm (0.34%B), corresponding to an applied load of 7.1 kN (Q_{aw}). Thereafter, σ_r' increased to a maximum value in a manner similar to that reported for S/S1 and S/S2.

In view of the smaller relative pile shaft/sand displacement, an increased ω_{sr}, typically 3.2 times greater than established for S/S1 and S/S2, was required in order to reduce δ' to zero.

The development of the pile shaft contact stresses within the clay were directly influenced by the prevailing pile shaft/soil boundary conditions, which varied with depth below the sand/clay interface. These were, for each pair of BOSTs:

Depth Below Sand/Clay Interface (mm)	Friction Angle (Deg)	Pile Shaft/Soil Boundary Condition
123	33.0^0	A 5.0 mm thick, continuous layer of sand between the pile shaft and the surrounding clay
309	27.5^0	Predominantly clay with widely dispersed sand grains
484	19.8^0	Clay

The rate of mobilization of f_z per unit ω_s within the clay was similar for all three boundary conditions and was relatively linear for pile shaft displacements of less than 1.01 mm (0.89%B, corresponding with Q_a of 11.7 kN ($166.7\%Q_{aw}$). Thereafter, f_z increased at a diminishing rate and approached a maximum value for a shaft displacement slightly in excess of 1.54 mm (1.35%B), corresponding with a Q_a of 13.9 kN ($200.0\%Q_{aw}$).

The development of σ_r within the underlying clay exhibited similar characteristics, to a greater or lesser extent, to those reported for the overlying sand. These were: a limited ω_s within which σ_r' remained relatively constant during the initial stages of loading; a progressively greater rate of increase in σ_r per unit ω_s to a maximum rate; a reducing rate of increase in σ_r per unit ω_s to the maximum value for a given depth.

The mobilization of δ within the clay may reasonably be expressed by Equation 7.10, where:

$$\alpha = \frac{\omega_s - \omega_{sr}}{0.5} = \frac{\omega'_{sr}}{0.5}$$

The limiting value of δ within the clay, varied directly with the pile shaft/soil boundary condition, reducing with greater dispersion of the sand grains.

7.4.3 Constant Rate of Uplift Test

7.4.3.1 Homogeneous Sand Profiles

The distribution of the post-compressive residual f_z (Figure 7.21) at the start of the CRU test compared favourably with that recorded at the conclusion of the ML test to within typically ± 0.5 kPa. This suggested that preparing the pile and loading system to undertake the CRU test, caused only minimal disturbance to the state of stress around the pile shaft at the end of the ML test.

Over the upper portion of the pile shaft, f_z attained a value of, on average, -2.2 kPa for a ω_s of typically -1.10 mm (0.96%B), corresponding to a Q_a of -2.1 kN. With further uplift f_z was observed to vary only marginally from this value. The essentially constant f_z extended to a depth of 800.0 mm (7.0B), below which f_z continued to increase with uplift. This resulted in a concentration of resistance to uplift over

the lower portion of the pile shaft. A similar concentration was observed by Williams (1981) and Reese and Cox (1976). The development of f_z over the lower portion of the pile shaft continued until Q_{sf} was attained for a pile uplift of, on average, -6.58 mm (5.77%B), corresponding with a Q_a of typically -2,68 kN. With greater pile uplift the distribution of f_z remained relatively constant until ω_s was equal to -11.91 mm (10.45%B), during which Q_a was also constant. Thereafter, below 292.0 mm (2.6B) above pile base level, f_z reduced dramatically and reached a value at 117.0 mm (1.0B) above pile base level which was comparable with the initial post-compressive residual f_z. This was accompanied by a limited increase in f_z of between 0.5 and 1.0 kPa within a region from 292.0 to 800.0 mm (2.5B to 7.0B) above the pile base. This may be explained as follows. The uplift of the pile formed a void in the sand below the pile base. Thus, sand from around the pile shaft, in the immediate proximity of the pile base, flowed into the void and resulted in a reduction in the stress intensity within the sand in this region. Above the region of flowing sand a zone of arching sand was formed, within which stress levels were increased. The increased stress levels within the sand arch were reflected in the progressive increase in σ'_r and f_z as the size of the flow zone increased throughout pile uplift (Figure 7.21). This is similar in concept to the mechanism proposed by Touma and Reese (1974) to account for the reduction in f_z above base level when loading a pile in compression.

The development of σ'_r mirrored that of f_z throughout pile uplift, since the limiting ratio of f_z/σ'_r equal to $-\text{Tan}\delta'$ was attained at all points along the pile shaft within the first increment of pile uplift. The increase in σ'_r with pile uplift suggested that σ'_z was also increased adjacent to the pile shaft. This does not agree with the supposition

that σ_z' is reduced adjacent to the shaft of a pile loaded in tension; thus, accounting for the lower ultimate tensile resistance of a pile shaft as compared with the ultimate compressive resistance (Broms, 1966; Birch-Hansen, 1968).

The inadvertant partial extraction of the pile at the end of pile installation during S/S1, gave an indication of the probable magnitude and distribution of the post-tensile residual f_z and σ_r' at the conclusion of the CRU test. The magnitude of f_z was positive and of a similar order to that developed for a Q_a of 4.6 kN (66.7%Q_{aw}) during the ML test. The reduced intensity of f_z over the lower portion of the pile shaft suggested that unloading alone was insufficient to neutralize the flow and arching zones developed within the sand around the pile base. The magnitude of the post-tensile residual σ_r' was similar to the distribution of σ_r' recorded at a Q_a of 6.9 kN (Q_{aw}) during the ML test, and was typically 4.0 kPa greater at all levels along the pile shaft than the post-compressive residual σ_r'.

7.4.3.2 Layered Soil Profile

The profiles of post-compressive residual f_z and σ_r' (Figures 7.23 and 7.24) developed within the sand to a depth of approximately 650.0 mm (5.7B), 625.0 mm (5.5B) above the sand/clay interface, experienced a limited increase throughout the CRU test. This suggested that the maximum mobilizable tensile f_z and σ_r' had already developed over this section of the pile shaft, possibly as a consequence of the greater post-compressive displacement recovery characteristics of the pile (Section 7.2.1.5 Refer). The magnitude of the maximum f_z acting over the

upper portion of the pile shaft, was comparable with that recorded during S/S1 and S/S2 of typically 2.2 kPa.

Below a depth of 650.0 mm (5.7B) the development of f_z and σ'_r within the overlying sand, departed from the behaviour previously observed in S/S1 and S/S2. This effect was most pronounced immediately above the sand/clay interface. However, the relationship f_z/σ'_r equal to $-\text{Tan}\delta'$ was sustained throughout the of the CRU test. The maximum stress acting on the shaft within the sand was recorded by a pair of BOSTs sited at approximately 30.0 mm (0.3B) above the sand/clay interface. At this depth the stress levels were typically 1.6 times greater than those recorded at the same depth during the ML test, and 3.3 times greater than those recorded at a comparable depth in S/S1 and S/S2 during the CRU test. This was a result of the upward displacement of the clay surface during the CRU test, which induced a localized increase in the stress levels within the sand directly above the sand/clay interface. Such behaviour was consistent with that previously reported in relation to the higher residual f_z recorded immediately above the sand/clay interface during pile installation, and is supported by data from the ELs and DPTs sited on the sand/clay interface (Sections 7.5.3.2 and 7.6.3.2 Refer).

Within the underlying clay the magnitude of f_z was observed to increase from the 'pseudo' post-compressive residual distribution at a diminishing rate throughout pile uplift, and tended to an upper limiting value equal to that recorded during pile installation (transposed), for a Q_a of -9.22 kN (Q_{sf}) and a ω_t of -11.12 mm (9.8%B).

The distribution of σ_r along the pile shaft within the clay varied only marginally for a ω_t of less than typically -2.11 mm (1.9%B). For ω_t in

excess of -2.11 mm (1.9%B), the rate of developement of σ_r increased and tended to a steady state for a Q_a of -9.22 kN (Q_{sf}), where the distribution of σ_r was comparable with that recorded during pile installation.

7.4.4 Stresses Developed on the Pile Shaft/Soil Interface During Both Compressive and Tensile Loading

To obtain an indication of the stress history adjacent to the pile shaft under both compressive and tensile loading, the variation in f_z with σ'_r was plotted for both the ML and CRU tests. These are presented on Figures 7.25(a), (b) and (c) for S/S1, S/S2 and S/M1 respectively, for various levels along the pile shaft.

7.4.4.1 Homogeneous Sand Profiles

The data presented on Figures 7.25(a) and (b) described what may loosely be termed a 'hyperbola', with asymtopic axes diverging from the origin at approximately $\pm 23.4^0$. Data from the CRU test was tangential to the $-\delta'$ envelope at stress levels significantly lower than those required to achieve initial tangency with the $+\delta'$ envelope during the ML test. The two limbs of the 'hyperbola' were not, therefore, symmetrical.

The post-compressive residual f_z, recorded prior to the ML test, was negative over the embedded length of the pile shaft. The magnitude of the post-compressive residual f_z, together with the associated σ'_r, was insufficient to lie on the $-\delta'$ envelope. This would appear to indicate

that the prevailing residual stresses were not associated with a state of shear failure within the sand adjacent to the pile shaft. However, this may not be the case, as will subsequently be shown (Section 7.4.4.3 Refer).

The first increment of Q_a, typically 2.3 kN ($33.3\%Q_{aw}$), was sufficient to reduce f_z to approximately zero at all levels along the pile shaft. This occurred in conjunction with a small ω_s of approximately 0.07 mm (0.06%B), resulting in a $\Delta f_z/\Delta\omega_s$ of typically 20.0 kPa/mm. The condition f_z equal to zero corresponded to the apex of the 'hyperbola' and, as such, required an associated reduction in σ'_r. The magnitude of the reduction in σ'_r was limited in S/S1 and S/S2, but was clearly evident within the overlying sand of S/M1 (Figure 7.20(c)). The greatest reduction in σ'_r occurred in association with the higher values of negative residual f_z, as would be expected from the nature of the f_z-σ'_r profiles. As Q_a increased, f_z developed at a diminishing rate whilst σ'_r increased at a progressively greater rate, until such time as the limiting condition f_z/σ'_r equal to $+\text{Tan}\delta'$, was reached (that is; the point of initial tangency with the $+\delta'$ envelope). For positive values of f_z up to the point of initial tangency with the $+\delta'$ envelope, $\Delta f_z/\Delta\omega_s$ was relatively consistent at 6.0 kPa/mm, 30.0% of that recorded in reducing the post-compressive residual f_z to zero. A further increase in Q_a resulted in an additional increase in both f_z and σ'_r, the probable cause of which was outlined in Section 7.4.2.3. Thoughout the latter stages of loading, f_z/σ'_r sustained the ratio 0.453 ($\text{Tan}24.3^0$) to a limiting value at all points along the pile shaft. This occurred in association with a reducing rate of $\Delta f_z/\Delta\omega_s$, which eventually tended to zero at Q_{sf}. Immediately above pile base level the development of stresses on the pile shaft, in excess of those associated with the condition of initial

tangency with the $+\delta'$ envelope, were limited due to the developement of arching and flow zones within the sand around and above the pile base (Touma and Reese, 1974).

The pile was unloaded from Q_{amax} in two equal increments, therefore only one set of intermediate data points are available for analysis, corresponding with a $\frac{1}{2}Q_{amax}$. When plotted, the data points were remote from the compressive loading curve of the f_z-σ'_r profiles, and were initially thought to be a spurious set of results, possibly as a consequence of 'shear lag' in the BOSTs. However, it was subsequently observed that in some instances a straight line passing through this data point, and that associated with the post-compressive residual stress, was parallel to the $+\delta'$ envelope ($+\delta'_u$). Additional support for this observation was obtained from data recorded as the pile was unloaded on completion of the CRP test. A possible explanation for this behaviour is offered subsequently in Section 7.4.4.3.

Data from the strain controlled CRU test lacked the small displacement increments associated with the initial stages of the ML test. As a consequence the first set of post-residual data was generally found to lie on the $-\delta'$ envelope. This occurred for stress levels and pile butt displacements which were approximately 50.0% of those required to attain initial tangency during the ML test. With further uplift of the pile there was an increase in both $-f_z$ and σ'_r, which sustained the ratio of -0.453 ($\text{Tan}24.3^0$) throughout loading.

For a pile uplift (ω_t) in excess of typically -11.91 mm (0.1B), the stresses acting on the pile shaft at 117.0 mm (1.0B) above base level reduced for the reasons previously outlined in Section 7.4.3.1. In doing

so the variation of f_z with σ'_r traversed the $-\delta'$ envelope, ultimately reducing to a value of less than the post-compressive residual stress recorded at that depth.

The post-tensile residual stresses, surmised from S/S1 at the end of pile installation (Section 7.2.2.1 Refer), are presented on Figure 7.25(a). Since each data point lay within the $+f_z$ sector of the f_z-σ'_r profile it may be assumed that the f_z-σ'_r profile described upon unloading on completion of the CRU test, was similar to that observed during the unloading phase of the ML test, and followed a path parallel to the $-\delta'$ envelope ($-\delta'_u$) over the latter stages. It is possible, however, to envisage a pile of sufficient self-weight to cause shear failure within the sand adjacent to the pile shaft when unloaded, in the absence of end bearing. Thus, the post-tensile residual stress need not lie on the compressive f_z-σ'_r profile at the point of initial intersection.

It is apparent from Figures 7.25(a) and (b) that the ratio f_{zmax}(tension)/f_{zmax}(compression) was not constant along the pile shaft. Above a depth of 800.0 mm (7.0B) the ratio was relatively constant at approximately 0.35. Below this depth, however, the ratio increased at a progressively greater rate and tended to unity in the vicinity of the pile base. Such a distribution compared favourably with the average value of Q_{sf}(tension)/Q_{sf}(compression) of typically 0.44.

7.4.4.2 Layered Soil Profile

The development of f_z and σ'_r within the overlying sand of S/M1 was generally similar to that reported for S/S1 and S/S2. The exception to

this being the elevated values of f_z and σ'_r recorded by the two pairs of BOSTs located immediately above the sand/clay interface. This difference was particularly pronounced during the CRU test for the reasons previously outlined in Section 7.4.1.2. The stresses recorded by the pair of BOSTs sited within the sand immediately above the sand/clay interface, deviated from the $-\delta'$ envelope during the latter stages of the CRU test. This may be attributed to σ'_r exceeding the calibration limits of the t = 0.6 mm BOSTs.

Below the sand/clay interface the upper two pairs of BOSTs exhibited broadly similar features to those reported within the sand. These included the progressive increase in f_z and σ_r beyond that required to achieve initial tangency with the $\pm\delta$ envelopes, and a $+\delta_u$ envelope.

The magnitude of δ varied only marginally with depth below the sand/clay interface, from an average of 32.4^0. In the case of the upper two pairs of BOSTs, δ was the same for both the CRU and ML tests, and was in-keeping with the values recorded at comparable depths during pile installation. However, this appeared to be excessive in the case of the lower pair of BOSTs, in view of the nature of the pile shaft/soil interface, and was only attained during the CRU test.

7.4.4.3 The State of Three Dimensional Stress Developed Within the Sand Adjacent to the Pile Shaft Throughout Pile Loading

On the basis of the results and discussions presented in Sections 7.4.4.1 and 7.4.4.2, it was considered that the idealised f_z-σ'_r history acting on a typical prismatic element of sand adjacent to the pile shaft, remote

from end effects, was of the form indicated on Figure 7.26(a). This shows, for simplicity, the $\pm\delta'_u$ envelopes intersecting at f_z equal to zero, there being insufficient data to establish this point with any certainty.

With regard to the idealised f_z-σ'_r profile, a number of tentative assumptions were made as to the behaviour of the pile shaft/sand interface and the magnitude of the cylindrical stresses acting on a prismatic element of sand adjacent to this boundary.

A detailed study of the behaviour of a metal/sand interface under shear was conducted by Yoshimi and Kishida (1981) using a ring torsion apparatus. They showed that for a machined metal surface which was slightly rough (R_{max} = 23.0 μm), shear zones developed within the sand near the interface immediately after slip had occurred at the interface. They also showed that the shear zone began to develop once f_z/σ'_r had exceeded 0.7 to 0.8 Tanδ', and that the shear zone was typically five to eight times the mean sand grain size in width. The surface roughness (R_{max}) of the author's pile was 25.0 μm. Thus, since it was shown by Yoshimi and Kishida (1981) that the type of sand had very little influence on the development of δ' for a surface roughness in excess of R_{max} equal to 20.0 μm, an equivalent mode of failure to that described above may be expected to develop along the pile shaft. This implied that shear failure occurs within the sand in conjunction with slip at the pile shaft/sand interface.

The state of stress at any depth (Z) adjacent to the pile shaft, remote from end effects, was considered. A convenient starting point was the condition at which f_z was equal to zero. By definition σ'_r, σ'_z and σ'_θ are

principal stresses, of which only σ'_r is known.

In order to ascertain the interdependance of the three axial cylindrical stresses in the sand adjacent to the pile shaft, consider the following:

In a weightless soil the condition f_z equal to zero along the shaft of a rigid pile, would imply zero elastic vertical strain within the sand adjacent to the pile shaft ($\varepsilon_z = 0$). However, since the soil is not weightless there must be an element of ε_z within the soil adjacent to the pile shaft. From the work of Hanna and Tan (1973) and Vesic (1963) it is suggested that σ'_z adjacent to a pile shaft at failure, is less than, or equal to, the initial effective overburden stress. The magnitude of σ'_z at failure must therefore contain an element of σ'_z induced by the action of f_z along the pile shaft. Thus, at f_z equal to zero, the magnitude of σ'_z adjacent to the pile shaft will be less than that at failure and, therefore, less than the initial effective overburden stress.

The DPTs sited at a depth of 1275.0 mm (11.2B) in tests S/S1 and S/S2, 570.0 mm (5.0B) above pile base level, indicated a reduction in σ'_z with proximity to the pile shaft, the magnitude of which was below that of the initial effective overburden stress under residual stress conditions. Extrapolation of the results indicated that the magnitude of σ'_z adjacent to the pile shaft, in absolute terms, was between 0.0 to 3.0 kPa. It was subsequently estimated that this was increased by less than 0.5 kPa due to the application of the first increment of Q_a, under which f_z tended to zero. Thus, as a first order approximation, ε_z adjacent to the pile shaft may be taken as zero.

With regard to the state of circumferential strain (ε_θ); Robinsky and

Morrison (1964) reported that vertical expansion occurred within the sand adjacent to the edge of a pile base during penetration. This was due to the downward movement of the sand below the pile base away from the previously compacted sand around and immediately above the pile base. It was also shown to be possible for a volumetric expansion of the sand to occur within this region (Section 7.3.2 Refer). The stresses acting on an element of sand adjacent to the pile shaft at base level may, therefore, be of a low order and any subsequent re-stressing of a prismatic element of sand adjacent to the pile shaft during pile installation may occur under conditions of zero elastic circumferential strain ($\varepsilon_\theta = 0$), assuming the pile to be rigid. It was estimated that the maximum ε_θ developed within the sand adjacent to the pile shaft, due to the diametral expansion of the pile when fully loaded, was 12.0 $\mu\varepsilon$. This was sufficiently small to be ignored. In support of this, data from the BOSTs located within the ALCs, where the axial load within the pile was transmitted through a central core (leaving the pile wall 'stress free'), was not perceptably different from that recorded by BOSTs located within sections of pile in which the load was transmitted directly through the pile wall.

Thus, as an approximation, from the equations of elasticity for the condition where $f_z = 0$ and $\varepsilon_z = \varepsilon_\theta = 0$, it can be shown that:

$$\sigma'_z = \sigma'_\theta = \left(\frac{\nu}{1 - \nu}\right) \sigma'_r = K_o \sigma'_r \qquad (7.11)$$

This stress condition is indicated on Figure 7.26(b).

Throughout loading $\sigma'_\theta = \sigma'_2$, where $\sigma'_2 = \nu(\sigma'_1 + \sigma'_3)$ and $\nu = 0.32$ for

$\phi' = 32^0$, since $\varepsilon_\theta = 0$.

Figures 7.16(a) and (b), and 7.18 show that the condition f_z equal to zero was attained, within acceptable limits, at all levels along the pile shaft within sand for a single value of Q_a in each test. Thus, σ'_r corresponding to f_z equal to zero was deduced from Figures 7.25(a), (b) and (c), and σ'_z and σ'_θ were evaluated taking $K_o = (1-\text{Sin}\phi')$. The variation in the cylindrical stresses with depth (Z), normalized with respect to the initial effective overburden stress (γZ), are presented on Figure 7.27.

Below 570.0 mm (5.0B) depth, the normalised cylindrical stresses reduced marginally with depth, with $\sigma'_z/\gamma Z$ and $\sigma'_\theta/\gamma Z$ attaining a value of approximately 0.24 (slightly less than K_a, 0.31), whilst $\sigma'_r/\gamma Z$ was about 0.46 (approximately equal to K_o, 0.47). Above a depth of 570.0.mm (5.0B), however, $\sigma'_z/\gamma Z$ and $\sigma'_\theta/\gamma Z$ increased progressively, and tended to unity near the surface. This would appear to indicate the progressive development of an arching mechanism within the sand around the pile shaft. The depth at which this mechanism was fully mobilized (5.0B) was of the same order as that at which the radial limit of the visible displacement envelope, reported by Robinsky and Morrison (1964) around a straight sided pile in loose sand, attained a maximum value. Further, it approximately coincided with the depth at which the base bearing capacity factor, N^*_q, attained a peak value (4.6B) (Section 7.2.1.3 Refer).

The possibility of the reduction in $\sigma'_r/\gamma Z$ with depth, over the upper portion of the pile shaft being erroneously deduced from the results of one pair of BOST at a depth of typically 200.0 mm (1.8B), was investigated. It was observed on Figures 7.25(a), (b) and (c) that the

magnitude of the residual σ'_r was comparable with that associated with the condition f_z equal to zero. The residual values of σ'_r recorded by all BOSTs throughout pile installation in S/S1 and S/S2 were, therefore, normalized with respect to the initial effective overburden stress (γz) to a depth of 950.0 mm (8.3B), and are presented on Figure 7.28. This shows σ'_r to reduce significantly with depth within the upper 570.0 mm (5.0B) of the sand, and confirmed the observations reported in relation to Figure 7.27. Although not indicated on Figure 7.28, due to the degree of scatter in the results, σ'_r may be expected to increase at a given depth with pile embedment (Section 7.4.1.4 Refer).

With regard to Figure 26(b), an increase in Q_a beyond that required to attain the condition f_z equal to zero, resulted in an clockwise rotation of the principal stress planes and an increase in the stress intensity acting on the prismatic element of sand adjacent to the pile shaft. This continued until such time as the f_z-σ'_r profile was tangential to the $+\delta'$ envelope, where slip occurred at the pile shaft/sand interface and shear failure developed within the sand adjacent to the shaft. The stress system at this juncture was, therefore, of the general form indicated on Figure 7.26(c). The system of stresses indicated on Figure 7.26(c) is applicable to all values of f_z and σ'_r which lie along the $+\delta'$ envelope. The stresses developed at the point of initial tangency coincided with the limits of acceptable linear load/settlement behaviour for the pile shaft. With further increase in Q_a, no additional rotation of the principal stress planes occurred. However, the magnitude of the stresses acting on the element of sand adjacent to the pile shaft, continued to increase.

The stress circle (σ'_2-σ'_3) appeared to be tangential to the $\pm\delta'$ envelope

whenever a state of shear failure existed within the sand. An explanation cannot be offered for this at present.

The magnitude of the principal and axial stresses, acting on a prismatic element of sand adjacent to the pile shaft at various depths, was evaluated at Q_{amax} for each test. These are presented on Figure 7.29, nomalized with respect to the initial effective overburden stress. The normalized axial and principal stresses evaluated from K_z, defined by Equation 7.5, were superimposed on the experimental results, with which they were in reasonable agreement. There was however, a tendency for the stresses derived during the ML test to be less over the upper section of the pile shaft, and greater within the central portion of the pile shaft, than those deduced from Equation 7.5. The results, however, show the stresses adjacent to the pile shaft to reduce with depth in relation to the initial effective overburden stress. At a depth of approximately 200.0 mm (1.8B), both σ_r' and σ_1' were in excess of K_p, whilst σ_z' was greater than the initial effective overburden stress. Over the central portion of the pile shaft, σ_z' was comparable with the initial effective overburden stress. Within a region extending to 650.0 mm (5.7B) above pile base level stresses were in accord with those evaluated from Equation 7.5.

Under the above system of stresses, the magnitude of the axial stresses generated within the sand adjacent to the pile shaft, were of the relative order $\sigma_r' > \sigma_z' > \sigma_\theta'$. Bennett and Gisbourne (1971) recorded axial stresses of similar relative proportions at a radius of 1.0B from the axes of a 25.4 mm diameter penetrometer jacked into loose sand, using an array of cubical three dimensional stress cells of sides 6.5 mm square.

As the pile was unloaded to $\frac{1}{2}Q_{amax}$ there was a reduction in stress intensity within the sand adjacent to the pile shaft, to a level less than that necessary to sustain a state of shear failure. This occurred in conjunction with an anticlockwise rotation of the principal stress planes. The stressed sand around the pile, when loaded to Q_{amax}, contained an element of 'elastic' recoverable vertical compressive strain. The condition was eventually reached during unloading where the shear stress developed along the pile shaft was insufficient to resist the elastic displacement recovery of the sand. This resulted in a net upward displacement of the sand relative to the pile shaft, the development of slip along the pile shaft/sand boundary, and shear failure within the sand adjacent to the pile shaft. It was possible, therefore, for the sand to be in a state of shear failure adjacent to the pile shaft, in conjunction with a positive f_z as the pile was unloaded. The stress system associated with the onset of shear failure within the sand and slip along the pile shaft/sand boundary is indicated in an idealized form on Figure 7.26(d). Beyond this point the variation in f_z with σ'_r traversed the $+\delta'_u$ envelope. This was associated with an anticlockwise rotation of the principal stress planes and a reduction in stress intensity. The stress condition described above appeared to be fully developed for an applied load of $\frac{1}{2}Q_{amax}$. The precise point at which the variation in f_z with σ'_r became tangential to the $+\delta'_u$ envelope is unknown.

In support of the above mechanism, a positive f_s was found to act on the pile shaft (Figures 7.7(a) and (b)) for $\frac{1}{2}Q_{amax}$, the magnitude of which was in reasonable agreement with f_z. Further, the soil displacement data (Figures 7.36(a), (b) and (c)) indicated that a significant portion of the elastic displacement recovery of the sand had occurred at $\frac{1}{2}Q_{amax}$. At the inner limit of instrumentation (1.4B) this amounted to typically

-0.05 mm (0.04%B) for an average shaft recovery of -0.09 mm (0.08%B). It is conceivable, therefore, for the displacement recovery of the sand adjacent to the shaft to be greater than that of the pile shaft. At $\frac{1}{2}Q_{amax}$, f_z tended to zero which suggested that the prevailing stresses along the pile shaft were at the limit of sand displacement recovery induced failure.

As the pile was unloaded from $\frac{1}{2}Q_{amax}$ to zero, the variation in f_z with σ'_r continued to traverse the $+\delta'_u$ envelope, maintaining the state of shear failure within the sand adjacent to the pile shaft. This resulted in the development of a negative f_z, since the pile shaft displacement recovery was greater than that of the surrounding sand due to the elastic displacement recovery of the pile and the highly compressed sand below the pile base. Thus, at zero applied load, the sand adjacent to the pile shaft was at a state of shear failure under the system of post-compressive residual stresses, as indicated on Figure 7.26(f).

If the pile was subsequently loaded in compression, a collapse of the post-compressive residual stress system would occur to a level below that necessary to sustain a state of shear failure within the sand adjacent to the pile shaft, together with a clockwise rotation of the principal stress planes. As the condition f_z equal to zero was approached the stresses would again tend to $K_o\sigma'_r = \sigma'_z = \sigma'_\theta$ (Figure 7.26(b)). If however, a tensile load was applied to the pile, the post-compressive stress system would not collapse and the state of shear failure within the sand adjacent to the shaft would be maintained, resulting in a gradual increase in stress intensity and a further anticlockwise rotation of the principal stress planes. This behaviour would continue until such time as the ratio of f_z to σ'_r attained the constant limiting value

defined by the $-\delta'$ envelope. Beyond the point of initial tangency with the $-\delta'$ envelope, the stresses would continue to increase to the maximum limiting value without further rotation of the principal stress planes.

The principal and axial stresses developed within the sand adjacent to the pile shaft, were evaluated for tensile Q_{sf} in all three tests. These are presented, normalized with respect to the initial effective overburden stress on Figure 7.30. This showed the stresses below a depth of 570.0 mm (5.0B) to be directly related to a constant portion of the initial effective overburden stress in S/S1 and S/S2, with σ_z' and σ_r' being typically $0.35\gamma Z$ and $0.64\gamma Z$ respectively. Above 570.0 mm (5.0B) depth, the normalized stresses increased progressively with proximity to the surface, where $\sigma_3'/\gamma Z$ appeared to approach unity. The stresses associated with S/M1 were of the same order as those reported for S/S1 and S/S2. However, at depth they increased progressively with proximity to the sand/clay interface for the reasons previously stated (Section 7.4.3.2 Refer).

The available data relating to the state of post-tensile residual stress along the pile shaft, was limited to that obtained from the inadvertant extraction of the pile during S/S1 (Section 7.2.2.1 Refer). The following discussion on the development of post-tensile residual stress is, therefore, purely speculative.

Soil displacement recorded during the CRU test indicated a general uplift of the sand adjacent to the pile shaft (Figures 7.39(a) and (b)). Upon unloading, a rapid collapse in the stress system around the pile shaft may be anticipated to an intensity below that necessary to sustain a state of shear failure within the sand adjacent to the pile shaft,

together with a clockwise rotation of the principal stress planes. This would continue until such time as the stress intensity adjacent to the pile shaft was insufficient to support the surrounding sand. As a consequence, the downward vertical displacement of the sand would be greater than that of the pile shaft at any depth, resulting in the development of a state of shear failure within the sand adjacent to the pile shaft together with a negative f_z (Figure 7.26(g)), at which point the f_z-σ'_r profile would be tangential to the $-\delta'_u$ envelope. As the pile was further unloaded, a state of shear failure would continue to exist within the sand adjacent to the pile shaft, in conjunction with a progressive reduction in stress intensity and a clockwise rotation of the principal stress planes. This would eventually result in the developement of a positive f_z due to the settlement of the pile under self-weight in the absence of end bearing (Figure 7.26(h)).

If a second CRU test was undertaken, the post-tensile residual stress system would collapse to an intensity less than that necessary to sustain a state of shear failure within the sand adjacent to the shaft, together with an anticlockwise rotation of the principal stress planes. For f_z equal to zero, the cylindrical stresses would again tend towards $K_o\sigma'_r = \sigma'_z = \sigma'_\theta$, beyond which they would develop in a manner similar to that described previously in relation to the compressive load test. However, a compressive load test would sustain the state of shear failure developed within the sand adjacent to the pile shaft, as previously outlined in relation to conducting a tensile load test immediately after a compressive load test.

No attempt was made to evaluate the axial and principal stresses developed adjacent to the pile shaft within the clay in S/M1, since the

precise nature of the stresses, in terms of total and effective stress, was unknown.

7.5 Soil Displacements

7.5.1 Pile Installation

It was evident from the vertical displacements generated during pile installation that the LVDT/piano wire arrangement, employed to monitor the vertical displacement of the EL in each train furthest from the pile axis, was successful. This is best illustrated by the displacements recorded at the radial limit of the third layer (I3) of ELs, 460.0.mm (4.0B) from the pile axis. Vertical displacements at this location were recorded by an above ground LVDT and compared favourably with those evaluated from the second layer (I2) of ELs, at the same radius, by an integration technique (Section 5.7 Refer).

An element of doubt must be expressed as to the validity of the results obtained using the Type 7650 ELs sited at a radius of 160.0 mm (1.4B) from the pile axis, since the rotations recorded were only marginally greater than those recorded by the Type 7660 ELs which were sited further from the pile axis. This was probably due to the relatively high aspect ratio of the type 7650 EL.

7.5.1.1 Homogeneous Sand Profiles

Vertical displacement profiles generated within the sand for various pile embedments during pile installation are presented on Figures 7.31(a) and (b).

Surface heave was evident for a pile penetration of less than about 200.0 mm (1.8B).

At depth, planes within the sand which were initially horizontal and below the pile base, were observed to 'dish' with the approach of the pile base. Dishing became progressively greater until the continuity of the sand layer under consideration was ruptured by the punching action of the pile base. The depth below the pile base at which rupture occurred was indeterminate from the author's data. However, from the work of Robinsky and Morrison (1964) rupture was estimated to occur at about 1.0B below pile base level. At approximately the same time as the onset of rupture, the development of subsurface heave was observed within the sand. The uplift of sand due to subsurface heave was confined to below pile base level, as illustrated on Figure 7.32. Additional vertical displacements were recorded within the sand above pile base level, which developed at a diminishing rate as pile installation progressed.

The development of vertical displacements (V) within the sand at a given radius (r) from the pile axis for each layer of ELs, is presented on Figure 7.32 as a function of pile embedment (D_b).

The maximum surface heave recorded at the inner limit of instrumentation, 310.0 mm (2.7B) from the pile axis, amounted to typically 0.27 mm

(0.24%B) and coincided with a pile embedment of approximately 110.0 mm (1.0B), at which it extended to a radius of 460.0 mm (4.0B) from the pile axis. Surface heave was reduced to zero for a pile embedment of 230.0.mm (2.0B). Further pile penetration resulted in settlement of the surface profile, which occurred at a diminishing rate throughout pile installation, and probably attained a quasi-constant limiting value for a pile embedment in excess of that attained during this study.

Support for the above was evident from the radioghaphic study conducted by Robinsky and Morrison (1964). They showed that the additional displacements generated near the surface, during the installation of a model pile in loose sand from an embedment of 8.6B to 17.2B, were inperceptable by the measuring techneques employed.

Throughout pile installation, the zone of disturbance generated within the sand below the pile base increased in size at a diminishing rate. This was indicated by the relatively small additional pile penetration required in order to produce measureable displacements at progressively greater depths within the sand. Vertical displacements within the sand, across a horizontal plane at a given depth, increased at a progressively greater rate with the approach of the pile base. This was observed until such time as the pile base was within typically 250.0 mm (2.2B) of the plane under consideration. With greater proximity of the pile base to the plane under consideration a reduction in $\Delta V/\Delta D_b$ was observed. After a further penetration of approximately 100.0 mm (0.9B), the onset of subsurface heave was observed, indicated by a negative $\Delta V/\Delta D_b$. This effect was observed to a radius of 460.0 mm (4.0B) at most from the pile axis where an inflection point was evident in the $V\text{-}D_b$ profiles. At greater radii from the pile axis a temporary reduction in $\Delta V/\Delta D_b$ was

observed. The maximum subsurface heave recorded at the inner limit of instrumentation, 160.0 mm (1.4B) from the pile axis, occurred at a depth of typically 30.0 mm (0.26B) below the pile base and varied between 0.2 mm (0.2%B) at a depth of 510.0 mm (4.5B) to 0.7 mm (0.6%B) at a depth of 1275.0 mm (11.2B). Once the pile base was at the same depth as the plane under consideration, subsurface heave had, in the main, ceased. After a further 100.0 mm (0.9B) pile penetration, sand displacements were 'free' of the immediate influence of the pile base and appeared to increase at a diminishing rate to a quasi-constant limiting value for a pile embedment greater than that achieved during this study.

A detailed analysis and discussion of the vertical displacement field around the base of a continuously penetrating pile, is undertaken in Section 7.5.1.4.

7.5.1.2 Layered Soil Profile

The vertical displacement profiles recorded within the overlying sand (Figure 7.31(c)) were comparable in magnitude to those observed in S/S1 and S/S2, within a radius of 460.0 mm (4.0B) from the pile axis. Beyond this radius, displacements were less than those recorded in S/S1 and S/S2, this was probably due to the influence of the secondary clay tank.

The V-D_b profiles presented on Figure 7.32 show the development of vertical displacements within the soil, in detail. The surface displacements, together with those recorded at a depth of 510.0 mm (4.5B), were comparable with the displacements recorded at the same depth in S/S1 and S/S2, provided D_b was less than the depth to the sand/clay

interface. Vertical displacements within the sand at a depth of 1020.0 mm (8.9B), and on the sand/clay interface, were initially detected at smaller pile embedments than those associated with the onset of vertical displacement at comparable depths in S/S1 and S/S2. Initially $\Delta V/\Delta D_b$ at the level of the I2 and I3 ELs, was less than that observed for S/S1 and S/S2. However, when the pile base was within 600.0 mm (5.3B) of the sand/clay interface the $V\text{-}D_b$ profiles were in accord, within acceptable limits, with those observed in S/S1 and S/S2.

As the pile base penetrated below the sand/clay interface, uplift of the clay surface was recorded at all radii, which continued until a penetration of approximately 200.0 mm (1.8B) below the sand/clay interface had been achieved. Uplift of the sand/clay interface affected the displacements recorded within the overlying sand, causing a significant deviation in the $V\text{-}D_b$ profiles. This was discernable at all depths within the overlying sand, even at the surface, to a radius of between 460.0 mm (4.0B) and 710.0 mm (6.2B) from the pile axis. This would tend to suggest that a significant portion of the additional displacement, generated within the sand around the pile shaft during installation, was attributable to the displacement mechanism local to the pile base.

The maximum heave recorded on the sand/clay interface was 1.4 mm (1.2%B), at a radius of 160.0 mm (1.4B) from the pile axis. This was twice that measured at a similar location in S/S1 and S/S2, and reduced to 0.1 mm (0.1%B) at a radius of 460.0 mm (4.0B) from the pile axis. Further pile penetration of the underlying clay resulted in a small increase in the vertical displacement of the sand/clay interface, which was reflected in the displacements recorded within the overlying sand.

7.5.1.3 Vertical Displacments Within the Soil Per Unit Pile Penetration

The additional vertical soil displacements generated on an initially horizontal plane at a depth of 1275.0 mm (11.2B), due to a unit penetration of the pile, are presented on Figure 7.33 relative to the location of the pile base. If a steady state displacement field is considered to exist around the pile base at this depth, which is not exactly correct, then the resulting values are a measure of the vertical strain (ε_z) generated around the base of a continuously penetrating pile in homogeneous loose sand.

Vesic (1965) evaluated the variation in ε_z around the base of a pile installed in loose sand from the displacement profiles presented by Robinsky and Morrison (1964). The strains were calculated within a series of elements which were originally at a radius of approximately 0.3B from the pile axis. These were subsequently displaced laterally above pile base level to a radius of 0.6B. The magnitude of the peak extensive and compressive strains were typically twenty times greater than those deduced by the author at a radius of 1.4B, assuming negligible lateral displacement of the soil instrumentation during pile installation. From the data, including that of Vesic (1965), it was evident that the magnitude of the maximum vertical compressive strain was approximately twice that of the maximum extensive strain at any given radii from the pile axis. Strains generated around the pile shaft remote from the influence of the base, were surmised to be extensive by Vesic (1965). However, within the limits of the author's instrumentation, the strains developed within the sand above pile base level were compressive, and of the order of 0.002 mm/mm at a radius of 160.0 mm (1.4B) from the

pile axis. This may, however, reflect the erroneous assumption of a steady state displacement field around the pile base.

For comparative purposes the loci of maximum and minimum σ'_z, together with that of σ'_z equal to the initial effective overburden stress, recorded below the pile base during pile installation in S/S1 and S/S2 are superimposed on the strain profiles. A good correlation was found to exist between the recorded stress and the deduced strain within a radius of 235.0 mm (2.1B) from the pile axis.

Displacements per unit pile penetration on the sand/clay interface in S/M1 were comparable with those recorded during S/S1 and S/S2 prior to the attainment of the maximum compressive ε_z in S/S1 and S/S2. For a greater pile penetration the results from the two types of soil profile diverged at a radius of 160.0 mm (1.4B) from the pile axis, with those deduced from S/M1 requiring an additional pile embedment of 65.0 mm (0.6B) to achieve a maximum rate of vertical displacement per unit penetration. The two strain profiles remained out of phase by this amount in terms of D_b with further pile embedment to a depth of 1500.0 mm (13.2B), 230.0 mm (2.0B) below the sand/clay interface. 'Out of phase' behaviour was also evident to a radius of 310.0 mm (2.7B) where it amounted to 30.0 mm (0.3B). The ratio of peak positive to peak negative $\Delta V/\Delta D_b$, however, varied nonuniformally with radius from the pile axis, from a maximum of 0.39 at radius of 235.0 mm (2.1B), to approximately 0.20 at radii of 160.0 and 310.0 mm (1.4 and 2.7B).

7.5.1.4 Vertical Displacement Zones Around the Base of a Continuously Penetrating Pile in Homogeneous Sand

An indication of the extent of the vertical displacements generated within loose sand around the pile base during pile installation was obtained by plotting prominent points from the V-D_b profiles (Figures 7.32(a) and (b)) relative to the position of the pile base (Figure 7.34). This showed the existance of two 'spear-head' shaped regions which extended out, and down from the edge of the pile base at approximately 20^0 to the horizontal. The outer region extended to a radius of 650.0 mm (5.7B) from the pile axis, and was comparable with the radial limit of volumetric strain (Figure 7.10). The inner region extended to a radius of 460.0 mm (4.0B) from the pile axis, and was comparable with the limit of radial displacement (Section 7.4.1.5 Refer). Six distinct zones were found to exist within the sand around the pile base, in each of which the behaviour described below was greatest close to the pile axis.

Zone I	Increasing rate of downward displacement
Zone II	Reducing rate of downward displacement
Zone III	Increasing rate of upward displacement
Zone IV	Reducing rate of upward displacement
Zone V	Increasing rate of downward displacement
Zone VI	'Steady' rate of downward displacement

The boundaries between these zones were significant in terms of ε_z.

I-II Maximum compressive strain.

This appeared to emanate from the apex of the active sand cone formed below the pile base. The radial limit of this

boundary, defined by the point of convergance with boundary V-VI, extended to a radius of 650.0 mm (5.7B) at a depth of 300.0 mm (2.6B) below pile base level.

II-III Zero strain.

This appeared to originate from the edge of the pile base and extended radially to 460.0 mm (4.0B) at a depth of 150.0 mm (1.3B) below pile base level.

III-IV Maximum extensive strain.

This also appeared to originate from the edge of the pile base and extended radially to the limit of boundaries II-III and IV-V.

IV-V Zero strain.

This too appeared to originate from a point near the pile base and extended to the radial limit of boundaries II-III and III-IV.

V-VI Onset of 'steady state' compressive strain.

This extended out and down from the pile shaft from a point approximately 110.0 mm (1.0B) above pile base level and converged with boundary I-II at a radius of 650.0 mm (7.2B).

The boundary between zones I and VI is not defined above since it was considered that the displacement patterns within each of these zones merged beyond the radial limit of zones II and V.

Boundary II-V identified the limits of the minimum rate of change of compressive strains generated within the sand. At the inner limit, 460.0 mm (4.0B) from the pile axis, compressive strains were reduced to zero, coinciding with an inflexion point in the $V\text{-}D_b$

profile (Figures 7.32(a) and (b)), before again increasing. At the outer limit, 650.0 mm (5.7B) from the pile axis, the development of V with D_b was 'unaffected' by the passage of the pile base.

7.5.1.5 Radial Displacements Generated in Homogeneous Sand Due to Pile Installation

The radial displacements generated within the sand at the conclusion of pile installation, were evaluated by determining the reduction in volume of a given mass of sand contained within an annular prism around the pile shaft as a result of densification. That proportion of the resulting volume change directly attributable to vertical compaction was calculated from the vertical displacements recorded within the sand. The remaining volume change was equated to the radial displacement of the inner radius of the annular prism of sand; the radial displacement of the outer radius being equated to the calculated radial displacement of the inner radius of the outer adjacent annular prism of sand.

The application of this method showed that beyond a radius of 460.0 mm (4.0B) from the pile axis, the vertical compression of the sand between two successive levels of ELs was sufficient to account for the recorded densification of the sand. Lateral displacements within the sand were therefore considered to be zero at radii of greater than 460.0 mm (4.0B) from the pile axis.

The radial displacements evaluated according to the above method are presented on Figure 7.31 for each soil profile. The results show a considerable variation, possibly as a consequence of the way in which

errors are compounded by the method of calculation.

The radial displacements evaluated at a given radii for all three soil profiles, together with average values, are presented in a normalized form on Figure 7.35. These results are compared with those deduced from the work of Robinsky and Morrison (1964) and Davidson et al (1981) for loose sand, together with the theoretical radial displacement profile for zero vertical and volumetric strain ($\varepsilon_z = \varepsilon_v = 0$) within the sand.

The evaluation of radial displacements from the work of Robinsky and Morrison (1964), undertaken on the basis of the measured radial displacement of individual lead shots, was not wholly successful. Displacements beyond a radius of 1.5B were found to be relatively constant at 0.15B. Further, all displacements were greater than those evaluated for the condition $\varepsilon_z = \varepsilon_v = 0$, which may only occur in a dilatant soil. The results were, therefore, adjusted linearly assuming the displacements evaluated at, and beyond, a radius of 1.5B from the pile axis to be zero. The adjusted values were in reasonable agreement with those of Davidson et al (1981).

The dimensionless radial displacement (2R/B) at any radius (2r/B) within a soil subjected to the condition $\varepsilon_z = \varepsilon_v = 0$ can be evaluated using Equation 7.12 (after Randolph et al, 1979(b)).

$$\frac{2R}{B} = \left[\left(\frac{2r}{B}\right)^2 + 1\right]^{\frac{1}{2}} - \frac{2r}{B} \qquad (7.12)$$

This equation may be used to evaluate the dimensionless radial displacements within a loose sand by the introduction of an empirical

compaction factor (C).

That is:

$$\frac{2R}{B} = C^{\left[\frac{2r}{B}\right]} \cdot \left(\frac{2R}{B}\right)_{\varepsilon_z=\varepsilon_v=0}$$

Acceptable agreement was achieved between the experimental and theorectical results for C equal to 0.78.

The results show radial displacements in loose sand to be insignificant beyond a radius of approximately 4.0B from the pile axis.

7.5.2 Maintained Load Test

7.5.2.1 Homogeneous Sand Profiles

The displacement profiles presented on Figure 7.36 show the vertical displacements generated within the sand, in excess of those developed during pile installation, at the conclusion of each loading increment throughout the ML test. For clarity, the two displacement profiles related to the unloading from, and the reapplication of, Q_{aw} have been omitted.

The magnitude of the displacements recorded in S/S2 for a given Q_a were

approximately twice those recorded in S/S1, an observation which cannot readily be explained. A fluctuation in the energizing voltage to the ELs was discounted since the surface displacements, which were of the same relative magnitude as those recorded at depth, were recorded directly using LVDTs energized from a power supply independent of that which energized the ELs. Further, the rate of change of ω_s per unit Q_a was practically the same for both tests. The only apparent physical difference between the two tests was the slightly higher initial sand density recorded in S/S1, which amounted to typically 26.5 kg/m^3. Vertical displacements generated throughout pile installation in S/S2 were also marginally greater than those of S/S1; this was also apparent for the CRU tests.

The sand displacement profiles associated with the first two loading increments were extended to the pile shaft, where the vertical displacement of the adjacent sand was assumed to be equal to ω_s. This was justified since Yoshimi and Kishida (1981) reported that no slip occurred at a metal/sand interface, regardless of the prevailing conditions, until the mobilized value of $Tan\delta'$ was equal to between 0.7 and $0.8Tan\delta'$, which was satisfied for applied loads up to and including Q_{aw}.

Vertical displacements within the sand were observed to increase approximatley linearly at a given radius from the pile axis per unit Q_a; an observation which was subsequently employed to develop a set of semi-normalized displacement curves of the form V/Q_a verses $2r/B$ (Section 7.5.2.3 Refer).

A large variation in the amount of elastic displacement recovery recorded

in the sand was observed as the pile was unloaded. The greatest amount of displacement recovery was recorded near to the pile. At $\frac{1}{2}Q_{amax}$, approximately 70.0% of the total elastic displacement recovery of the sand had occurred, amounting to typically 30.0% of the maximum sand displacement recorded at Q_{amax}.

No elastic displacement recovery of the sand was recorded at the surface. However, this may be indicative of the lack of sensitivity of the surface displacement transducers to small displacement reversals.

7.5.2.2 Layered Soil Profile

Within the layered soil profile the vertical displacements recorded at the surface, and at a depth of 510.0 mm (4.5B), were comparable with those recorded in S/S2 at similar depths.

Displacements recorded at a depth of 1020.0 mm (8.9B), 255.0 mm (2.0B) above the sand/clay interface, were significantly greater, by as much as a factor of two, than those recorded at the same depth in S/S1 and S/S2. Further from the pile axis the soil displacements diminished rapidly, ultimately tending to values which were comparable with those observed in S/S1 and S/S2 at the outer limit of instrumentation.

Displacement profiles recorded on the sand/clay interface suggested that the secondary clay tank was of insufficient diameter to fully model the behaviour of an underlying clay layer, since the extrapolated displacement profiles appeared to tend to zero at the outer limit of the secondary clay tank. This would explain the observed reduction in

vertical displacements within the sand immediately above the sand/clay interface at radii of greater than about 600.0 mm (5.3B) from the pile axis.

The relatively large vertical displacements observed on the sand/clay interface, resulted in the development of extensive strains within the overlying sand. This resulted in a reduction in the magnitude of the vertical effective stress (σ'_{zi}) over a major portion of the sand/clay interface during pile loading (Section 7.6.2.2 Refer).

Upon unloading the pile to $\frac{1}{2}Q_{amax}$ the displacement recovery of the sand/clay interface amounted to typically 28.0% of the maximum vertical displacement recorded at Q_{amax}. A similar amount of displacement recovery was recorded within the overlying sand. Associated with this displacement pattern was a negative f_z which acted on the pile shaft within the sand, with the exception of a short length of shaft immediately above the sand/clay interface. The negative values of f_z over the upper portion of the pile shaft indicated that the full elastic displacement recovery of the sand had been attained adjacent to this portion of the pile shaft. Any additional vertical displacement recovery within the sand was, therefore, due to the uplifting effect of the elastic displacement recovery of the pile and underlying clay. The positive f_z over the lower portion of the pile shaft within the overlying sand was a result of the limited relative displacement generated between the pile shaft and the adjacent sand at this depth.

Upon complete removal of Q_a, the total displacement recovery of the sand/clay interface was approximately 75.0% of the maximum vertical displacement recorded at Q_{amax}. The amount of vertical displacement

recovery, recorded within the overlying sand, diminished with height above the sand/clay interface, resulting in the development of compressive strains within the overlying sand and an increase in the vertical effective stress (σ'_{zi}) on the sand/clay interface. The latter was confirmed by the results from the DPTs (Section 7.6.2.2. Refer).

7.5.2.3 Semi-Normalized Vertical Displacement Profiles Derived from the Maintained Load Tests in Homogeneous Sand

Soil displacements recorded during the ML test in S/M1 were not normalized due to their variation with depth, and the adverse influence of the secondary clay tank.

It was previously reported that vertical displacements within the sand, remote from the immediate proximity of the pile shaft, increased approximately linearly with Q_a and were relatively constant with depth at a given radius from the pile axis. The variation in V/Q_a with $2r/B$ was found to be non-linear when examined in the light of the theory proposed by Cooke et al (1979), in which V was shown to vary approximately linearly with $\log_e(2r/B)$. Cooke et al (1979) stated that non-linearity of the resulting plot was due to the assumption of a constant shear modulus (G) for the soil at all radii from the pile axis, and that the shear stress (τ) varied inversely with radius (r) from the pile axis throughout the soil.

When the parameters V/Q_a and $2r/B$ were plotted on logarithmic axes a linear relationship was found to exist between the two variables with the exception of the displacements recorded at a radius of 160.0 mm (1.4B)

from the pile axis. This further supported the doubts previously expressed by the author as to the validity of the results obtained from the Type 7650 ELs. Two displacement functions were established, one for each test (S/S1 and S/S2), defining the variation in V/Q_a with $2r/B$. These are presented on Figures 7.37(a) and (b), and are compared with the actual values of V/Q_a. The average of the two functions, Equation 7.14, was reasonably acceptable to both sets of data and is also plotted on Figures 7.37(a) and (b).

$$\frac{V}{Q_a} = 0.087 \left(\frac{2r}{B}\right)^{-1.854} \qquad (7.14)$$

The constant of 0.087 was equivalent to ω_s/Q_a, and compared favourably with the recorded values of this ratio up to Q_{aw} (Figures 7.37(a) and (b) Refer).

7.5.2.4 Variation in the Shear Modulus of Homogeneous Sand with Radius from the Pile Axis at Working Load

The initial tangent shear modulus for the sand was estimated as 11.4 MN/m^2 from the average of the two drained triaxial samples which gave the lowest value of ϕ' (typically 32.4^0) when deriving the $\phi'-\rho_d$ relationship (Section 3.2.5 Refer). Poulos and Davis (1980) suggested that the average value of elastic modulus for loose sand, in association with driven piles, was between 27.2 and 55.0 MN/m^2. For ν equal to 0.32, the corresponding shear modulus was between 10.4 and 20.8 MN/m^2, which is in agreement with that deduced by the author.

The variation in shear modulus with radius from the pile axis (Figure 7.38(a)) was evaluated directly from the vertical displacements recorded within the sand during the ML tests, as indicated on Figure 7.36(b), for an applied load of Q_{aw}. At Q_{aw}, no slip was assumed to have occurred between the pile shaft and the adjacent sand (Section 7.5.2.1 Refer). The shear modulus of the sand contained within an annular prism around the pile shaft, to a radius of 160.0 mm (1.4B) from the pile axis, was evaluated assuming V_2 equal to ω_s. For comparative purposes the variation in shear modulus with radius from the pile axis was calculated using Equation 7.14, with which the individual results were in reasonable agreement.

The results derived from Equation 7.14 show the shear modulus to increase with radius from the pile axis at a progressively greater rate from 0.1 MN/m^2 adjacent to the pile shaft, to a constant limiting value of 11.4 MN/m^2 (the initial tangent modulus) at a radius of 520.0 mm (4.6B) from the pile axis. The radius at which the back figured shear modulus was equal to the initial tangent shear modulus, was approximately midway between the radial limit of volumetric strain and radial displacement within the sand (Sections 7.3.2 and 7.5.1.5 Refer). The resulting radial variation in shear modulus was of a similar nature to that reported by Cooke et al (1979) around the shaft of a loaded pile in London Clay.

7.5.3 Constant Rate of Uplift Test

The soil displacements reported in this section are those associated with the pile displacement increments considered in Section 7.4.3. However, for clarity the soil displacement profiles associated with some of the

initial pile displacement increments have been omitted.

7.5.3.1 Homogeneous Sand Profiles

The sand displacement profiles recorded during the CRU tests (Figures 7.39(a) and (b)) were consistent with those recorded during the ML tests, in that displacements recorded in S/S2 were greater than those of S/S1.

The upward displacement of the pile and the resulting negative f_z developed along the pile shaft limited the settlement of the sand to a radius of approximately 460.0 mm (4.0B) from the pile axis. Immediately adjacent to the pile shaft a gross uplift of the sand was recorded during the initial stages of each test.

The downward displacement of the sand was due to the movement of a volume of sand from around and below the pile base into the void formed below the pile base during pile uplift. At maximum uplift, typically 30.0 mm (0.3B), the volume of the 'void' formed beneath the pile base could be equated to an average vertical downward displacement of 0.04 mm (0.04%B) over the surface area of the sand profile. This compared favourably with the recorded values in S/S2.

Vertical displacements within the sand to a radius of 310.0 mm (2.7B) from the pile axis, experienced an increased uplift with depth, which resulted in the development of compressive strains within the overlying sand and an increase in σ'_z. This was evident from the progressive increase in f_z and σ'_r observed over the lower portion of the pile shaft during the CRU test (Section 7.4.3.1 Refer). An increase in σ'_z within

the sand adjacent to the pile shaft may also be deduced from the results of the DPTs sited at a depth of 1275.0 mm (11.2B) (Section 7.6.3.1 Refer).

Beyond a radius of 310.0 mm (2.7B) from the pile axis, vertical soil displacements were relatively constant with depth.

7.5.3.2 Layered Soil Profile

It should be noted that the vertical soil displacements evaluated at levels I2 and I3 in S/M1 are plotted to one tenth the scale of those for I1 and the surface displacement transducers.

Throughout the CRU test, vertical displacements within the sand, and on the sand/clay interface, were negative (upward). On the sand/clay interface vertical displacements reached a maximum of -0.58 mm (0.48%B) at a radius of 160.0 mm (1.4B) from the pile axis. For pile displacements in excess of -11.12 mm (0.1B), corresponding with Q_{sf}, the upward vertical displacement of the sand/clay interface continued to increase. The increase in upward vertical displacements with depth resulted in the development of compressive strains within the overlying sand and a corresponding increase in σ'_z. This would account for the elevated values of f_z and σ'_r, recorded on the pile shaft immediately above the sand/clay interface, and σ'_{zi}, as recorded by the DPTs.

7.6 Stresses Generated on a Horizontal Plane at a Depth in a Soil Profile

7.6.1 Pile Installation

7.6.1.1 Homogeneous Sand Profiles

The radial distribution of the change in effective vertical stress ($\Delta\sigma'_z$), as recorded by the DPT's at a depth of 1275.0 mm (11.2B) during pile installation, is presented on Figures 7.40(a) and (b). The increments of pile embedment associated with the reported stress profiles are the same as those for which vertical displacements within the sand are reported on Figures 7.31(a) and (b). The variation in $\Delta\sigma'_z$ at a given radius from the pile axis throughout pile installation is shown on Figure 7.41(a).

With referance to these two figures, it was observed that for a pile embedment of less than 300.0 mm(2.6B), 975.0 mm (8.6B) above the plane of the DPTs, a small negative $\Delta\sigma'_z$ was recorded by the DPTs which amounted to typically -1.0 kPa. This was within the limits of accuracy for the DPTs and may not, therefore, be significant. It was however, evident in all tests.

Mogami and Kishida (1961) and Kishida (1964) reported the changes in vertical effective stress at depth below, and in line with the axis of, a single model pile pushed into loose sand. Their results showed a gradual reduction in the intensity of the vertical effective stress to a level below that of the initial effective overburden stress during the initial

stages of pile installation. A minimum value of σ'_z was recorded when the base of the pile was at 7.5 to 10.0B above the plane of instrumentation (increasing with greater pile diameter). No explanation was offered for the above behaviour. With further pile penetration, the vertical effective stress was observed to increase at a progressively greater rate.

It was observed on Figure 7.41(a) that for a pile embedment of less than 1275.0 mm (the depth of the DPTs), a peak value for $\Delta\sigma'_z$ was first recorded at the outer radial limit of the DPTs, 480.0 mm (4.2B) from the pile axis. With further pile penetration, peak values of $\Delta\sigma'_z$ of increasing magnitude were recorded closer to the pile axis. From the peak positive value at any radii, $\Delta\sigma'_z$ reduced to a peak negative value which was less than the initial overburden stress. A peak negative $\Delta\sigma'_z$ was first recorded at the outer radial limit of the DPTs and moved progressively closer to the pile axis with further pile penetration. The intensity of the peak negative $\Delta\sigma'_z$, however, diminished with proximity to the pile axis, probably due to the positive vertical effective stress induced in the sand adjacent to the pile shaft by the action of the shaft friction. The above obervations were in-keeping with a 'bulbous' distribution of $\Delta\sigma'_z$ below the pile base.

The depths at which peak positive and negative values of $\Delta\sigma'_z$ were recorded at a given radius, are plotted relative to the pile base on Figure 7.33 (Section 7.5.1.3 Refer).

From the work of Kishida (1964) it was observed that σ'_z reduced to below that of the initial effective overburden stress at a radius of 6.0B from pile axis on a plane 2.8B below the pile base, during the incremented

loading to failure of a model pile in loose sand. At pile failure, σ'_z was equal to the initial effective overburden stress at a radius of 4.5B from the pile axis. This was in reasonable agreement with that observed by the author of 360.0 mm(3.2B) for an equivalent vertical clearance of 320.0 mm (2.8B) between the DPTs and the pile base.

As the pile base approached the plane of the DPTs, $\Delta\sigma'_z$ decreased from the peak negative value and tended to zero at all radii when the pile base was at the same depth as the DPTs. This suggested that the full effective overburden stress acted on the horizontal plane within the sand at pile base level. This is contrary to the suppositions of other investigators who have suggested that σ'_z is less than the initial effective overburden stress at this level (Brezantzev et al, 1961; Meyerhof, 1976).

For pile embedments of greater than 1275.0 mm (11.2B), for which the pile base was below the plane of the DPTs, there was a rapid reduction in σ'_z to below that of the initial effective overburden stress. This was most pronounced at the inner radial limit of the DPTs, 180.0 mm (1.6B) from the pile axis.

At full pile embedment, 570.0 mm (5.0B) below the plane of the DPTs, σ'_z tended to a constant limiting value. The intensity of σ'_z was less than the initial effective overburden stress within the radial limits of the DPTs, and reduced with proximity to the pile axis. This appeared to indicate the existence of an arching mechanism within the sand around the pile shaft.

The above observations are in agreement with the statement made by Vesic

(1969(a)). This was that σ'_z generally increased under the pile base and generally decreased, at least over a certain length, above pile base level. The author's findings, however, showed no tendancy for the reduction in σ'_z to be confined to a short distance above the pile base.

The variation in residual vertical effective stress within the sand with pile embedment during pile installation is presented on Figure 7.41(b). The residual $\Delta\sigma'_z$ reduced from zero to typically -1.5 kPa during the first 200.0 mm (1.8B) of pile embedment at all radii within the limits of the DPTs, at which it remained until D_b was equal to 600.0 mm (5.3B). Further pile embedment resulted in a progressive increase in the residual $\Delta\sigma'_z$ at a radius of 180.0 mm (1.8B). This coincided with the depth at which vertical elastic displacement recovery of the sand was first recorded at a radius of 160.0 mm (1.4B) from the pile axis (Section 7.2.1.5 Refer). The increase in residual $\Delta\sigma'_z$, due to the vertical elastic displacement recovery of the sand, was limited to a radius of 280.0 mm (2.5B) from the pile axis, and was sufficient at a radius of 180.0 mm (1.6B) from the pile axis to induce a net positive residual vertical effective stress with a peak value of approximately 1.0 kPa. The pile embedment associated with the peak residual $\Delta\sigma'_z$ was equivalent to that at which the peak positive $\Delta\sigma'_z$ was recorded during pile installation.

As the pile base penetrated below the plane of the DPTs, the residual and installation vertical effective stresses developed within the sand at a radius of 180.0 mm (1.6B) from the pile axis, converged for a limited pile embedment of between 1360.0 and 1480.0 mm (11.9 and 13.0B). These limits increased to between 1400.0 and 1640.0 mm (12.3 and 14.4B) at a radius of 280.0 mm (2.5B). The behaviour outlined above was not apparent at a radius of 480.0 mm (4.2B) from the pile axis, due to the variable

nature of the vertical effective stress recorded during pile installation and under residual load conditions. For pile embedments in excess of the limits quoted above, the installation and residual values of $\Delta\sigma'_z$ diverged, with those recorded during pile installation being the greater due to the increase in σ'_z developed locally to the pile shaft by the positive shaft friction.

The magnitude of the residual σ'_z recorded below the pile base at the end of each penetration increment, showed no indication of the relatively high positive displacement stresses reported by Mogami and Kishida (1961) and Kishida (1964).

7.6.1.2 Layered Soil Profile

The initial development of $\Delta\sigma'_{zi}$ on the sand/clay interface exhibited similar features to the developement of vertical displacements at the same depth. The initial rate of development of $\Delta\sigma'_{zi}$ was greater for radii of less than, or equal to, 280.0 mm (2.5B) from the pile axis than was observed in S/S1 and S/S2. Further, as with the vertical displacement profiles, $\Delta\sigma'_{zi}$ was comparable with that recorded during S/S1 and S/S2 at a pile embedment of about 800.0 mm (7.0B). Parity between the results from S/M1 with those of S/S1 and S/S2 was sustained without signficant deviation until such time as D_b was equal to the depth to the sand/clay interface.

As the pile base penetrated below the sand/clay interface a rapid increase in $\Delta\sigma'_{zi}$ was recorded by the DPTs at radii of 180.0 mm (1.6B) and 280.0 mm (2.5B) from the pile axis. A maximum value of 4.7 kPa was

recorded for a pile embedment of 25.0 mm below the sand/clay interface, at which $\Delta\sigma'_{zi}$ remained relatively stable for a further 100.0 mm (0.9B) of pile embedment. For a pile embedment in excess of 125.0 to 200.0 mm (1.1 and 1.8B) below the sand/clay interface, σ'_{zi} tended to less than the initial effective overburden stress within the radial limits of the DPTs. The above depths were approximately the limits to which heave of the sand/clay interface was recorded (Figure 7.33). Throughout the latter stages of pile installation, the reduction in σ'_{zi} was greatest at the inner radial limit of the DPTs, 180.0 mm (1.6B) from the pile axis, and tended to a quasi-constant limiting value at any given radius from the pile axis. The lower value of σ'_{zi} at the inner radial limit of the DPTs, 180.0 mm (1.6B) from the pile axis, was probably due to the developement of vertical extensive strains within the sand immediately above the sand/clay interface, as was evident from Figure 7.36(c) during the ML test.

For D_b less than the depth to the sand/clay interface, significant peaks and troughs in the residual $\Delta\sigma'_{zi}$ - D_b profile correlated with maxima in the $\Delta\sigma'_{zi}$ - D_b profile recorded during pile installation. The maximum positive residual $\Delta\sigma'_{zi}$ attained 20.0% of the installation value at a radius of 180.0 mm (1.6B) from the pile axis. This reduced to 17.0% at a radius of 280.0 mm (2.5B) from the pile axis. The relatively high positive residual $\Delta\sigma'_{zi}$ was probably due to the greater elastic displacement recovery characteristics of the sand/clay interface, as compared with that of S/S1 and S/S2.

During the initial stages of pile penetration below the sand/clay interface, the residual $\Delta\sigma'_{zi}$ was generally greater than that recorded during pile installation. The D_b associated with the maximum positive

residual $\Delta\sigma'_{zi}$ recorded at radii of 180.0 mm (1.6B) and 280.0 mm (2.5B), corresponded approximately with the on-set of steady state rebound on the sand/clay interface (Figure 7.5(c)). At full pile embedment the residual σ'_{zi} tended to the initial effective overburden stress at all radii.

Included on the sand/clay interface were four pairs of Interface Shear Stress Transducers (ISSTs), the inner two and outer pairs of which were sited at the same radii from the pile axis as the DPTs. The fourth pair of ISSTs were installed at a radius of 380.0 mm (3.3B) from the pile axis.

The shear stress (τ_i) developed on the sand/clay interface (Figure 7.42) initially increased at a slower rate than the vertical effective stress at a given radius. However, with further pile embedment the rate of increase in τ_i became progressively rapid. Peak positive values of τ_i ranging between 42.0 kPa and 5.0 kPa, 1.4 to 3.0 times greater than the associated peak $\Delta\sigma'_{zi}$, were attained at pile penetrations of between 920.0 and 1100.0 mm (8.1 and 9.6B). For pile penetrations in excess of those associated with the peak positive τ_i at a given radius, τ_i reduced rapidly and became negative. This was achieved at all radii for a pile embedment of 1250.0 mm (11.0B), 25.0 mm (0.2B) above the sand/clay interface. The reversal in direction of the shear stresses indicated that the lateral displacement of the clay surface, relative to the overlying sand, had changed direction. In this instance a negative τ_i indicated a movement of the clay away from the pile relative to the overlying sand. For a pile embedment of approximately 1300.0 mm (11.4B), 25.0 mm (0.2B) below the sand/clay interface, the distribution of τ_i was relatively uniform within the radial limits of the ISSTs, and amounted to approximately -2.9 kPa. Further pile embedment

resulted in a second direction reversal for τ_i within a radius of less than 480.0 mm (5.2B) from the pile axis. Thereafter, τ_i increased at a diminishing rate, with the greatest rate of increase occurring at the inner radial limit of the ISSTs, 180.0 mm (1.6B) from the pile axis. During the latter stages of pile installation there was a slight reduction in τ_i. This was greatest at the inner radial limit of the ISSTs, 180.0 mm (1.6B) from the pile axis. The ultimate extent of the reduction in τ_i was indeterminate due to the limited penetration of the pile into the clay. At the end of pile installation the direction of τ_i was complementary to f_z along the pile shaft.

The development of the residual τ_i (Figure 7.42(b)), for D_b less than the depth to the sand/clay interface, complemented the developement of τ_i during pile installation. Peak values were attained at given radii from the pile axis for an equivalent pile embedment. At a radius of 180.0 mm (1.6B) from the pile axis, the peak positive residual τ_i was approximately equal to 20.0% of the peak installation τ_i. However, at the outer limit of instrumentation, 480.0 mm (5.2B) from the pile axis, the residual τ_i deviated only marginally from zero until a pile embedment of approximately 1000.0 mm (8.8B) was achieved. As the pile base approached the sand/clay interface the direction of the residual τ_i was reversed. For D_b equal to the depth of the sand/clay interface, the magnitude of τ_i was approximately constant at -2.8 kPa within the radial limits of the ISSTs. For a pile embedment of 1375.0 mm (12.1B), 100.0 mm (0.9B) below the sand/clay interface, the residual τ_i attained a peak negative value of about -7.0 kPa at a radius of 180.0 mm (1.6B) from the pile axis. With greater pile embedment, peak values of τ_i of reducing magnitude were recorded at progressively greater radii from the pile axis. Throughout the latter stages of pile installation a slight

reduction in the intensity of the residual τ_i was recorded at all radii. The direction of the residual τ_i was complementary to the residual f_z on the pile shaft at the end of pile installation.

7.6.1.3 Vertical Effective Stress Generated Around and Below a Vertically Loaded Pile in Homogeneous Loose Sand

The probable distribution of the change in vertical effective stress ($\Delta\sigma_z'$) generated within a sand mass by a pile of unit length, loaded to plunging failure, is presented in the form of a dimensionless stress coefficient 'I' plotted against dimensionless axes r/D_b and Z/D_b (Figures 7.43(a) and (b)). The coefficent 'I' was evaluated throughout pile installation from Equation 7.15

$$I = \frac{\Delta\sigma_z' D_b}{Q_t} \qquad (7.15)$$

where:

$\Delta\sigma_z'$ = change in vertical effective stress recorded by the DPTs,

D_b = foundation depth,

Q_t = total pile resistance (applied load + self weight).

Geddes (1966) derived a series of equations for 'I' due to various subsurface loading conditions which were based on the work of Mindlin (1936). Using the equation presented by Geddes (1966) for a uniform vertical subsurface line load of unit length, 'I' was evaluated for Q_b/Q_t equal to 0.86 (the average value during pile installation) and is

presented on Figure 7.43(c) for comparison with those derived experimentally from S/S1 and S/S2.

The stress coefficents derived experimentally and theoretically were in general agreement and exhibited a number of common features. These were:

(i) A bulbous distribution of stress coefficents below the pile, which reduced in intensity with increased distance from the pile base.

(ii) The development of a region above the pile base within which the stress coefficent were negative.

(iii) A transition zone between the regions defined in (i) and (ii). For the experimental data this consisted principally of a spur shape zone which extended outwards and upwards from the pile base, within which the stress coefficents tended to zero. In the theoretical study the above was comparable with an abrupt deviation in the stress coefficient contours.

The results of S/M1 were not analysed as above, since the layered soil profile was not compatible with the assumptions inherent in the evaluation procedure.

7.6.1.4 A Two Dimensional Analysis of the Stresses Generated on the Sand/Clay Interface During Pile Installation

Throughout pile installation the radial shear stress (τ_i) and the change in vertical effective stress ($\Delta\sigma'_{zi}$) was recorded on the sand/clay interface at 180.0 mm, 280.0 mm and 480.0 mm from the pile axis. The

interdependance of these boundary stresses, with the initial effective overburden stress added to $\Delta\sigma'_{zi}$, is presented on Figure 7.44. Certain tentative assumptions were made with regard to the magnitude of the radial effective stress acting within the sand immediately above the sand/clay interface. This allowed a supposition to be made with regard to the state of two dimensional stress generated on the sand/clay interface throughout pile installation.

It was observed that a number of consecutive data points corresponding to a pile embedment of approximately 1200.0 mm (10.5B), for the variation in τ_i with σ'_{zi} at a radius of 180.0 mm from the pile axis, lay on a straight line which passed through the origin and subtended an angle (ψ') of 53.1 to the horizontal. This suggested that a state of shear failure existed on the sand/clay interface at this point. It was assumed, for practical purposes, that ψ' was equal to ϕ' due to roughness of the sand/clay interface.

The stress profile recorded at a radius of 280.0 mm (2.5B) from the pile axis exhibited a similar feature to that outlined above, however, ψ' was equal to 42.5^0.

The variation in τ_i with σ'_{zi} at a radius of 480.0 mm (4.2B) from the pile axis showed no indication of the development of a state of shear failure on the sand/clay interface.

From the above results, the direction of the major principal effective stress (σ'_1) associated with the point of initial tangency of the $\tau_i - \sigma'_{zi}$ profile with the ψ' envelope, was evaluated and plotted relative to the prevailing pile/soil geometry (Figure 7.45). It was observed that σ'_1

appeared to emanate from a point which was typically 48.8 mm (0.4B) below the pile base. This was consistent with the formation of a dense sand cone (active wedge) below the flat base of a driven pile (Koizumi, 1973). Further, Meyerhof (1959) stated that the elastic major principal stress, developed below a pile base, acted radially from the centre of the pile base. Throughout pile penetration in the vicinity of the sand/clay interface it was assumed that the major principal stress 'radiated' from a point 48.8 mm below the pile base. Thus, additional information relating to the state of stress on the sand/clay interface could be established. Of particular interest was the point at which σ'_{zi} was equal to σ'_{ri}, which occurred when σ'_1 was inclined at 45^0 to the horizontal. The pile embedments corresponding to the above condition at radii of 180.0 mm, 280.0 mm and 480.0 mm (1.6B, 2.5B and 4.2B) were estimated and the associated stress circles plotted on Figure 7.44.

With due consideration to the above assumptions, it is suggested that an element of sand on the sand/clay interface within a radius of 280.0 mm (2.5B) from the pile axis, was subjected to the following sequence of stress changes during pile installation.

It was assumed that the stresses acting on an element of sand immediately above the sand/clay interface, prior to pile installation, were equivalent to the 'at-rest' state; that is, σ'_{zi} was equal to the initial effective overburden stress and σ'_{ri} equal to $K_o\sigma'_{zi}$.

From the K_o condition the intensity of both σ'_{zi} and τ_i increased, accompanied by an anticlockwise rotation of the principal stress planes. This continued until the condition was reached where σ'_{zi} was equal to σ'_{ri}, which approximately coincided with σ'_{zimax}. Further pile

penetration resulted in an additional increase in τ_i and a reduction in σ'_{zi}, throughout which the principal stress planes continued to rotate anticlockwise, and resulted in σ'_{ri} being greater than σ'_{zi}.

At a radius of 180.0 mm (1.6B) from the pile axis, for a pile embedment of between 1100.0 and 1190.0 mm (9.6 to 10.4B), 175.0 to 85.0 mm (1.5 to 0.7B) above the sand/clay interface, the variation in σ'_{zi} with τ_i experienced an abrupt deviation in stress path, as indicated by the intermediate data points. The intermediate data points appeared to lie, within reasonable limits, around the arc of a circle constructed to be tangential to the ψ' envelope at the point at which the $\sigma'_{zi} - \tau_i$ profile first became tangential to the ψ' envelope. This suggested that failure initially developed, or came very close to developing, within the sand rather than across the sand/clay interface.

Beyond the point of initial tangency with the ψ' envelope, it is suggested that the general stress intensity reduced with no further rotation of the principal stress planes. This occurred with the pile base between 85.0 mm (0.7B) and 60.0 mm (0.5B) above the sand/clay interface. An abrupt deviation in the $\sigma'_{zi} - \tau_i$ profile away from the ψ' envelope was observed when the pile base was less than 60.0 mm (0.5B) above the sand/clay interface, during which τ_i experienced a significant reduction in association with a small increase in σ'_{zi}. This suggested that a rapid clockwise rotation of the principal stress planes occurred, whilst possibly maintaining a state of shear failure within the sand and, in doing so, reverting to the original stress condition where σ'_{zi} was greater than σ'_{ri}. The $\sigma'_{zi} - \tau_i$ profile intersected the abscissa at a value of σ'_{zi} approximately equal to the initial effective overburden stress. The above stress changes were observed until such time as the

pile base was within 20.0.mm (0.2B) of the sand/clay interface. With further pile penetration there was a reversal in the direction of τ_i and a noteable increase in σ'_{zi}. Such a stress variation was indicative of heave on the sand/clay interface and the greater outward radial displacement of the clay surface relative to the overlying sand. For a pile embedment of greater than 200.0 mm (1.8B) below the sand/clay interface, uplift of the sand/clay interface ceased and settlement commenced. This resulted in a reduction in σ'_{zi}, a reversal in the direction of action of τ_i and an anticlockwise rotation of the principal stress planes. Over the latter stages of pile penetration a quasi-steady state of stress was observed to act across the sand/clay interface.

Similar reasoning to that outlined above may be applied to the state of stress recorded at a radius of 280.0 mm (2.5B) from the pile axis.

With regard to the magnitude and radial distribution of σ'_{ri} associated with the quasi-steady state of stress developed across the sand/clay interface during the latter stages of pile installation. A σ'_{ri} of typically 24.4 kPa was recorded adjacent to the pile shaft by the BOSTs at the level of the sand/clay interface during pile installation. It was assumed that the radial variation in σ'_{ri} within the sand was inversely proportional to the radius, enabling the state of two dimensional stress at radii of 180.0 mm (1.6B) and 280.0 mm (2.5B) from the pile axis to be established. This is plotted on Figure 7.44. It would appear from these results that the sand immediately above the sand/clay interface within a radius of at least 280.0 mm(2.5B), was at, or near to, a state of shear failure, since the resulting stress circles were approximately tangental to their respective ψ' envelopes.

The variation in σ'_{zi} with τ_i, at a radius of 480.0 mm (4.2B) from the pile axis, followed a path generally similar to that reported at a radii of 180.0 mm (1.6B) and 280.0 mm (2.5B) from the pile axis. However, the stress levels were much reduced and appeared to be insufficient to develop shear failure within the sand during pile installation. Since both σ'_{zi} and τ_i tended to their respective initial value during the latter stages of pile installation, it was considered probable that σ'_{ri} was again equal to $K_o\sigma'_{zi}$.

On the basis of the above, the probable radial variation in the quasi-steady state of stress within the sand immediately above the sand/clay interface, was deduced for the pile loaded to plunging failure at full embedment (Figure 7.46). The associated state of stress adjacent to the pile shaft was evaluated in accordance with the assumptions outlined in Section 7.4.4.3, and is indicated on Figure 7.46. The results show a good degree of consistancy between the stress levels acting on the sand/clay interface and the pile shaft contact stresses. The reduction in τ_i with increased radius from the pile axis was almost linear and tended to zero at a radius of 450.0 mm (3.9B). By definition, therefore, σ'_{zi} and σ'_{ri} were principal stresses and were approximately equal to γz_i and $K_o\gamma z_i$ respectively.

7.6.2 Maintained Load Test

7.6.2.1 Homogeneous Sand Profiles

The change in the vertical effective stress ($\Delta\sigma'_z$), recorded by the DPTs

at a depth of 1275.0 mm (11.2B) throughout the ML test, was evaluated and is presented on Figures 7.47(a) and (b). The datum value from which the change in vertical effective stress was evaluated, was the average of the three values associated with the post-compressive residual stress condition recorded during the ML test. In the case of S/S1, only two sets of results were averaged in order to establish a datum, since that recorded immediately prior to commencing the ML test was greater than those recorded subsequently by typically 2.0 kPa.

The datum residual vertical effective stress profiles are presented on Figures 7.47(a) and (b) relative to the initial effective overburden stress. The intensity of σ'_z was less than the initial effective overburden stress within the radial limits of the DPTs and reduced with proximity to the inner radial limit, 180.0 mm (1.6B) from the pile axis. σ'_z was evaluated adjacent to the pile shaft for the post-compressive residual stress condition, as recorded by the BOSTs, on the basis of the assumptions outlined in Section 7.4.4.3. This was found to be, in absolute terms, 3.1 and 3.5 kPa respectively for S/S1 and S/S2, and was in acceptable agreement with the distribution of σ'_z recorded by the DPTs.

The magnitude of $\Delta\sigma'_z$ was small and less than the limits of accuracy of the transducers. However, a good degree of consistency and repeatability was observed in the results. Throughout pile loading there was a tendency for σ'_z to increase at all radii within the radial limits of the DPTs, with the greatest increase occurring near the pile shaft. For pile loads equal to, or in excess of, $200\%Q_{aw}$, the change in σ'_z tended to an upper limiting value at all radii and was associated with Q_{sf}. The radial distribution of σ'_z, relative to the initial effective overburden stress for Q_{amax}, is presented on Figures 7.47(a) and (b) together with

the associated value of σ'_z evaluated adjacent to the pile shaft. It was observed that σ'_z did not exceed the initial effective overburden stress within a radius of 480.0 mm (4.2B) from the pile axis.

At Q_{amax}, the increase in σ'_z adjacent to the pile shaft was estimated at 12.1 kPa and 11.1 kPa for S/S1 and S/S2 respectively. Geddes (1969) undertook the integration of Boussinesq's (1885) equation to evaluate the stress distribution developed within a semi-infinite isotropic medium, due to a uniform vertical line load. Using the equation derived by Geddes (1969), the theoretical radial distribution of $\Delta\sigma'_z$ was evaluated for the calculated $\Delta\sigma'_z$ adjacent to the pile shaft. The resulting theoretical distribution was in excellent agreement with the experimential results for radii of less than, or equal to, 280.0 mm (2.5B) from the pile axis. At greater radii the theoretical vertical effective stress tended to be slightly less than that recorded. The above gave further support to the proposed state of stress along the pile shaft (Section 7.4.4.3 Refer).

As the pile was unloaded to $\frac{1}{2}Q_{amax}$, $\Delta\sigma'_z$ reduced to typically 25.0% of the maximum value recorded at any given radius from the pile axis. This gave support to the supposition of a rapid collapse in the intensity of the stress system adjacent to the shaft as the pile was unloaded (Section 7.4.4.3 Refer).

7.6.2.2 Layered Soil Profile

The intensity and radial distribution of the average post-compressive residual σ'_{zi}, used as datum throughout this test, is presented on

Figure.7.47(c). Within the radial limits of the DPTs σ'_{zi} was approximately equal to, or slightly in excess, of the initial effective overburden stress. The average magnitude of σ'_{zi} adjacent to the pile shaft, under post-compressive residual stress conditions, was evaluated as 4.6 kPa, 14.0 kPa less than the initial effective overburden stress.

Throughout pile loading, $\Delta\sigma'_{zi}$ reduced within the radial limits of the DPTs. This agreed with the observed displacement behaviour for S/M1, which showed the developement of extensive strains within the sand immediately above the sand/clay interface (Section 7.4.2.2 Refer). However, on the basis of the discussions presented in Section 7.3.5, $\Delta\sigma'_{zi}$ increased adjacent to the pile shaft throughout loading.

At Q_{amax}, $\Delta\sigma'_{zi}$ attained a minimum value within the radial limits of the DPTs. However, adjacent to the pile shaft, $\Delta\sigma'_{z}$ increased due to the wedging action of the sand between the pile shaft and the sand/clay interface.

Upon unloading the pile to $\frac{1}{2}Q_{amax}$, σ'_{zi} reduced to typically 75.0% of the maximum value recorded at any given radius from the pile axis. This compared favourably with the corresponding degree of displacement recovery recorded on the sand/clay interface, of 28.0% (Section 7.5.2.2 Refer).

7.6.3 Constant Rate of Uplift Test

7.6.3.1 Homogeneous Sand Profiles

The radial distribution of post-compressive residual vertical effective stress (σ'_z) recorded by the DPTs at depth of 1275.0 mm (11.2B), immediately prior to the CRU test, together with that evaluated adjacent to the pile shaft, is presented on Figures 7.48(a) and (b). The changes in σ'_z, during the CRU test, relative to the residual stress distribution recorded by DPTs are also shown on Figures 7.48(a) and (b). Throughout the CRU test $\Delta\sigma'_z$ was relatively small, less than the limits of accuracy for the DPTs.

The reduction in σ'_z during the CRU test was greatest, within the radial limits of the DPTs, at a radius of 480.0 mm (4.2B) from the pile axis. The trends of the $\Delta\sigma'_z$ profiles indicated a small increase in σ'_z adjacent to the pile shaft. This was confirmed by the results of the BOSTs, from which an increase in σ'_z of typically 3.2 kPa was evaluated at a depth of 1275.0 mm (11.2B) for Q_{sf}. The radial distribution of σ'_z at Q_{sf} is shown on Figures 7.48(a) and (b) relative to the initial effective overburden stress. The change in the radial distribution of σ'_z was compatible with the vertical displacement profiles recorded at the same depth (Figures 7.39(a) and (b)). These showed the development of compressive strains within the sand to a limited radius around the pile shaft.

7.6.3.2 Layered Soil Profile

The radial distribution of the post-compressive residual vertical effective stress (σ'_{zi}), used as datum throughout the CRU test, is shown on Figure 7.48(c). Changes in σ'_{zi} relative to the datum value indicated an increase in the intensity of σ'_{zi} which was greatest at the inner limit of the DPTs, 180.0 mm (1.6B) from the pile axis. This was in agreement with the vertical displacement recorded on the sand/clay interface (Figure 7.39(c)), which showed an increase in uplift of the sand/clay interface with proximity to the pile shaft, resulting in the developement of compressive strains within the overlying sand.

The increase in $\Delta\sigma'_{zi}$ recorded by the DPTs, tended to an upper limiting value which was attained at a pile uplift of -6.67 mm (5.9%B). Further pile uplift resulted in only a small increase in $\Delta\sigma'_{zi}$, irrespective of the continued upward displacement of the sand/clay interface.

The radial distribution of σ'_{zi} across the sand/clay interface for a pile uplift of -11.1 mm (0.1B), corresponding to Q_{sf}, is presented relative to the initial effective overburden stress on Figure 7.48(c). This shows the upper limiting value of σ'_{zi} to increase almost linearly from about 18.6 kPa (1.0 times the initial effective overburden stress) at a radius of 480.0 mm (4.2B), to approximately 27.0 kPa (1.4 times the initial effective overburden stress) at a radius of 180.0 mm (1.6B) from the pile axis.

The continued uplift of the pile resulted in no further increase in σ'_{zi} at radii of greater than 160.0 mm (1.6B) from the pile axis. However, σ'_{zi} continued to increase adjacent to the pile shaft, as was evident from

the increase in f_z and σ'_r recorded by the BOSTs located immediately above the sand/clay interface. At the conclusion of the CRU test the magnitude of σ'_r recorded by the BOSTs located immediately above the sand/clay interface, exceeded the calibration limits for the t = 0.6 mm BOSTs, σ'_r was, therefore, calculated from $f_z/\text{Tan}\delta'$. The magnitude of σ'_{zi} was evaluated assuming the stress geometry defined previously in Section 7.4.4.3. This showed the distribution of σ'_{zi}, at the conclusion of the CRU test, to increase approximately linearly across the sand/clay interface reaching a maximum value of 31.1 kPa (1.7 times the initial effective overburden stress) adjacent to the pile shaft. The distribution of σ'_{zi} reported above, lends further support to the proposed stress variation adjacent to the pile shaft (Section 7.4.4.3 Refer).

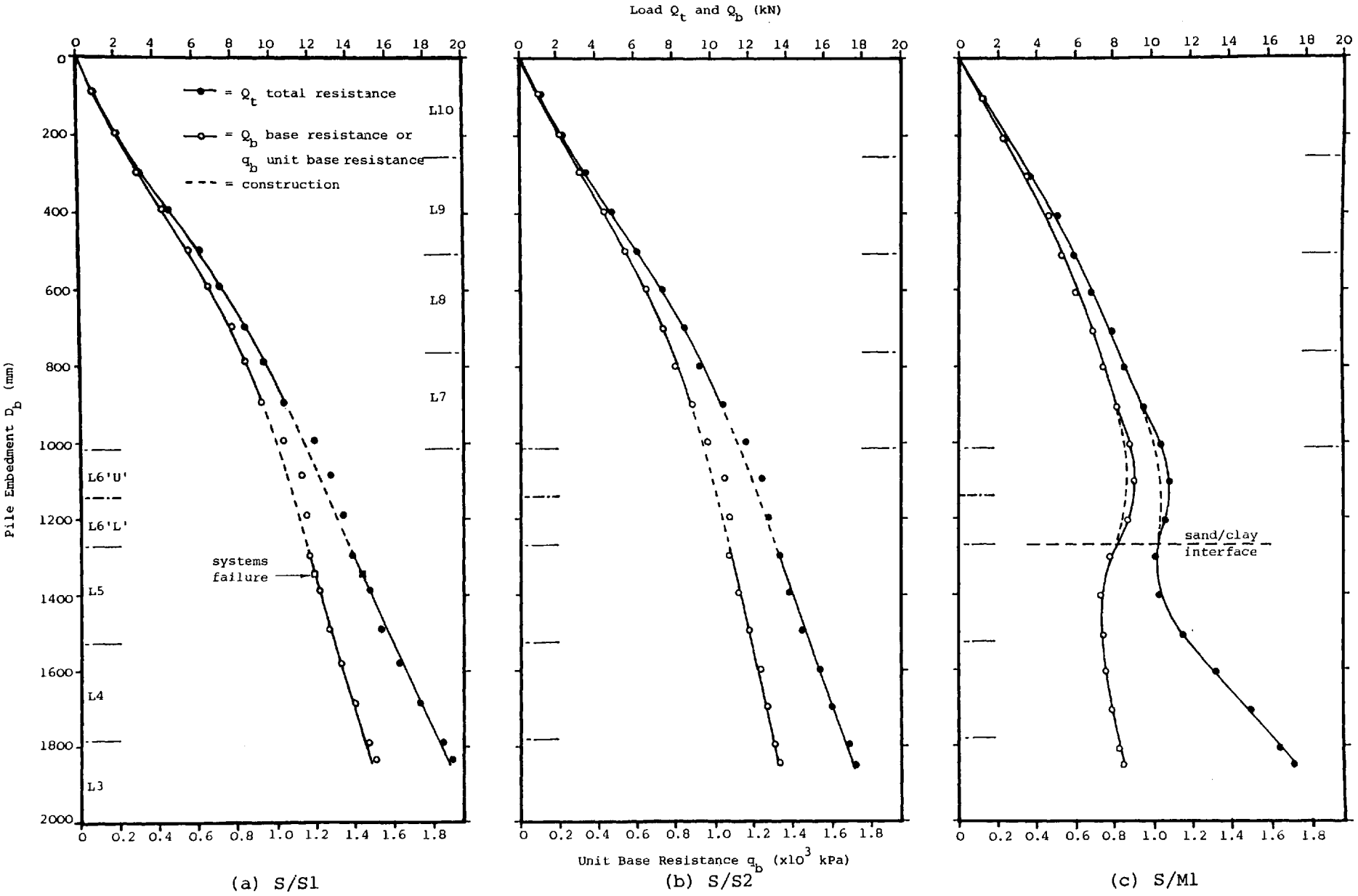

DEVELOPMENT OF TOTAL AND BASE RESISTANCE WITH PILE EMBEDMENT DURING INSTALLATION

FIGURE 7.1

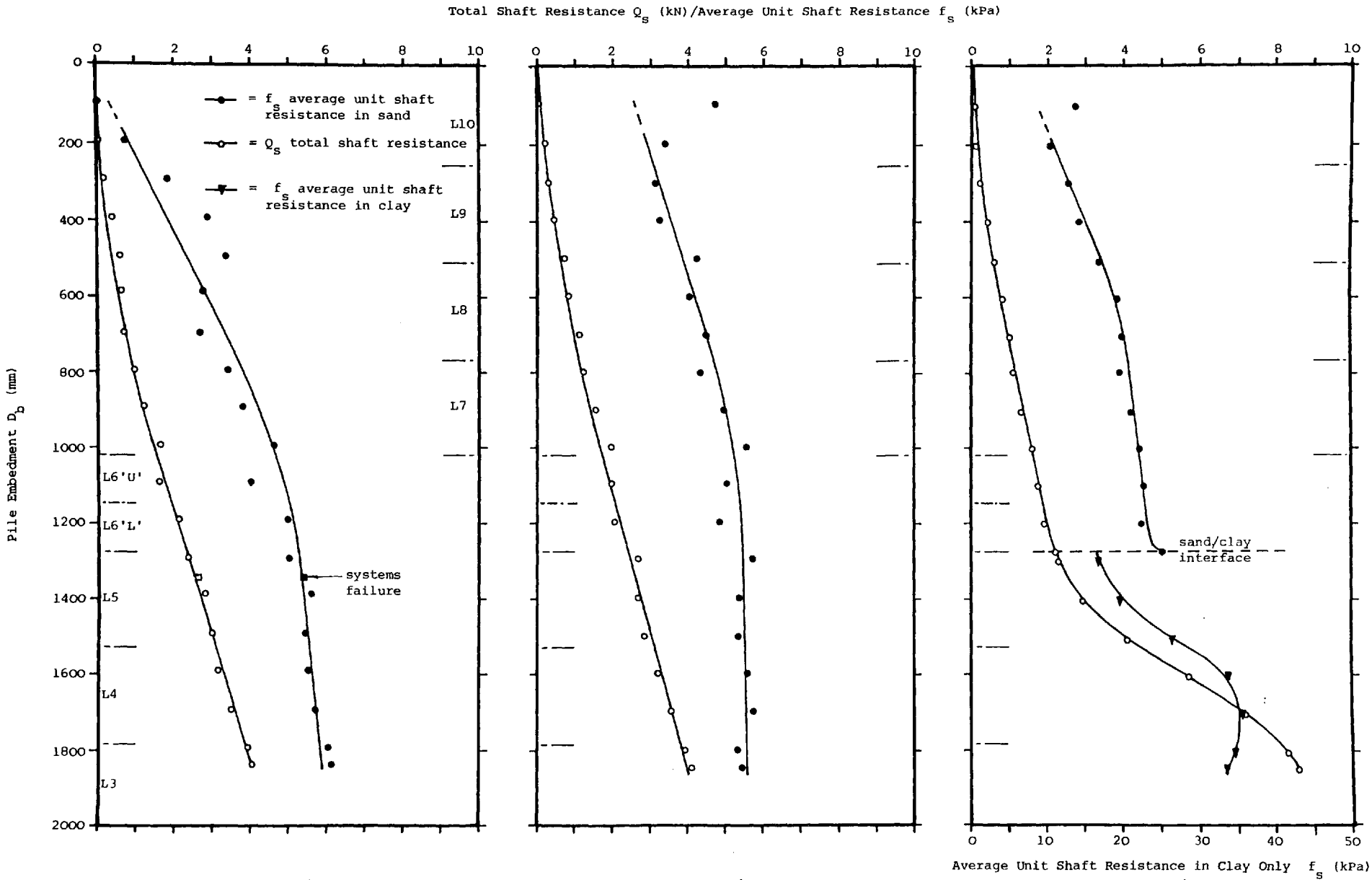

DEVELOPMENT OF TOTAL AND UNIT SHAFT RESISTANCE WITH PILE EMBEDMENT DURING INSTALLATION

FIGURE 7.2

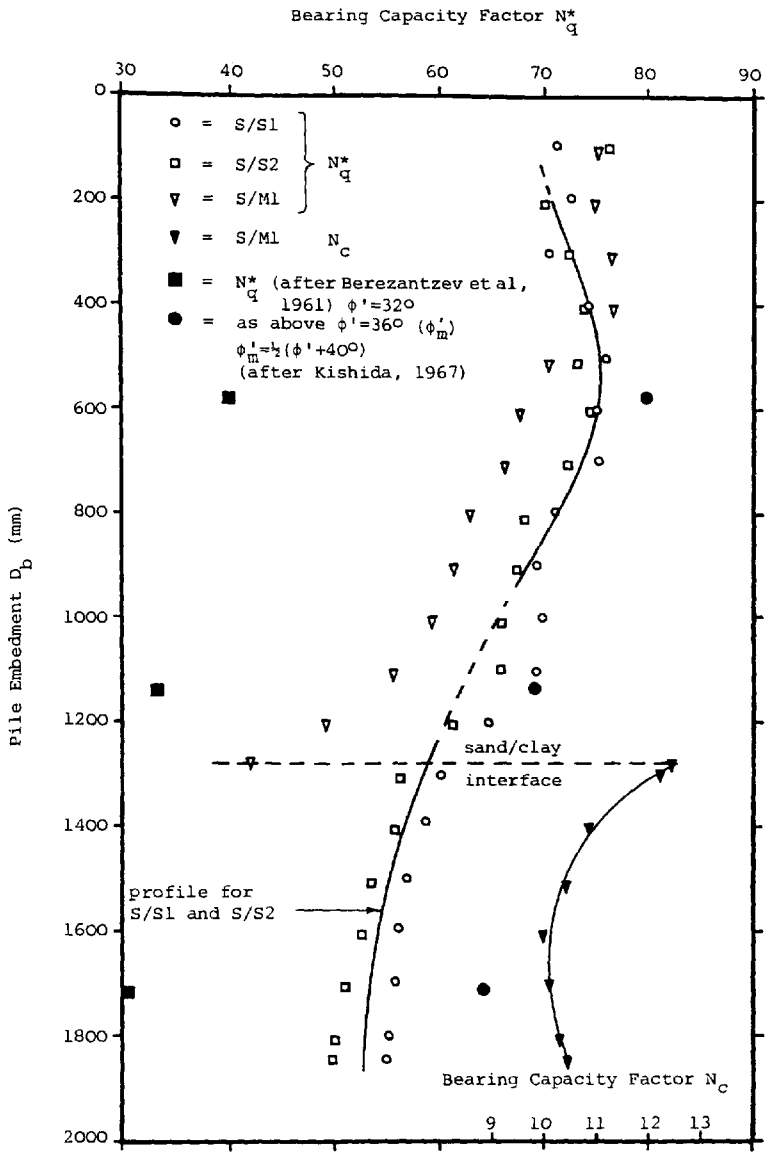

VARIATION IN BASE BEARING CAPACITY FACTORS WITH PILE EMBEDMENT DURING INSTALLATION

FIGURE 7.3

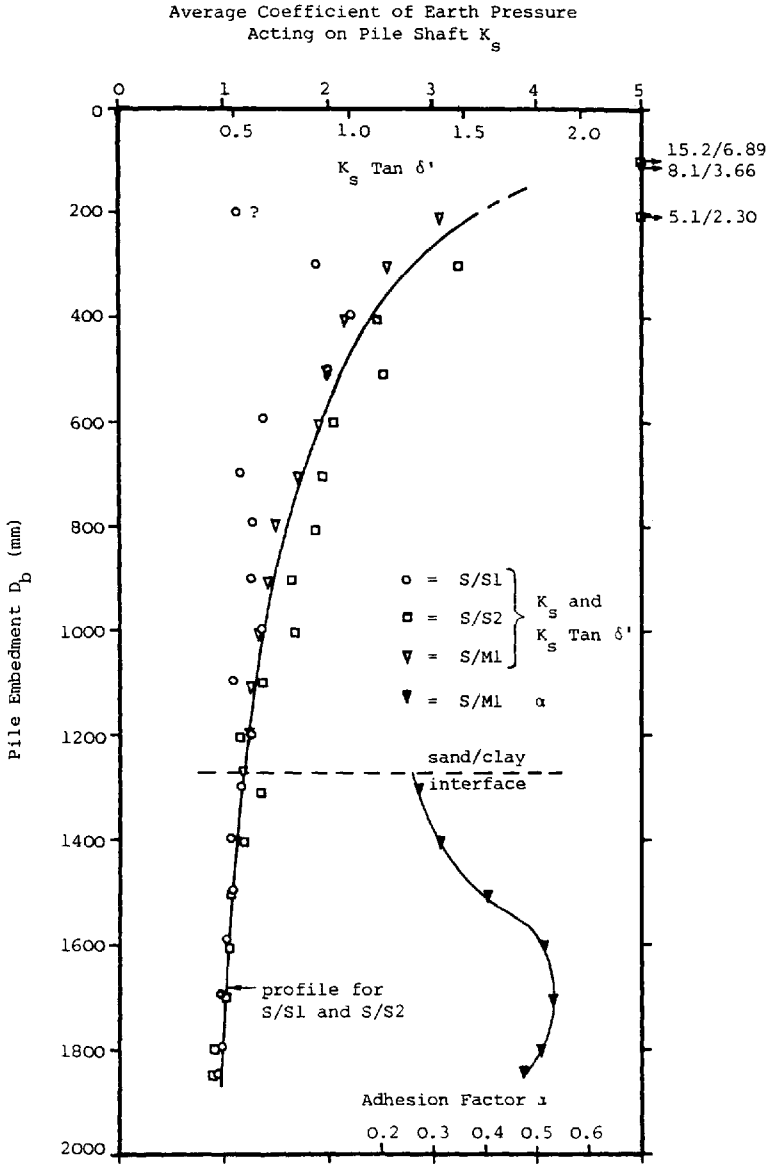

VARIATION IN AVERAGE SHAFT BEARING CAPACITY FACTORS WITH PILE EMBEDMENT DURING INSTALLATION

FIGURE 7.4

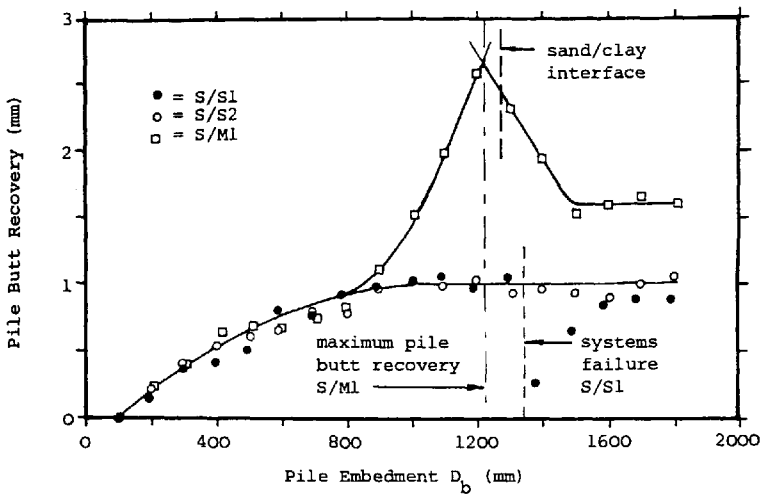

(a) Pile Butt Recovery

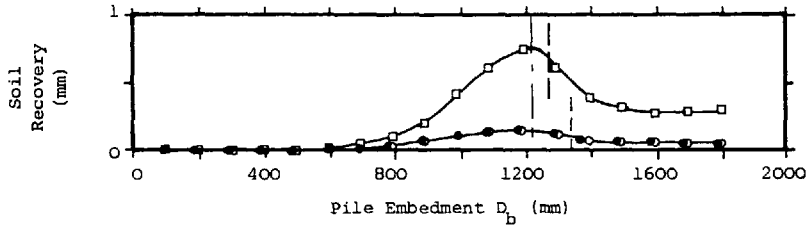

(b) Soil Recovery at Z = 1275.0 mm (Zi) and r = 160.0 mm

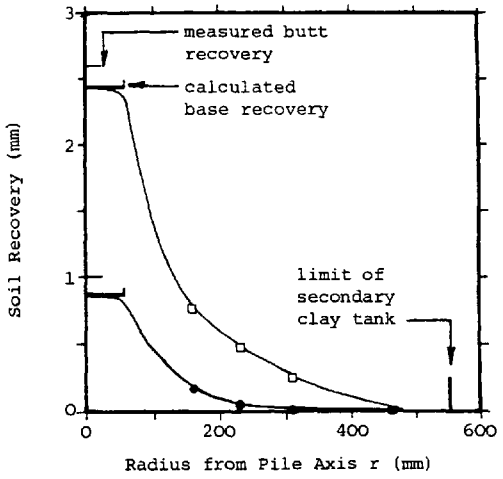

(c) Radial Profile of Maximum Soil Recovery Z = 1275.0 mm (Zi), Db = 1225.0 mm

PILE BUTT AND SOIL RECOVERY DURING INSTALLATION

FIGURE 7.5

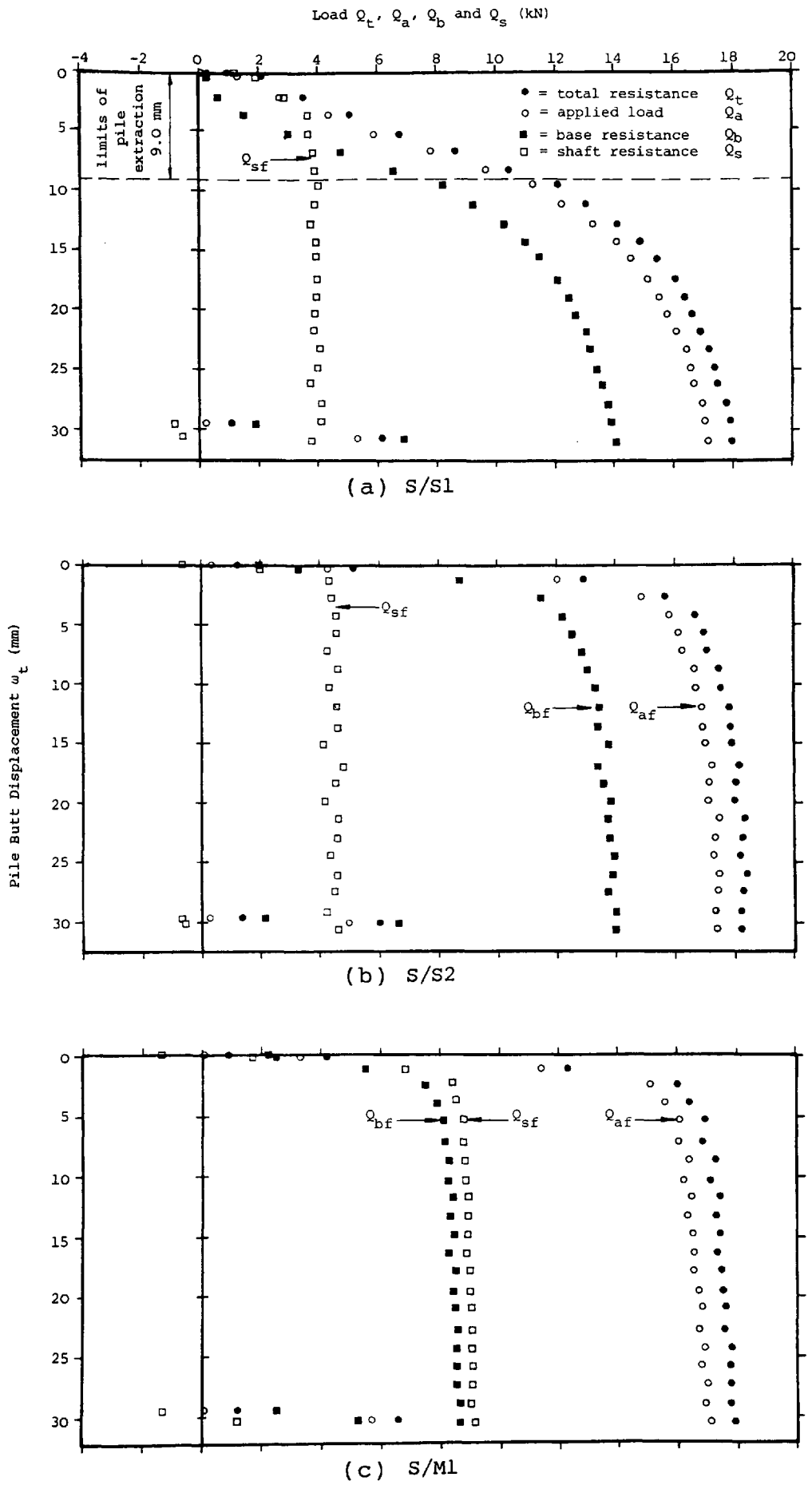

CONSTANT RATE OF PENETRATION TEST
(RATE = 1.524 mm/min)

FIGURE 7.6

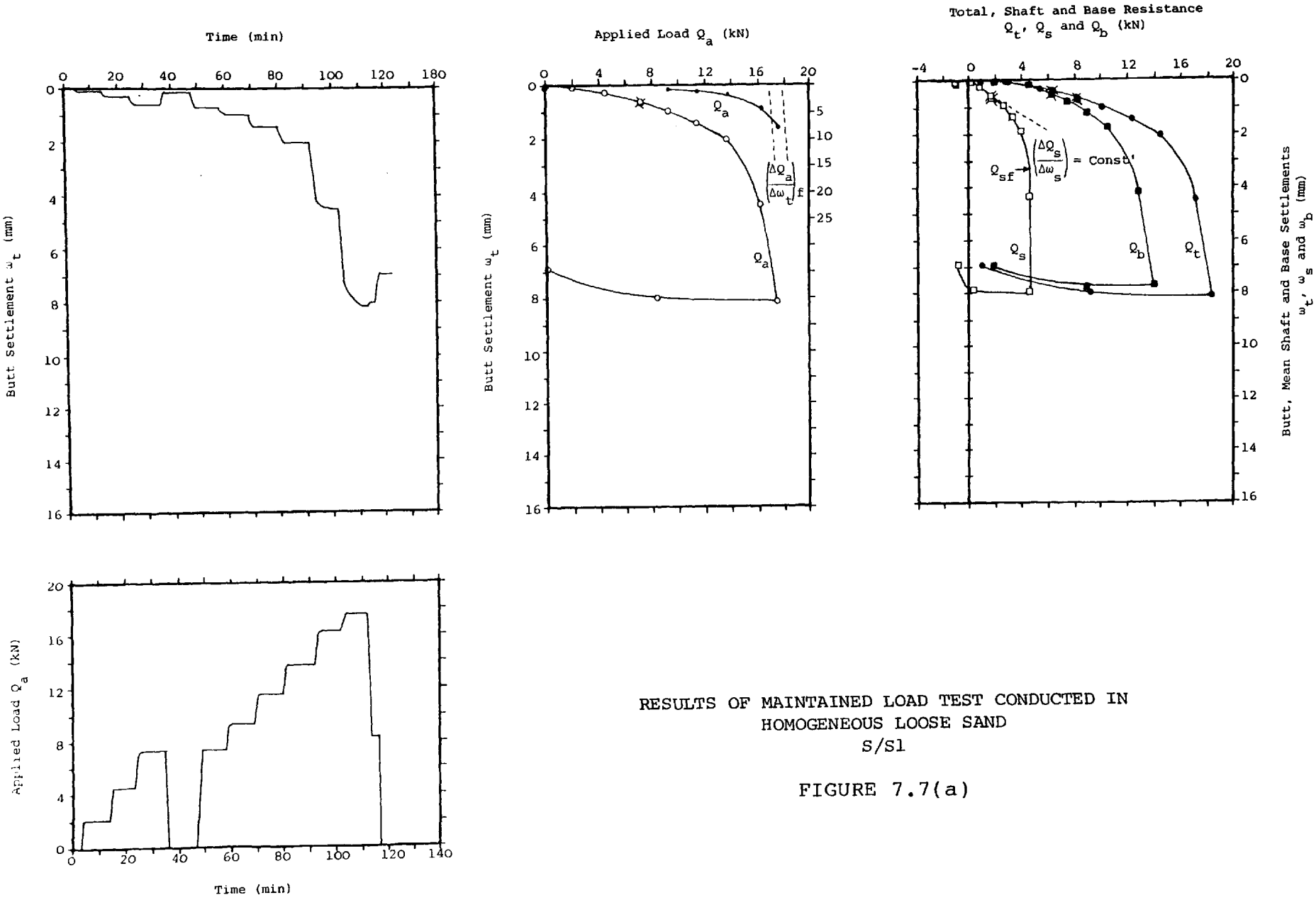

RESULTS OF MAINTAINED LOAD TEST CONDUCTED IN
HOMOGENEOUS LOOSE SAND
S/S1

FIGURE 7.7(a)

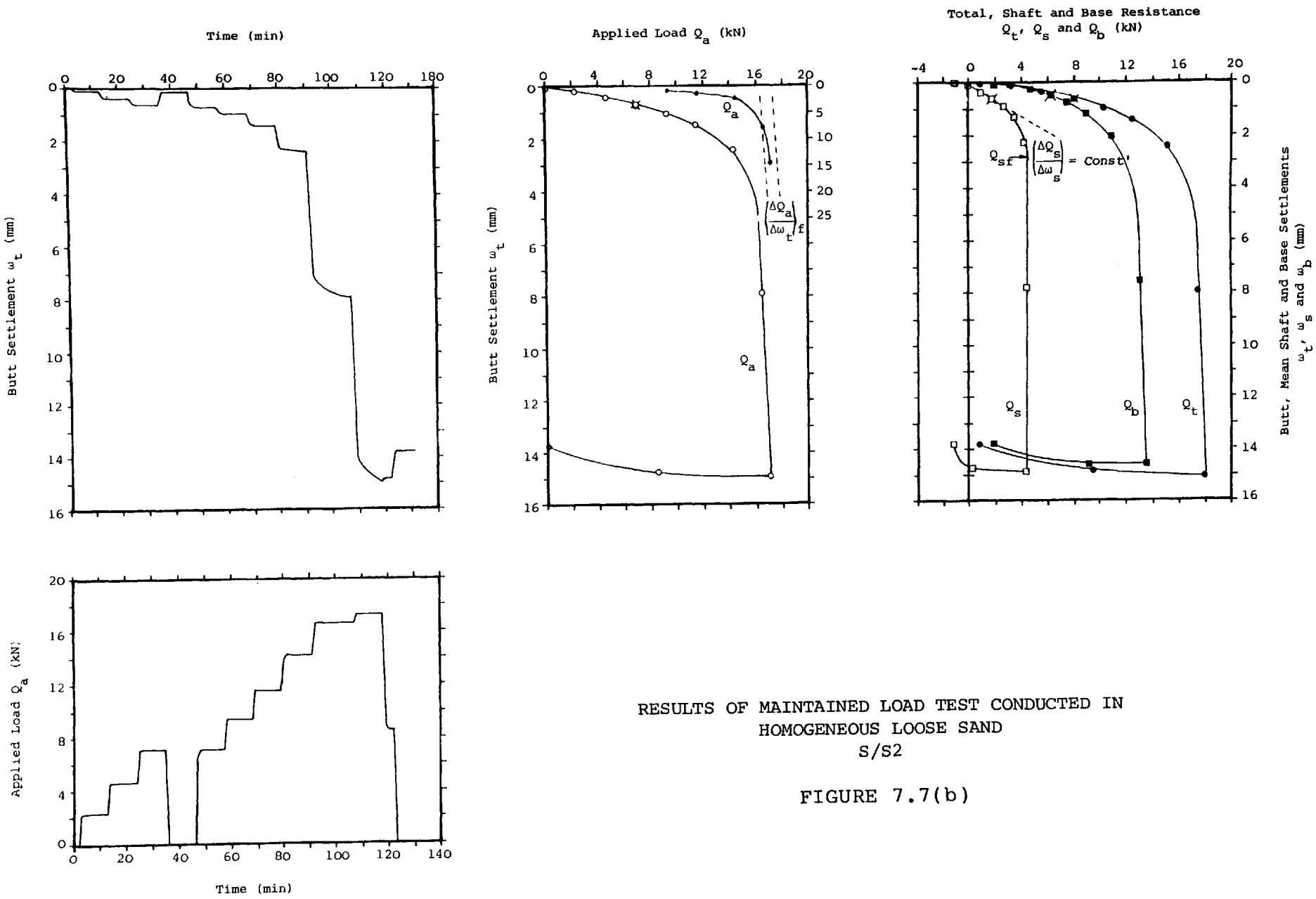

RESULTS OF MAINTAINED LOAD TEST CONDUCTED IN
HOMOGENEOUS LOOSE SAND
S/S2

FIGURE 7.7(b)

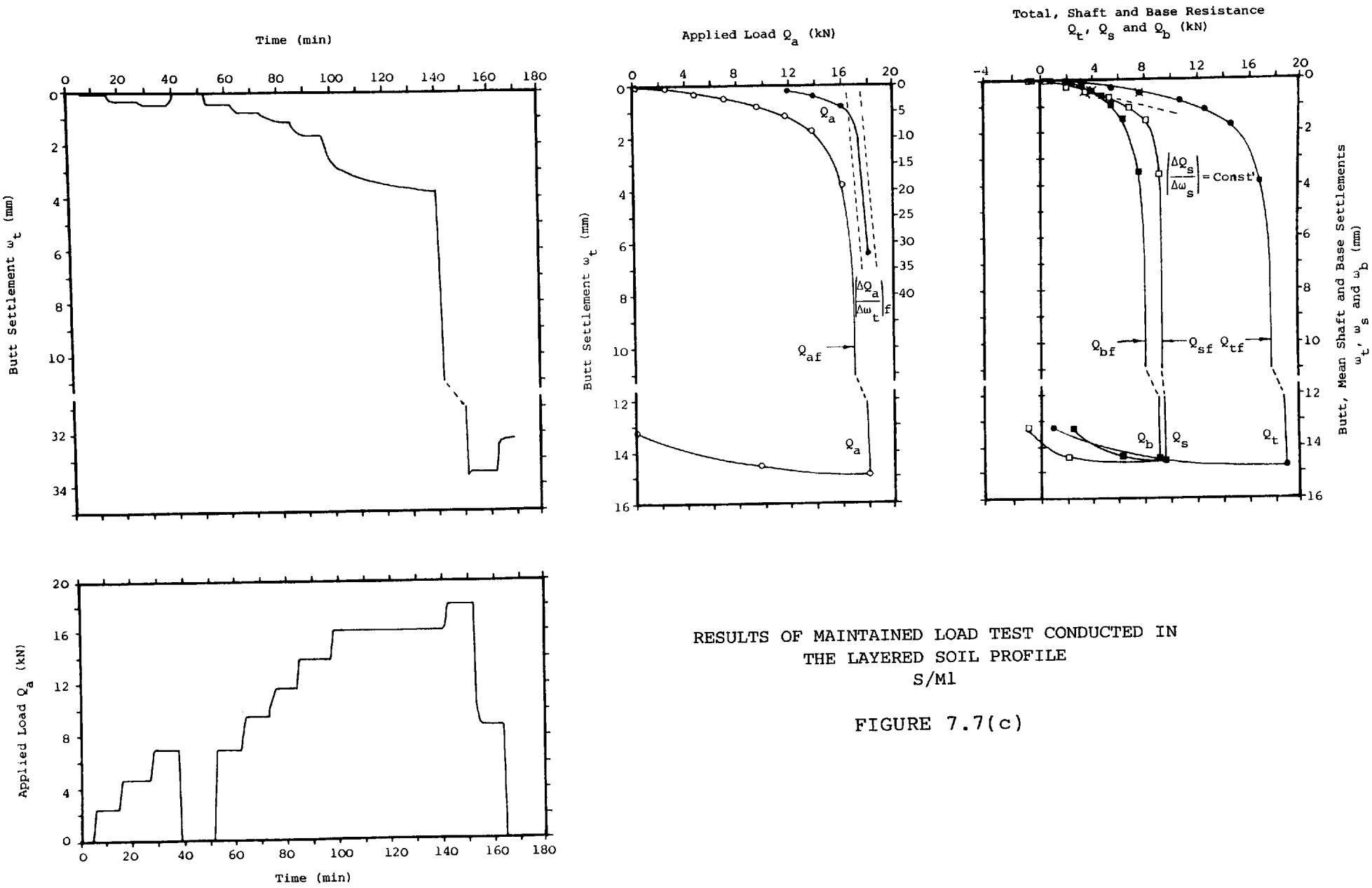

RESULTS OF MAINTAINED LOAD TEST CONDUCTED IN THE LAYERED SOIL PROFILE S/M1

FIGURE 7.7(c)

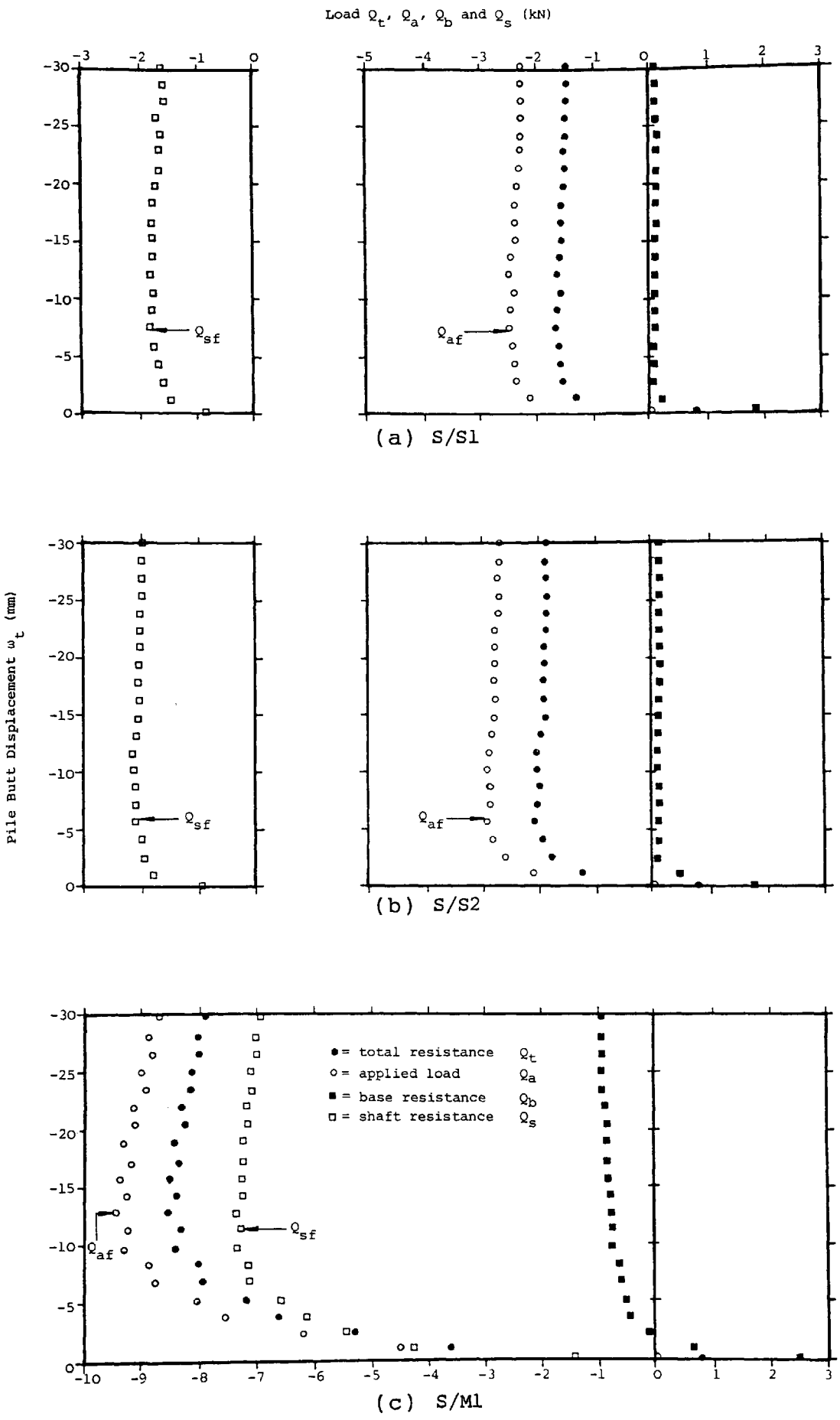

CONSTANT RATE OF UPLIFT TEST
(RATE = 1.524 mm/min)

FIGURE 7.8

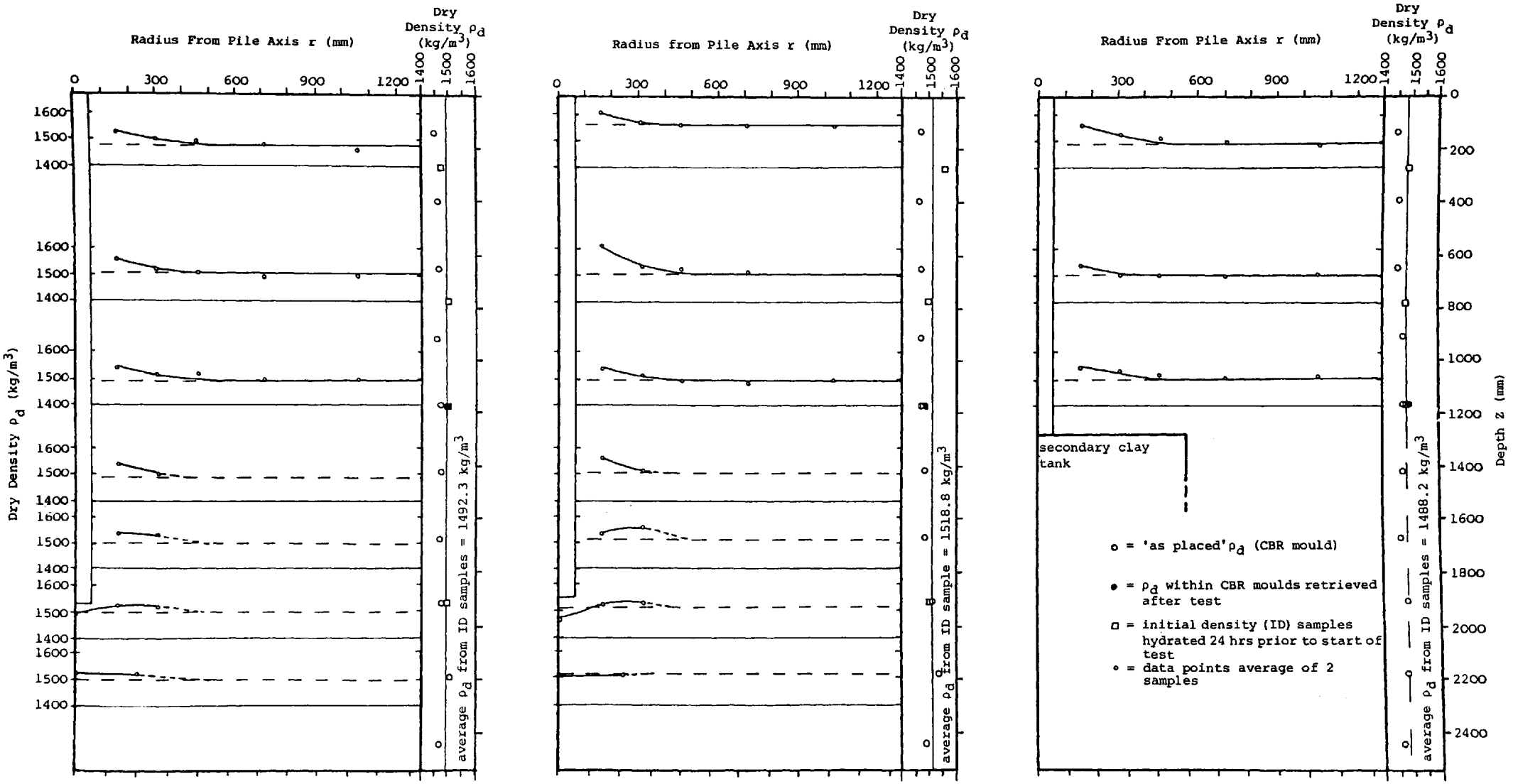

(a) S/S2 (b) S/S1 (c) S/M1

AS-PLACED AND INITIAL DENSITY PROFILES, AND THE DENSITY VARIATION DUE TO PILE INSTALLATION AS DEDUCED FROM SAND/PLASTER DENSITY SAMPLES

FIGURE 7.9

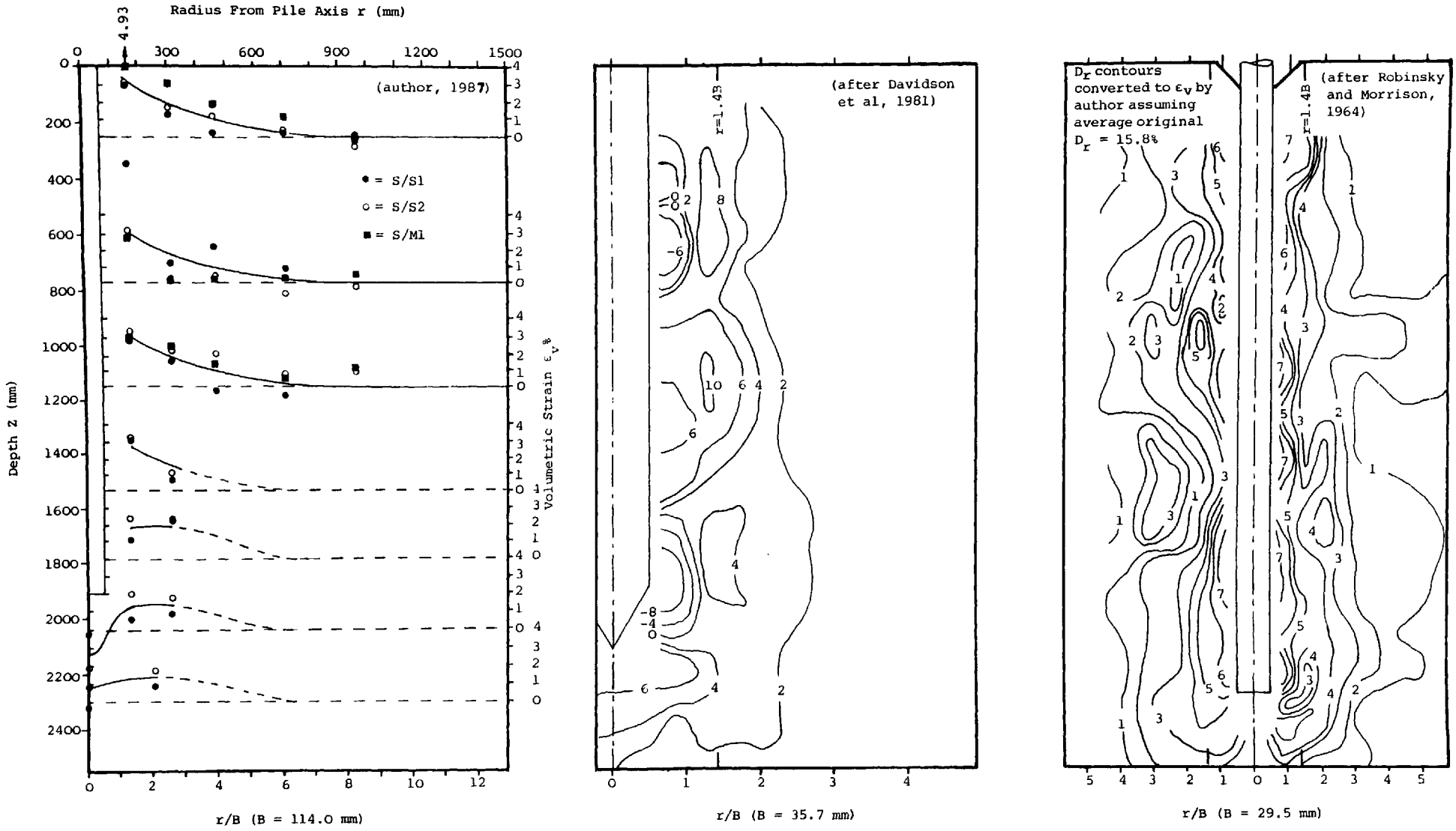

VOLUMETRIC STRAINS IN LOOSE SAND DUE TO PILE INSTALLATION

FIGURE 7.10

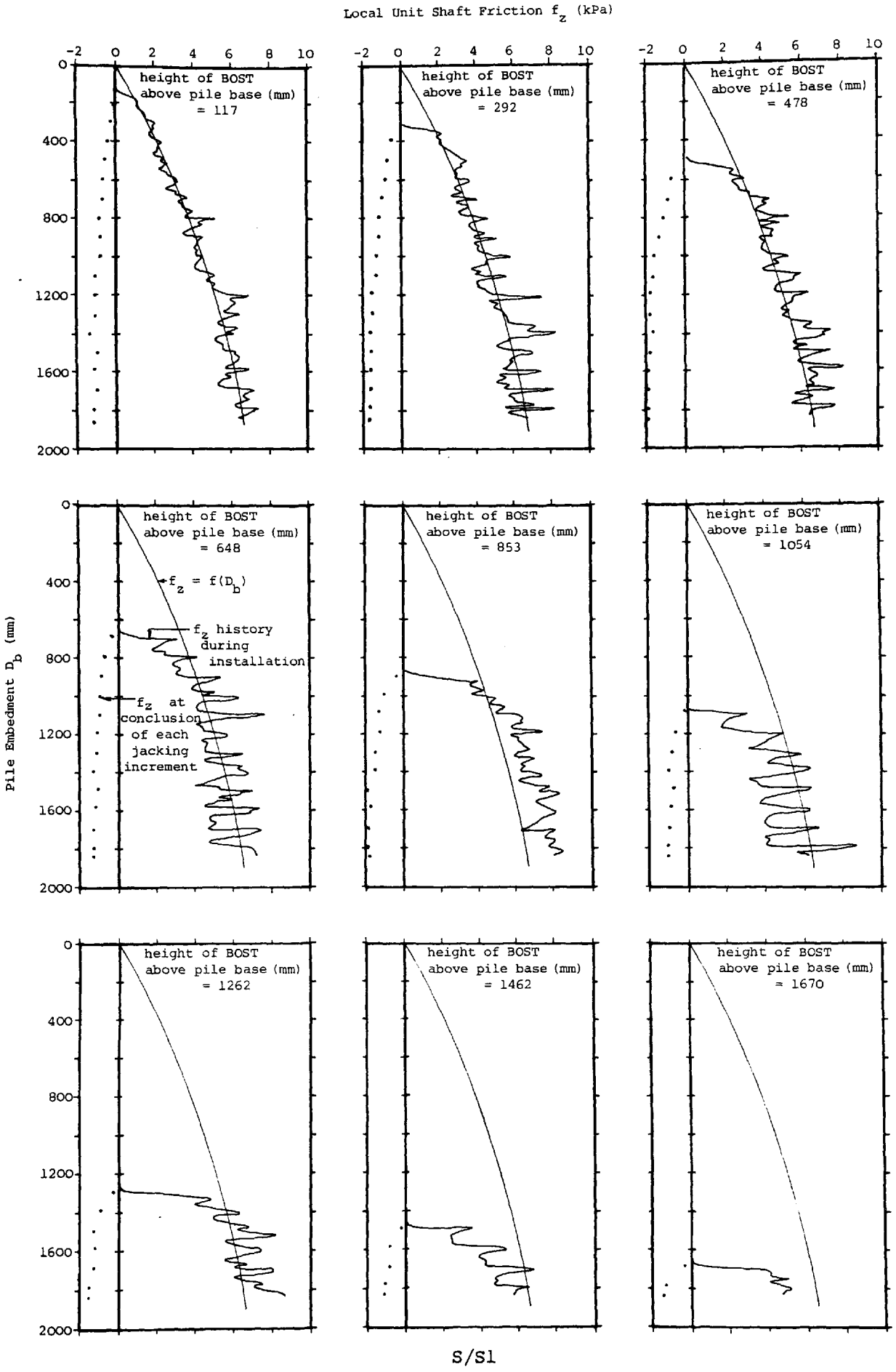

DEVELOPMENT OF LOCAL UNIT SHAFT FRICTION WITH PILE EMBEDMENT DURING INSTALLATION

FIGURE 7.11(a)

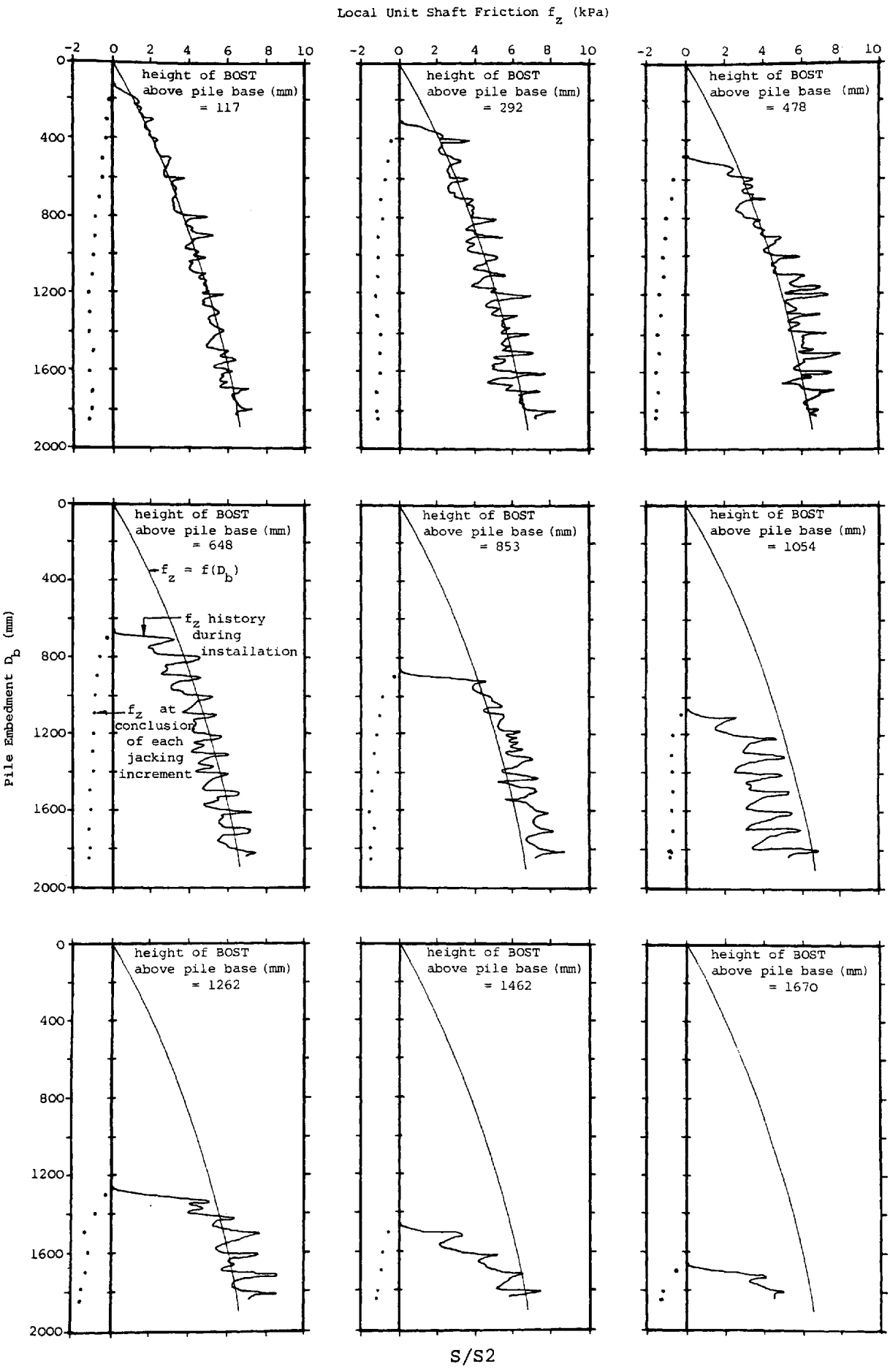

DEVELOPMENT OF LOCAL UNIT SHAFT FRICTION WITH PILE EMBEDMENT DURING INSTALLATION

FIGURE 7.11(b)

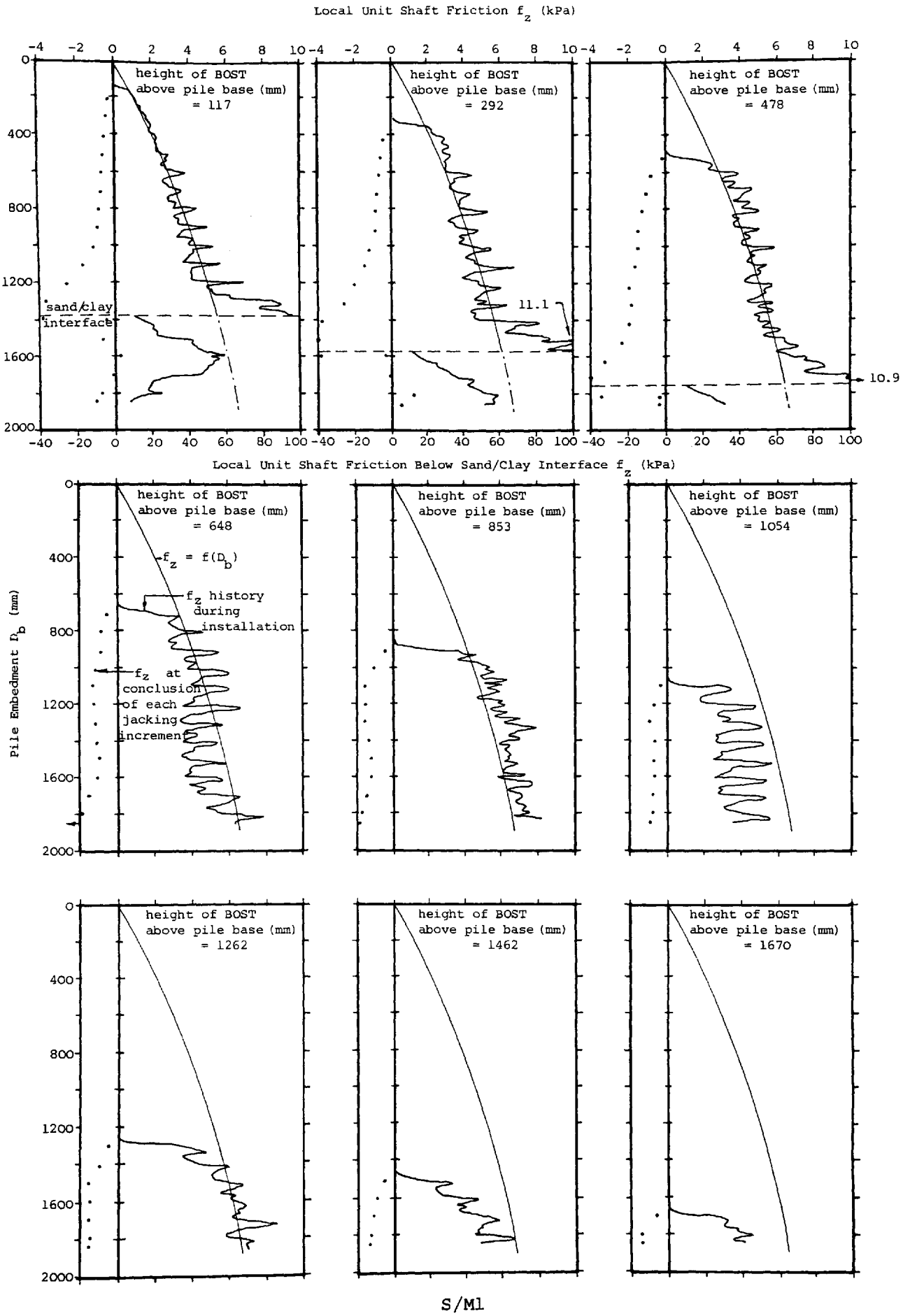

DEVELOPMENT OF LOCAL UNIT SHAFT FRICTION WITH PILE EMBEDMENT DURING INSTALLATION

FIGURE 7.11(c)

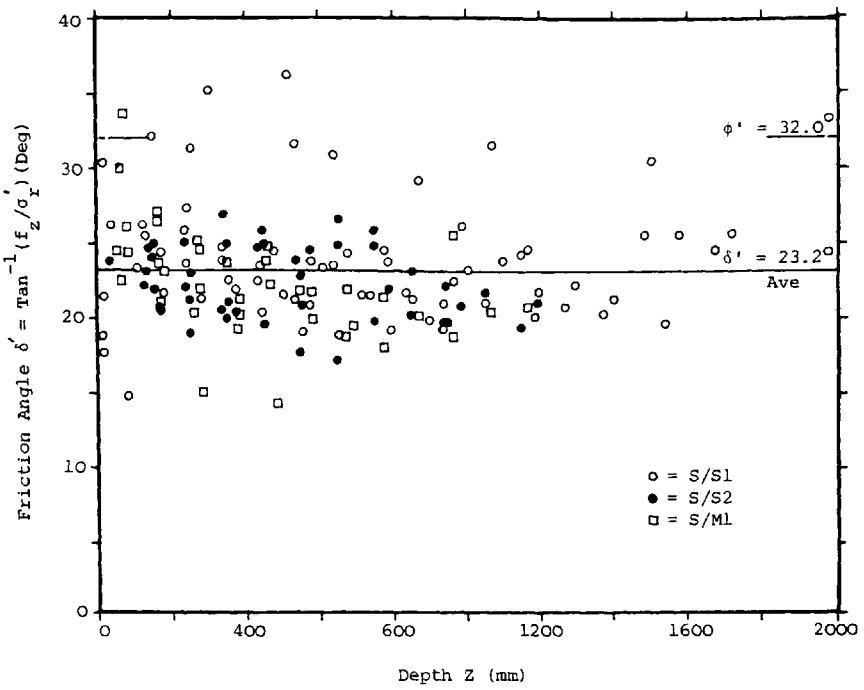

VARIATION IN FRICTION ANGLE DEVELOPED BETWEEN THE PILE SHAFT AND SAND WITH DEPTH DURING INSTALLATION

FIGURE 7.12

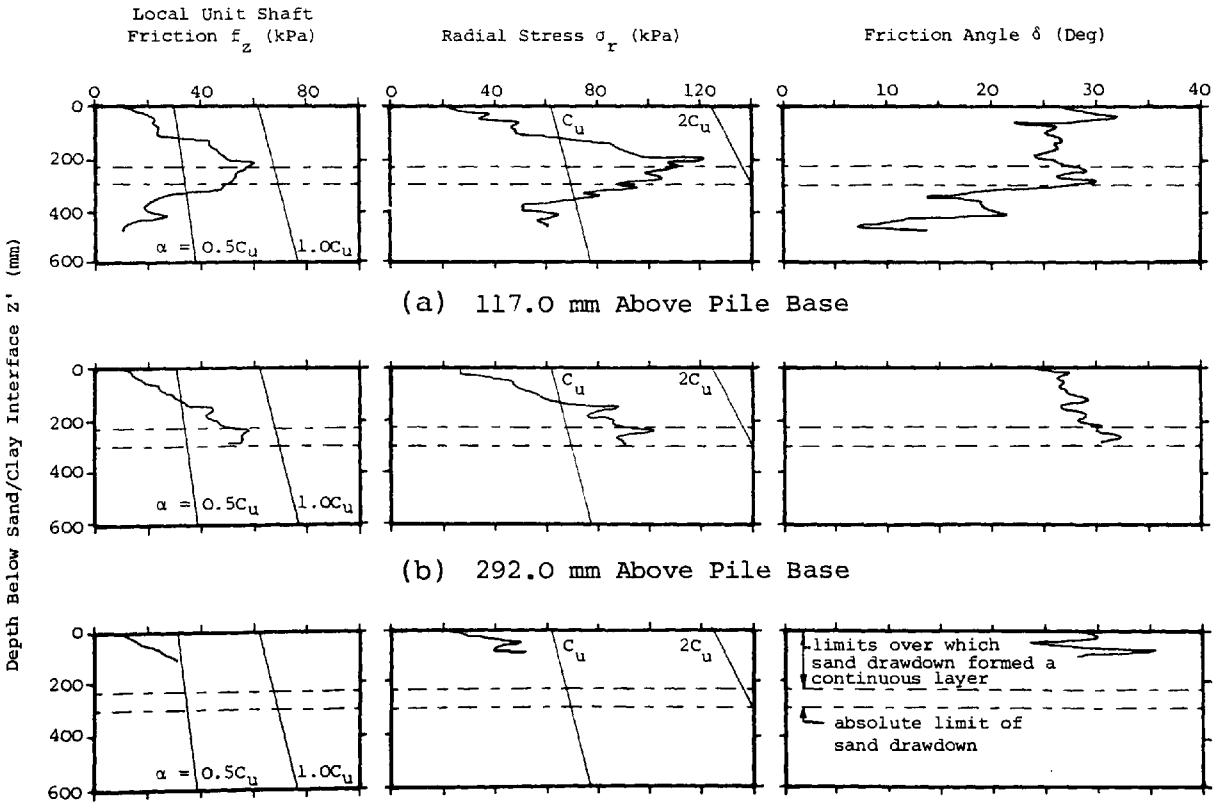

VARIATION IN LOCAL UNIT SHAFT FRICTION, RADIAL STRESS AND FRICTION ANGLE ALONG THE PILE SHAFT WITHIN THE CLAY DURING INSTALLATION

FIGURE 7.13

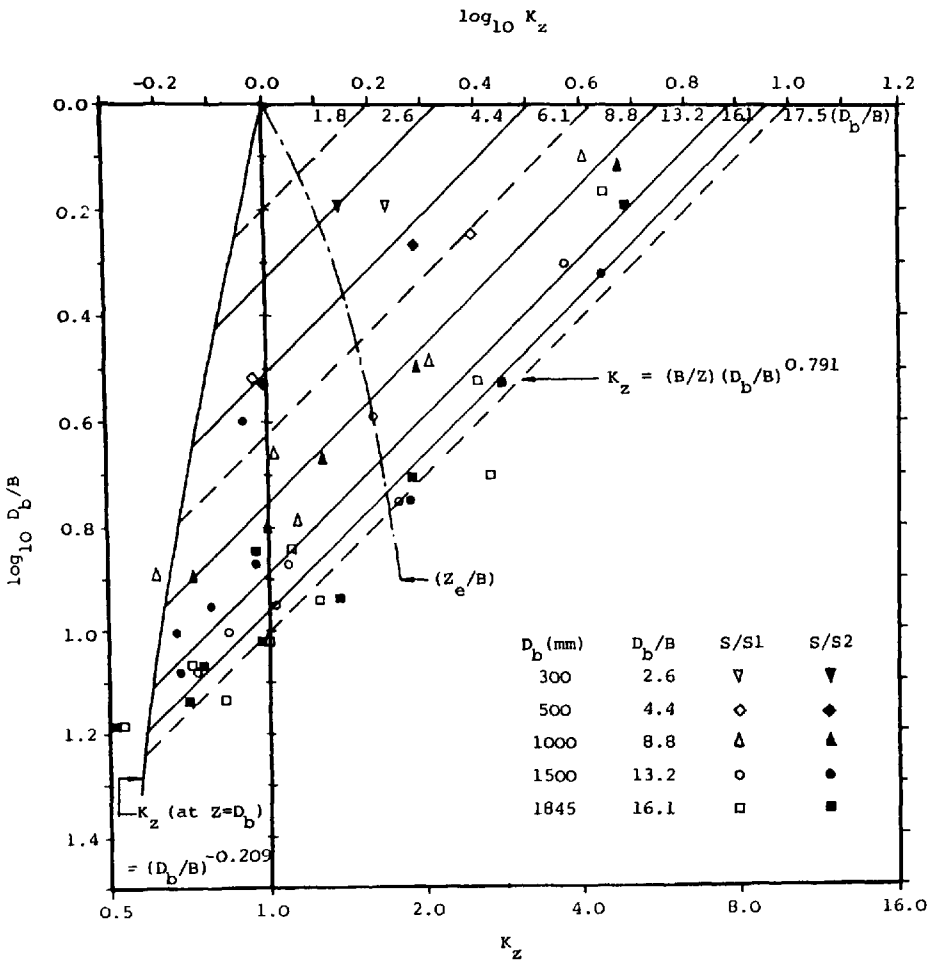

VARIATION IN THE LOCAL COEFFICIENT OF EARTH PRESSURE WITH DEPTH AND EMBEDMENT

FIGURE 7.14

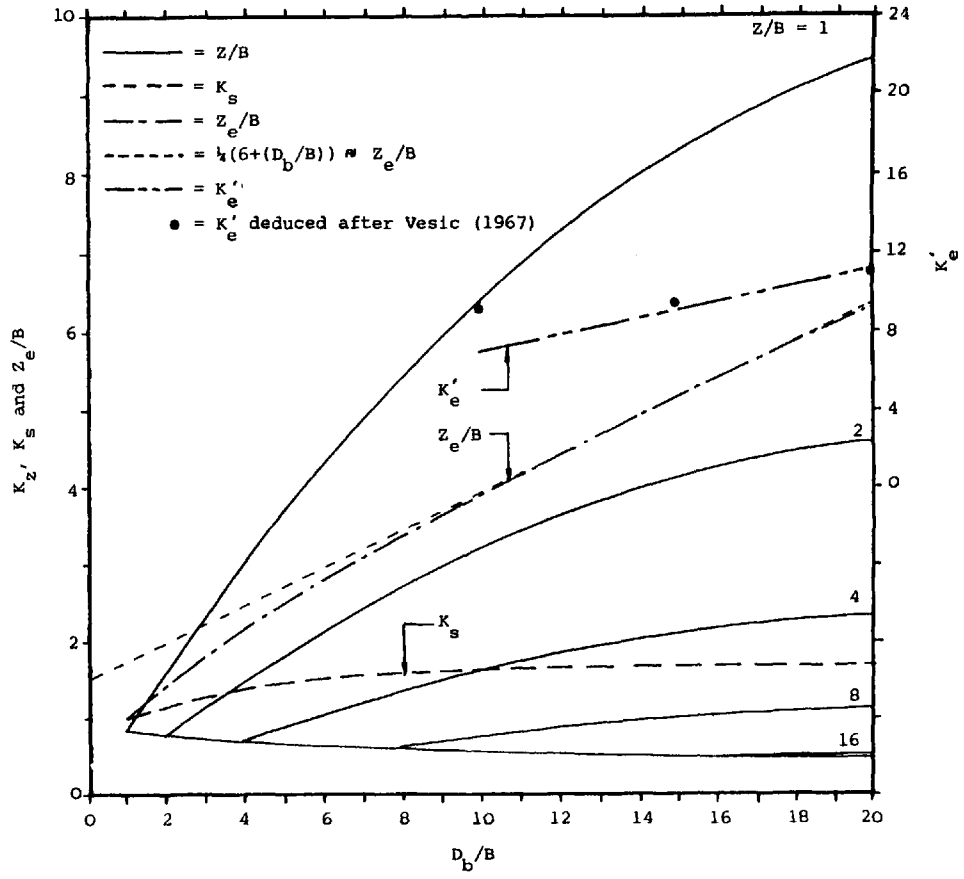

VARIATION IN THE LOCAL AND AVERAGE COEFFICIENTS OF EARTH PRESSURE (K_z AND K_s), DEPTH AT WHICH $K_z = K_s$ (Z_e/B) AND SHAFT BEARING CAPACITY FACTOR (K'_e) WITH EMBEDMENT

FIGURE 7.15

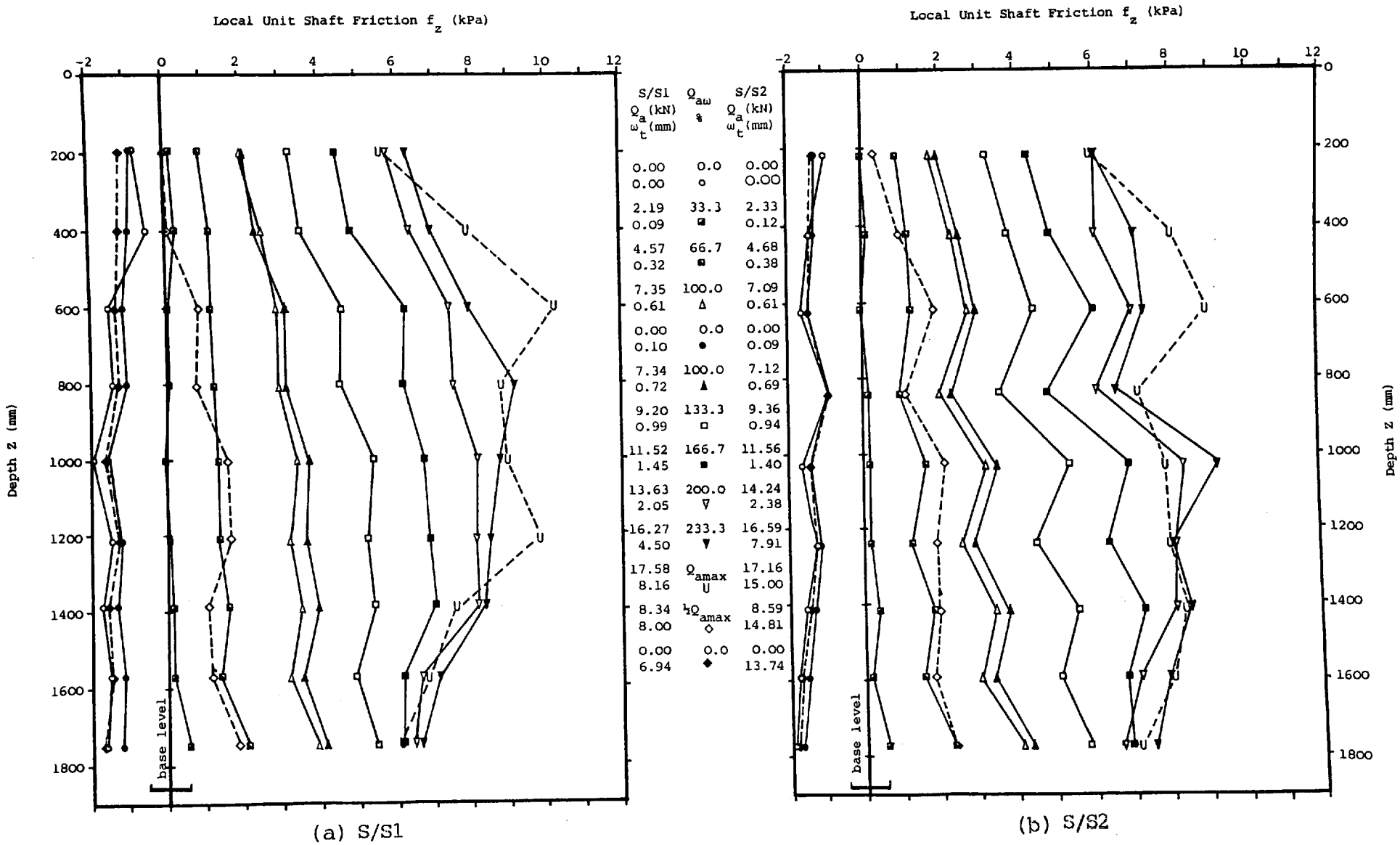

DEVELOPMENT OF LOCAL SHAFT FRICTION DURING THE MAINTAINED LOAD TEST

FIGURE 7.16

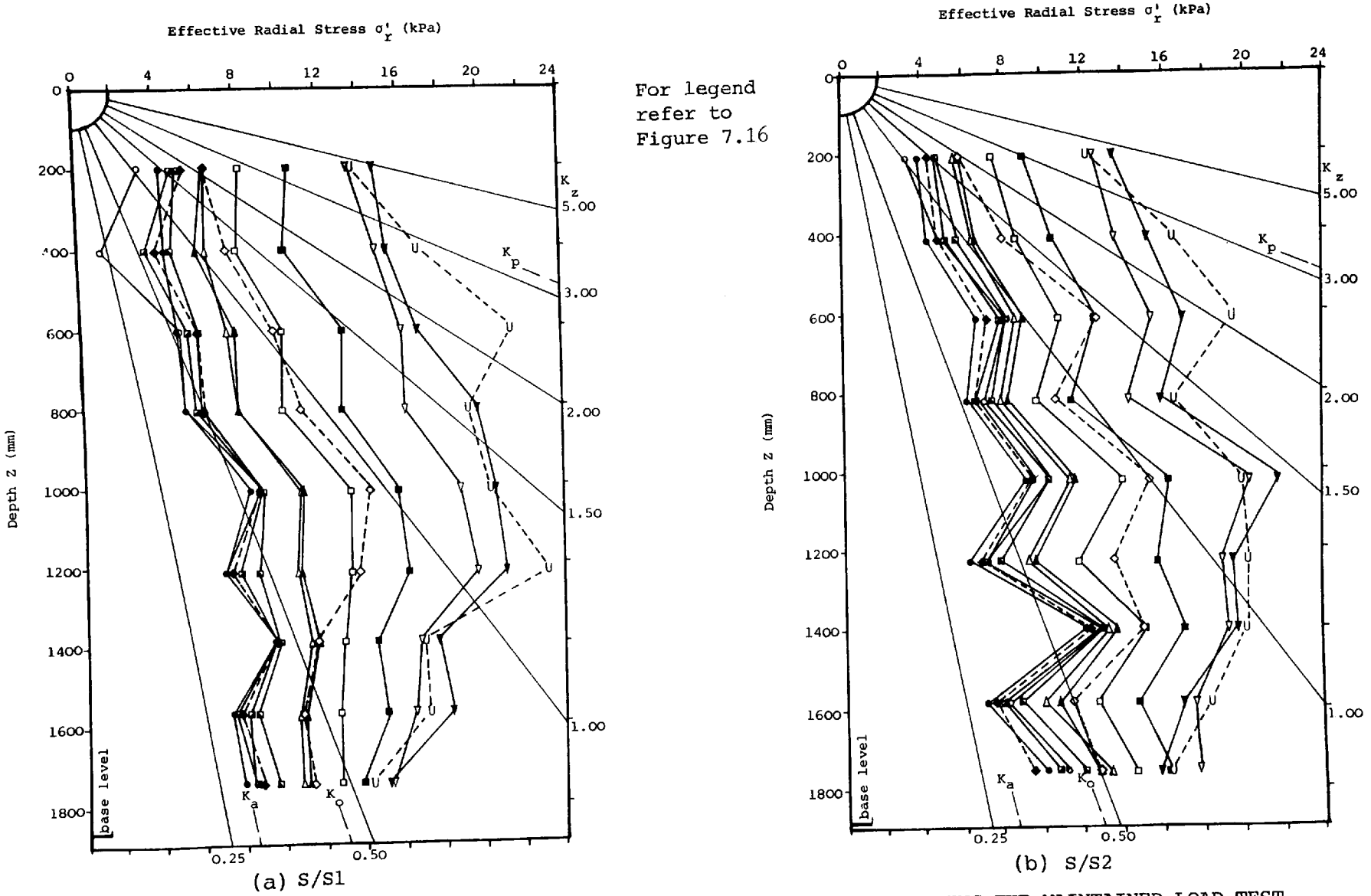

For legend refer to Figure 7.16

DEVELOPMENT OF EFFECTIVE RADIAL STRESS ACTING ON THE PILE SHAFT DURING THE MAINTAINED LOAD TEST

FIGURE 7.17

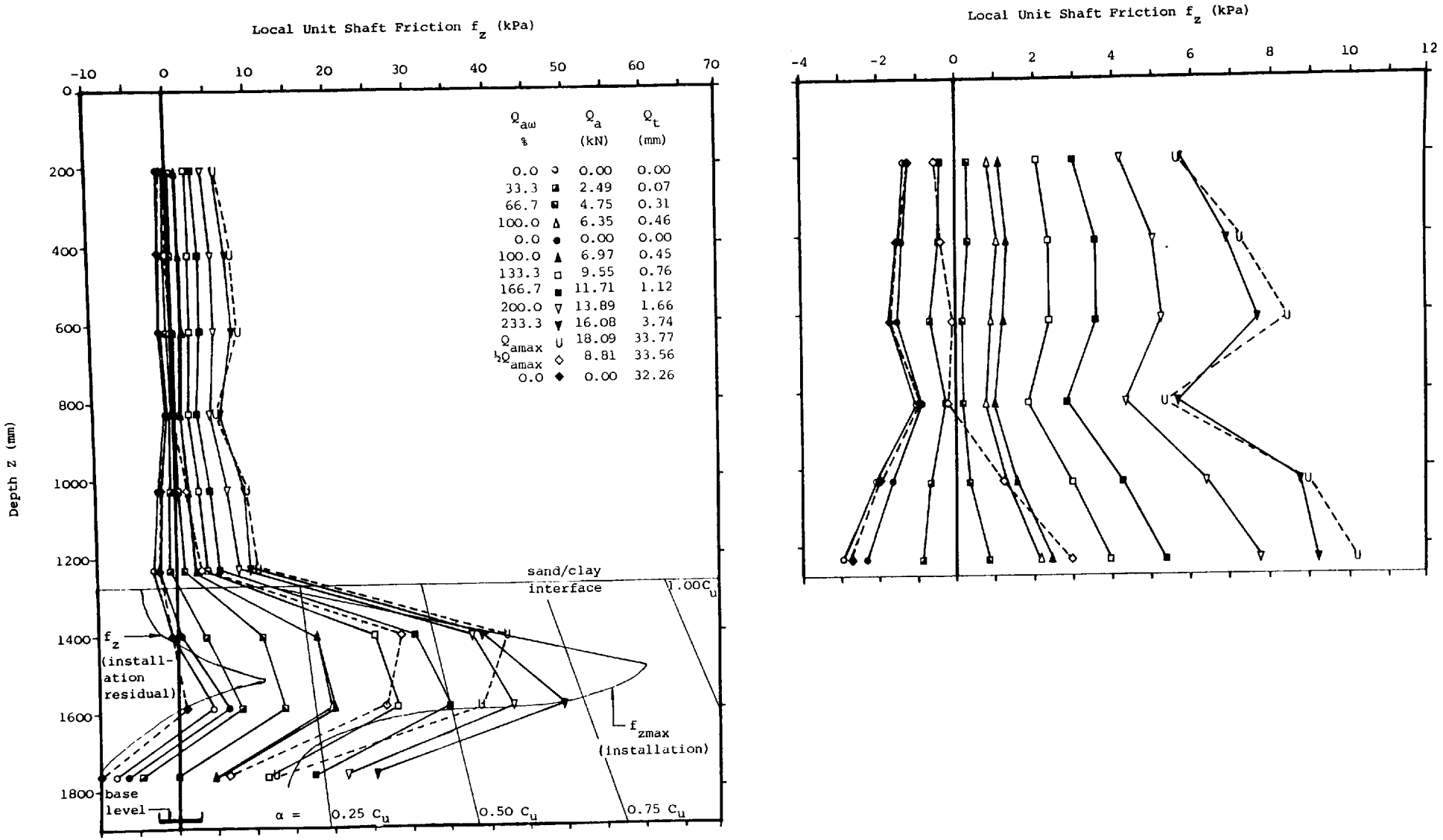

S/M1

DEVELOPMENT OF LOCAL UNIT SHAFT FRICTION DURING THE MAINTAINED LOAD TEST

FIGURE 7.18

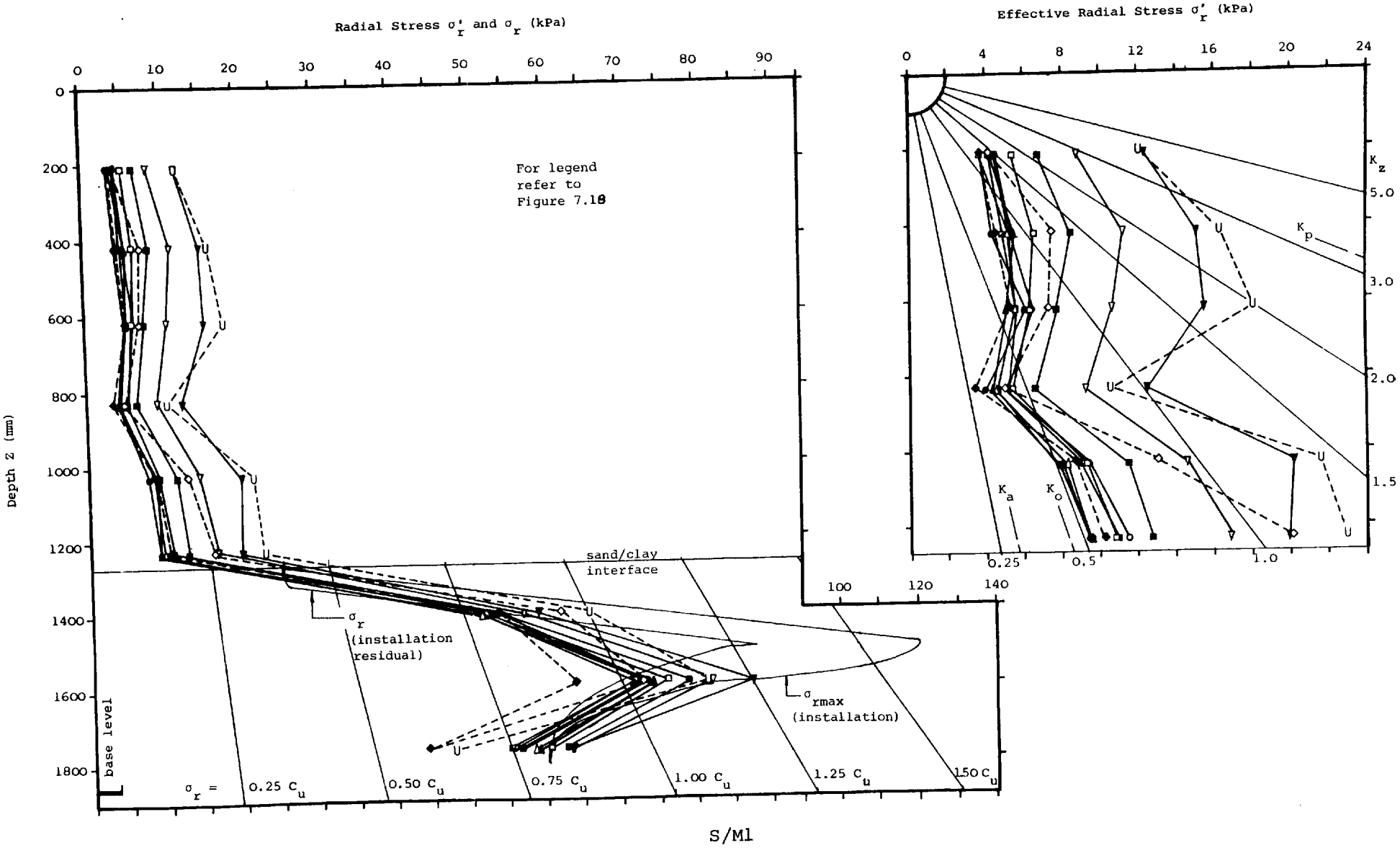

DEVELOPMENT OF RADIAL STRESS ACTING ON THE PILE SHAFT DURING THE MAINTAINED LOAD TEST

FIGURE 7.19

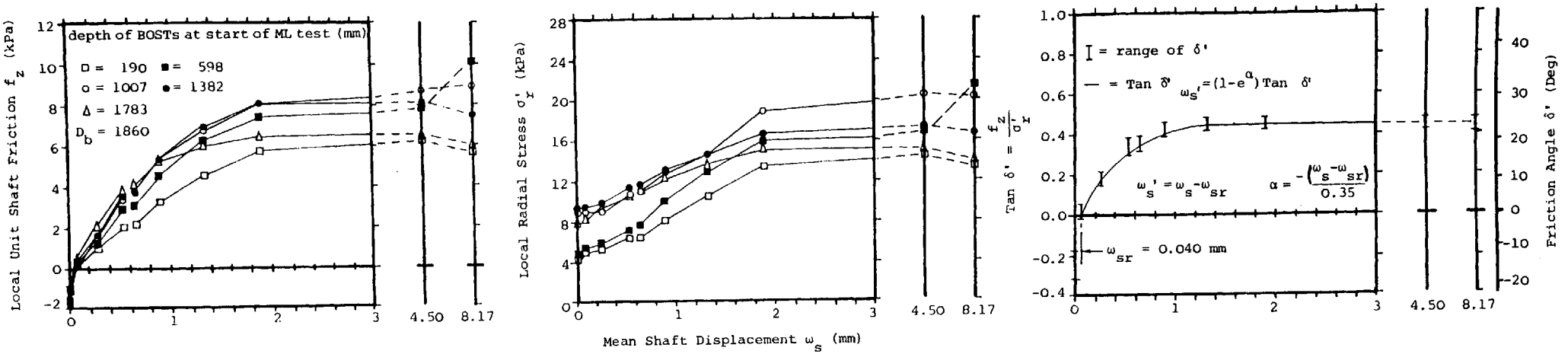

(a) S/S1

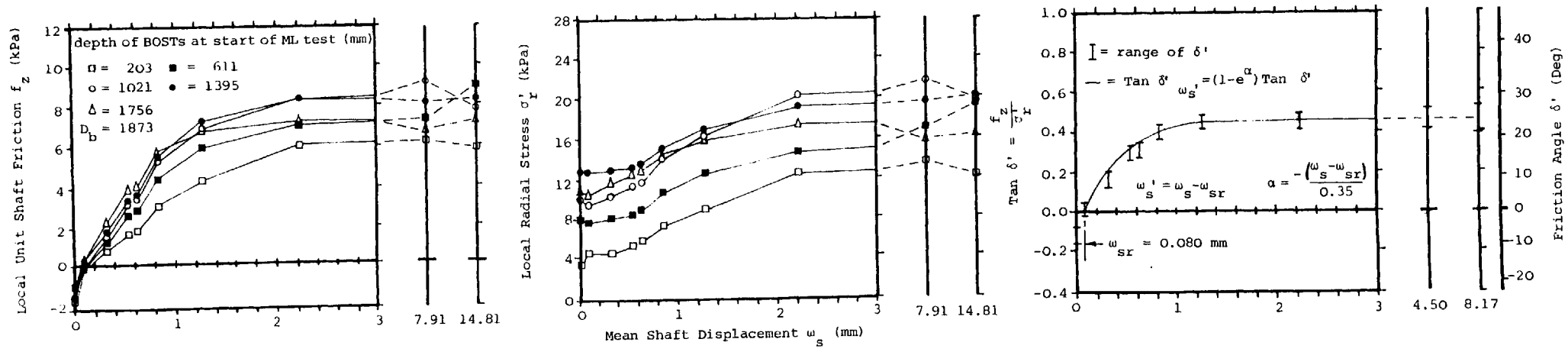

(b) S/S2

MOBILIZATION OF LOCAL UNIT SHAFT FRICTION, RADIAL STRESS AND FRICTION ANGLE AT VARIOUS LEVELS ALONG THE PILE SHAFT WITH MEAN SHAFT DISPLACEMENT DURING THE MAINTAINED LOAD TEST

FIGURE 7.20(a) and (b)

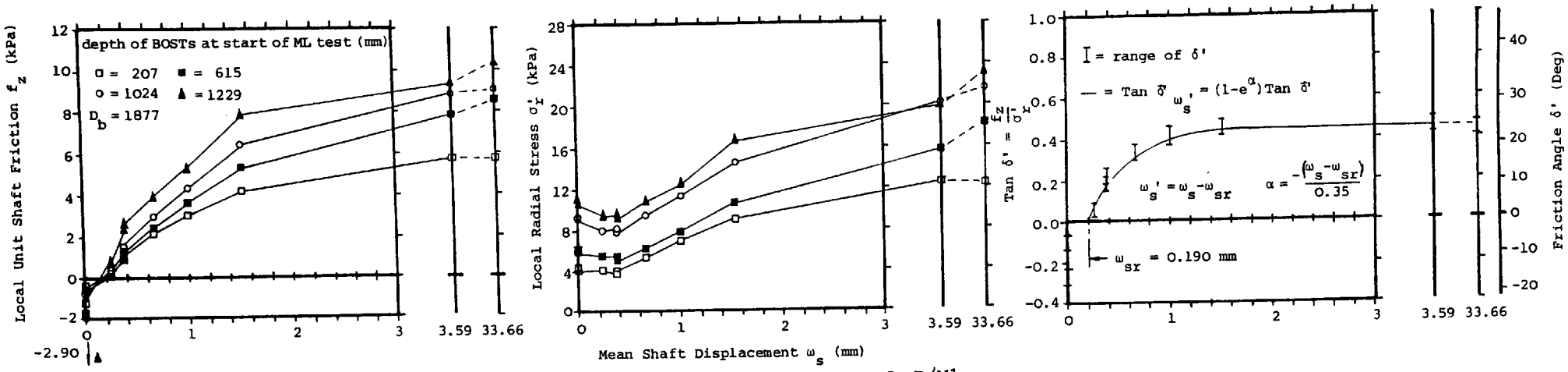

(c) Within the Overlying Sand S/M1

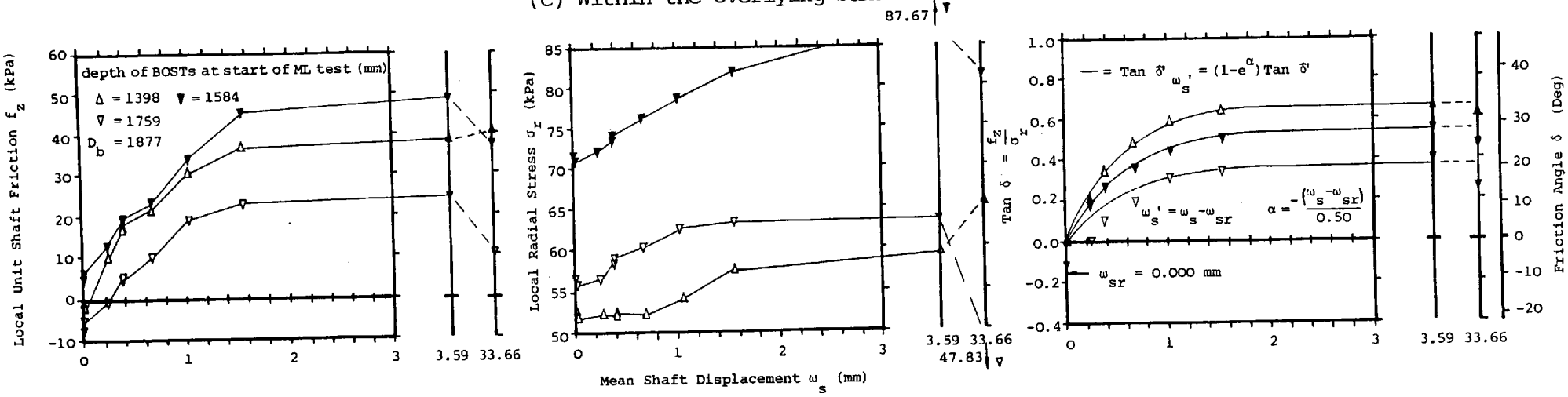

(d) Within the Underlying Clay S/M1

MOBILIZATION OF LOCAL UNIT SHAFT FRICTION, RADIAL STRESS AND FRICTION ANGLE AT VARIOUS LEVELS ALONG THE PILE SHAFT WITH MEAN SHAFT DISPLACEMENT DURING THE MAINTAINED LOAD TEST

FIGURE 7.20(c) and (d)

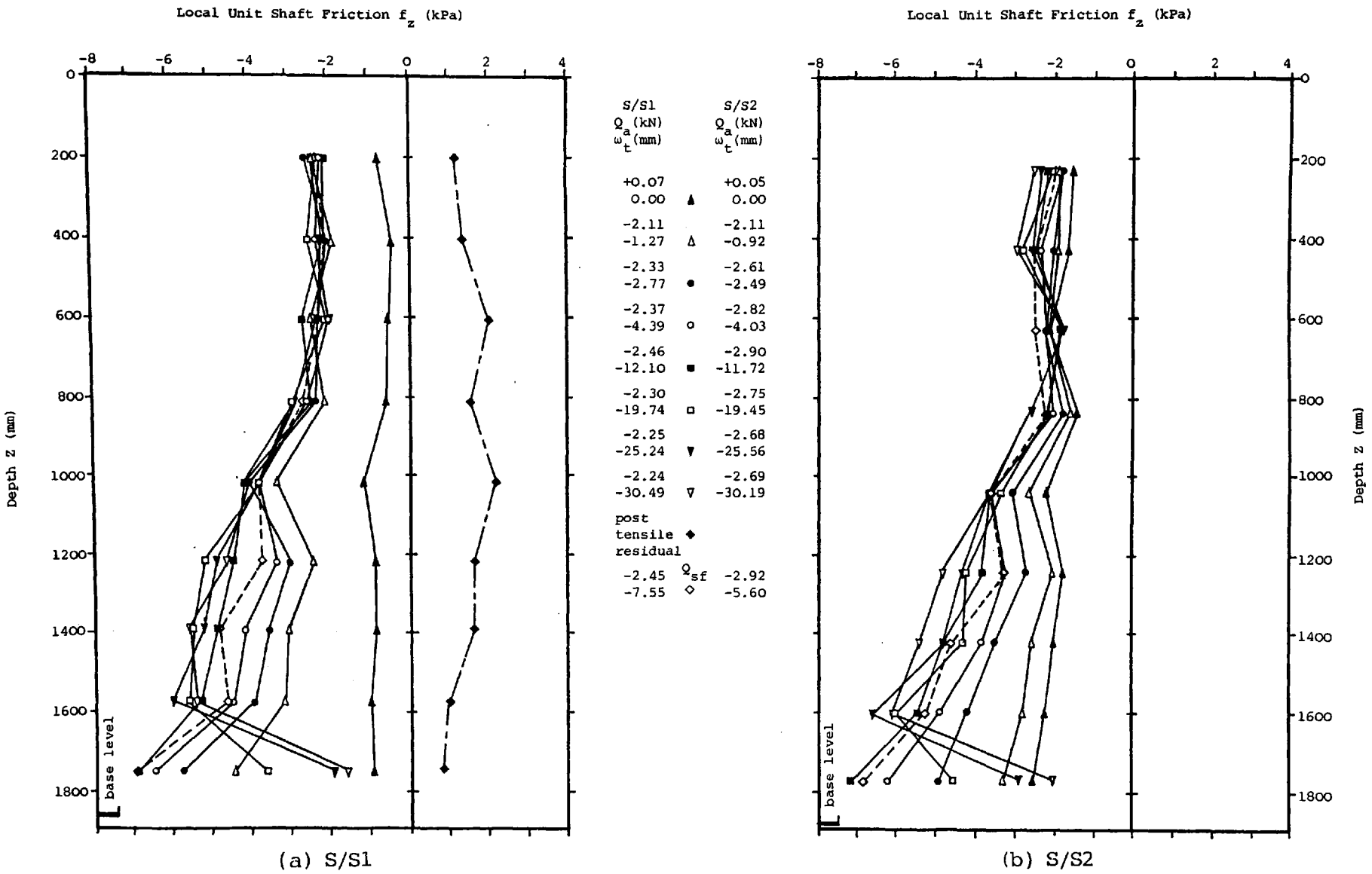

(a) S/S1

(b) S/S2

DEVELOPMENT OF LOCAL UNIT SHAFT FRICTION DURING THE CONSTANT RATE OF UPLIFT TEST

FIGURE 7.21

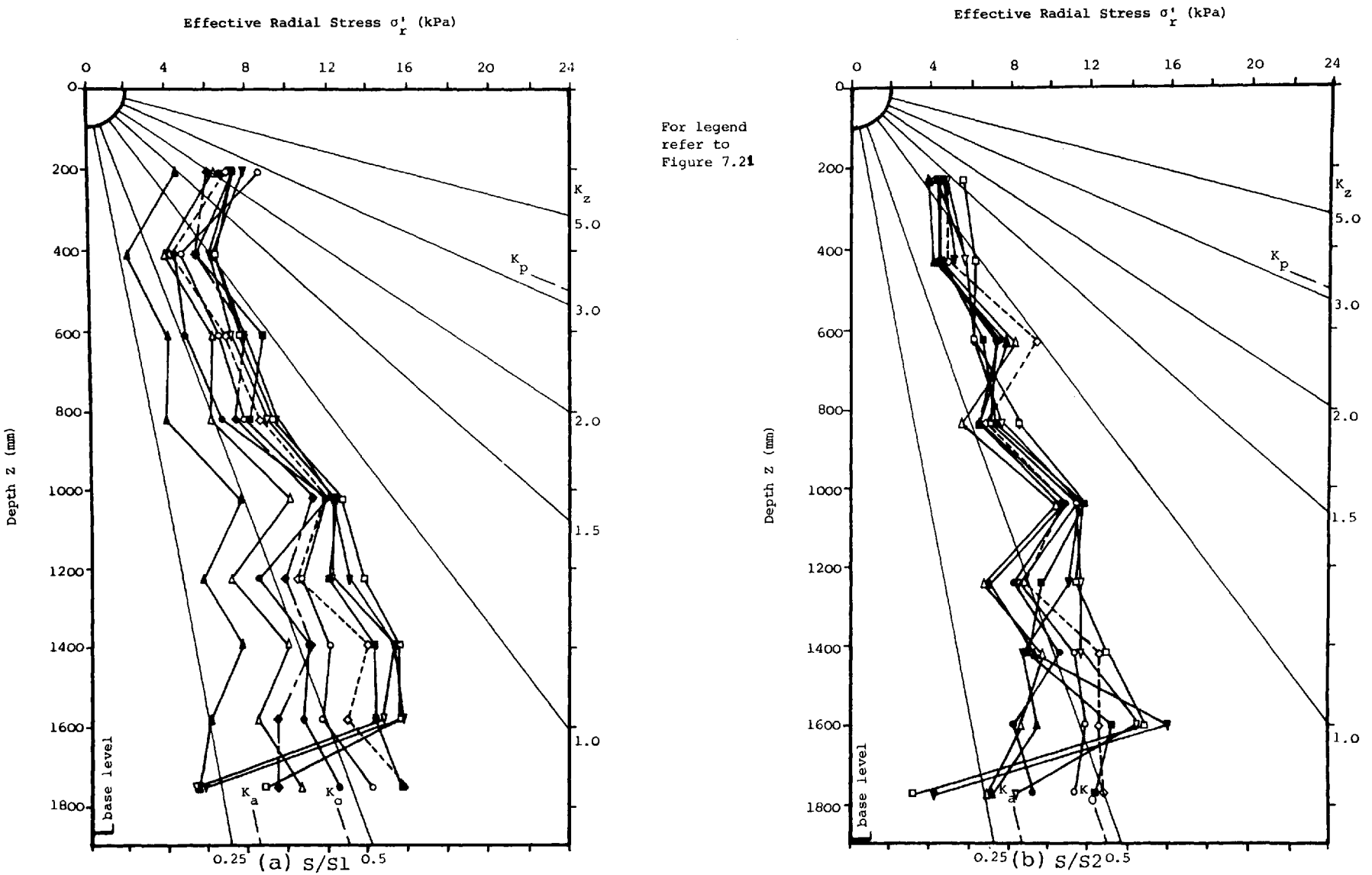

DEVELOPMENT OF EFFECTIVE RADIAL STRESS ACTING ON THE PILE SHAFT DURING THE CONSTANT RATE OF UPLIFT TEST

FIGURE 7.22

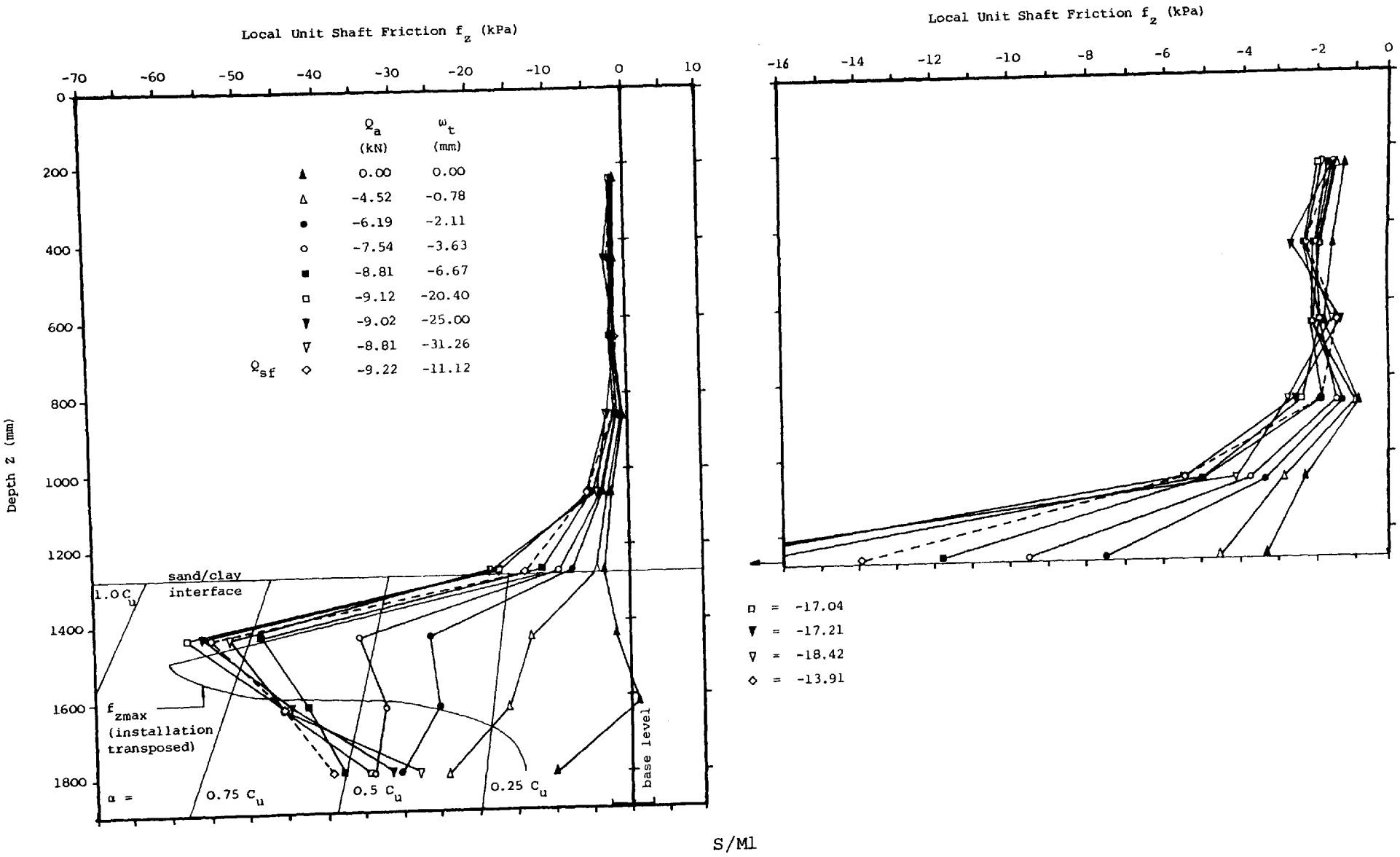

S/M1

DEVELOPMENT OF LOCAL UNIT SHAFT FRICTION DURING THE CONSTANT RATE OF UPLIFT TEST

FIGURE 7.23

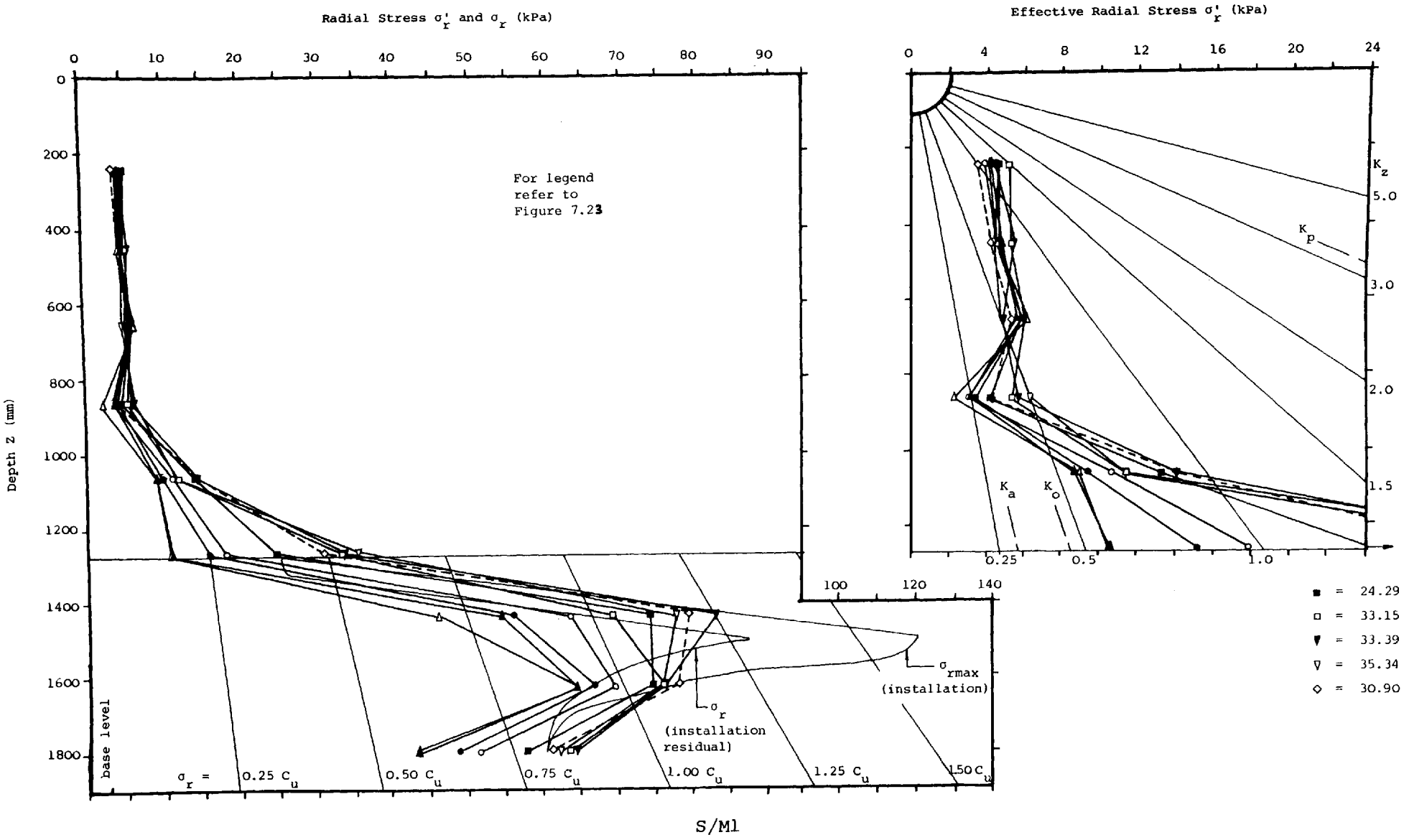

DEVELOPMENT OF RADIAL STRESS ACTING ON THE PILE SHAFT DURING THE CONSTANT RATE OF UPLIFT TEST

FIGURE 7.24

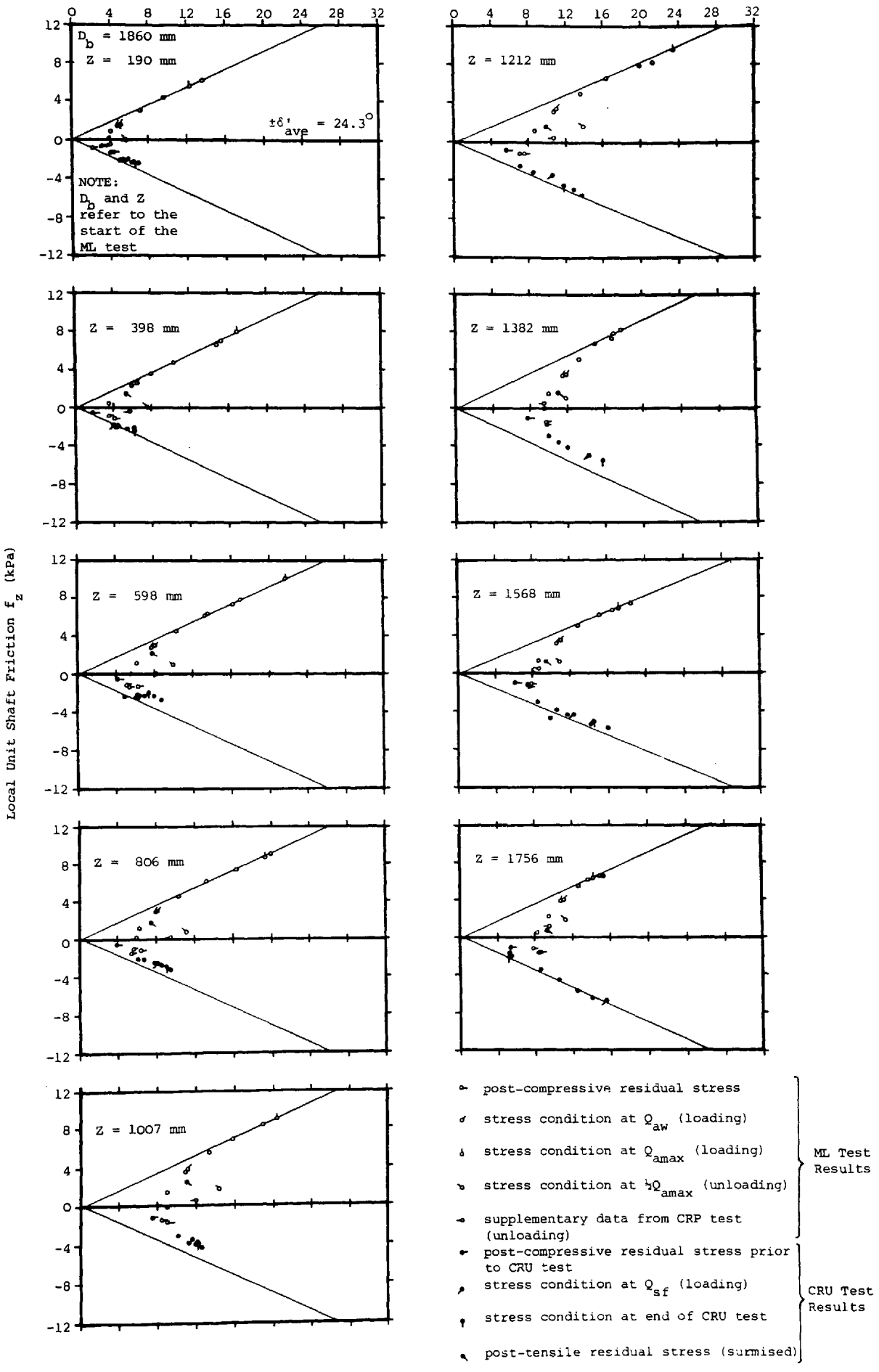

S/S1

DEVELOPMENT AND INTERDEPENDENCE OF THE LOCAL UNIT SHAFT FRICTION WITH THE LOCAL RADIAL STRESS AT VARIOUS LEVELS ALONG THE PILE SHAFT DURING THE MAINTAINED LOAD AND CONSTANT RATE OF UPLIFT TESTS

FIGURE 7.25(a)

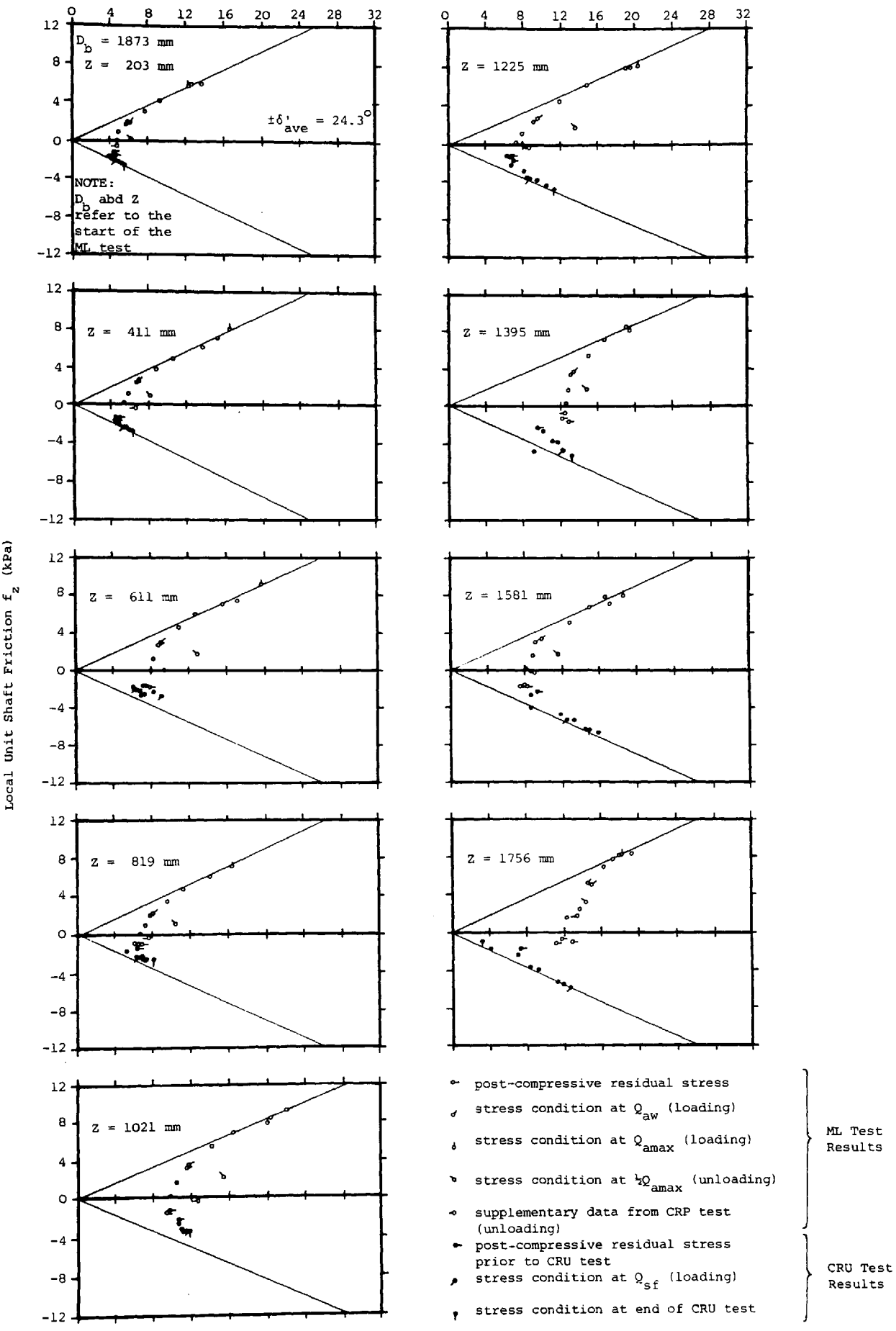

S/S2

DEVELOPMENT AND INTERDEPENDENCE OF THE LOCAL UNIT SHAFT FRICTION WITH THE LOCAL RADIAL STRESS AT VARIOUS LEVELS ALONG THE PILE SHAFT DURING THE MAINTAINED LOAD AND CONSTANT RATE OF UPLIFT TESTS

FIGURE 7.25(b)

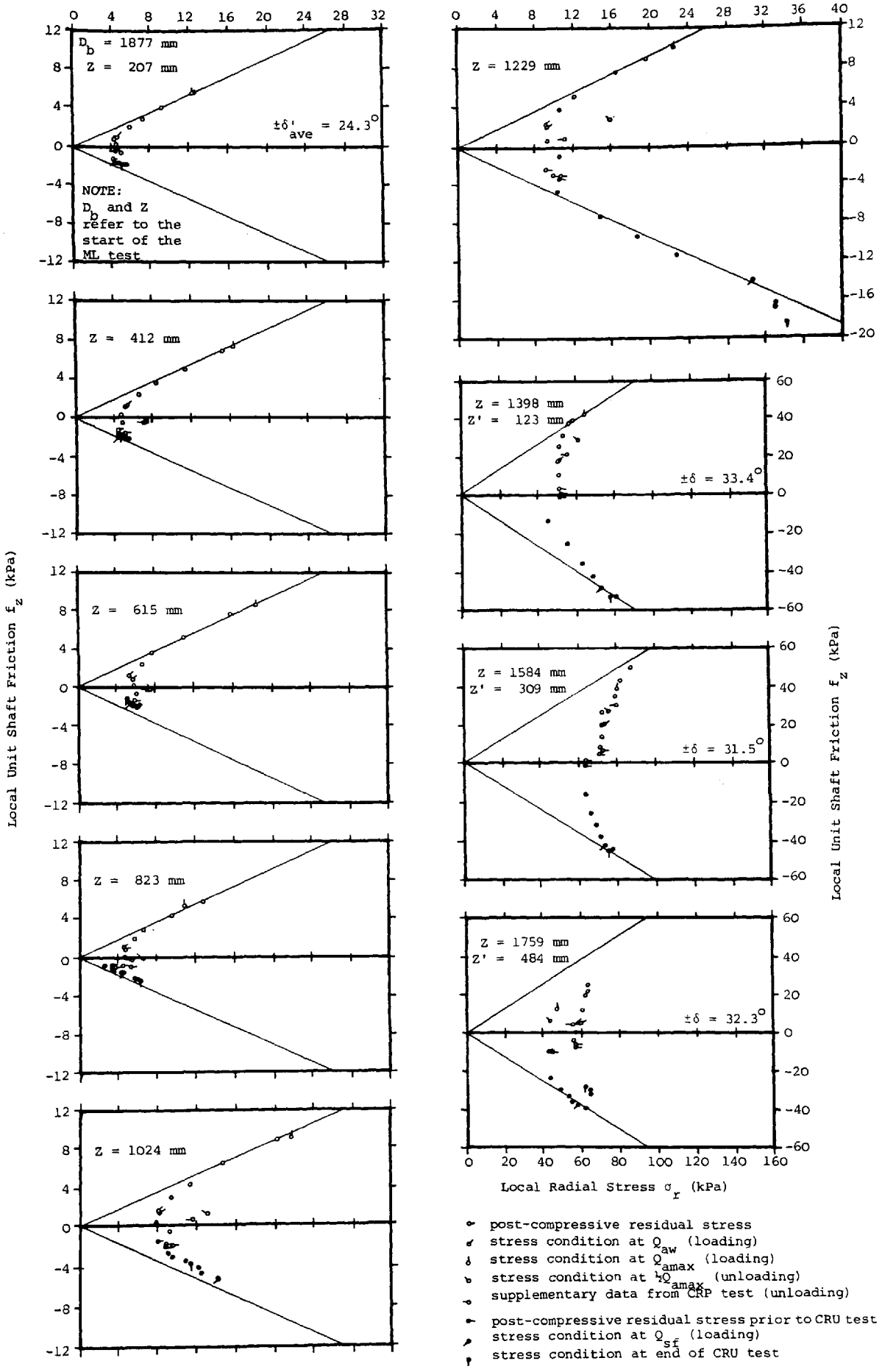

S/M1

DEVELOPMENT AND INTERDEPENDENCE OF THE LOCAL UNIT SHAFT FRICTION WITH THE LOCAL RADIAL STRESS AT VARIOUS LEVELS ALONG THE PILE SHAFT DURING THE MAINTAINED LOAD AND CONSTANT RATE OF UPLIFT TESTS

FIGURE 7.25(c)

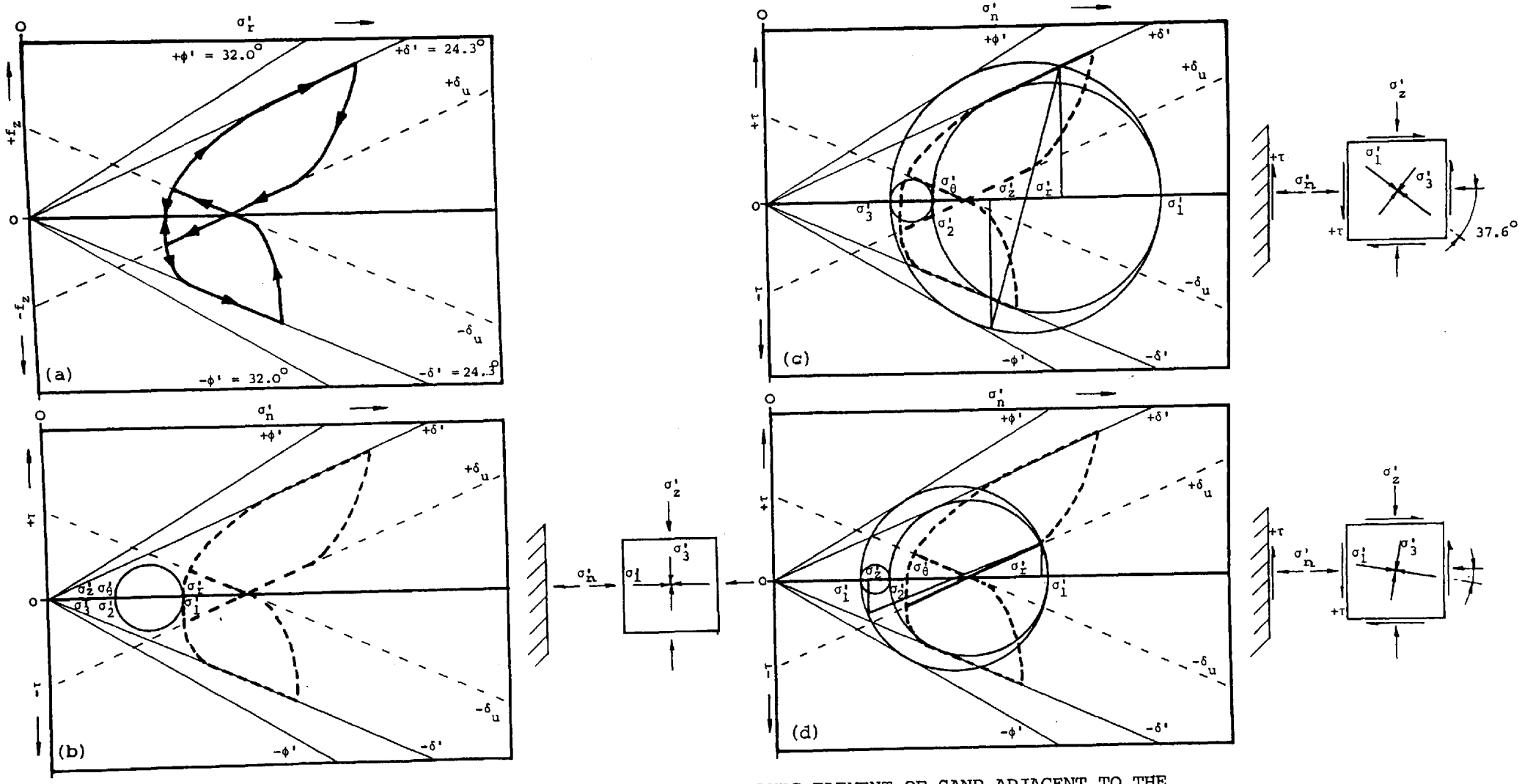

IDEALIZED EFFECTIVE STRESS HISTORY ACTING ON A PRISMATIC ELEMENT OF SAND ADJACENT TO THE PILE SHAFT DURING COMPRESSIVE AND TENSILE PILE LOADING

FIGURE 7.26(a) to (d)

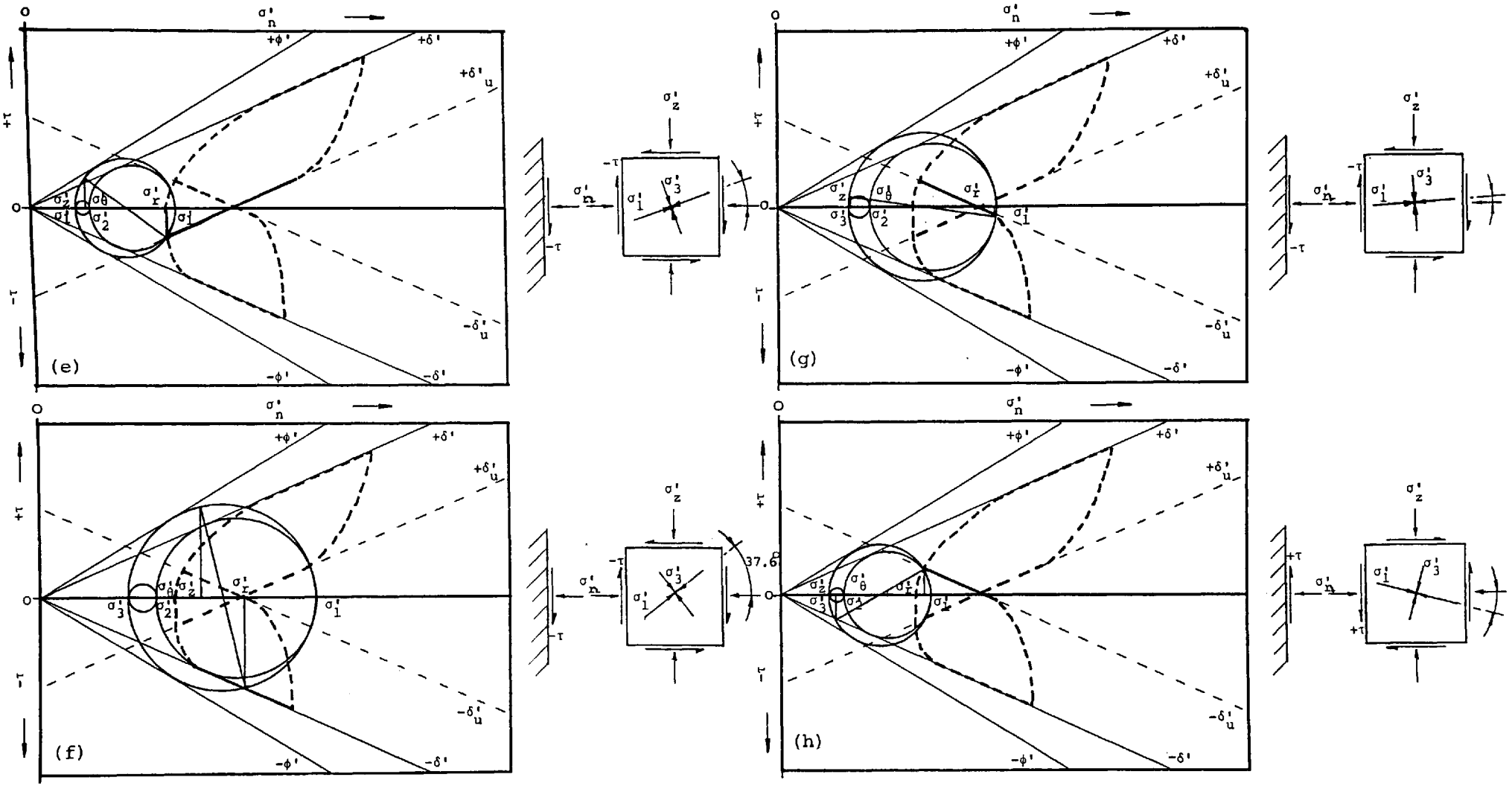

IDEALIZED EFFECTIVE STRESS HISTORY ACTING ON A PRISMATIC ELEMENT OF SAND ADJACENT TO THE PILE SHAFT DURING COMPRESSIVE AND TENSILE PILE LOADING

FIGURE 7.26(e) to (h)

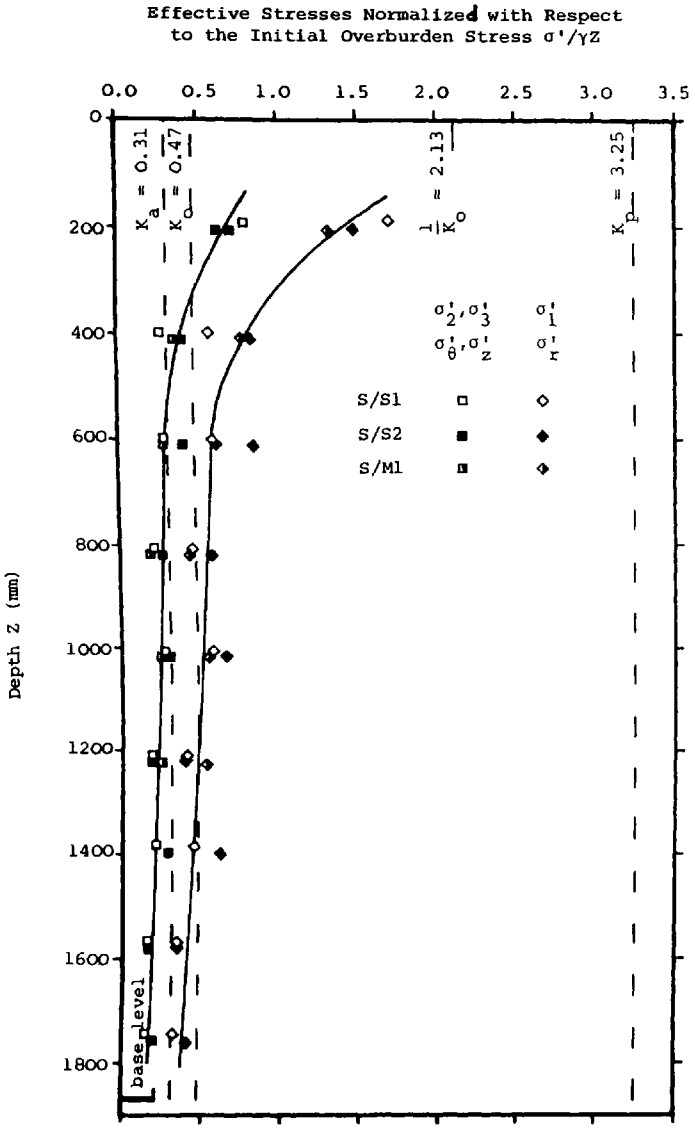

VARIATION IN THE NORMALIZED EFFECTIVE PRINCIPAL STRESSES ACTING ON A PRISMATIC ELEMENT OF SAND ADJACENT TO THE PILE SHAFT WITH DEPTH FOR ZERO LOCAL UNIT SHAFT FRICTION

FIGURE 7.27

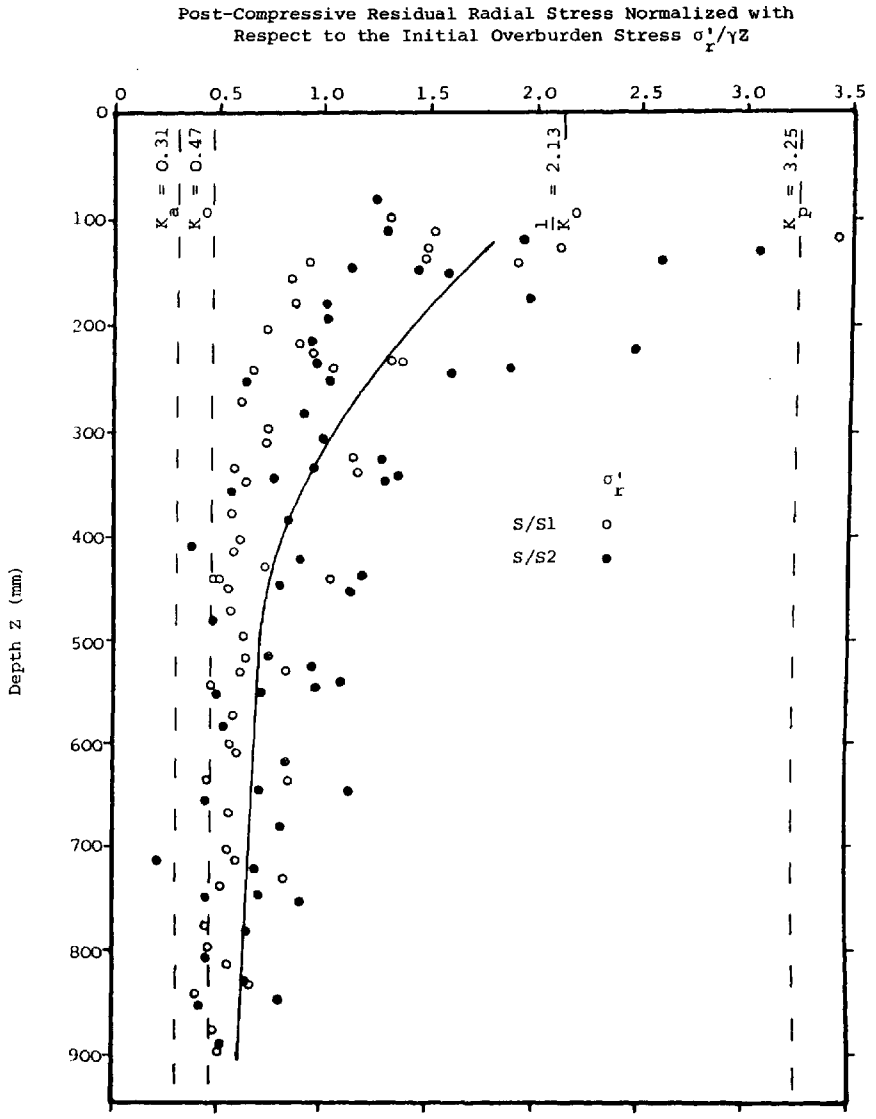

VARIATION IN THE NORMALIZED POST-COMPRESSIVE RESIDUAL EFFECTIVE RADIAL STRESS WITH DEPTH OVER THE UPPER PORTION OF THE SAND PROFILES THROUGHOUT PILE INSTALLATION

FIGURE 7.28

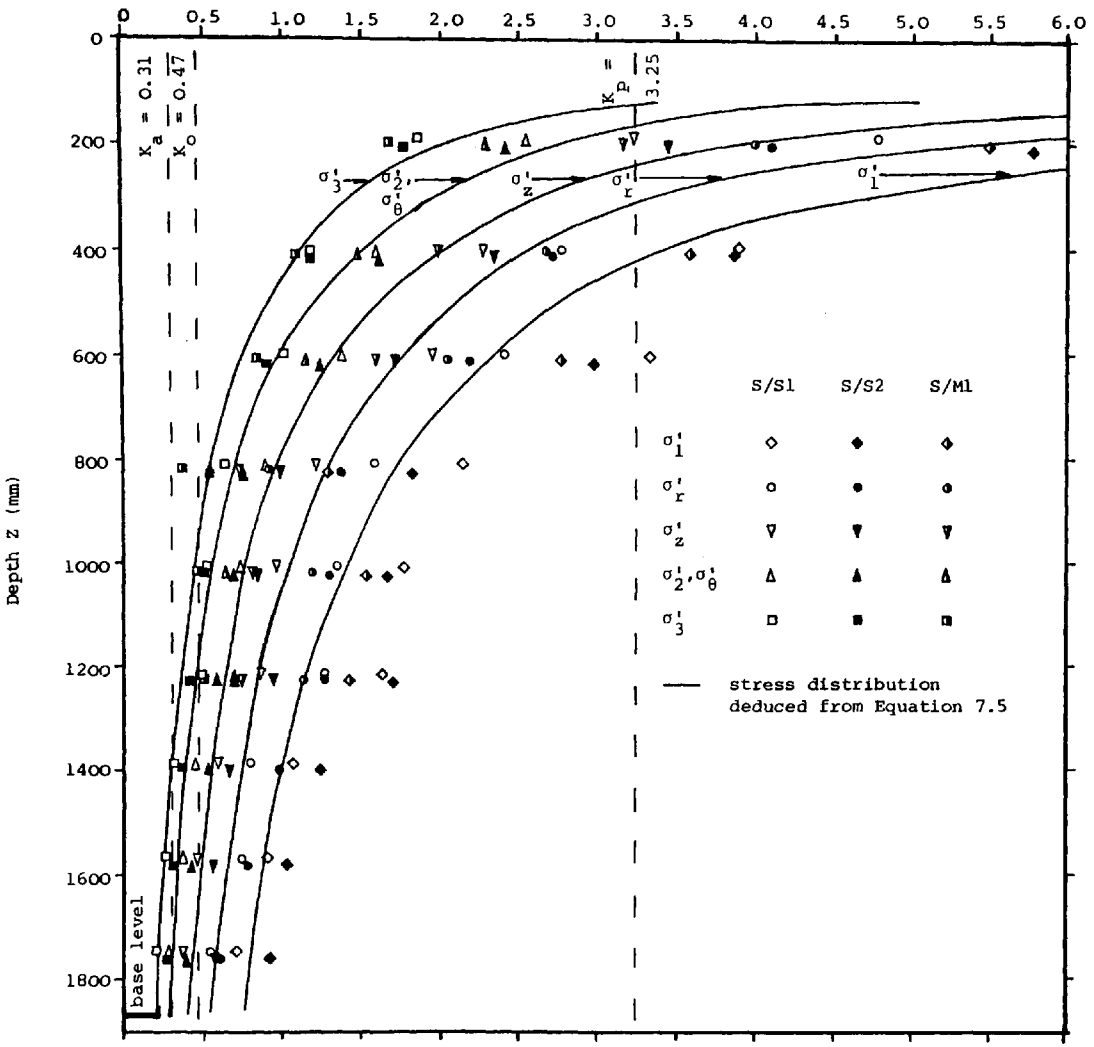

VARIATION IN THE NORMALIZED EFFECTIVE STRESSES ACTING ON A PRISMATIC ELEMENT OF SAND ADJACENT TO THE PILE SHAFT WITH DEPTH AT THE MAXIMUM APPLIED COMPRESSIVE LOAD

FIGURE 7.29

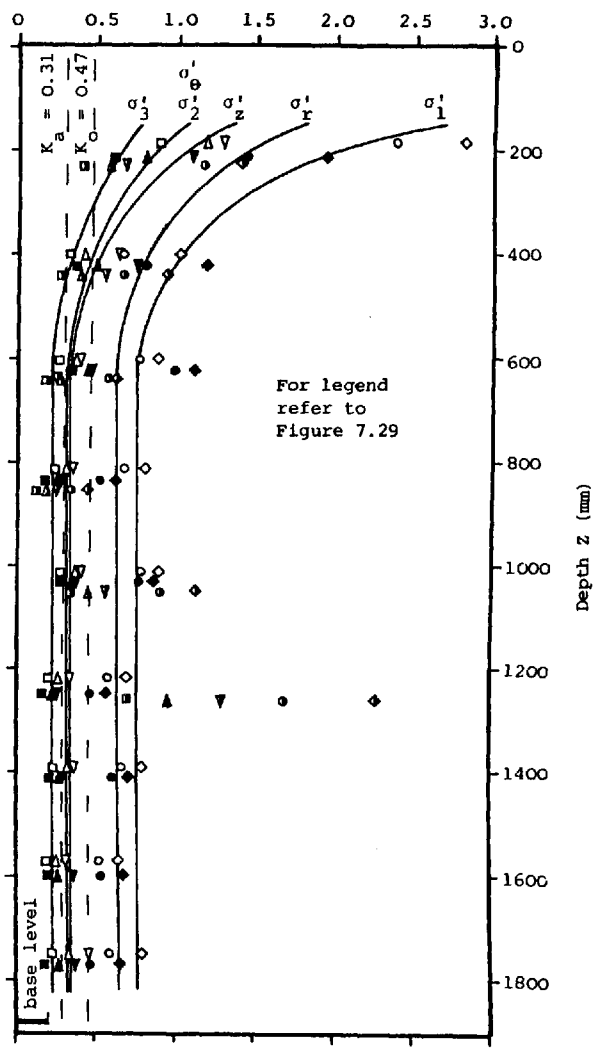

VARIATION IN THE NORMALIZED EFFECTIVE STRESSES ACTING ON A PRISMATION ELEMENT OF SAND ADJACENT TO THE PILE SHAFT WITH DEPTH AT MAXIMUM TENSILE SHAFT RESISTANCE

FIGURE 7.30

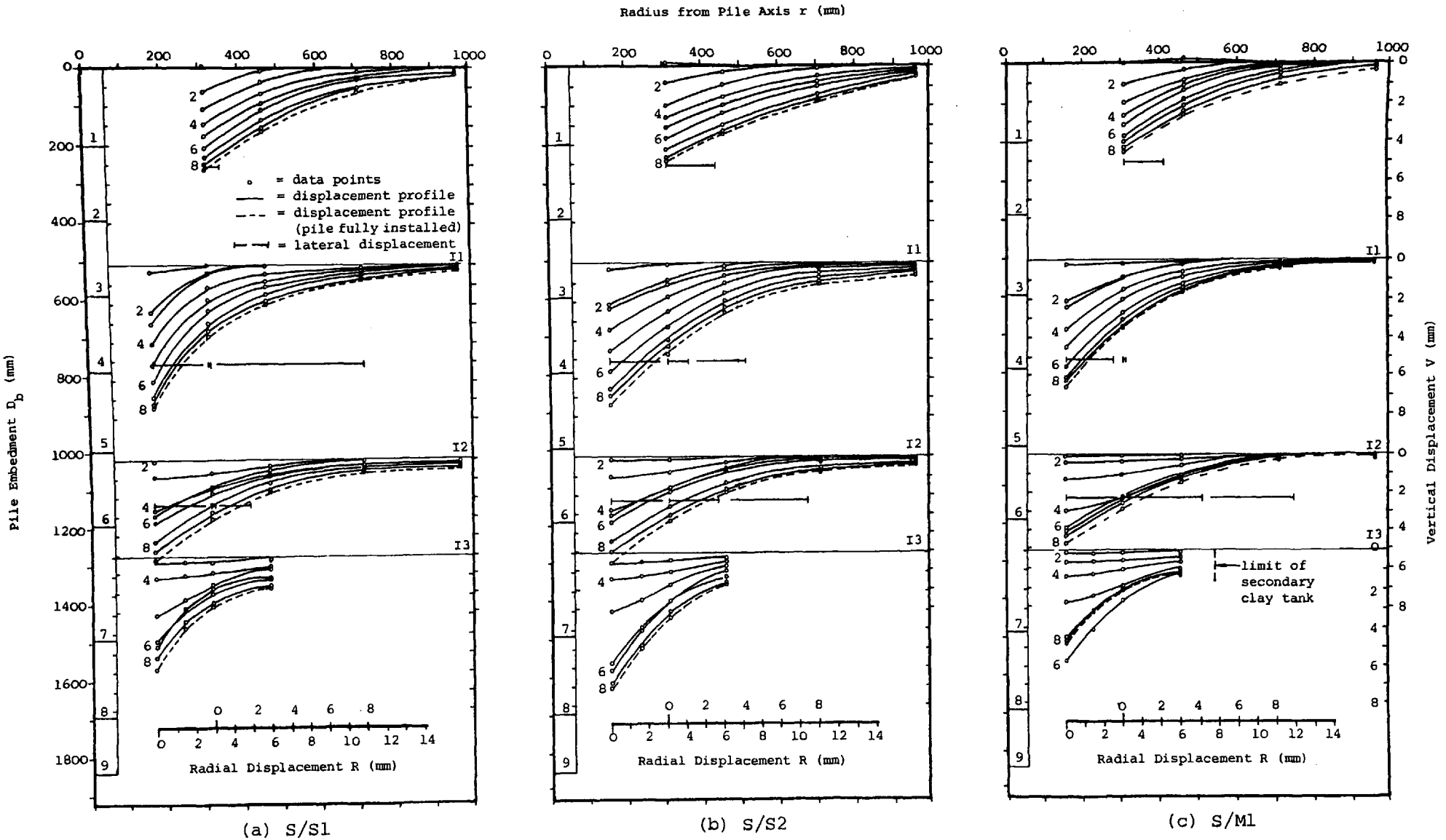

DEVELOPMENT OF VERTICAL SOIL DISPLACEMENTS DURING PILE INSTALLATION AND CALCULATED RADIAL SOIL DISPLACEMENT AT THE END OF PILE INSTALLATION

FIGURE 7.31

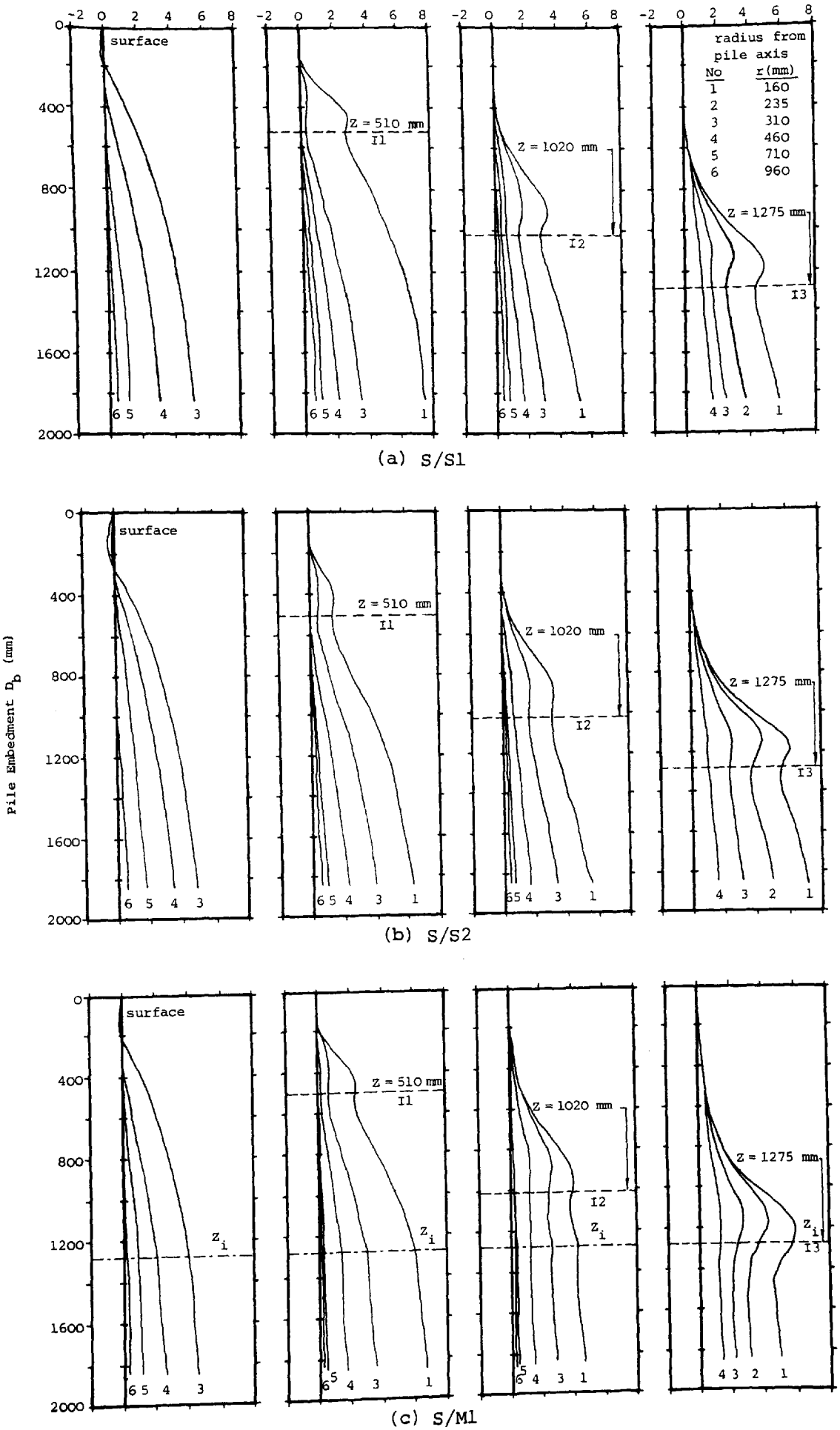

DEVELOPMENT OF VERTICAL SOIL DISPLACEMENTS DURING PILE INSTALLATION

FIGURE 7.32

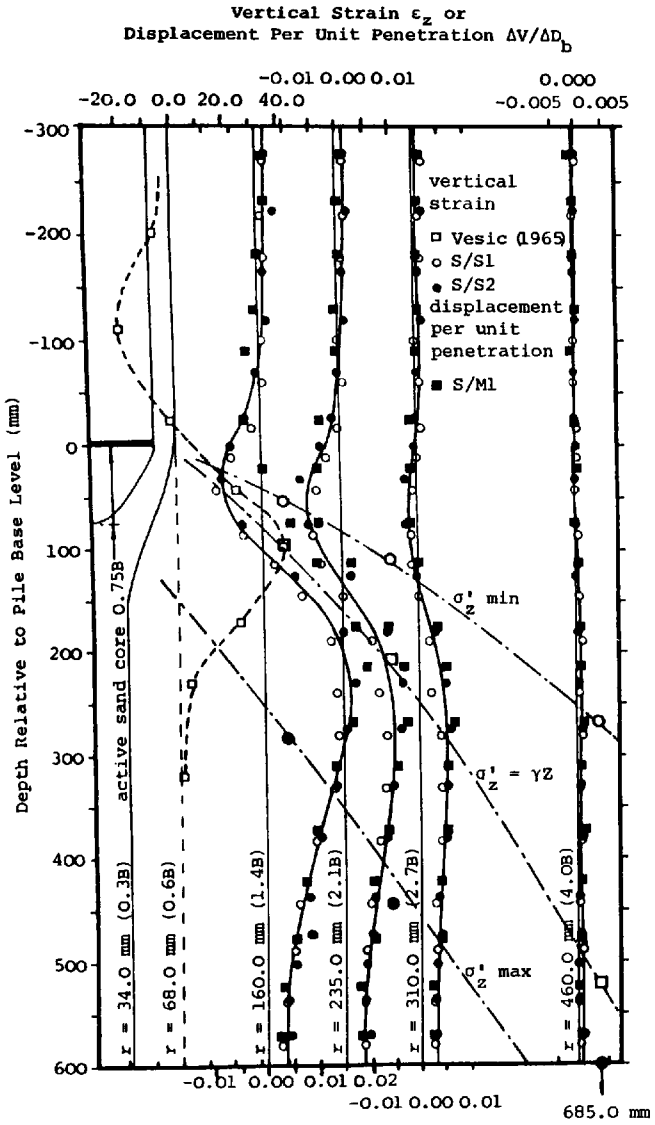

VERTICAL STRAIN, OR DISPLACEMENT PER UNIT PENETRATION, FIELD AROUND THE BASE OF A CONTINUOUSLY PENETRATING PILE

FIGURE 7.33

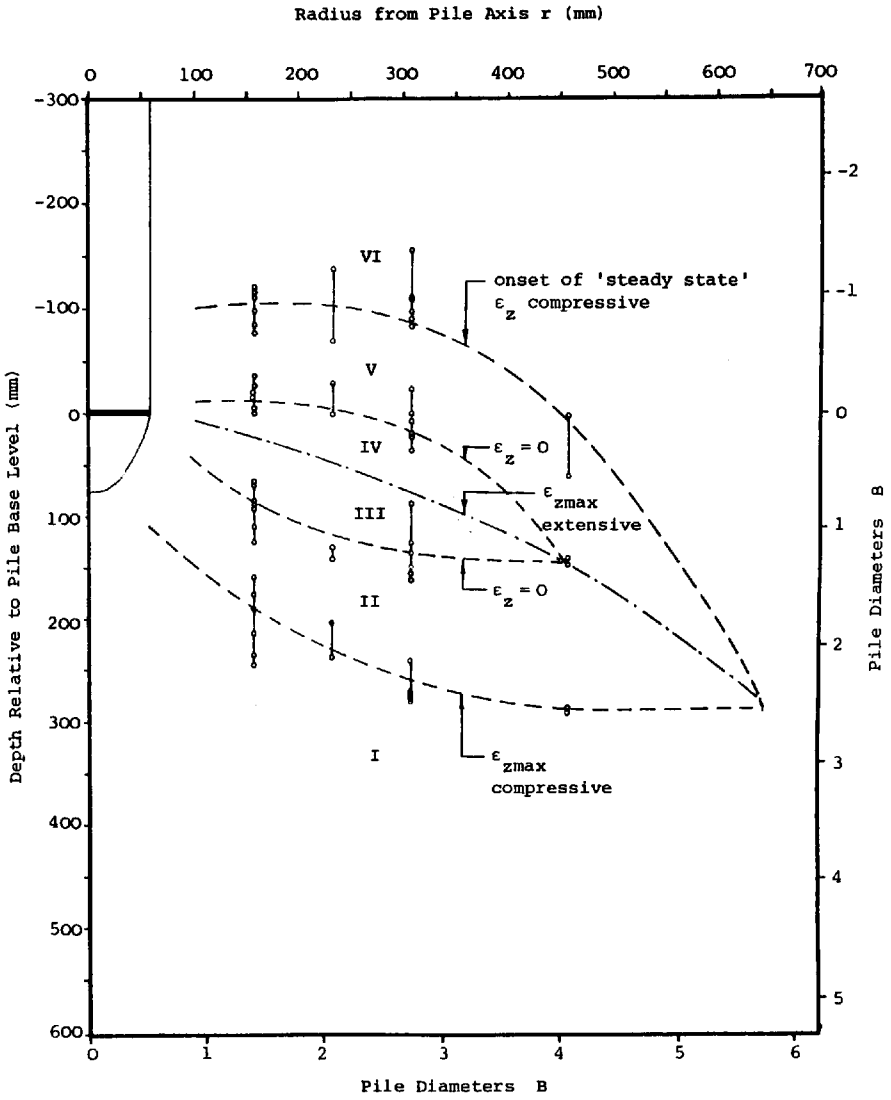

VERTICAL DISPLACEMENT ZONES AROUND THE BASE OF A CONTINUOUSLY PENETRATING PILE IN LOOSE SAND

FIGURE 7.34

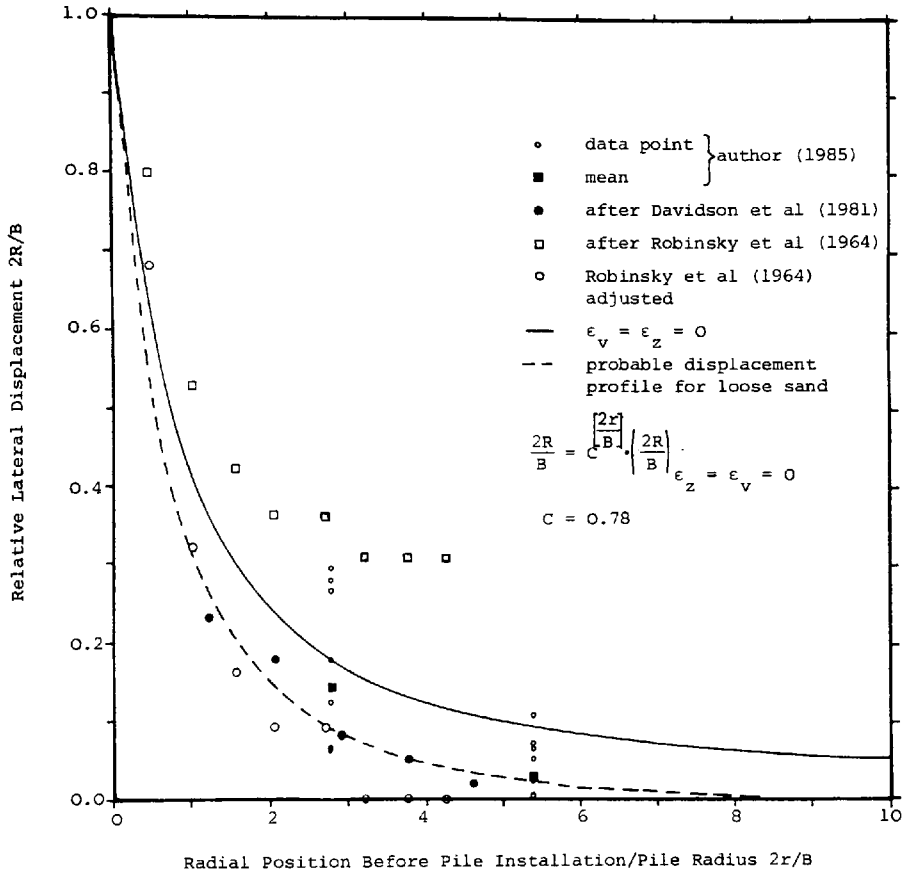

NORMALIZED RADIAL DISPLACEMENTS IN LOOSE SAND DUE TO PILE INSTALLATION

FIGURE 7.35

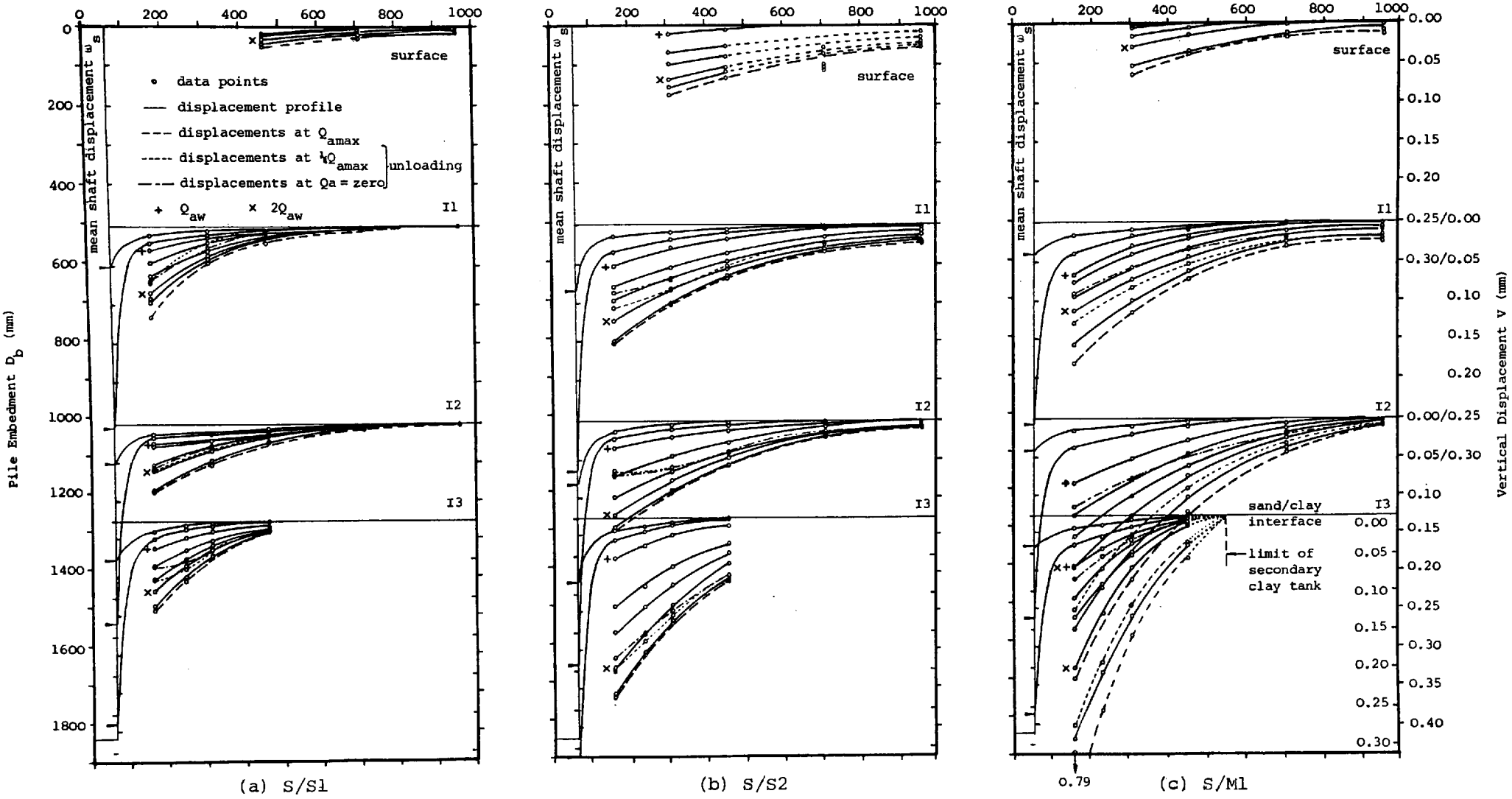

DEVELOPMENT OF VERTICAL SOIL DISPLACEMENTS DURING THE MAINTAINED LOAD TESTS

FIGURE 7.36

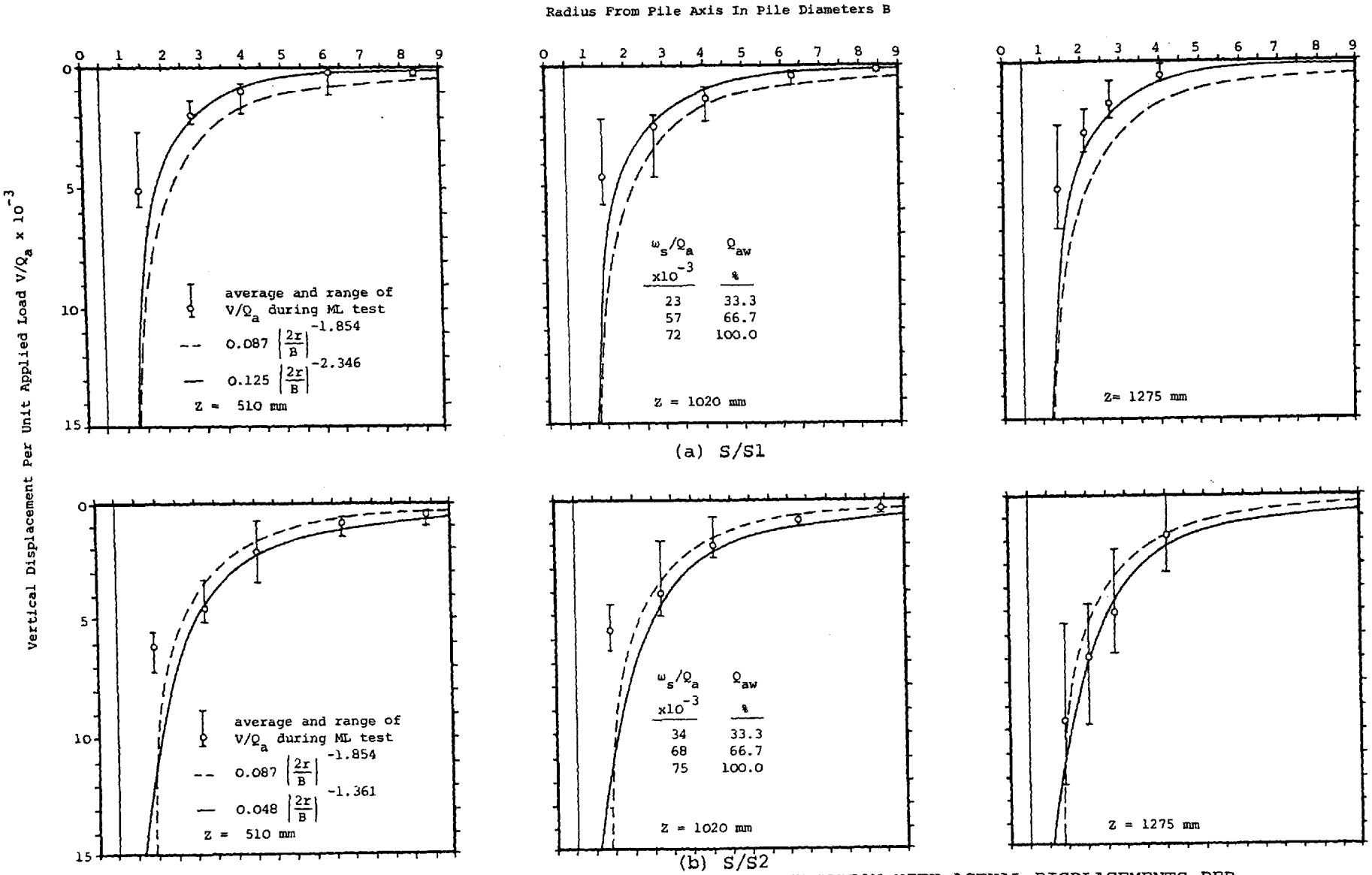

COMPARISON OF NORMALIZED SOIL VERTICAL DISPLACEMENT FUNCTION WITH ACTUAL DISPLACEMENTS PER UNIT OF APPLIED LOAD

FIGURE 7.37

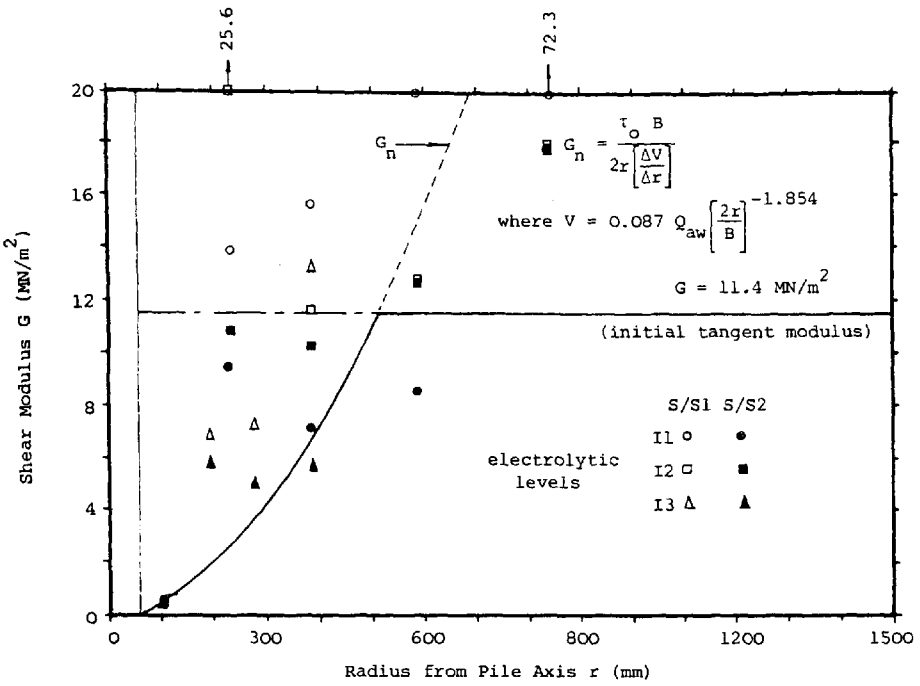

(a) Variation in Soil Shear Modulus with Radius from the Pile Axis at Working Load

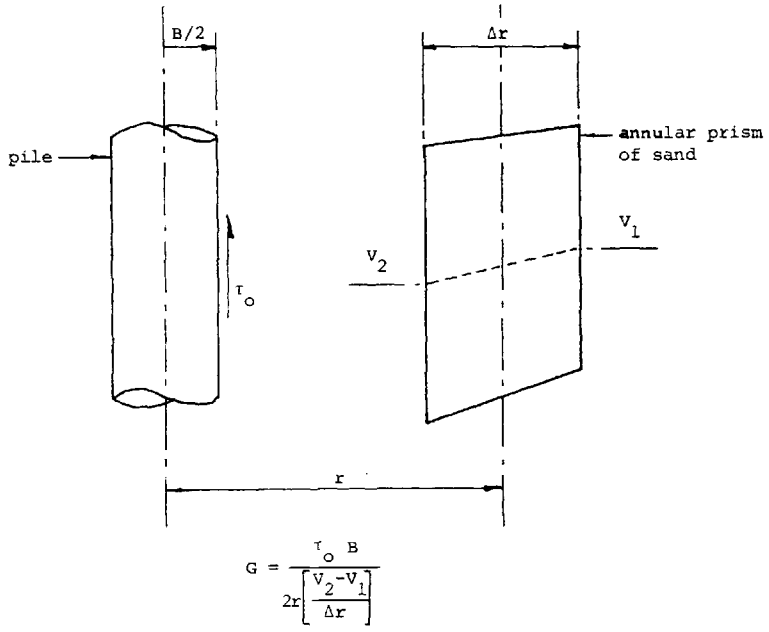

(b) Method of Evaluating Soil Shear Modulus from Displacements

VARIATION IN SOIL SHEAR MODULUS WITH RADIUS FROM THE PILE AXIS AT WORKING LOAD AND THE METHOD OF EVALUATION

FIGURE 7.38

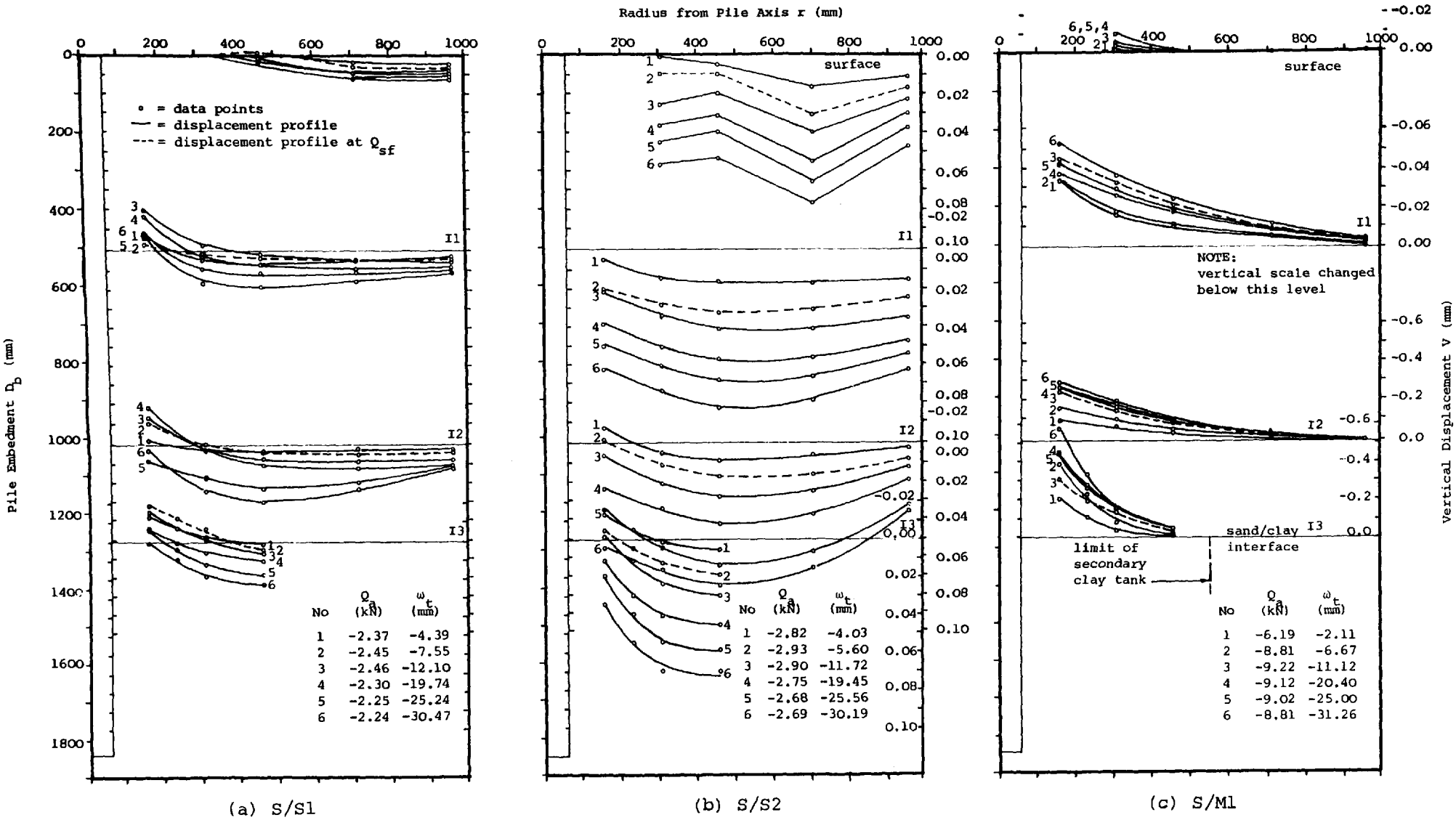

(a) S/S1 (b) S/S2 (c) S/M1

DEVELOPMENT OF VERTICAL SOIL DISPLACEMENTS DURING THE CONSTANT RATE OF UPLIFT TEST

FIGURE 7.39

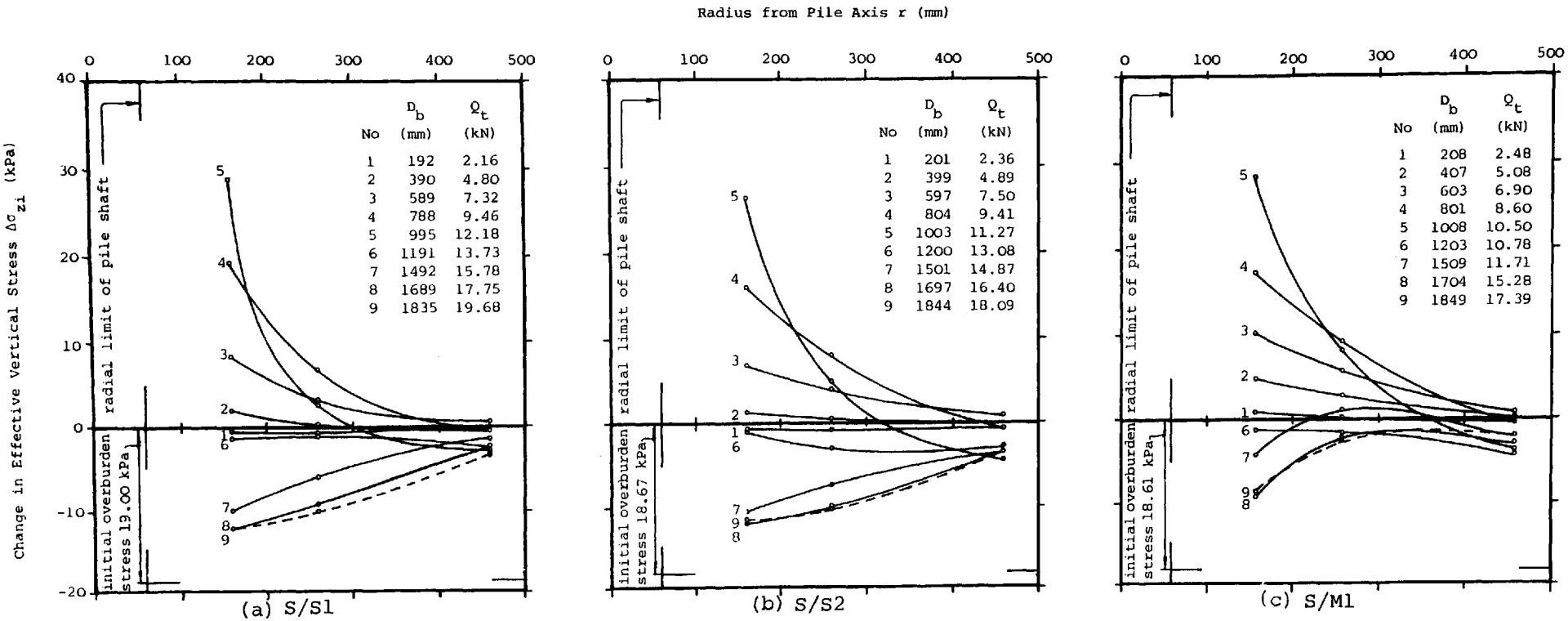

CHANGE IN, AND RADIAL DISTRIBUTION OF, THE EFFECTIVE VERTICAL STRESS ACTING ON A HORIZONTAL PLANE WITHIN THE SOIL PROFILE AT A DEPTH OF 1275.0 mm (EQUIVALENT TO THE LEVEL OF THE SAND/CLAY INTERFACE IN S/M1) DURING PILE INSTALLATION

FIGURE 7.40

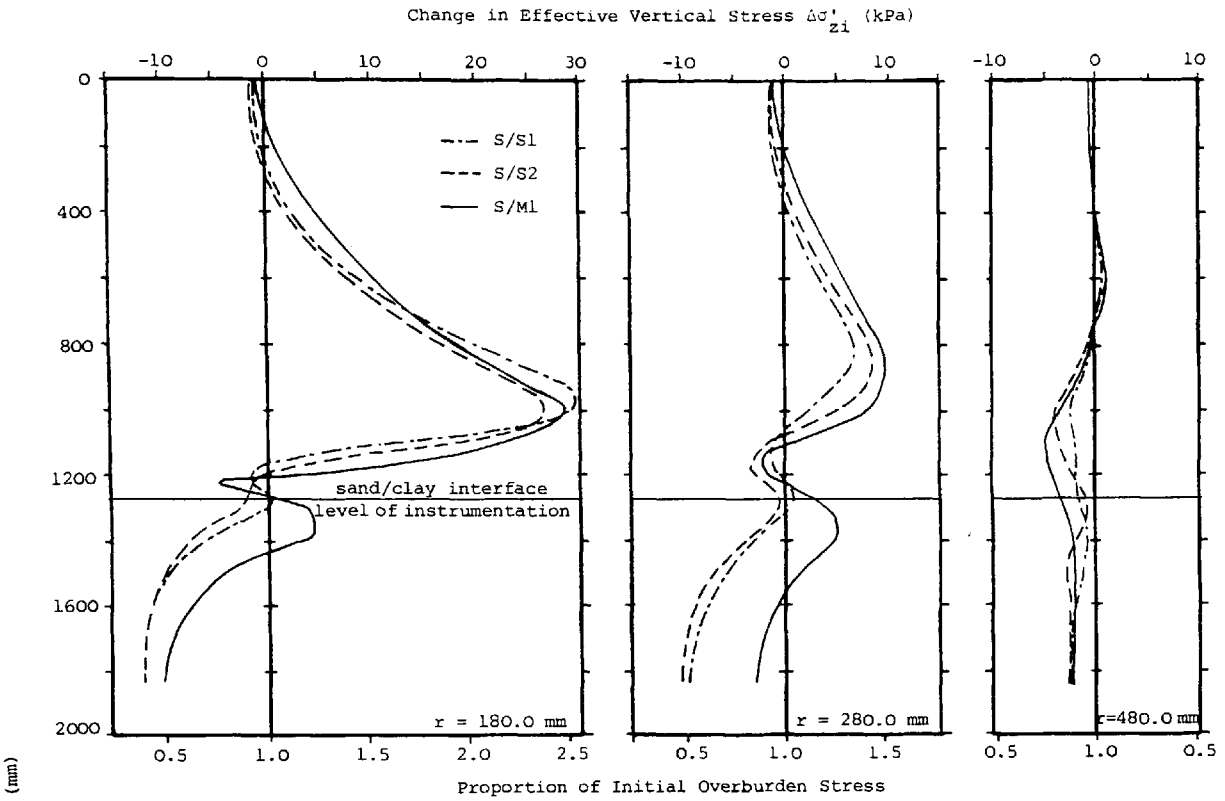

(a) Stress History During Pile Installation

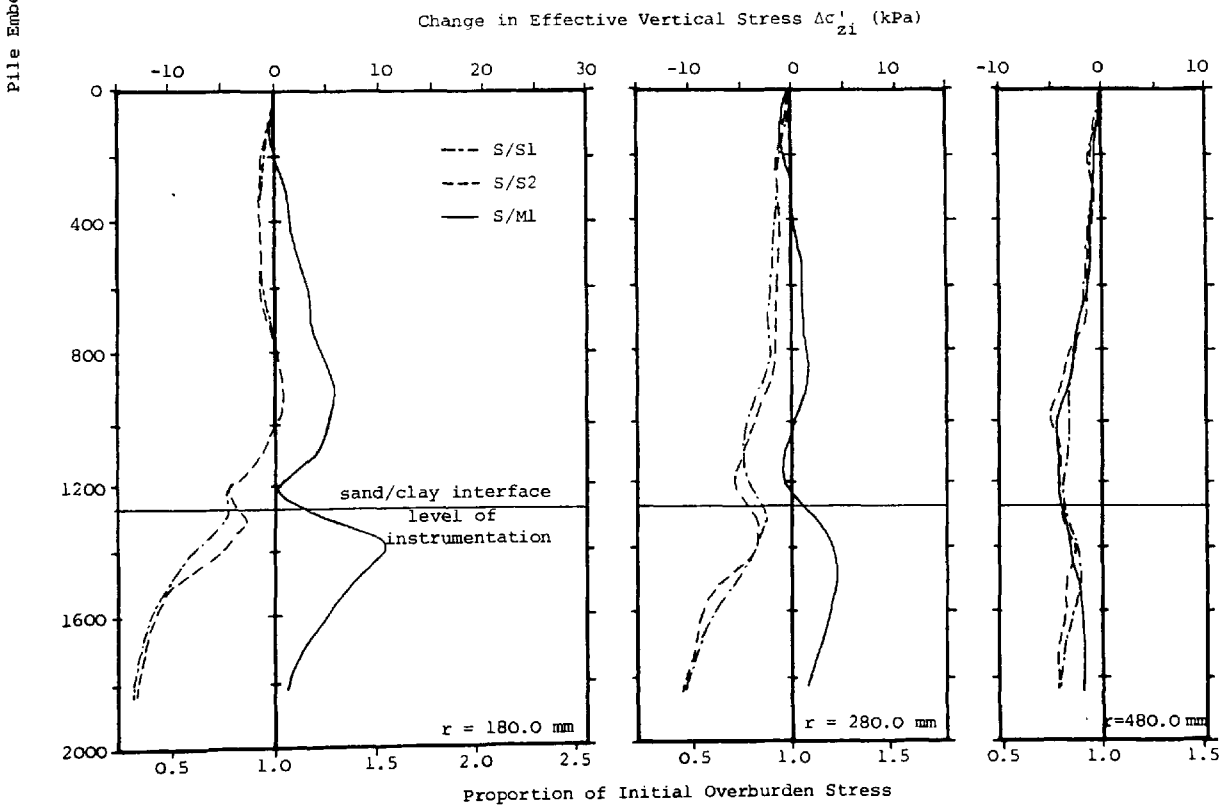

(b) Stress History Under Residual Stress Conditions During Pile Installation

THE CHANGE IN EFFECTIVE VERTICAL STRESS ACROSS A HORIZONTAL PLANE WITHIN THE SOIL PROFILE AT A DEPTH OF 1275.0 mm (EQUIVALENT TO THE LEVEL OF THE SAND/CLAY INTERFACE IN S/M1), AND THE ASSOCIATED RESIDUAL STRESS, WITH EMBEDMENT DURING PILE INSTALLATION

FIGURE 7.41

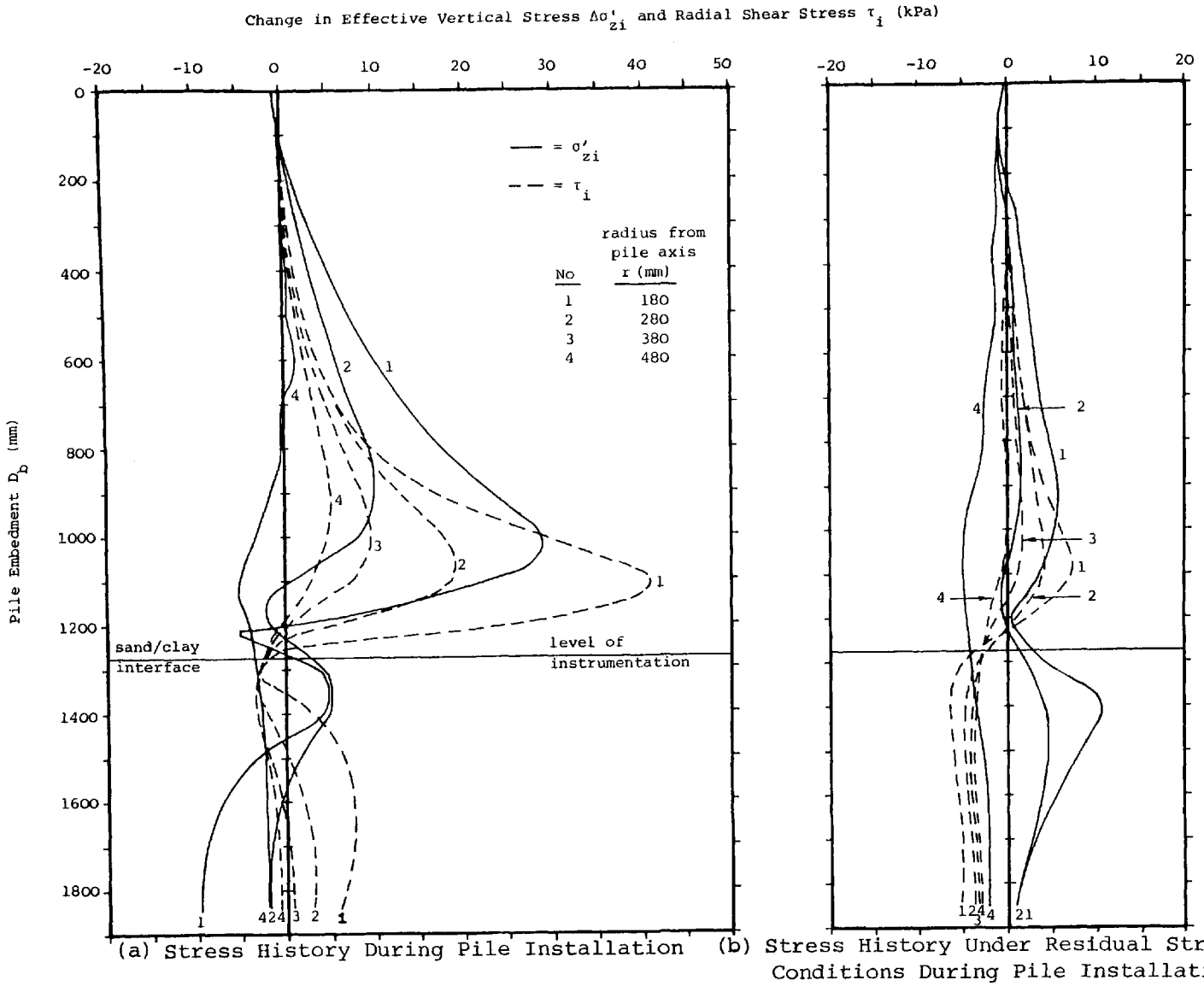

HISTORY OF THE CHANGE IN EFFECTIVE VERTICAL STRESS AND RADIAL SHEAR STRESS ACROSS THE SAND/CLAY INTERFACE, TOGETHER WITH THE ASSOCIATED RESIDUAL STRESSES, WITH EMBEDMENT DURING PILE INSTALLATION

FIGURE 7.42

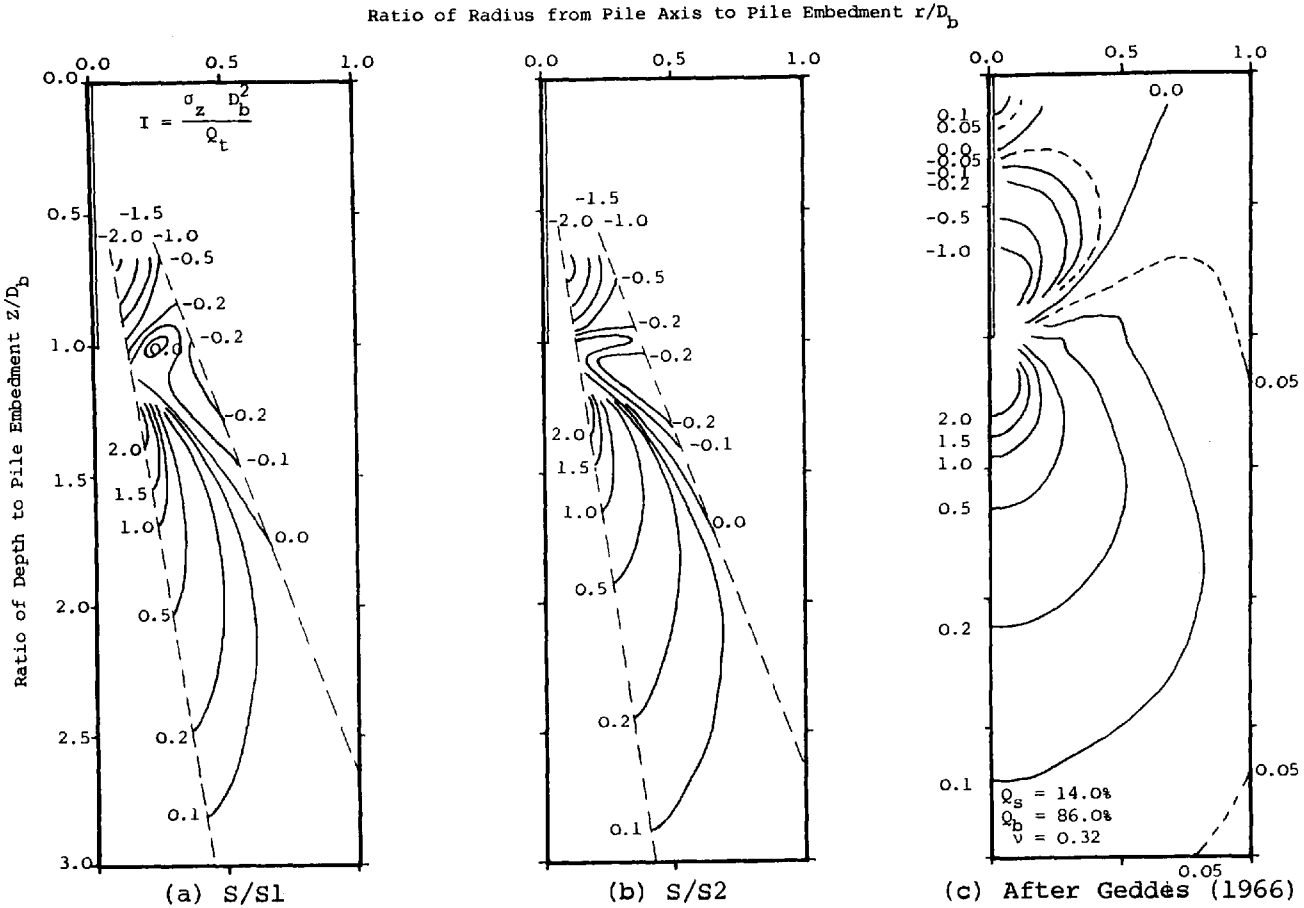

EXPERIMENTAL AND THEORETICAL DIMENSIONLESS STRESS COEFFICIENTS FOR THE CHANGE IN EFFECTIVE VERTICAL STRESS INDUCED IN LOOSE SAND BY A VERTICALLY LOADED PILE

FIGURE 7.43

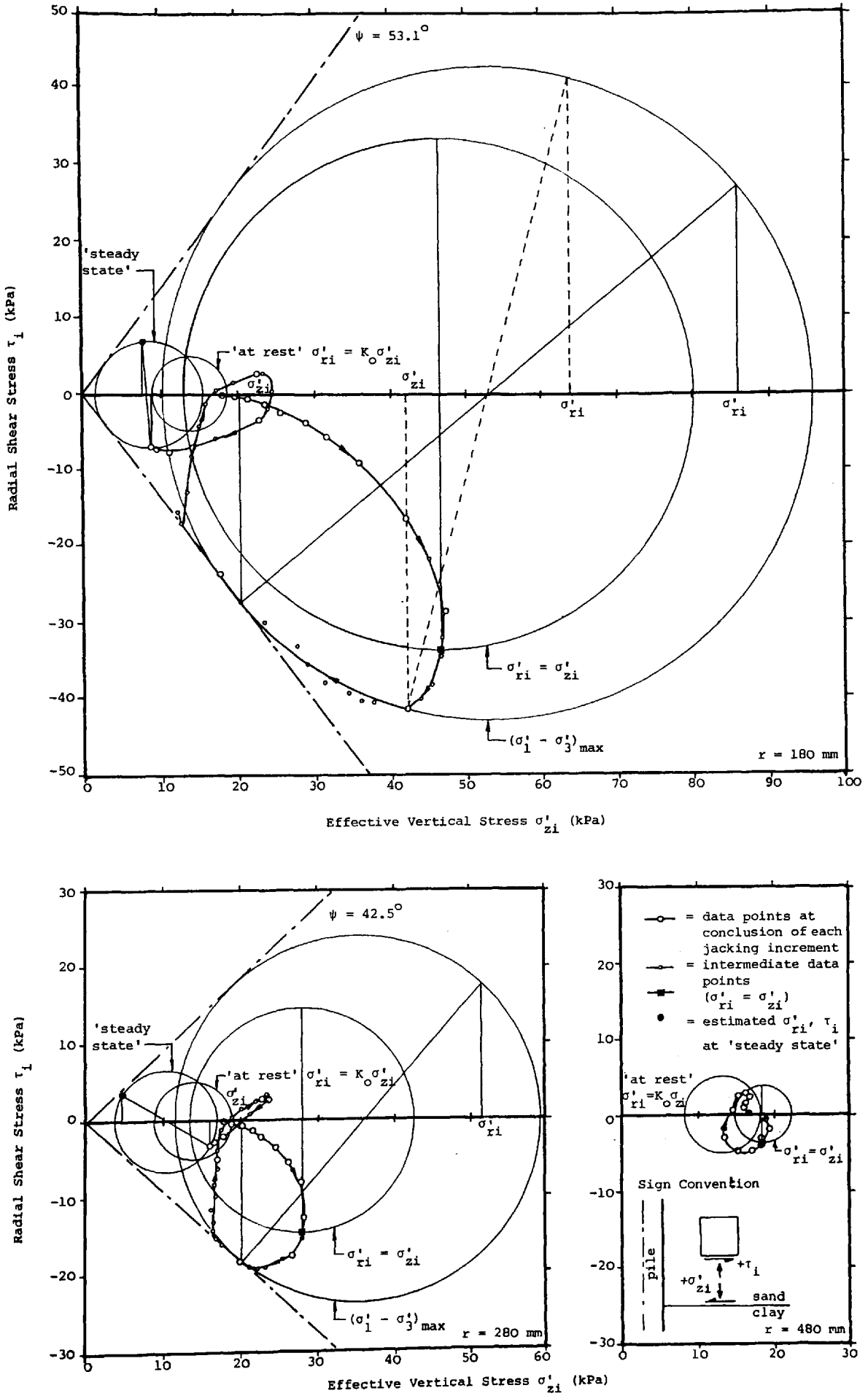

TWO DIMENSIONAL EFFECTIVE STRESS HISTORY ACTING ON AN ELEMENT OF SAND ADJACENT TO THE SAND/CLAY INTERFACE DURING PILE INSTALLATION

FIGURE 7.44

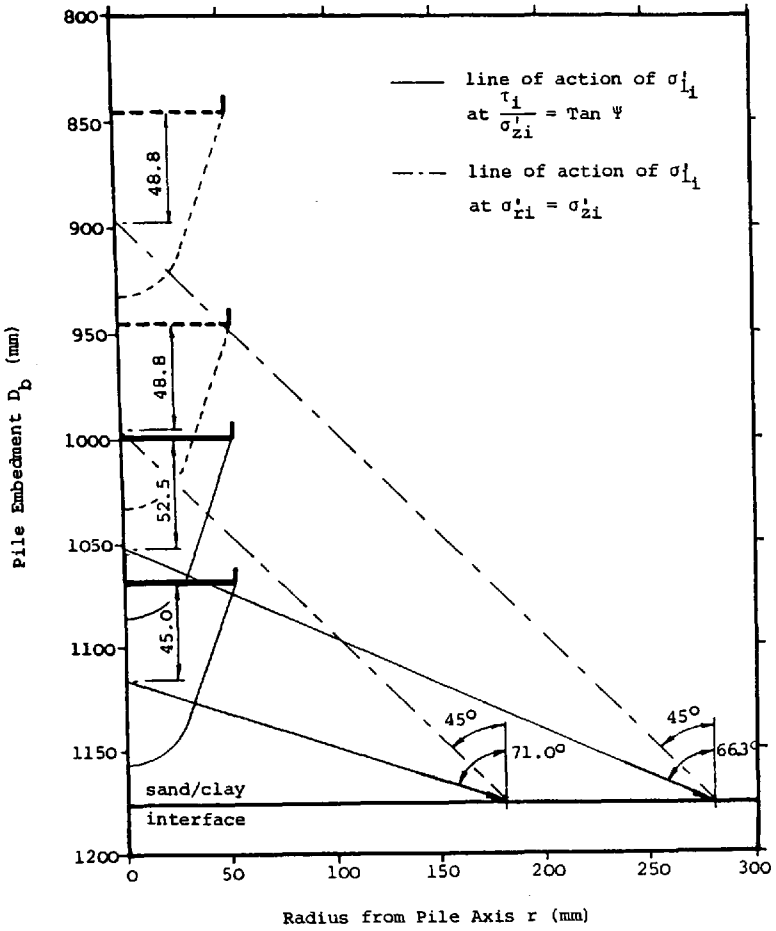

SOIL/PILE GEOMETRIES ASSOCIATED WITH THE MAXIMUM MAJOR EFFECTIVE PRINCIPAL STRESS AND THE ONSET OF SHEAR FAILURE IN THE PLANE OF THE SAND/CLAY INTERFACE AT RADII OF 180 mm AND 280 mm FROM THE PILE AXIS

FIGURE 7.45

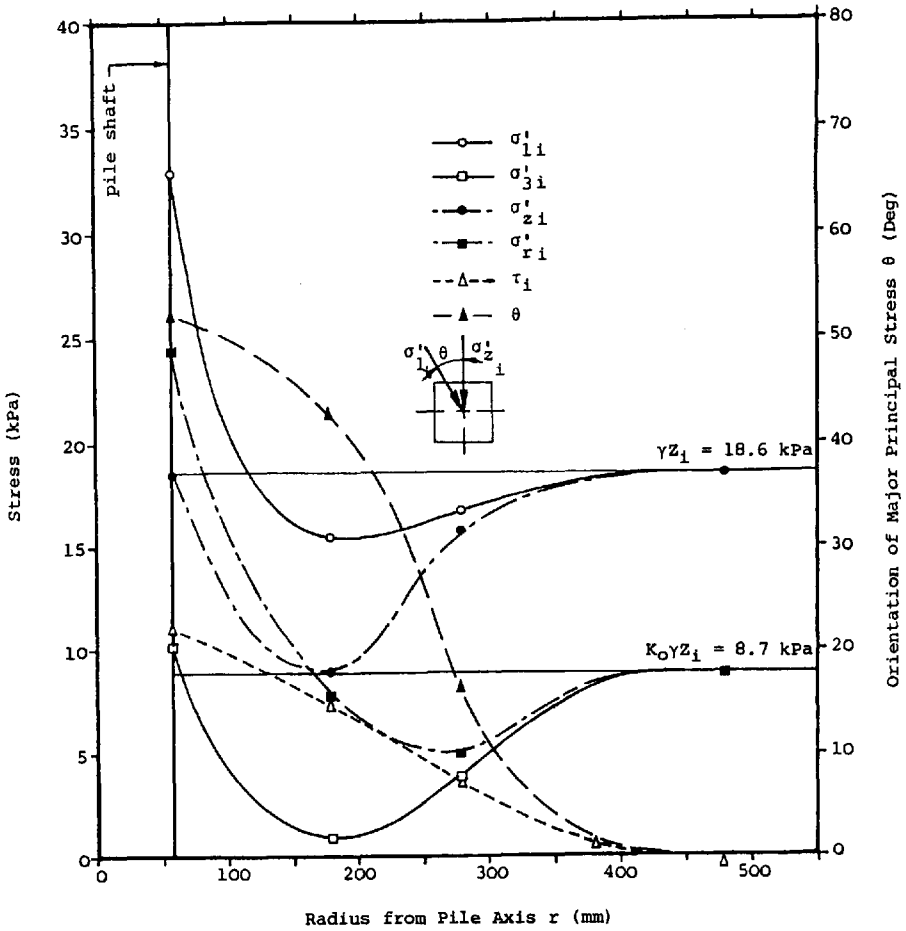

STEADY STATE EFFECTIVE STRESS PROFILE ACTING ACROSS THE SAND/CLAY INTERFACE ASSOCIATED WITH THE FULLY EMBEDDED PILE LOADED TO PLUNGING FAILURE

FIGURE 7.46

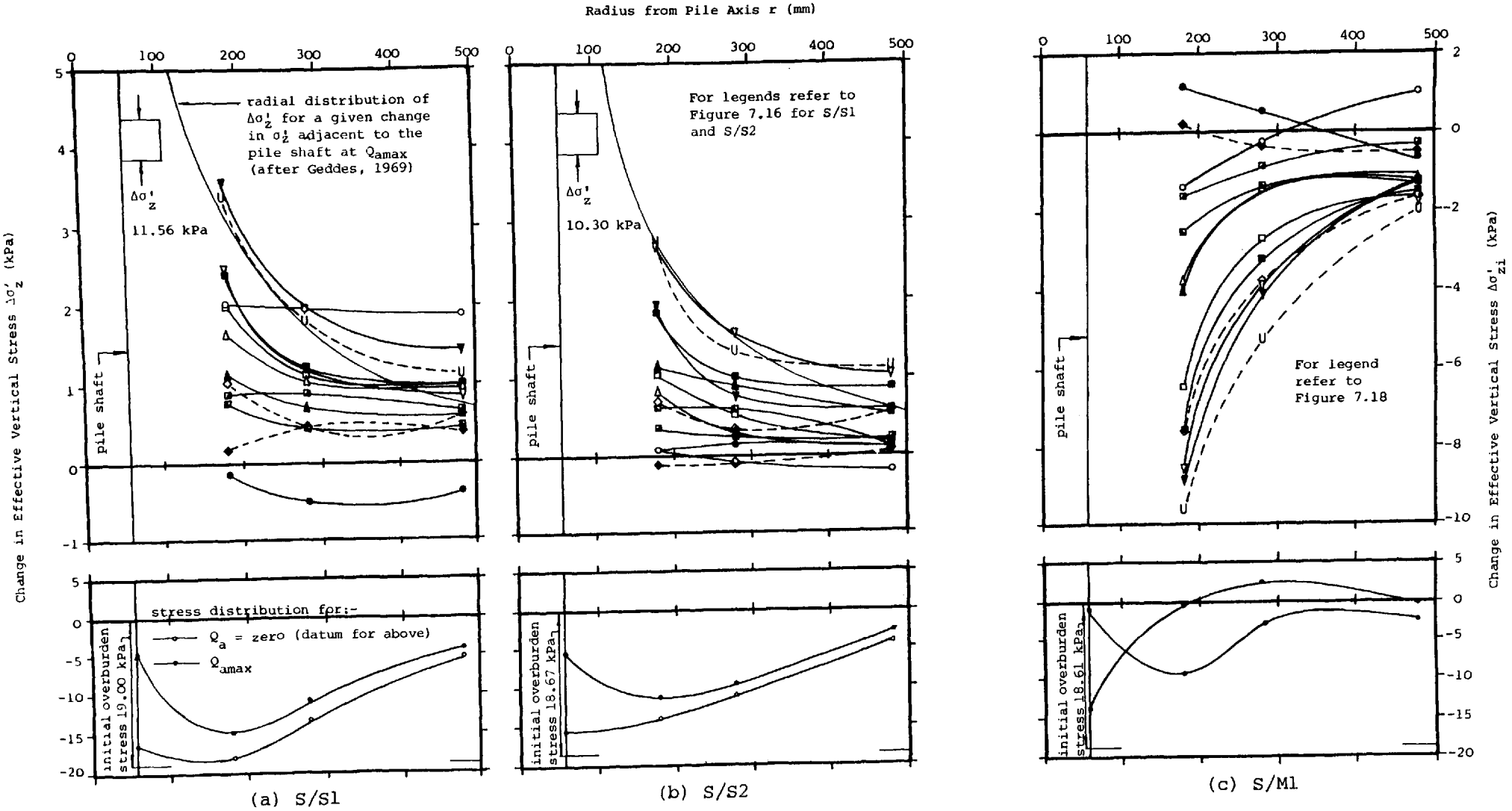

RELATIVE CHANGE IN AND ACTUAL (RELATIVE TO THE INITIAL OVERBURDEN STRESS) EFFECTIVE VERTICAL STRESS ACTING ON A HORIZONTAL PLANE WITHIN THE SOIL PROFILE AT A DEPTH OF 1275.0 mm (EQUIVALENT TO THE LEVEL OF THE SAND/CLAY INTERFACE) DURING THE MAINTAINED LOAD TEST

FIGURE 7.47

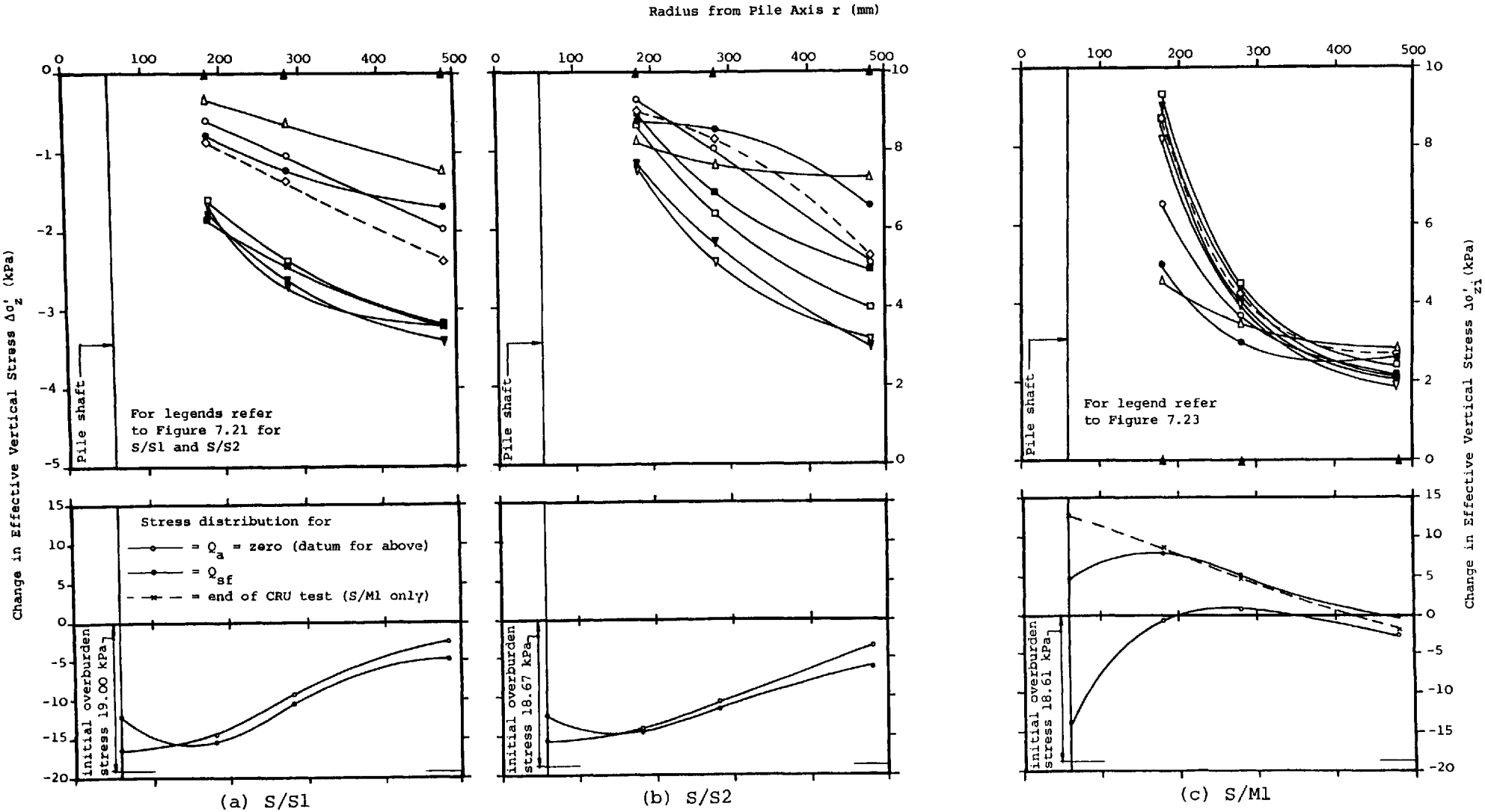

RELATIVE CHANGE IN AND ACTUAL (RELATIVE TO THE INITIAL OVERBURDEN STRESS) EFFECTIVE VERTICAL STRESS ACTING ON A HORIZONTAL PLANE WITHIN THE SOIL PROFILE AT A DEPTH OF 1275.0 mm (EQUIVALENT TO THE LEVEL OF THE SAND/CLAY INTERFACE) DURING THE CONSTANT RATE OF UPLIFT TEST

FIGURE 7.48

CHAPTER 8

CONCLUSIONS AND PROPOSALS FOR FUTURE WORK

CHAPTER 8

CONCLUSIONS AND PROPOSALS FOR FUTURE WORK

8.1 Introduction

The conclusions presented in this chapter are based upon the observations reported in Chapter 7 and are, therefore, only applicable to the conditions encounted during this investigation. Due consideration should therefore be given to the points raised in this study before any are applied to conditions in the field.

8.2 Performance of the Monitoring System

Without the aid of micro-electronics in the form of a micro-computer, data logger and wave form generator, a project of this size would be impractical. The operational success of this project was primarily founded on the 'Management' program which unified and controlled all the peripheral devices and handled and reduced the incoming data. The 'Management' program also prompted the operating personnel to perform various tasks during a test.

The overall performance of the monitoring system was excellent, the only exception being a systems failure which occurred during pile installation in S/S1, due to unknown causes. No significant modifications to the monitoring system are considered necessary.

8.3 Performance of the Instrumentation

The overall performance of the instrumentation was good. The operating limits of the instrumentation proved to be within the design and calibration limits, with the exception of the pair of BOSTs situated immediately above the sand/clay interface in S/M1 during the CRU test.

If required, proposed changes to specific types of instrumentation are outlined in the following sections.

8.3.1 'Core' Axial Load Cells

Data derived from the ALCs, other than from that located at the pile base, was not reported in this thesis since the quality of the data was poor relative to that from the BOSTs. This was due to a small variation in the calibration characteristics of the ALCs when loaded as discrete units in the Instron Universal Materials Testing Machine, as compared with loading as part of an integral pile.

The difference in load transmitted through adjacent ALCs within the pile at full embedment, was typically 1.0 kN for the maximum applied load of approximately 17.0 kN. A variation in the calibration factors of around ±2.0% was sufficient to render the data virtually unusable for the purpose of evaluating the distribution of shaft friction. In the event, a maximum variation of +8.0% was estimated for one of the ALCs. It is obvious, therefore, that although ALCs are probably the simplest means of instrumenting a pile, the design and subsequent calibration of these cells requires considerable thought.

8.3.2 Boundary Orthogonal Stress Transducers

The overall performance of the BOSTs was better than had been anticipated by the author. It was initially considered that the stiffness of the BOSTs in shear, which was necessarily low in order to optimise their response to radial stresses, would be too low to monitor boundary shear stresses other than those associated with a state of shear failure at the pile shaft/soil interface.

The radial stress component recorded by the BOSTs was affected by drift in the zero value during pile installation. Further, the resolved radial stress was also influenced by cross-sensitivity from an applied shear stress. Both of these factors were dealt with satisfactorily.

8.3.3 Sand/Plaster Density Samples

The performance of this method of density determination proved to be satisfactory, since the initial sand densities agreed well with those evaluated by direct measurement. In regions of potentially high volumetric strain, such as below the pile base, the accuracy of this technique is in doubt due to the excessive deformation of the sand/plaster sample. Consideration should, therefore, be given to examining the effects of sample geometry on the calibration factor.

8.3.4 Surface Vertical Displacement Transducers

The performance of the system for monitoring vertical displacements on

the surface of the sand, generally proved to be satisfactory. However, very small displacement reversals, such as those associated with pile unloading during the ML test, were not detected by this system. It may therefore, have been better to have employed an array of surface ELs which have been shown to be capable of monitoring small reversal in displacement. However, the 'direct' measurement of surface displacements proved useful in that it offered an independant check on vertical displacements evaluated within the body of the sand using the ELs.

8.3.5 Electrolytic Levels

The use of ELs to evaluate vertical displacements within the sand was very successful. Calculated displacements were in reasonable agreement with those recorded 'directly' on the surface using LVDTs. The performance of the Type 7650 ELs (±0.70 rad) proved not to be as good as that of the Type 7660 ELs (±0.21 rad) due to a higher aspect ratio which inhibited rotation.

8.3.6 Diaphragm Pressure Transducers

An indication of the performance and reliability of the DPTs may be obtained by comparing the recorded data with stresses evaluated from other types of instrumentation or from theory.

For a pile embedment of less than the depth to the DPTs:

(i) The distribution of the vertical effective stress coefficient

'I', evaluated by back analysis, was in good agreement with that calculated from theory.

(ii) The loci of maximum and minimum vertical effective stress, relative to the pile base, was in accord with the maximum vertical compressive and extensive strain generated within the sand to a radius of 235.0 mm (2.0 B) from the pile axis.

For a pile embedment of greater than the depth to the DPTs:

(i) The intensity and distribution of vertical effective stress recorded by the DPTs, which was less than the initial overburden stress, was compatible with that evaluated adjacent to the pile shaft at both the ultimate and residual load condition.

(ii) The theoretical radial distribution of the change in σ'_z within the sand, due to an evaluated increase in σ'_z adjacent to the pile shaft at ultimate load, was in acceptable agreement with that recorded by the DPTs.

On the basis of the above it would appear that the performance of the DPTs was satisfactory. However, the possibility of some arching occurring across the active face of the DPTs cannot be dismissed.

8.3.7 Interface Shear Stress Transducers

The mode of operation of the ISSTs was deemed not to be applicable to the homogeneous sand profiles. They were not, therefore, employed in S/S1 and S/S2. However, on reflection this approach was incorrect since the

results could have been ignored if found to be 'meaningless'.

The performance of the ISSTs on the sand/clay interface proved to be satisfactory in view of the compatibility of the data with that recorded by the DPTs. Further, at full pile embedment the shear stress acting across the sand/clay interface was complementary to that acting along the pile shaft under both ultimate and residual load. At ultimate load the magnitude of f_z, recorded by the BOSTs immediately above the sand/clay interface, was in accord with the radial distribution of shear stress acting across the sand/clay interface as recorded by the ISSTs.

8.4 Results, Analysis and Discussion

8.4.1 Total, Base and Shaft Resistance

8.4.1.1 Pile Installation

Homogeneous Sand Profiles:

(i) The critcal depths (D_c) relative to q_b and f_s were attained simultaneously for a pile embedment of 1200.0 mm (10.5B). For a pile embedment of greater than D_c, f_s tended to a quasi-constant limiting value of between 5.0 to 6.0 kPa, whilst q_b continued to increase linearly with D_b at typically 0.5 kPa/m embedment.

(ii) The back analysed base bearing capacity factor, N_q^*, attained

a maximum value at D_b equal to 540.0 mm (4.6B), equivalent to 0.45 D_c. At full pile embedment, 1845.0 mm (16.1B), N_q^* tended to a value of approximately 50.

(iii) The variation in K_s with D_b, obtained by back analysis, showed K_s to reduce from greater than K_p for shallow pile embedments, to a lower limiting value of approximately unity at full pile embedment, 1845.0 mm (16.1B).

Layered Soil Profile:

(i) The underlying clay did not affect the development of Q_b until the pile base was at 250.0 mm (2.2B) above the sand/clay interface. This was reflected in a significant increase in the rate of reduction of N_q^* with D_b.

(ii) The maximum value of Q_b within the overlying sand was recorded at 170.0 mm (1.5B) above the sand/clay interface.

(iii) The effect of the underlying clay on the development of Q_s was first evident at D_b equal to 1175.0 mm, 100.0 mm (0.9B) above the sand/clay interface, and resulted in an apparent increase in f_s.

(iv) The base bearing capacity factor, N_c, evaluated at the sand/clay interface was approximately twice that for a circular surface footing on clay.

(v) At depths greater than 350.0 mm (3.0B) below the sand/clay interface, N_c tended to 9.

(vi) The shaft adhesion factor, α, mobilized within the underlying clay showed no tendency towards the high values reported by Tomlinson (1970), and attained a maximum value of 0.54.

(vii) The drawdown of sand around the pile shaft was continuous to

a depth of 230.0 mm (2.0B). The absolute limit of drawdown was 285.0 mm (2.5B).

8.4.1.2 Maintained Load Test

Homogeneous Sand Profiles:

(i) Both ω_s and ω_b were insignificant until Q_a was sufficient to overcome the residual Q_s.

(ii) For Q_a in excess of that necessary to overcome the residual Q_s, the development of Q_s per unit ω_s was linear at typically 3.2 kN/mm to $0.4Q_{amax}$ (Q_{aw}).

(iii) Q_{sf} was attained at a ω_s of typically 2.9 mm (2.5%B), and was constant with further ω_s.

(iv) Q_{bf} was probably attained at a ω_b of 14.6 mm (12.8%B), and continued to increase with further ω_b.

(v) Upon unloading to $\frac{1}{2}Q_{amax}$, both Q_s and Q_b reduced by approximately equal amounts.

Layered Soil Profile:

(i) ω_s and ω_b were insignificant until Q_a was sufficient to overcome the residual Q_s.

(ii) For Q_a in excess of that required to overcome the residual Q_s, the development of Q_s per unit ω_s was linear at approximately 8.0 kN/mm. This was greater than for S/S1 and S/S2 due to the major contribution of the underlying clay to the development of Q_s. Linearity was maintained to an

applied load of $0.4Q_{amax}$ (Q_{aw}).

(iii) Q_{sf} and Q_{bf} appeared to have been attained simultaneously for a ω_s and ω_b of approximately 10.0 mm (8.8%B).

(iv) Upon unloading to $\frac{1}{2}Q_{amax}$, Q_s became negative within the overlying sand due to the greater elastic displacement recovery of the pile and the underlying clay.

8.4.1.3 Constant Rate of Uplift Test

Homogeneous Sand Profiles:

(i) The pile uplift necessary to attain Q_{sf} was typically twice the pile settlement required to achieve Q_{sf} during the CRP test.

(ii) The magnitude of Q_{sf} was typically 44.4% of that recorded during the CRP test. Thus, assuming all other terms in Equation 7.1 to be equal, K_s (tension) is approximately equal to 0.44 K_s (compression).

(iii) For a pile uplift of greater than that associated with Q_{sf}, Q_s reduced due to the development of flow and arching zones within the sand around the pile shaft immediately above pile base level.

Layered Soil Profile:

(i) A negative base resistance was recorded within the underlying clay due, at least in part, to the development of a 'suction' force.

(ii) The pile uplift necessary to attain Q_{sf} was typically twice that required to achieve Q_{sf} during the CRP test.

(iii) The magnitude of Q_{sf} recorded during the CRU test was 85.0% of that recorded during the CRP test.

8.4.2 Sand Density

(i) Density variations within the overlying sand of S/M1 appeared to be unaffected by the underlying clay.

(ii) Around the pile shaft, remote from end effects, the zone of densification extended to a radius of 750.0 mm (6.6B). Within this region volumetric strains reduced to zero at a diminishing rate from about 3.0% at a radius of 180.0 mm (1.4B) from the pile axis.

(iii) The existance of a transition zone was evident in the vicinity of the pile base, within which ε_v was relatively constant at about 1.0 to 2.0% between 160.0 mm (1.4B) and 310.0 mm (2.7B) from the pile axis.

(iv) The total reduction in void content of the sand was estimated at between 170.0 and 190.0% of the embedded volume of the pile.

8.4.3 Boundary Orthogonal Stress Transducers

8.4.3.1 Pile Installation

Homogeneous Sand Profiles:

(i) The magnitude of f_z at a given depth was related to D_b and increased at a diminishing rate with greater D_b. The distribution of f_z along the pile shaft was constant for a given D_b.

(ii) During the initial stages of embedment for a pair of BOSTs, f_z increased at approximately 100.0 kPa/m embedment to the limiting value dictated by the prevailing D_b.

(iii) The magnitude and distribution of the residual f_z was related to D_b and increased at a decreasing rate with greater D_b. The magnitude of the residual f_z was approximately 25.0% of that recorded during pile installation.

(iv) The δ' developed on the pile shaft/sand interface appeared to reduce by about 2^0 over the upper 400.0 mm of the sand profile. Throughout pile embedment an average value of 23.2^0 was recorded.

(v) The magnitude of the local coefficient of earth pressure (K_z) on the pile shaft was greater near the surface. A logorithmic plot of the variation in K_z with Z/B, for a given D_b/B, was linear with a slope of unity. This implied that the ratio of K_z recorded at any two points on the pile shaft, for a given D_b, was equal to the inverse ratio of the depth to the two points under consideration.

(vi) The integration of K_z between the limits of one to D_b/B, where D_b/B was greater than one, showed that K_s tended to 1.7 for D_b/B greater than 10.

Layered Soil Profile:

(i) The development of f_z within the overlying sand was, with the exception of a zone which extended to 170 mm (1.5B) above the sand/clay interface, comparable with that recorded in S/S1 and S/S2. Within the zone immediately above the sand/clay interface f_z increased rapidly to a peak value of typically 10.2 kPa, approximately twice that recorded at the same depth in S/S1 and S/S2, due to the wedging action of the sand between the pile shaft and the clay surface.

(ii) The residual f_z within the overlying sand was affected by the underlying clay once the pile base was within 575.0 mm (5.0B) of the sand/clay interface. The peak value of residual f_z, recorded immediately above the sand/clay interface, was typically -4.0 kPa. This was approximately twice that recorded at the same depth in S/S1 and S/S2, and was due to the greater elastic displacement recovery of both the pile and the sand/clay interface as the pile was unloaded.

(iii) The variation in pile shaft boundary stresses, and the friction angle (δ) within the underlying clay, was directly influenced by the prevailing pile shaft/soil boundary conditions, and reflected the limits to which sand was drawn down into the clay around the pile shaft.

8.4.3.2 Maintained Load Test

Homogeneous Sand Profiles:

(i) The distribution of post compressive residual f_z varied approximately linearly from -1.0 kPa near the surface to -1.7 kPa in the vicinity of the pile base. It was reduced to zero at all points along the pile shaft for a ω_s of typically 0.06 mm (0.05%B) and was associated with a limited decrease in σ'_r.

(ii) For the condition f_z equal to zero, σ'_r tended to $0.47\gamma z$ over the middle portion of the pile shaft. At the upper and lower limits of the pile shaft, σ'_r tended to $1.3\gamma z$ and $0.31\gamma z$ respectively.

(iii) The development of f_z with ω_s was linear for ω_s between 0.06 and 0.87 mm (0.05 and 0.73%B). The greatest rate of increase was associated with the BOSTs at depth. This was accompanied by an increase in σ'_r which developed at a progressively greater rate with ω_s.

(iv) For Q_a of less than $66.7\%Q_{aw}$, the increase in σ'_r per unit Q_a was limited.

(v) For Q_a in excess of $133\%Q_{aw}$, the distribution of f_z tended to a 'Dee' shape.

(vi) At Q_{amax}, K_z varied from approximately $5.0\gamma z$ (greater than K_p, 3.25) near the surface to about $0.6\gamma z$ in the vicinity of the pile base.

(vii) The size of the flow and arching zones developed within the sand in the proximity of the pile base increased with greater ω_b.

(viii) For ω_b in excess of that required to overcome the post compressive residual shaft friction, the mobilization of δ' with ω_s was definable by an exponential relationship.

(ix) The ω_s required to fully mobilize δ' (24.3^0) was typically 1.2 mm (1.1%B), at which both f_z and σ'_r were approximately 80.0% of their respective maximum values at any point along the pile shaft.

Layered Soil Profile:

(i) The intensity of the post compressive residual f_z acting on the pile shaft immediately above the sand/clay interface, was greater than that recorded at a comparable in depth S/S1 and S/S2.

(ii) A ω_s of 0.19 mm (0.17%B) was required to overcome the post compressive residual f_z recorded within the overlying sand, 3.2 times greater than that required in S/S1 and S/S2.

(iii) The development of f_z and σ'_r within the overlying sand was generally similar to that observed in S/S1 and S/S2. However, within the sand immediately above the sand/clay interface, the rate of development of f_z per unit ω_s increased rather than decreased during the latter stages of loading. This was also evident for σ'_r.

(iv) The magnitude of f_z and σ_r developed on the pile shaft within the underlying clay, was directly influenced by the prevailing pile shaft/soil boundary conditions.

(v) Residual and peak values of f_z and σ_r recorded within the underlying clay, generally conformed with the limits recorded during pile installation.

(vi) The residual value of σ_r lay between the limits 0.75 to $1.05C_u$ and increased by typically $0.24C_u$ for Q_{amax}.

8.4.3.3 Constant Rate of Uplift Test

Homogeneous Sand Profiles:

(i) A maximum value of f_z was attained over the upper 800.0 mm (7.0B) of the pile shaft for a ω_s of -1.1 mm (1.0%B), corresponding to a Q_a of -2.1 kN. Below this depth f_z continued to increase with further pile uplift, resulting in a concentration of f_z over the lower portion of the pile shaft.

(ii) At Q_{sf}, σ'_r was equal to a constant portion of the initial effective overburden stress of between 0.6 and $0.7\gamma Z$ below a depth of approximately 450.0 mm (3.5B).

(iii) For a pile uplift in excess of that associated with Q_{sf}, the intensity of both f_z and σ'_r reduced in the vicinity of the pile base due to the development of flow and arching zones with the sand.

Layered Soil Profile:

(i) Within a zone which extended to about 625.0 mm (5.5 B) above the sand/clay interface, the development of both f_z and σ'_r was significantly different from that observed during S/S1 and S/S2. Both f_z and σ'_z increased rapidly with proximity to the sand/clay interface due to the increase in σ'_z generated

within the overlying sand by the uplift of the sand/clay interface.

(ii) Within the underlying clay the pile shaft stresses were affected by the prevailing pile shaft/clay boundary conditions, and were generally comparable in magnitude with those recorded during pile installation (f_z transposed).

8.4.3.4 The State of Stress Developed Within the Sand Adjacent to the Pile Shaft During both Compressive and Tensile Loading

(i) The variation in f_z with σ_r' described what could loosely be termed as a hyperbola, with assumtopic axes diverging from the origin at $\pm 24.3^0$ to the σ_r' axis. Initial tangency of the data to the $\pm\delta'$ envelopes (that is; $f_z/\sigma_r' = \text{Tan}\,\delta'$) was observed for higher stress levels during the ML test than in the CRU test. The two limbs of the hyperbola were therefore, not symmetrical.

(ii) The increase in both f_z and σ_r' beyond that associated with initial tangency to the $\pm\delta'$ envelopes, was greater over the upper portion of the pile shaft.

(iii) The limit of acceptable linear behaviour between Q_s/ω_s, or f_z/ω_s, coincided with the initial tangency of the variation in f_z with σ_r', with the $\pm\delta'$ envelope.

(iv) The ratio f_{zmax} (tension)/f_{zmax} (compression) was not constant along the pile shaft, but varied non-linearly from approximately 0.35 near the surface to about unity near the pile base.

(v) The changes in the axial and principal stresses generated

within the sand adjacent to the pile shaft on loading, were complex. It was deduced that:

(a) For f_z equal to zero during pile loading, σ_r' was the major principal stress, and σ_z' and σ_θ' were equal and equivalent to the minor and intermediate principal stresses, σ_3' and σ_2'. Further, the intensity of σ_z' was less than the initial overburden stress.

(b) Pile loading resulted in a rotation of the principal stress planes and a global increase in the intensity of both the axial and principal stresses.

(c) Shear failure developed in the sand adjacent to the pile shaft at the same time as 'slip' occurred at the pile shaft/sand interface.

(d) The relative magnitude of the axial stresses developed within the sand adjacent to the pile shaft at Q_{amax} was $\sigma_\theta' < \sigma_z' < \sigma_r'$.

(e) As the pile was unloaded a rapid collapse occurred in the stress intensity adjacent to the pile shaft, accompanied by a rotation of the principal stress planes. The complex interaction between the pile shaft and the stressed sand resulted in the development of shear failure within the sand adjacent to the pile shaft and 'slip' on the pile shaft/sand interface.

8.4.4 Soil Displacements

8.4.4.1 Pile Installation

Homogeneous Sand Profiles:

(i) For a pile embedment of less than 200.0 mm (1.8B), heave was recorded on the surface of the sand within a radius 460.0 mm (4.0B) from the pile axis.

(ii) The zone of disturbance generated within the sand below the pile base increased in size with pile embedment.

(iii) The rate of vertical displacement per unit of pile embedment within the sand, on a given horizontal plane, increased at a progressively greater rate with proximity to both the pile axis and pile base until the pile base was within about 250.0 mm (2.2B) of the plane under consideration.

(iv) Within a zone which extended to between 250.0 mm (2.2B) below and 100.0 mm (0.9B) above the pile base, the rate of increase in vertical soil displacement per unit pile penetration reduced and ultimately resulting in the development of subsurface heave within a radius of 460.0 mm (4.0B) from the pile axis.

(v) Above the zone of immediate influence of the pile base, vertical displacements per unit pile penetration within the sand increased at a diminishing rate and tended to a quasi-constant limiting value.

(vi) Six distinct displacement zones were identified around the pile base, within each of which the vertical displacement

behaviour of the sand was different. The boundaries between these zones were significant in terms of vertical strain.

(vii) Vertical strains generated within the sand below the pile base reduced in intensity with distance from the pile axis. Generally, the maximum compressive strain was twice the maximum extensive strain at any given radius.

Layered Soil Profile:

(i) Whilst the pile base was above the level of the sand/clay interface, vertical displacements within the sand at a depth of 510.0 mm (4.5B) or less were unaffected by the underlying clay. However, below a depth of 510.0 mm (4.5B), soil displacements were recorded for shallower pile embedments than those associated with S/S1 and S/S2.

(ii) Heave occurred on the sand/clay interface as the pile base penetrated the underlying clay. This resulted in a reduction in the rate of increase in vertical displacement per unit pile penetration within the overlying sand.

(iii) The maximum recorded heave on the sand/clay interface was 1.4 mm (1.2%B), at a radius of 160.0 mm (1.4B) from the pile axis. This was twice that recorded at the same location in S/S1 and S/S2.

8.4.4.2 Maintained Load Test

Homogeneous Sand Profiles:

(i) Vertical displacements within the sand above pile base level, increased approximately linearly at any given radius from the pile axis per unit Q_a.

(ii) The variation in $\log_e(V/Q_a)$ with $\log_e(2r/B)$ was approximately linear.

(iii) The shear modulus of the sand increased from approximately 0.1 MN/m^2 adjacent to the pile shaft, to the upper limiting value of 11.4 MN/m^2 at a radius of 520.0 mm (4.6B) from the pile axis.

(iv) As the pile was unloaded to $\frac{1}{2}Q_{amax}$, approximately 70.0% of the total elastic displacement recovery of the sand occurred, amounting to typically 30.0% of the maximum vertical displacement recorded at Q_{amax}.

Layered Soil Profile:

(i) The vertical displacements within the overlying sand, to a depth of 510.0 mm, were comparable with those recorded in S/S2.

(ii) Vertical displacements within the overlying sand at 255.0 mm (2.0B) above and on the sand/clay interface, were greater than those at a similar depths in S/S1 and S/S2.

(iii) Throughout pile loading, extensive strains developed within the sand immediately above the sand/clay interface. This was consistent with a reduction in σ'_z as recorded by the DPTs

located on the surface of the underlying clay.

(iv) Upon complete removal of Q_a, the displacement recovery of the sand/clay interface amounted to 78.0% of the maximum vertical displacement recorded at Q_{amax}. The displacement recovery within the overlying sand reduced with height above the sand/clay interface, resulting in the development of compressive strains. This was evident from the increase in σ'_z as recorded by the DPTs located on the surface of the underlying clay.

8.4.4.3 Constant Rate of Uplift Test

Homogeneous Sand Profiles:

(i) The net upward displacement of the sand increased with depth to a radius of approximately 310.0 mm (2.7B) from the pile axis. This resulted in the development of compressive strains and an increase in σ'_z within the sand adjacent to the pile shaft.

(ii) The magnitude of the average vertical displacement at the surface could be equated to the volume of pile extracted.

Layered Soil Profile:

(i) Throughout the CRU test all vertical displacements within the overlying sand were upward.

(ii) Vertical displacements generated within the overlying sand increased with depth. This resulted in the development of

compressive strains and an increase σ'_z within the overlying sand.

8.4.4.4 Radial Displacements in Homogeneous Sand due to Pile Installation

(i) Radial displacements within the sand extended to a radius of 480.0 mm (4.0B) from the pile axis, and may be evaluated at any given radius by applying an emperical compaction factor to the theoretical radial displacement evaluated assuming $\varepsilon_v = \varepsilon_z = 0$, Equation 7.13.

8.4.5 Stresses Developed on a Horizontal Plane at Depth in a Soil Profile

8.4.5.1 Pile Installation

Homogeneous Sand Profile:

(i) The normalized stress coefficients 'I', derived throughout pile installation, show the distribution of vertical effective stress below the pile base to be in-keeping with the formation of 'pressure-bulbs'.

(ii) When D_b was equal to the depth to the plane of the DPTs, σ'_z as equal to the initial overburden stress at all radii within the radial limits of the DPTs.

(iii) When D_b was greater than the depth to the plane of the DPTs, σ'_z was less than the initial overburden stress and reduced with proximity to the pile axis.

(iv) The magnitude of σ'_z at any given radius from the pile axis appeared to tend to a constant limiting value at 570.0 mm (5.0B) above pile base level.

(v) The development of residual σ'_z with D_b followed a similar variation to that recorded during pile installation. However, although there was some evidence of 'locked-in' displacement stresses these were not as great as those reported in literature.

Layered Soil Profile:

(i) Throughout penetration of the overlying sand the development of σ'_{zi} on the sand/clay interface was comparable with that recorded in S/S1 and S/S2 at the same depth. However, the associated residual stresses were greater than those recorded in S/S1 and S/S2, due to the greater displacement recovery of the sand/clay interface.

(ii) As the pile base penetrated the sand/clay interface an increase in σ'_{zi} was recorded, which corresponded with the development of heave on the sand/clay interface.

(iii) As the pile approached full embedment, σ'_{zi} tended to a constant limiting value which was less than the initial overburden stress within the radial limits of the DPTs.

(iv) During penetration of the underlying clay the residual σ'_{zi} was in excess of the initial effective overburden stress. This reflected the greater elastic vertical displacement

recovery of the sand/clay interface as compared with the sand in S/S1 and S/S2. As the pile approached full embedment, the residual σ'_{zi} tended to the initial overburden stress within the radial limits of the DPTs.

(v) For the pile base immediately above the sand/clay interface, and for a limited penetration below the sand/clay interface, τ_i was negative. This was due to the displacement of the clay surface away from the pile axis relative to the overlying sand, and was associated with the onset of heave at the clay surface.

(vi) Over the latter stages of pile installation, τ_i became positive across the sand/clay interface and was complementary to f_z. The magnitude of τ_i was greatest at the inner limit of instrumentation and tended to zero at the radius of between 320.0 mm (3.3B) and 480.0 mm (4.2B) from the pile axis.

8.4.5.2 The State of Two Dimensional Stress Developed on the Sand/Clay Interface

(i) The stresses acting on an element of sand immediately above the sand/clay interface prior to pile installation, were those associated with the 'at-rest' state.

(ii) The major principal stress (σ'_1) acting on the sand/clay interface throughout pile installation, appeared to emanate from a point which was typically 48.8 mm (0.4B) below the pile base.

(iii) The stress changes generated on the sand/clay interface

during pile installation, were complex. They gradually increased in intensity, accompanied by a rotation of the principal stress planes, as the pile base approached the sand/clay interface. For a limited pile embedment immediately above the sand/clay interface, σ'_{ri} was greater than σ'_{zi}. A rapid reduction in stress intensity and a counter rotation of the principal stress planes, occurred as the pile penetrated below the sand/clay interface.

(iv) Over the latter stages of pile penetration a quasi-constant state of stress was observed to act across the sand/clay interface.

8.4.5.3 Maintained Load Test

Homogeneous Sand Profiles:

(i) The radial distribution of residual σ'_z was in accord with the magnitude of residual σ'_z evaluated adjacent to the pile shaft.

(ii) σ'_z increased within the radial limits of the DPTs throughout pile loading. The greatest increase in σ'_z was recorded by the DPT closest to the pile axis.

(iii) For pile loads equal to, or greater than, $200\%Q_{aw}$, $\Delta\sigma'_z$ tended to an upper limiting value at all radii within the limits of the DPTs.

(iv) Between the outer radial limit of the DPTs and the pile shaft, σ'_z was less than the initial overburden stress throughout pile loading.

Layered Soil Profile:

(i) Under post-compressive residual stress conditions σ'_{zi} was approximately equal to, or slightly in excess of, the initial overburden stress within the radial limits of the DPTs.

(ii) During pile loading, σ'_{zi} reduced within the radial limits of the DPTs. However, adjacent to the pile shaft σ'_{zi} was increased.

8.4.5.4 Constant Rate of Uplift Test

Homogeneous Sand Profiles:

(i) σ'_z underwent a progressive reduction throughout pile loading which was greatest at the outer limit of the DPTs 480.0 mm (4.2B) from the pile axis. The trends observed in the radial distribution of $\Delta\sigma'_z$ indicated a small increase in σ'_z adjacent to the pile shaft. This was confirmed by the results from the BOSTs.

Layered Soil Profile:

(i) The radial distribution of σ'_{zi} across the sand/clay interface at Q_{sf}, increased approximately linearly from about 18.6 kPa (1.0 times the initial overburden stress) at a radius of 480.0 mm (4.2B), to approximately 26.0 kPa (1.4 times the initial overburden stress) at 180.0 mm (1.6B) from the pile axis.

8.5 The Significance of this Study to the Design of Full-Scale Piles

This study highlights the over-simplification of current design methods for the evaluation of shaft friction on full scale piles. On the basis of this study alone, it would be imprudent to propose a new design procedure. Further investigations must be undertaken in order to quantify the effects of a number of variables; that is: pile diameter and embedment, method of installation, sand density and ground water level. However, the study does offer an insight into the mechanics of shaft friction in granular soil.

With regard to the layered soil profile, it would appear that the sand/clay interface affects the development of shaft friction within a zone which extends to 2.5B above and below the sand/clay interface. In relation to field piles this is insignificant and, therefore, the effects of the interface on the development of shaft friction may be ignored for design purposes.

8.6 Proposals for Future Work

A considerable amount of time and effort was expended both by the author and the technical staff at the Polytechnic on the development and construction of the testing equipment employed in this research project. Any future project should, therefore, where possible aim to employ the same equipment.

It is considered that there is sufficient scope for a further project dealing solely with the behaviour of a single pile in sand.

The project should aim to:

(i) Verify, or otherwise, the stress variation developed within the sand adjacent to the pile shaft on loading. This may be achieved by subjecting the pile to cyclic loading between the limits of tensile and compressive shaft failure.

(ii) Although a general indication of the distribution in vertical effective stress within the sand was gained by normalizing the data recorded during pile installation in the form of stress coefficients, the variation due to pile loading is indeterminate. For this reason the inclusion of additional DPTs should be considered. Further, in order to gain an overall picture of the stress variation within the sand, the DPTs should be installed normal to the three cylindrical axes.

(iii) Vertical displacements have been adequate monitored during this project. However, it would be to the advantage of any future project to verify, or otherwise, the radial displacement profile proposed by the author.

(iv) The effects of sand density on the state of stress should be considered.

(v) The effects of the method of pile installation should be considered.

(vi) After investigating, in detail, the behaviour of a single pile in homogeneous sand, future investigations should consider the effects of an underlying clay layer.

(vii) A further logical extension to the proposed future work is to study the effect of pile interaction within a pile group.

BIBLIOGRAPHY

ACER, Y.B., DURGUNOGLU, H.T. & TUMAY, M.T. (1982). 'Interface Properties of Sand', Journal of the Geotechnical Engineering Division, ASCE, Vol.108, No.GT4, pp 684-654.

AGARWAL, S.L. & VENKATESAN, S. (1965). 'An Instrument to Measure Skin Friction and Normal Earth Pressure on Deep Foundations', Instruments and Apparatus for Soil and Rock Mechanics, ASTM STP 392, American Society of Testing Materials, pp 152-169.

AKROYD, T.N.W. (1957). 'Laboratory Testing in Soil Mechanics', The Marshall Press Limited, London.

ARTHUR, J.R.F. & ROSCOE, M.A. (1961). 'An Earth Pressure Cell for the Measurement of Normal and Shear Stresses', Civil Engineering and Public Works Review, Vol.56, pp 765-770.

BENNETT, D.H. & GISBOURN, R. (1971). 'Stress Strain Behaviour of Soils', Proceedings of the Roscoe Memorial Symposium, Cambridge University, pp 459-466.

BEREZANTZEV, V.G., KHRISTOFORAV, V.S. & GOLUBKOV, V.N. (1961). 'Load Bearing Capacity and Deformation of Piled Foundations', Proceedings of the 5th International Conference on Soil Mechanics and Foundation Engineering, Vol.2, pp 11-15.

BERGDAHL, U. & WENNERSTRAND, J. (1976). 'Bearing Capacity of Driven Piles in Loose Sand', Proceeding of the 6th European Conference on Soil Mechanics and Foundation Engineering, Wien, Vol.2.1, pp 355-360.

BISHOP, A.W. & HENKEL, D.J. (1961). 'The Measurement of Soil Properties' in The Triaxial Test, Edward Arnold Limited, London.

BISHOP, R.F., HILL, R. & MOTT, N.F. (1945). 'The Theory of Indentation and Hardness Test', Proceedings of the Physical Society, 57, pp 147-159.

BRANSBY, P.L. (1973). 'Cambridge Contact Stress Transducers', Lecture Notes for the Course on 'Research Techniques and Equipment in Soil Mechanics' held at Cambridge.

BRITISH STANDARDS INSTITUTION (1972). 'Code of Pratice for Foundations', CP2004, The British Standards Institution.

BRITISH STANDARDS INSTITUTION (1975). 'Methods of Testing Soils for Civil Engineering Purpose', BS1377, The British Standards Institution.

BRINCH HANSEN, J. (1968). 'A theory for Skin Friction in Piles', The Danish Geotechnical Institute, Bulletin No.25, Copenhagen.

BROMS, B.B (1966). 'Methods of Calculating the Ultimate Bearing Capacity of Piles', Sols Soils, Vol.5, pp 21-32.

BROMS, B.B. & SILBERMAN, J.O. (1964). 'Skin Friction Resistance for Piles in Cohesionless Soils', Sols Soils, No.10, pp 33-41.

BROWN, S.F. (1973). 'Measurement of Insitu Stress and Strain in Soils', Symposium on Field Instrumentation in Geotechnical Engineering, London, Part 1, pp 38-52.

BROWN, J.D. & MERYERHOF, G.G. (1969). 'Experimental Study of Bearing Capacity in Layered Clays', Proceedings of the 7th International Conference on Soil Mechanics and Foundation Engineering, Vol.2, pp 45-51.

BUTTERFIELD, R. & ANDRAVES, K.Z. (1972). 'On the Angle of Friction Between Sand and Plane Surfaces', Journal of Termechanics, Vol.8, No.4, pp 15-23.

BUTTERFIELD, R. & BANNERJEE, P.K. (1970). 'The Effect of Porewater Pressures on the Ultimate Bearing Capacity of Driven Piles', Proceedings of the 2nd South East Asian Conference on Soil Engineering, Bangkok, pp 385-394.

BUTTERFIELD, R. & GHOSH, N. (1977). 'The Response of Single Piles in Clay to Axial Load', Proceedings of the 9th International Conference on Soil Mechanics and Foundation Engineering, Vol.1, pp 451-457.

BUTTERFIELD, R. & JOHNSTON, I.W. (1973). 'The Stress Acting on a Continuously Penetrating Pile', Proceedings of the 8th International Conference on Soil Mechanics and Foundation Engineering, Vol.2.1, pp 39-42.

CLARK, J.I. & MEYERHOF, G.G. (1972). 'The Behaviour of Piles Driven in Clay. Part I. An Investigation of Soil Stress and Pore Water Pressure as Related to Soil Propnrties', Canadian Geotechnical Journal, Vol.9, pp 351-373.

CLARK, J.I. & MEYERHOF, G.G. (1973). 'The Behaviour of Piles Driven in Clay. Part II. Investigation of the Bearing Capacity Using Total and Effective Stress Parameters', Canadian Geotechnical Journal, Vol.10, pp 86-102.

CLEMENTS, S.P. & BRUMUND, W.F. (1975). 'Large Scale Model Test of Drilled Pier in Sand', Journal of the Geotechnical Engineering Division, ASCE, Vol.101, No.GT6, pp 537-550.

COOKE, R.W. & PRICE, G. (1973(a)). 'Horizontal Inclinometers for the Measurement of Vertical Displacement in the Soil Around Experimental Foundations', Proceedings of the Symposium on Field Instrumentation in Geotechnical Engineering, London, pp 112-125.

COOKE, R.W. & PRICE, G. (1973(b)). 'Strains and Displacements Around Friction Piles', Proceedings of the 8th International Conference on Soil Mechanics and Foundation Enginering, Moscow, Vol.2, No.1, pp 53-60.

COOKE, R.W. PRICE, G. & TARR, K. (1979). 'Jacked Piles in London Clay: A Study of Load Transfer and Settlement Under Working Conditions', Geotechnique, Vol.29, No.2, pp 113-147.

COOKE, R.W. & WHITAKER, T. (1961). 'Experiments in Model Piles with Enlarged Bases', Geotechnique, Vol.11, No.1, pp 1-13.

COYLE, H.M. & CASTELLO, R.R. (1979). 'A New Look at Bearing Capacity Factors for Piles', 11th Annual Offshore Technology Conference, Houston, Texas, Vol.1, pp 427-431.

COYLE, H.M. & CASTELLO, R.R. (1981). 'New Design Correlations for Piles in Sand', Journal of the Geotechnical Engineering Division, ASCE, Vol.107, No.GT7, pp 965-986.

COYLE, H.M. & SULAINMAN, I.H. (1967). 'Skin Friction on Steel Piles in Sand', Journal of Soil Mechanics and Foundation Engineering Division, ASCE, Vol.93, No.SM6, pp 261-278.

DAVIDSON, J.L., MORTENSEN, R.A. & BARREIRO, D. (1981). 'Deformations in Sand Around a Cone Penetrometer Tip', Proceedings of 10th International Conference on Soil Mechanics and Foundation Engineering, Stockholme, Vol.2, pp 467-470.

ESRIG, M.E. & KIRBY, R.C. (1979(a)). 'Advances in General Effective Stress Method for the Prediction of Axial Capacity for Driven Piles in Clay', 11th Annual Offshore Technology Conference, Houston, Texas, Vol.1, pp 437-443.

ESRIG, M.E. & KIRBY, R.C. (1979(b)). 'Soil Capacity for Supporting Deep Foundation Members in Clay', Behaviour of Deep Foundations, ASTM STP620, American Society for Testing Materials, pp 27-63.

FEDA, J. (1963). 'Skin Friction on Piles due to Dilatancy', Proceedings of the Budapest Soil Mechanics Conference, pp 243-252.

FEDA, J. (1976). 'Skin Friction of Piles', Proceedings of the 6th European Conference of Soil Mechanics and Foundations Engineering, Wien, Vol.2.1, pp 423-361.

FRANCESON, M. (1982). 'Model Pile Tests in Clay: Stresses and Displacements due to Installation and Axial Loading', Ph.D Thesis, Cambridge University, Cambridge.

GEDDES, J.D. (1966). 'Stresses in Foundation Soils due to Vertical Subsurface Loading', Geotechnique, Vol.16, No.3, pp 231-255.

GEDDES, J.D. (1969). 'Boussinesq-Based Approximations to the Vertical Stresses Caused by Pile-Type Subsurface Loadings', Geotechnique, Vol.19, No.4, pp 509-514.

GETZLER, Z, KOMORNIK, A. & MAZURIK, A. (1968). 'Model Study on Arching Above Buried Structures', Journal of the Soil Mechanics and Foundation Division, ASCE, No.SM5, pp 1123-1141.

GREGERSEN, O.S., AAS, G. & DIBIAGIO, E. (1973). 'Load Tests on Friction in Loose Sand', Proceedings of the 8th International Conference on Soil Mechanics and Foundation Engineering, Moscow, Vol.2.1, pp 109-117.

HANNA, T.H. (1969). 'The Mechanics of Load Mobilization in Friction Piles', Journal of Materials, JMLSA, Vol.4, No.4, pp 924-937.

HANNA, T.H. & TAN, R.H.S. (1971). 'The Load Movement Behaviour of Long Piles', Journal of Materials, JMLSA, Vol.6, No.3, pp 532-554.

HANNA, T.H. & TAN, R.H.S. (1973). 'The Behaviour of Long Piles Under Compressive Loads in Sand', Canadian Geotechnical Journal, Vol.10, No.3, pp 311-340.

HEALY, K.A. & MEITZLER, G. (1968). Discusssion on 'Skin Friction for Steel Piles in Sand', Journal of Soil Mechanics and Foundations Division, ASCE, No.SM3, pp 811.

HOLLOWAY, D.M., CLOUGH, G.W. & VESIC, A.S. (1978). 'The Effects of Residual Driving Stresses on Pile Performance Under axial Loads', 10th Annual Offshore Technology Conference, Houston, Texas, Vol.4, pp 2225-2236.

HOLINQUIST, D.V. & MATLOCK, H. (1976). 'Resistance-Displacement Relationships for Axially-Loaded Piles in Soft Clay', 8th Annual Offshore Technology Conference, Houston, Texas, Vol.1, pp 553-569.

KAY, W.R. (1980). 'The Development of Skin Friction in Semi-Full Sclae Piles Passing Through Granular Soils', Ph.D Thesis, The Polytechnic of Wales, Pontypridd.

KERISEL, J. (1961). 'Deep Foundations in Sand: Variation of Ultimate Bearing Capacity with Soil Density, Depth, Diameter & Speed', Proceedings of the 5th Internation Conference on Soil Mechanics & Foundation Engineering, Vol.2, pp 73-83.

KERISEL, J. (1964). 'Deep Foundations-Basic Experimental Facts', Proceedings on the Conference on Deep Foundations, Mexico City, Vol.1, pp 5-44.

KIRBY, R.C. & ESRIG, M.I. (1979). 'Further Development of a General Effective Stress Method for Prediction of Axial Capacity for Driven Piles in Clay', Conference on Recent Developments in the Design and Constitution of Piles, The Institution of Civil Engineers, London.

KISHIDA, H. (1964). 'Stress Distribution by Model Piles in Sand', Soil and Foundation, Vol.5, No.1, pp 1-23.

KISHIDA, H. (1967). 'Ultimate Bearing Capacity of Piles Driven into Loose Sand', Soil and Foundations, Vol.7, No.3, pp 20-29.

KOIZUMI, Y. (1971). 'Field Tests on Piles in Sand', BCP Committee, Soils and Foundations, Vol.11, No.2, pp 29-49.

LAMBE, T.W. & WHITMAN, R.V. (1979). 'Soils Mechanics, SI Version', John Wiley and Sons, New York.

MANSUR, C.I. & KAUFMAN, R.I. (1956). 'Pile Tests, Low-Sill Structure, Old River, Louisiana', Journal of the Soil Mechanics and Foundation Division Transactions, Vol.123, pp 435-466.

MAZURKIEWICZ, B.K. (1968). The Danish Geotechnical Institute, Bulletin No.25, Copenhagen.

MEYERHOF, G.G. (1951). 'The Ultimate Bearing Capacity of Foundations', Geotechnique, Vol.2, No.4, pp 301-332.

MEYERHOF, G.G. (1956). 'Penetration Tests and Bearing Capacity of Cohesionless Soils', Journal of Soil Mechanics and Foundation Engineering Division, ASCE, No.SM1, pp 1-19.

MEYERHOF, G.G. (1959). 'Compaction of Sands and Bearing Capacity of Piles', Journal of the Soil Mechanics and Foundations Division, ASCE, Vol.85, No.SM6, pp 1-29.

MEYERHOF, G.G. (1963). 'Some Recent Research on the Bearing Capacity of Foundations', Canadian Geotechnical Journal, Vol.1, No.1, pp 16-26.

MEYERHOF, G.G. (1976). 'Bearing Capacity and Settlement of Pile Foundations', Journal of the Geotechnical Engineering Division, Vol.102, No.GT3, pp 195-228.

MEYERHOF, G.G. & SASTRY, V.V.R.N. (1978(a)). 'Bearing Capacity of Piles in Layered Soils: Part 1, Clay Overlying Sand', Canadian Geotechnical Journal, Vol.15, No.2, pp 171-182.

MEYERHOF, G.G. & SASTRY, V.V.R.N. (1978(b)). 'Bearing Capacity of Piles in Layered Soils: Part 2, Sand Overlying Clay', Canadian Geotechnical Journal, Vol.15, No.2, pp 183-189.

MEYERHOF, G.G & VALSANGKAR, A.J. (1977). 'Bearing Capacity of Piles in Layered Soils', Proceedings of the 9th International Conference on Soil Mechanics and Foundation Engineering, Japan, Vo.1, pp 645-650.

MOGAMI, T. & KISHIDA, H. (1961). 'Some Piling Problems', Proceedings of the 5th International Conference on Soil Mechanics and Foundation Engineering, Vol.2, pp 111-115.

MOHAN, D., JAIN, G.S. & KUMAR, V. (1963). 'Load-Bearing Capacity of Piles', Geotechnique, Vol.13, No. , pp 76-86.

NORLAND, R.L. (1963). 'Bearing Capacity of Piles in Cohesionless Soils', Journal of Soil Mechanics and Foundations Division, ASCE, No.SM3, pp 1-35.

PERREN, F.J. (1978). 'A Case History of Piling in the Glacial Material of South Wales', M.Phil. Thesis, CNAA, London, UK.

PLANTEMA, G. (1952). 'A Soil Pressure Cell and Calibration Equipment', Proceedings of the 3rd International Conference on Soil Mechanics and Foundation Engineering, Vol.1, pp 283-286.

PLANTEMA, G. & NOLET, C.A. (1957). 'Influence of Pile Driving on the Sounding Resistances in a Deep Sand Layer', Proceedings of the 4th International Conference on Soil Mechanics and Foundation Engineering, London, Vol.II, pp 52-55.

POTYONDY, J.G. (1961). 'Skin Friction Between Various Soils and Construction Materials', Geotechnique, Vol.11, No.4, pp 339-353.

POULOS, H.G. & DAVIS, E.H. (1980). 'Pile Foundation Analysis and Design', John Wiley and Sons, New York.

RANDOLPH, M.F., CARTER, J.P. & WROTH, C.P. (1979(a)). 'Driven Piles in Clay - The Effects of Installation and Subsequent Consolidation', Geotechnique, Vol.29, No.4, pp 361-393.

RANDOLPH, M.F., STEENFELT, J.S. & WROTH, C.P. (1979(b)). 'The Effect of Pile Type on Design Parameters for Driven Piles', Proceedings of the 7th European Conference on Soil Mechanics and Foundation Engineering, Brighton, Vol.2, pp 107-114.

REESE, L.C. & COX, W.R. (1976). 'Pullout Tests of Piles in Sand', 8th Annual Offshore Technology Conference, Houston, Texas, Vol.1, pp 527-538.

REESE, L.C. & SEED, H.B. (1955). 'Pressure Distribution Along Friction Piles', Proceedings of the ASTM, Vol.55, pp 1156-1182.

ROBINSKY, E.I. & MORRISON, C.F. (1964). 'Sand Displacement & Compaction Around Model Friction Piles', Canadian Geotechnical Journal, Vol.1, No.2, pp 81-93.

ROBINSKY, E.I., SAGAR, W.L. & MORRISON, C.F. (1964). Effect of Shape and Volume on the Capacity of Model Piles in Sand. Canadian Geotechnical Journal, Vol.1, No.4, pp 189-204.

SEED, H.B. & REESE, L.C. (1955). 'The Action of Soft Clay Along Friction Piles', Transactions, ASCE, Vol.122, pp 731-754.

SHERMAN, W.C. Jr., HOLLOWAY, D.M. & TREHAN, C.C. (1974). 'Analysis of Pile Tests', Army Engineer Waterways Experiment Station, Vicksburg, Mississippi, Technical Report S-74-3.

SKEMPTON, A.W. (1951). 'The Bearing Capacity of Clays', Proceedings of the Building Research Congress, London, Vol.1, pp 180-189.

TAVENAS, F.A. (1971). 'Load Tests Results on Friction Piles in Sand', Canadian Geotechnical Journal, Vol.8, pp 7-22.

TEJCHMAN, A. (1971). 'Skin Friction on a Model Pile Driven in Sand', The Danish Geotechnical Institute, Bulletin No.29, Copenhagen.

TOMLINSON, M.J. (1970). 'Adhesion of Piles in Stiff Clay', Construction Industry Research and Information Association Research Report 26, November, pp 1-47.

TOMLINSON, M.J. (1971). 'Some Effects of Pile Driving on Skin Friction', Conference on Behaviour of Piles, Institution of Civil Engineers, London, pp 107-114.

TOUMA, F.T. & REESE, L.C. (1974). 'Behaviour of Bored Piles in Sand', Journal of Geotechnical Engineering Division, ASCE, Vol.100, No.GT7, pp 749-761.

TROLLOPE, D.H. & CURRIE, D.T. (1960). 'Small Embedded Earth Pressure Cells - Their Design & Calibration', Proceedings of the 3rd Australian & New Zealand Conference on Soil Mechanics & Foundation Engineering, Sydney, Australia, pp 145-151.

VESIC, A.S. (1963). 'Bearing Capacity of Deep Foundations in Sand', National Acadamy of Science, National Research Council, Highway Research Record 39, pp 112-153.

VESIC, A.S. (1964). 'Investigations of Bearing Capacity of Piles in Sand', Proceedings of North American Conference on Deep Foundations, Mexico City, Vol.1, pp 197-224.

VESIC, A.S. (1965). 'Ultimate Loads and Settlements of Deep Foundations in Sand', Proceedings of a Symposium on Bearing Capacity and Settlement of Foundations, Duke University, Durham, N.C., pp 53-68.

VESIC, A.S. (1967). 'A Study of Bearing Capacity of Deep Foundations', Final Report Project B189, School of Civil Engineering Georgia Institute of Technology, Atlanta.

VESIC, A.S. (1969(a)). 'Load Transfer, Lateral Loads and Group Action of Deep Foundations', Performance of Deep Foundation, ASTM STP444, American Society for Testing Materials, pp 5-14.

VESIC, A.S. (1969(b)). Discussion : Proceedings of 7th Conference on Soil Mechanics and Foundation Engineering, Vol.3, pp 242-244.

VESIC, A.S. (1970). 'Tests on Instrumented Piles, Ogeechee River Site', Journal of the Soil Mechanics and Foundations Division, ASCE, Vol.96, No.SM2, pp 561-585.

VESIC, A.S. (1977). 'Design of Pile Foundations', Synthesis of the Highway Practice No.42, National Co-operative Highway Research Programme, Transport Research Board, National Research Council, Washington D.C., pp 68.

WELTMAN, A.J. (1980). 'Pile Load Testing Procedures', Construction Industry Research and Information Association Report PG7.

WELTMAN, A.J. & HEALY, P.R. (1978). 'Piling in 'Boulder Clay' and Other Glacial Tills', Construction Industry Research and Information Association Report PG5.

WERSCHING, S.N., DELPAK, R. & ROWLANDS, G.O. (1983). 'A Method of Estimating the Insitu Density of Dry, Uniformally Graded Sand Under Controlled Conditions of Placement', Geotechnical Testing Journal, ASTM, Vol.6, No.4, pp 196-200.

WHITAKER, T. (1963). 'The Constant Rate of Penetration Test for the Determination of the Ultimate Bearing Capacity of a Pile', Proceedings of ICE, Vol.26, pp 119-123.

WHITAKER, T. & COOKE, R.W. (1961). 'A New Approach to Pile Testing', 5th International Conference on Soil Mechanics & Foundation Engineering, Paris, Vol.2, pp 171-176.

WILLIAMS, D.J. (1979). 'The Behaviour of Model Piles in Dense Sand Under Vertical and Horizontal Load', Ph.D Thesis, Cambridge University, Cambridge.

YOSHIMI, Y. & KISHIDA, T. (1981). 'Friction Between Sand and Metal Surface', 10th International Conference on Soil Mechanics and Foundation Engineering, Stockholme, Vol.1, pp 831-834.